

INCREASED RESURGENT SODIUM CURRENTS (I_{NaR}) IN INHERITED AND
ACQUIRED DISORDERS OF EXCITABILITY

Andrew D. Piekarz

Submitted to the faculty of the University Graduate School
in partial fulfillment of the requirements
for the degree
Doctor of Philosophy
in the Department of Pharmacology and Toxicology
Indiana University

February 2012

Accepted by the Faculty of Indiana University, in partial fulfillment of the requirements for the degree of Doctor of Philosophy

Theodore R. Cummins, Ph.D., Chair

Andy Hudmon, Ph.D.

Doctoral Committee

Rajesh Khanna, Ph.D.

Grant D. Nicol, Ph.D.

November 10, 2011

Michael R. Vasko, Ph.D.

DEDICATION

This work is dedicated to my thesis mentor, Dr. Theodore R. Cummins and my friends and family, especially my parents, Frank and Theresa Piekarz, my sister, Katherine, my brother, Michael, my grandmother Lillian Schall, and my great uncle Ignatius Piekarz.

ACKNOWLEDGEMENTS

This dissertation would not have been possible without the inspiration, guidance, and support of many people who have impacted my life and shaped my experiences both personally and professionally. I have been extremely fortunate to have been influenced by some truly extraordinary people and I know that I owe all that I have done and will do in my lifetime to them. In the paragraphs below I would like to acknowledge several people who made significant contributions to my life and academic training.

First and foremost, I would like to thank my family. To my mother, Teri, and father, Frank, your dedication and sacrifice as parents has made many of my achievements possible. You have given me the unwavering support to pursue my interests and instilled me with a confidence in my abilities. You have provided me with significant guidance during periods of struggle, yet have exhibited patience and given me the freedom to learn for myself. To my sister, Katie, and my brother, Michael, your consistent support and competitive spirit have motivated me to be not only a better scientist but also a better person. To my grandmother Lillian, and my great uncle Ignatius, your support and significant sacrifice has been truly inspirational to me.

I would especially like to thank my mentor, Dr. Theodore Cummins. I am deeply indebted to Dr. Cummins for providing me with the ideal environment to learn and develop as a training scientist. As a mentor Dr. Cummins has given me the freedom to pursue and develop an independent research plan, provided expert assistance during periods of trouble shooting, and allowed me to cultivate collaborations and receive additional scientific training by other investigators. In many ways Dr. Cummins embodies the ideal PhD mentor and has served as an excellent personal and professional role model. Dr. Cummins is highly respected among his colleagues and

previous trainees and I have been very fortunate to have been guided through my graduate training by such a remarkable person.

I would also like to thank the members of my thesis committee, Dr. Grant Nicol, Dr. Michael Vasko, Dr. Rajesh Khanna, and Dr. Andy Hudmon for their guidance, suggestions, and constructive critiques. Each of you has had a positive impact in shaping my training and experiences as a graduate student that will not be forgotten as I progress in my scientific career. Although each of the members of my committee has provided mentorship in one form or another during my progression in graduate school, I would especially like to thank Dr. Nicol and Dr. Khanna for their patience, mentorship, and training in collaborative projects.

Aside from my committee, I would like to thank the faculty of the department of Pharmacology and Toxicology and the members of the Stark Neurosciences Research Institute (SNRI) for all your guidance and support. I would like to acknowledge Dr. Xiao-Ming Xu, Dr. Naikui Liu, and Qingbo Lu for their contributions to the spinal cord injury project. I would like to acknowledge Kathryn Hodgdon for her ideas and assistance in quantifying voltage-gated sodium channel gene expression following contusive spinal cord injury. I would especially like to thank all the faculty members for their advice and critiques following departmental seminars—especially Dr. Oxford for challenging me with technical questions related to my research and electrophysiology and Dr(s) Vasko and Hingtgen for helping me focus my scientific questions. I would also like to thank the staff of the Department of Pharmacology and Toxicology, the Stark Neurosciences Research Institute, and the Graduate School who have made my experiences as a graduate student as painless as possible. A special thanks for all your hard work and patience is order for Amy Lawson, Lisa King, Miriam Barr, Dan Smith, Nastassia Belton, Amy Doherty, Lisa Parks-Connell, Brittany Veal, and Ali Miller. Thanks again for limiting my stress, putting up with my ignorance, and taking care of the myriad of background

responsibilities that made it possible for me to focus on research. Additionally I would like to thank Debra Barker for her help editing and formatting my dissertation. Finally, I would like to thank the students in the Department of Pharmacology and Toxicology and the students in the Stark Neuroscience Research Institute for all of their critiques and input during formal and informal presentations. I would especially like to thank Stacy Dixon, Brian Schmutzler, Weihua Song, Sherry Phillips, Natalia VanDuyn, Matt Brittan, Joel Brittan, Sarah Wilson, Nicole Ashpole, and Karl Koelher for keeping me on my toes and making my experiences as a graduate student more enjoyable.

I would also like to show my gratitude to the members, past and present, of the Cummins Lab. Having excellent lab mates can impact the trajectory of a graduate student on a level that approaches that of the mentor, and I have been very fortunate to wonderful people. I would like to recognize Dr. Patrick Sheets, James Jackson II, Dr. Brian Jarecki, Dr. Yucheng Xiao, and Dr. Jonathan Theile for all their help during my graduate studies. Patrick, during my first two years in the lab you were very much like a second mentor and, in many ways, a big brother to me. You were always willing to take time to teach me better experimental technique and lab practices. We developed a friendship outside the lab and I have missed your advice and light hearted banter every day since you left. Having recently learned that you just accepted a position at IU South Bend, I am very confident that you will find success as both a scientist and mentor. Brian, your grasp of the literature and attention to detail in your work has been inspiring to me during my graduate training. I thank you for spending time critiquing my experimental design and data analysis. Yucheng, your productivity and ability to multitask is refreshing—I hope to someday embody your habits as a scientist. Jon, I found our conversations about experimental design and career development particularly helpful and I look forward to hopefully joining you in an industrial career. James, I thank you for all of your help with harvests and molecular biology. You have influenced my

personal and professional development in many ways as my lab manager, my spiritual mentor, my confidant, and my friend. I have enjoyed our conversations about all things including science—I think these conversations have helped expand my horizons and enrich my perspectives. Lastly, I would like to thank Tumare for his help with laboratory maintenance.

Finally, I would like to thank several individuals who influenced me to consider a career in scientific research. I would like to thank Mrs. Barbara Babiar, Mr. Frank DeSerto, Mr. Lynn Schultz, Father Barney Barry S.J., Father Michael Doody, Dr. David Barnett, and Dr. Mark Knuepfer. Each of you had a profound impact on shaping me both personally and academically and I am positive I would not have made it to graduate school without you.

A special thanks to the NINDS of NIH for funding much of this research through a predoctoral NRSA training grant (1F31NS066663-01).

It may not take a village to raise a child but it certainly takes a village, or equivalent, to train a scientist...

ABSTRACT

Andrew D Piekarz

Increased resurgent sodium currents (I_{NaR}) in inherited and acquired disorders of excitability

Voltage-gated sodium channels (VGSCs) are dynamic membrane spanning proteins which mediate the rapid influx of Na^+ during the upstroke of the action potential (AP). In addition to the large inward Na^+ currents responsible for the upstroke of the AP, some VGSC isoforms produce smaller, subthreshold Na^+ currents, which can influence the excitable properties of neurons. An example of such a subthreshold current is resurgent Na^+ current (I_{NaR}). These unusual currents are active during repolarization of the membrane potential, where the channel is normally refractory to activity. I_{NaR} exhibit slow gating kinetics and unusual voltage-dependence derived from a novel mechanism of channel inactivation which allows the channel to recover through an open configuration resulting in membrane depolarization early in the falling phase of the AP, ultra-fast re-priming of channels, and multiple AP spikes. Although originally identified in fast spiking central nervous system (CNS) neurons, I_{NaR} has recently been observed in a subpopulation of peripheral dorsal root ganglion (DRG) neurons. Because I_{NaR} is believed to contribute to spontaneous and high frequency firing of APs, I have hypothesized that increased I_{NaR} may contribute to ectopic AP firing associated with inherited and acquired disorders of excitability. Specifically, this dissertation explores the mechanisms which underlie the electrogenesis of I_{NaR} in DRG neurons and determines whether the biophysical properties of these unique currents were altered by mutations that cause inherited muscle and neuronal channelopathies or in an experimental model of nerve injury. The results demonstrate that (1) multiple Na^+ channel isoforms are capable of producing I_{NaR} in DRG neurons, including NaV1.3, NaV1.6, and NaV1.7, (2) inherited muscle and neuronal channelopathy mutations that

slow the rate of channel inactivation increase I_{NaR} amplitude, (3) temperature sensitive I_{NaR} produced by select skeletal muscle channelopathy mutations may contribute to the triggering of cold-induced myotonia, and (4) I_{NaR} amplitude and distribution is significantly increased two weeks post contusive spinal cord injury (SCI). Taken together, results from this dissertation provide foundational knowledge of the properties and mechanism of I_{NaR} in DRG neurons and indicates that increased I_{NaR} likely contributes to the enhanced membrane excitability associated with multiple inherited and acquired disorders of excitability.

Theodore R. Cummins, Ph.D., Chair

TABLE OF CONTENTS

LIST OF TABLES	xv
LIST OF FIGURES	xvi
LIST OF ABBREVIATIONS	xx
FOREWARD	xxiv
I. Introduction.....	1
A. Historical perspective on the mechanism underlying action potential generation.....	2
1. Ionic theory of membrane excitation and the development and description of the Hodgkin-Huxley model of membrane excitability	2
2. Role of inward sodium current in action potential generation.....	5
B. Voltage-gated sodium channels	6
1. Discovery and structural features of voltage-gated sodium channels	6
2. The dynamic sodium channel structure: voltage-dependent conformational change	11
3. Diversity of voltage-gated sodium channels in mammals.....	15
4. Altered expression and dysfunction of voltage-gated sodium channels is associated with inherited and acquired disorders of excitability	18
C. Voltage-gated sodium channel auxiliary β -subunits structure and function	21
D. Resurgent Sodium Currents	24

1. Resurgent sodium current results from an alternative form of channel inactivation.....	25
2. Mechanism and molecular determinants of resurgent sodium current in cerebellar Purkinje neurons.....	29
a. The NaV1.6 channel isoform is the major carrier of resurgent sodium current in cerebellar Purkinje neurons	29
b. The C-terminus of the auxiliary β_4 -subunit serves as the open channel blocker responsible for resurgent inactivation kinetics.....	30
c. Regulation of open channel block and resurgent sodium current generation	31
3. Resurgent sodium current contributes to burst firing of action potentials in CNS neurons.....	33
E. Hypothesis and specific aims	34
II. <i>Materials and methods</i>	37
A. cDNA vectors	37
B. Mutagenesis of voltage-gated sodium channels	39
C. Harvest and culture of rat DRG neurons.....	42
D. Biolistic transfection of rat DRG neurons.....	46
E. Electrophysiology Recordings Solutions	48
1. Standard extracellular bathing solution for electrophysiology recordings	48
2. Standard CsF dominant electrode solution for electrophysiology recordings	48
F. Whole-cell voltage-clamp recordings in DRG neurons	49
G. Isolation of transfected recombinant voltage-gated sodium currents in DRG neurons.....	52
H. Computational simulations of a DRG neuron and a cardiac myocyte	56
1. DRG neuron simulation.....	56

2. Cardiac myocyte simulation	57
I. Contusive spinal cord injury model	62
J. Conventional- and real-time- reverse transcriptase polymerase chain reaction (RT-PCR)	63
K. Immunocytochemistry: staining acutely cultured rat DRG neurons	67
L. Data analysis	68
1. Electrophysiology data analysis	68
2. Resurgent sodium current quantification and analysis	69
3. qPCR data analysis	72
III. <i>Characterization of resurgent sodium currents (I_{NaR}) properties and distribution in rat dorsal root ganglion (DRG) neurons</i>	74
A. Introduction	74
B. Original experimental results	76
1. Resurgent sodium currents in native rat DRG neurons	76
2. Sodium channel auxiliary NaV β_4 subunit is expressed in rat DRG neurons	82
3. Resurgent sodium currents can be produced by multiple voltage-gated sodium channels in rat DRG neurons.....	86
C. Discussion.....	89
IV. <i>Mutations that slow the rate of channel inactivation and cause neuronal and muscle channelopathies increase I_{NaR} amplitude and frequency</i>	94
A. Introduction and hypothesis rationale	94
B. Original experimental results	99
1. NaV1.7 PEPD mutations which slow the rate of channel inactivation increase resurgent sodium currents	99

2. Increased resurgent sodium currents augment neuronal excitability	103
3. A NaV1.5 LQT-3/SIDS mutation which slows the rate of channel inactivation increased resurgent sodium currents and elongates the cardiac action potential Q-T interval	105
4. NaV1.4 PMC mutations that slow the rate of channel inactivation increased resurgent sodium currents	108
C. Discussion.....	112
V. <i>Differential temperature dependence of resurgent sodium currents in muscle and neuronal channelopathies</i>	115
A. Introduction	115
B. Original experimental results	117
1. Cold temperature induces slowing of NaV1.4 and NaV1.7 channel inactivation kinetics	117
2. Cold temperature increases I_{NaR} in NaV1.4-R1448P PMC mutant but not NaV1.7-I1461T mutant channels.....	120
3. Temperature sensitivity of I_{NaR} is determined, at least in part, by the location of the mutation	124
C. Discussion.....	129
VI. <i>Increased resurgent sodium currents in rat DRG neurons following contusive spinal cord injury (SCI)</i>	135
A. Introduction	135
B. Original experimental results	137
1. 14 days post T10 contusive SCI, VGSC TTX-S, TTX-R, and persistent current densities are unaltered in acutely dissociated L1-L6 DRG neurons	139
2. 14 days post contusive SCI resurgent sodium current (I_{NaR}) amplitude is increased	143
3. Increased I_{NaR} in SCI neurons does not result from slowed rate of channel open-state inactivation	148

4. Increased DRG excitability and I_{NaR} amplitude is not supported by gene expression increases in voltage-gated sodium channel isoform and associated β -subunits	150
C. Discussion.....	154
1. Future directions	159
a. Does increased I_{NaR} in L1-L6 DRG neurons correlate to augmented excitability and pain following SCI?.....	159
b. What mechanisms are responsible for increased I_{NaR} in L1-L6 DRG neurons following contusive SCI?.....	161
VII. Thesis unifying discussion.....	166
A. Multiple VGSC isoforms can produce I_{NaR}	167
B. Rate of channel inactivation is an important factor which regulates I_{NaR} generation but it is not the sole determinant	172
C. Resurgent sodium current (I_{NaR}) is increased in inherited and acquired disorders of excitability.....	182
1. Inherited channelopathy mutations which slow the rate of channel inactivation increase resurgent sodium currents (I_{NaR})	183
2. Resurgent sodium currents (I_{NaR}) are increased by contusive spinal cord injury (SCI)—a model of peripheral nerve injury	188
D. Final summation.....	190
VIII. Reference list.....	193
APPENDICES	217
A. Author permissions.....	217
B. Human voltage-gated sodium channel mutations that cause inherited neuronal and muscle channelopathies increase resurgent sodium currents.....	221
CURRICULUM VITAE	

LIST OF TABLES

Table 1: Diversity of voltage-gated sodium channels (VGSCs).....	17
Table 2: Transition rate expressions for NaV1.7 conductance simulations in a modeled DRG neuron.....	60
Table 3: Transition rate expressions for NaV1.5 conductance simulations in a modeled cardiac myocyte	61
Table 4: Primers used for qPCR experiments.....	66
Table 5: Biophysical properties of wild-type and mutant channels	111
Table 6: Comparison of NaV1.7 and NaV1.4 wild-type and mutant channel biophysical properties	128
Table 7: Biophysical properties of naïve, sham, and SCI L1-L6 DRG neurons 14 days post contusive SCI.....	152
Table 8: Multiple VGSC isoforms can produce I_{NaR}	170
Table 9: Relationship between rate of channel inactivation and I_{NaR} amplitude in wild-type VGSCs.	178
Table 10: VGSC channelopathy mutations that are likely to increase resurgent sodium current (I_{NaR})	186

LIST OF FIGURES

Figure 1: Topography of a voltage-gated sodium channel (VGSC)	9
Figure 2: Simplified scheme of the different conformational states of the dynamic voltage-gated sodium channel (VGSC).....	13
Figure 3: Structure and subunit stoichiometry of the voltage-gated sodium channel (VGSC) complex.....	23
Figure 4: Model of channel state configurations with and without resurgent sodium current (I_{NaR})	27
Figure 5: Rat DRG harvest flow chart	45
Figure 6: Reduced NaV1.8 currents following biolistic transfection of NaV1.8 shRNA	55
Figure 7: Diagram of the Markov models used for voltage-gated sodium channel conductances.....	59
Figure 8: Standard resurgent current (I_{NaR}) voltage clamp protocol.....	69
Figure 9: Quantification of resurgent sodium current amplitude	71
Figure 10: Resurgent sodium currents (I_{NaR}) detected in some, but not all, DRG neurons.....	78

Figure 11: Distribution of native resurgent sodium currents (I_{NaR}) in rat DRG neurons	79
Figure 12: Properties of resurgent sodium currents (I_{NaR}) in rat DRG neurons	81
Figure 13: Suspected resurgent sodium current (I_{NaR}) open channel blocker, $NaV\beta_4$, mRNA and protein are expressed in rat DRG neurons	84
Figure 14: Resurgent sodium currents (I_{NaR}) are produced by recombinant wild-type $NaV1.6$, -1.7 , and -1.3 channels expressed in rat DRG neurons	88
Figure 15: Rationale for increased I_{NaR} frequency and amplitude with slowed rate of channel inactivation	97
Figure 16: Resurgent current amplitude and frequency are increased in $NaV1.7$ -I1461T PEPD mutant channels	101
Figure 17: Computer simulation of sodium conductances and DRG neuron excitability.....	104
Figure 18: Increased I_{NaR} amplitude in $NaV1.5$ -F1486L mutant channel contributes to elongated cardiac action potential	106
Figure 19: Paramyotonia congenital mutations induce I_{NaR} in $NaV1.4$ mutants that slow the rate of channel inactivation.....	110

Figure 20: Temperature slows channel open-state inactivation in NaV1.7-WT, NaV1.4-WT, NaV1.7-I1461T, and NaV1.4-R1448P	119
Figure 21: Temperature alters resurgent current (I_{NaR}) amplitude from the NaV1.4-R1448R (PMC) but not NaV1.7-I1461T (PEDP) mutant channels.....	122
Figure 22: Temperature slows channel open-state inactivation in NaV1.7-R1599P and increases I_{NaR} amplitude	126
Figure 23: No change in TTX-S, TTX-R, or persistent sodium current density 14 days post contusive SCI.....	141
Figure 24: Increased resurgent sodium current (I_{NaR}) amplitude in small and medium/large soma diameter DRG neurons 14 days post contusive SCI.....	144
Figure 25: Following contusive SCI resurgent sodium current (I_{NaR}) is found in a broader population of DRG neurons.....	147
Figure 26: Increased resurgent sodium current (I_{NaR}) amplitude following contusive SCI is not explained by slowed rate of channel open-state inactivation (τ_h).....	149
Figure 27: No change in voltage-gated sodium channel (VGSC) subunit expression following contusive SCI.....	151
Figure 28: NaV β_4 mRNA expression is augmented in SCI neurons with resurgent sodium current	165

Figure 29: Rate of channel inactivation correlates to I_{NaR} amplitude for recombinant VGSCs expressed in DRG neurons..... 174

Figure 30: Summary of average correlation between rate of channel inactivation and I_{NaR} amplitude for wild-type VGSC isoforms 177

Figure 31: Working hypothesis: Factors which influence I_{NaR} generation and amplitude..... 181

LIST OF ABBREVIATIONS

α -subunit	Pore forming subunit of Voltage-Gated Sodium Channel with 24 transmembrane spanning segments)
β -subunits	Sodium channel auxiliary β -subunits
τ_h	Tau-h (referring to the Hodgkin and Huxley kinetic time constant of channel inactivation)
τ_m	Tau-m (referring to the Hodgkin and Huxley kinetic time constant of channel activation)
ANOVA	Analysis of Variance
AP	Action Potential
CAM	Cell Adhesion Molecule
CIP	Congenital Insensitivity to Pain (Nonsense channelopathy where NaV1.7 channel is not expressed in patients—resulting loss of pain sensation) also referred to as Hereditary Sensory Neuropathy Type IV (HSN-IV).
CNS	Central Nervous System
Ct	Cycle Threshold (PCR cycle where fluorescence crosses the threshold of detection)
DI-DIV	Domains of the Voltage-Gated Sodium Channel
BfDMEM	Bicarbonate Free Dulbecco's Modified Eagle Medium
DMEM	Dulbecco's Modified Eagle Medium
DsRed	28-kDa fluorescent protein responsible for the red coloration around the oral disk of a coral of the Discosoma genus. (similar to green fluorescent protein)
GFP	Green Fluorescent Protein
hEK293	Human Embryonic Kidney Cells
h_∞	Steady-State Channel Fast Inactivation

IC ₅₀	Concentration of drug where a measured biological effect is inhibited by 50%
IFM particle	Corresponding to the Isoleucine, Phenylalanine, and Methionine putative inactivation gate
I _{NaR}	Resurgent Sodium Current
I _{Na}	Sodium Current
I _K	Potassium Current
IRES	Internal Ribosome Entry Site
IV	Current Voltage Relationship
K ⁺	Potassium ion
LQT-3	Long-QT Type 3 (NaV1.5 channelopathy which results in elongated Q-T interval of cardiac action potential)
Na ⁺	Sodium Ion
NaV	Voltage-Gated Sodium Channel (referring to channel isoforms NaV1.1-1.9)
NaVβ ₄	Voltage-Gate Sodium Channel auxiliary β ₄ -subunit
NTC	No Template Control
NGF	Nerve Growth Factor
ORF	Open Reading Frame
OSI	Open-State channel inactivation
PCR	Polymerase Chain Reaction
PEPD	Paroxysmal Extreme Pain Disorder (NaV1.7 channelopathy which results in extreme pain in the ocular, submandibular, and rectal regions)
PMC	Paramyotonia Congenita (NaV1.4 channelopathy which results in cold-induced myotonia of skeletal muscle)
PNS	Peripheral Nervous System
ProTx-II	Prototoxin-II (tarantula toxin that inhibits voltage-gated calcium and sodium channels)

PVP	Polyvinylpyrrolidone
qPCR	Referring to semi-quantitative polymerase chain reaction methodology
RT	Reverse Transcriptase
S1-S6	Inter-domain Segments of the Voltage-Gated Sodium Channel
SCI	Spinal Cord Injury
SEM	Standard Error of the Mean
SIDS	Sudden Infant Death Syndrome (NaV1.5 channelopathy which results in sudden cardiac failure in infants)
TEA	Tetraethylammonium Ion
TTX	Tetrodotoxin
TTX-S	Tetrodotoxin Sensitive (in reference to sodium channel isoforms which are pharmacologically inhibited by TTX at relatively low concentrations (< 500nM))
TTX-R	Tetrodotoxin Resistant (in reference to sodium channel isoforms which are pharmacologically inhibited by TTX at relatively high concentrations(>1μM))
WT	Wild-type
$V_{1/2}$	The voltage at which 50% of channels have transitioned to a new state conformation
VGSC	Voltage-Gated Sodium Channel

“A good Ph.D. [dissertation] often raises more questions than it solves, so you should not be surprised if your work changes direction.”

-Raymond Gosling, Ph.D.
Emeritus professor, University of London

“It is not the mountain we conquer but ourselves...”

-Sir Edmund Hillary
Mountaineer

FOREWORD

Voltage-gated sodium channels (VGSCs) are complex proteins that transition to different conformations in response to changes in the transmembrane voltage. Located in the plasma membrane, these dynamic proteins mediate the influx of Na^+ ions across the cell that causes membrane depolarization and the rapid upstroke of the action potential in nerve and muscle tissue. Consequently, VGSCs play a fundamental role in regulating excitability and have important roles in a diverse array of physiological processes ranging from nerve and muscle excitation to learning and memory.

In addition to the large, classic inward sodium currents which contribute to initiation and propagation of action potentials, some VGSC isoforms produce smaller, subthreshold sodium currents that can influence the excitable properties and signal processing functions of neurons. One example of a subthreshold sodium current that can impact excitability in neurons is resurgent sodium current (I_{NaR}). Resurgent sodium currents are unusual sodium currents that activate during the falling phase of the action potential at voltages where sodium channels are normally refractory to activation. Although relatively small in amplitude (~3% of peak transient current), I_{NaR} exhibit slow gating kinetics and unusual voltage-dependence resulting from a novel mechanism of recovery from an inactivated state through an open, ion conducting configuration which produces depolarizing driving early in the falling phase of the action potential and subsequent action potential spikes. Originally identified in cerebellar Purkinje neurons, I_{NaR} are crucial to the high frequency firing in several areas of the central nervous system (CNS).

This dissertation explores the mechanism and molecular determinants of resurgent sodium currents (I_{NaR}) and their role in inherited and acquired disorders of excitability in peripheral dorsal root ganglion (DRG) neurons. Specifically this

manuscript addresses questions related to the mechanism of I_{NaR} , including which VGSC isoforms are capable of producing I_{NaR} in DRG neurons and how the rate of channel inactivation influences I_{NaR} generation in DRG neurons. Additionally, this dissertation explores whether the biophysical properties of I_{NaR} are altered (1) by mutations that cause inherited muscle and neuronal channelopathies or (2) following contusive spinal cord injury. In pursuit of these goals the sections which follow outline information concerning the properties of voltage-gated sodium channels, the discovery and mechanism of I_{NaR} , and results and discussion of original data collected from experiments designed to address questions related to the mechanism of I_{NaR} and its proposed involvement in pathophysiology. The Introduction (**Chapter I**) discusses information about the structure and function of voltage-gated sodium channels—including an in depth discussion of their roles in nerve and muscle tissue physiology and evidence for their involvement in disease processes—and information on the properties and mechanism of resurgent sodium currents. The Methods section (**Chapter II**) details the experimental techniques used through the thesis. The experimental work has been divided into four separate chapters (**Chapters III-VI**) each with a short introduction, followed by results, and a brief discussion. **Chapter III** will characterize the properties of I_{NaR} in rat DRG neurons. **Chapter IV** will explore if the biophysical properties of I_{NaR} are altered in neuronal and muscle channelopathies with impaired rate of channel inactivation. **Chapter V** examines if increased I_{NaR} amplitude observed in select mutant channels is temperature dependent. Finally, **Chapter VI** examines if the biophysical properties of I_{NaR} are changed following an experimental model of contusive spinal cord injury. A thesis-unifying discussion (**Chapter VII**) is followed by a comprehensive list of all works cited.

Chapter I: *Introduction*

How do cells communicate? In multicellular organisms cell-to-cell communication is complex, requiring rapid transmission of information over distances ranging from micrometers to meters to regulate tissue specific cellular and metabolic processes. Intercellular communication is dependent on the transport of organic signaling molecules and ions from the extracellular environment across a cell membrane. Eukaryotic cells are partitioned from the external aqueous environment by a cell membrane composed of a hydrophobic lipid bilayer that is a major barrier to the movement of organic signaling molecules and ions¹. In order to overcome this physical barrier to communication, cells have evolved eloquent mechanisms to transduce signals to/from neighboring cells and the surrounding environment. Cells can communicate via many dissimilar processes including direct contact between receptors of neighboring cells, diffusion of chemical signaling molecules through gap junctions, or secretion of chemical signaling molecules into the extracellular environment that diffuse and bind to receptors on neighboring cells. In excitable cells, such as nerve and muscle tissue, communicated information is encoded by an impulse known as an action potential. The generation and propagation of this electrochemical impulse is a highly regulated and controlled process that is involved in a diverse array of physiological functions ranging from nerve-muscle excitation contraction coupling, learning and memory, and sensory signal transduction. Understanding the mechanisms which contribute to action potential initiation and propagation is of paramount importance because dysregulation of action potential signaling has been linked to a variety of pathological conditions including cardiac arrhythmias, weakness and paralysis of skeletal muscle, extreme pain, and epilepsy. This dissertation focuses on resurgent sodium current (I_{NaR}), a unique sodium current, which is hypothesized to contribute to high frequency action potential firing in

some neurons of the central nervous system. To begin, I discuss the ionic basis of the action potential and highlight the role of sodium currents in the generation of the action potential.

A. *Historical perspective on the mechanism underlying action potential generation*

1. *Ionic theory of membrane excitation and the development and description of the Hodgkin-Huxley model of membrane excitability*

The action potential is the basic unit of signaling used by nerve and muscle tissue for cellular communication. Research performed by Kenneth Cole, Howard Curtis, Sir Alan Hodgkin, Sir Andrew Huxley, and Benard Kratz during the period now known as the era of classical biophysics (1935-1952) defined the ionic theory of membrane excitation—which today serves as the foundation of our understanding of how the selective diffusion of ions across the plasma cell membrane results in the generation and propagation of action potentials in excitable tissues. These pioneering biophysicists applied principles of electrochemistry and electrical engineering to determine how an electrical impulse might be generated in organic tissues. Specifically, they studied the passive membrane properties and defined the ionic basis of the propagated action potential in the squid giant axon.

Although the origin of action potentials, or action currents as they were originally described, were initially debated, a series of experiments by Hodgkin demonstrated that action potentials were an electric signal of ionic origin^{2,3}. Research by Cole and Curtis suggested that the electrical action potential resulted from an increase in membrane permeability to different ion species⁴⁻⁶. Subsequent experiments by Rothenberg⁷ and Keynes⁸ demonstrated that propagation of the action potential is associated with an inward flow sodium ions and the outflow of potassium ions. Additional experiments by Hodgkin and Katz⁹ demonstrated that the rate of rise and amplitude of the action

potential were dependent on the concentration of sodium in the extracellular bath solution. Taken together, results from this early period of classical biophysics defined the ionic theory of membrane excitation which states that an action potential is an electrochemical impulse that is driven by the selective transport of ions across the plasma cell membrane.

With the development and optimization of the voltage clamp technique, the ionic theory of membrane excitation was proven and given a strong quantitative basis^{6,9,10}. The voltage clamp technique allows ionic currents to be measured when the cell membrane is maintained (“clamped”) at a uniform voltage. Using this technique in the squid giant axon, Hodgkin and Huxley were able to determine the following: (1) transient inward and sustained outward ionic currents moved enough charge to account for the rapid rate of rise and fall of the action potential¹¹ and (2) the selective permeability of the membrane to individual ion species is voltage-dependent¹². By removing ions from the extracellular medium individually and replacing them one at a time with a membrane impermeant molecule, Hodgkin and Huxley determined that the two major ionic components of the squid giant axon action potential were an inward sodium current (I_{Na}) and an outward potassium current (I_K)¹³. Subsequent experiments determined that both I_{Na} and I_K were voltage-dependent¹², and I_{Na} was also time dependent—where I_{Na} rises rapidly and then decays during a step depolarization¹⁴. Accordingly, Hodgkin and Huxley suggested that the selective permeability of sodium and potassium ions is governed by voltage-dependent movement of membrane gates, thus introducing, for the first time, the concept of voltage-dependent gating. Because the sodium conductance contained two separate phases it was said to be controlled by two separate gates: an activation gate—responsible for the rapid rising phase of the sodium conductance and an inactivation gate—responsible for the slow decay phase of the sodium conductance¹⁴. Finally, Hodgkin and Huxley developed a mathematical model to

describe how ion fluxes and permeability changes of the excitable cell membrane contributed to the generation of the action potential¹⁵. Accordingly to their model, ionic current was divided into components carried by sodium and potassium ions (I_{Na} and I_K) and a small leakage current (I_L). A system of differential equations was defined for each component of the ionic current as determined by several factors, including the voltage-dependent permeability coefficient, the membrane voltage, the equilibrium potential for the ionic species, and gating characteristics of the ionic component. The solution to the differential equation defined the individual ion conductance at a given voltage. According to the Hodgkin and Huxley model the action potential waveform is predicted to result from three components: a rising depolarizing phase dominated by activated sodium conductance (inward sodium current pushes the membrane voltage positively towards the equilibrium potential for sodium), a repolarizing phase, where potassium conductance activates and the sodium conductance inactivates (outward potassium current pushes the membrane voltage negatively towards the equilibrium potential for potassium), and a recovery phase where multiple ionic conductances reset the membrane voltage to the resting potential. The works described above by Hodgkin and Huxley have been foundational to our understanding of how individual ion fluxes contribute to the generation and propagation of action potentials in nerve and muscle tissue. Indeed, experiments described in this thesis make use of the voltage-clamp recording technique and inward sodium currents from several experiments are fit according to Hodgkin Huxley parameters (defined by their quantitative model) [see **Chapters IV-VI**].

2. Role of inward sodium current in action potential generation

The experiments described above defined how the selective movement of ions across the plasma cell membrane contributes to action potential propagation. Importantly, results from several studies suggested that inward sodium conductance contributed to the regenerative, rapid upstroke of the action potential in axons. More specifically, inward sodium (Na^+) current was described to contribute to the upstroke of the action potential because an influx of Na^+ ions coincided with upstroke of the action potential⁷ and the membrane permeability to Na^+ transiently increased during membrane depolarization^{12,13}. Because permeability of Na^+ through the membrane was controlled by the membrane voltage it was described as a voltage dependent ionic conductance controlled by different “gating configurations”¹⁴. Based on these data, mechanisms which govern inward Na^+ flux are believed to be critical determinants of excitability in excitable tissues. Our theoretical understanding of mechanisms which govern membrane excitability have come a long way since the days of Hodgkin and Huxley. For example, we now know that the transient increase in membrane permeability to Na^+ ions, responsible for the upstroke of the action potential, is controlled by sodium selective ion channels (referred to as voltage-gated sodium channels or VGSCs) that undergo conformational change, or gating, in response to a change in the membrane voltage. The following section provides background on voltage-gated sodium channels relevant to experiments described in this dissertation.

B. *Voltage-gated sodium channels (VGSCs)*

Voltage-gated sodium channels (VGSCs) are complex proteins that transition to different conformations in response to changes in the transmembrane voltage. Located in the plasma membrane, these dynamic proteins mediate the influx of Na⁺ ions into the cell that underlies the rapid depolarizing phase of the action potential in nerve and muscle tissue¹³. Voltage-gated sodium channels isolated from mammalian neurons exist in heteromultimeric complexes consisting of a highly processed, pore forming α -subunit (~260 kDa)¹⁶, and one or more auxiliary β -subunits (22-36 kDa)¹⁷⁻¹⁹, and, in some cases, other accessory proteins such as calmodulin²⁰ or annexin II²¹. The VGSC α -subunit is the principle subunit of the channel complex, responsible for pore formation, drug binding, ion selectivity, and ion conduction. Although expression of the VGSC α -subunit is sufficient to produce functional Na⁺ current, channel trafficking, anchoring, localization, and channel conformational change are all suggested to be modulated by the presence of the VGSC auxiliary subunits²⁰⁻²².

1. *Discovery and structural features of voltage-gated sodium channels*

Although work from Hodgkin and Huxley suggested the presence of membrane proteins that “gated” in response to voltage, the identification of channel proteins responsible for individual ion flux was realized only after (1) the discovery of high affinity neurotoxins which labeled individual channel families and (2) development of biochemical techniques for detergent solubilization and purification of labeled channel proteins^{23,24}. Using such techniques the sodium channel complex was initially identified by Beneski and Catterall²⁵ and later purified from rat brain^{26,27}. Subsequent molecular and biochemical characterization, culminating in the cloning of the VGSC first from the eel²⁸ and later from rat^{29,30}, provided the first insights into the structural composition and arrangement of the sodium channel.

The mammalian VGSC α -subunits are large proteins—composed of around 2000 amino acid residues. Sequence analysis and hydropathy mapping indicated that the channel sequence is composed of four homologous repeats, referred to as domains (DI-IV), containing six transmembrane spanning segments (S1-S6) with α -helical topography. In addition residues which link the four domains of the sodium channel and the N- and C-termini are located on the cytoplasmic side of the membrane (Figure 1A). The arrangement of the residues and order of the sodium channel topography resemble that of the evolutionarily related voltage-gated calcium channel (VGCC) and that of a tetrameric voltage-gated potassium channel (VGPC) complex. Close examination of the VGSC sequence and predicted secondary structure reveal several key structural elements which are important for channel function and are conserved among other voltage sensing ion channels. For example, the S4 segment of each domain contains several positively charged amino acids believed to be involved in the voltage-sensing mechanism that results in channel conformational change^{31,32}. Additionally, strong evidence suggests the S5-S6 regions of each domain contribute to the pore structure of the sodium channel—with the extracellular loops and transmembrane “P-loop” region between S5 and S6 contributing to the ion selectivity filter and extracellular mouth of the pore, and the distal section of each S6 segment comprising the cytoplasmic half of the channel pore³³. Although the tertiary structure of the VGSC had long been debated, recent publication of the bacterial sodium channel (*Arcobacter butzleri*) crystal structure, by Catterall and colleagues, shed light on the spatial arrangement of key channel elements³⁴. According to the crystal structure of the bacterial Na⁺ channel, the four homologous domains of mammalian VGSCs are predicted to assemble in four-fold symmetry around a central channel pore (Figure 1-C). Interestingly, each channel domain is segregated into two functional units: the voltage-sensor, comprised of S1-S4 segments, and the pore structure, comprised of the S5-S6 segments³⁴ (Figure 1-B).

Finally, the last structural feature which is important for channel function is the inactivation gate (see Figure 1A). Voltage clamp experiments by Hodgkin and Huxley described a voltage-dependent sodium conductance with two phases- a rapid *activation* phase followed by a slowly decaying *inactivation* phase¹⁴. According to the Hodgkin Huxley model the distinct nature of the two phases resulted from separate gates or modes of channel function. Early structure function studies employing site directed mutagenesis identified the DIII-IV linker as an area of the channel important for the inactivation process (slow decay of Na⁺ current)³¹. Further characterization of the DIII-IV linker identified three key amino acid residues— Isoleucine, Phenylalanine, and Methionine—which are critically important for channel inactivation and are collectively referred to as the channel inactivation gate or IFM particle³⁵. It is believed that following channel opening the IFM particle folds into the channel pore and blocks ion conduction from the cytoplasmic side.

Figure 1:

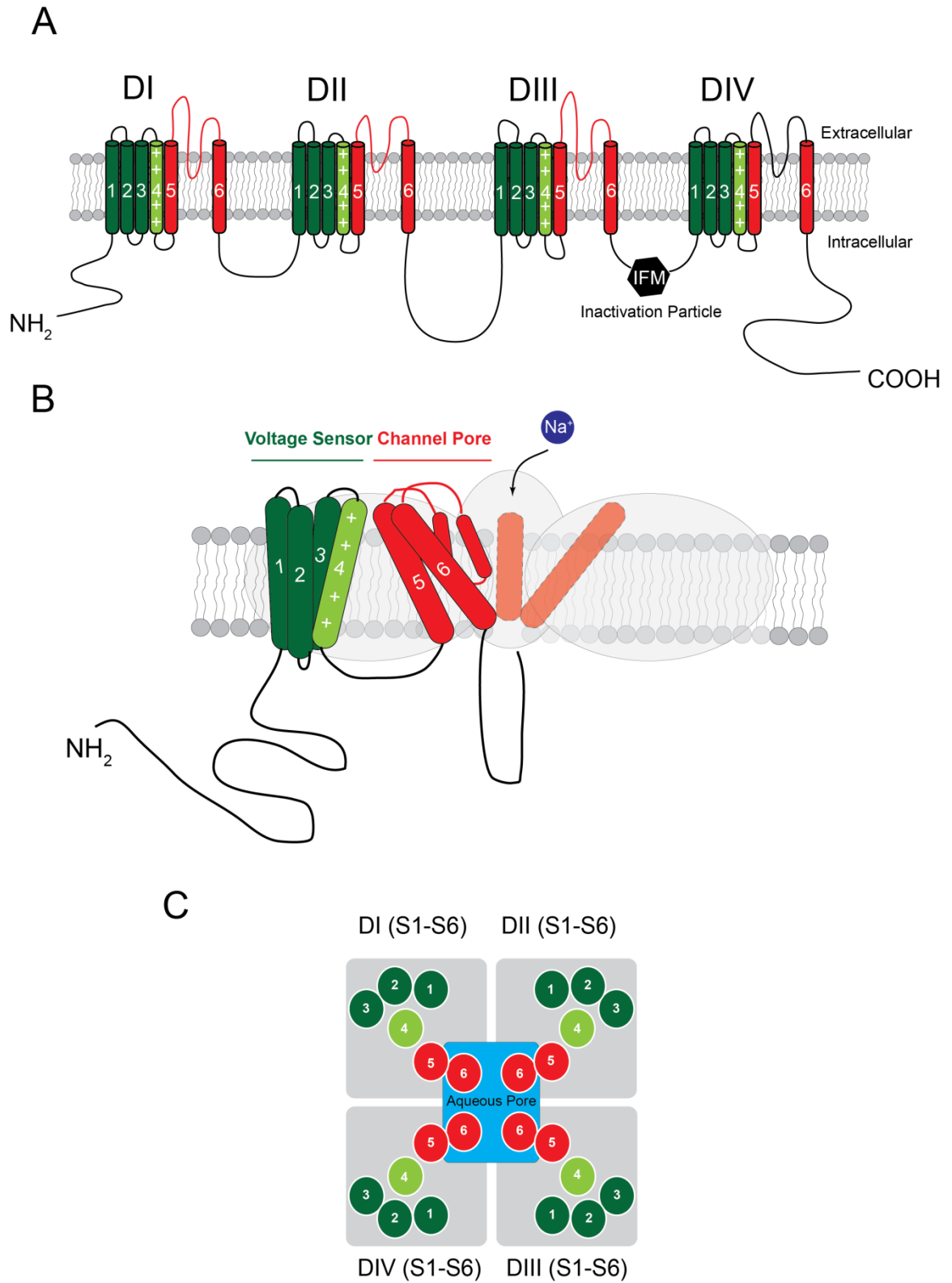


Figure 1: Topography of a voltage-gated sodium channels (VGSC). **(A)** Linear representation of the α -subunit of the voltage gated sodium channel with four domains (DI-DIV) each with six transmembrane spanning segments (S1-S6). Key structure features important for channel function are highlighted. The mobile voltage sensing segments important for channel activation in each domain are highlighted in lime green. The IFM particle in the DIII-DIV linker important for channel inactivation is highlighted with a black hexagon. Pore forming segments are highlighted in red. **(B)** 3-dimensional cartoon of the VGSC. The crystal structure of the bacterial VGSC indicates the channel is divided into two core elements: the channel voltage sensor (shown in green) and the channel pore (shown in red)³⁴. **(C)** Top down extracellular view of the aqueous VGSC pore surrounded by the transmembrane segments. These figures were created using Adobe Illustrator CS4 and were adapted from several models in the literature^{34,36,37}.

2. *The dynamic sodium channel structure: voltage-dependent conformational change.*

Voltage-gated sodium channels are dynamic proteins that facilitate the influx of Na⁺ ions across the plasma membrane. Sodium flux through these gated pores is dependent on a series of complex conformational changes in response to altered membrane voltage. In the most generalized scheme, VGSCs can exist in one of three state conformations: closed (primed), open (activated), or inactivated (Figure 2). In this case the closed, ion impermeant configuration of the channel is observed at hyperpolarized voltages, near the resting membrane potential; in the closed state the channel is said to be primed and available to open with membrane depolarization (Figure 2-A). As the membrane voltage is depolarized the VGSCs transition from a closed state to an open, ion-conducting configuration in less than a millisecond, allowing Na⁺ ions to flow down their electrochemical gradient and into the cell (Figure 2-B). Channel activation and opening in response to depolarization of the membrane is dependent on the mobility of multiple channel voltage-sensors. Specifically it is believed that displacement of the DI-DIII S4 segments are crucial for channel activation with membrane depolarization; transient displacement of S4 segments produces a conformational change that causes the tightly packed pore-forming segments of each domain (S5-S6 segments) to splay open^{34,38}. Within a few milliseconds of opening, VGSCs transition to a non-conducting, inactivated conformation (Figure 1-C). The transition to the inactivated configuration of the channel is mediated by the translocation of DIII-DIV inactivation (IFM) particle, which is hypothesized to bind within the pore and obstructs the influx of Na⁺ ions³⁵. The rate and extent to which VGSCs undergo inactivation shows apparent voltage-dependence and appears greater at depolarized potentials. The voltage dependence of the inactivation gate is hypothesized, by some, to result from the translocation of the DIV-S4 segment in response to membrane

depolarization. According to this hypothesis, the mechanism for channel activation and subsequent inactivation result from the coordinated translocation of the voltage-sensors in response to a membrane depolarization. Once inactivated, the channels are refractory to further activity and are not available to open again until the cell membrane is repolarized to negative potentials for many milliseconds. The time course for the onset of- and recovery from channel inactivation is very important in modulating the duration and firing frequency of action potentials in excitable cells. Understanding the normal sequence of sodium channel gating is important for understanding key elements of my central hypothesis and the mechanism of I_{NaR} , as cells which produce resurgent sodium current undergo a different form of channel inactivation.

Figure 2:

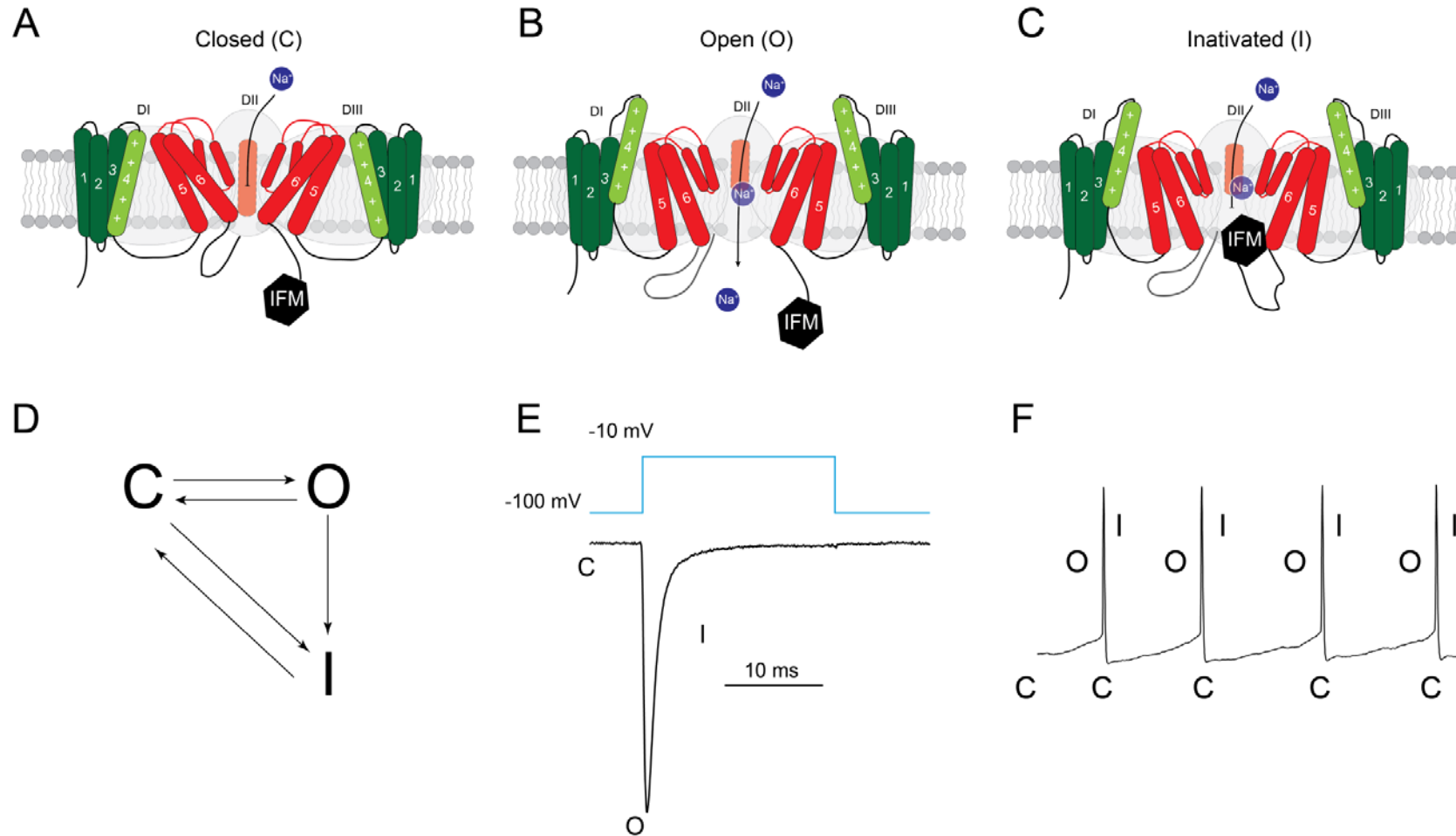


Figure 2: Simplified scheme of the different conformational states of the dynamic voltage-gated sodium channel (VGSC). (A-C) Cartoon of the state conformations of the VGSC. In the most simplified scheme VGSCs exist in one of three state conformations: closed, open, or inactivated. At very negative voltages the channel is closed and ready to open (A). As the membrane is depolarized the S4 segments of each channel domain are mobilized and the channel undergoes a rapid conformational change and opens (B) allowing sodium ions to flow down their electrochemical gradient. In less than a millisecond the same conformational change that causes the channel to open causes the channel to assume an inactivated (non-ion conducting) conformation (C). The DIII-IV linker IFM particle mediates channel inactivation. (D) State diagram of the VGSC gating transitions. It is important to note that once channels inactivate the channels must pass through a non-ion conducting closed state before reopening. (E) Representative current trace of sodium current recorded from DRG neurons. The downward deflection reflects the inward movement of sodium ions in response to a depolarizing pulse to -10 mV from a holding potential of -100 mV. Note that no sodium current is observed in the closed state; as the membrane is depolarized the channel opens resulting in a rapid influx of sodium ions; inactivation of the sodium channel results in the slow decay phase of the inward sodium current. (F) Drawing of a representative action potential showing the state conformation of the VGSC through the phases of action potential. VGSCs are closed (C) near the resting membrane potential, open (O) in response to membrane depolarization resulting in the rapid upstroke of the action potential, and then inactivate (I), aiding in repolarization of the membrane potential. The action potential in (F) was provided by Dr. Andrei Milosh.

3. *Diversity of voltage-gated sodium channels in mammals*

Voltage-gated sodium channels comprise a major gene family populated by multiple channel isoforms with conserved structural elements and function. To date nine distinct VGSC pore forming α -subunits (NaV1.1 to NaV1.9) have been identified in mammals,¹⁶ each of which differ in terms of their tissue distribution, electrophysiological properties, and pharmacology. As a group, VGSCs exhibit significant amino acid sequence homology (~50% among all VGSC isoforms) that is believed to contribute to similarities in functional properties of the channels. Sequence homology among the VGSC isoforms results from the evolutionarily conserved structural features of the channel, including the transmembrane segments, ion selectivity filter, pore, voltage sensors, and channel inactivation particle (see **Chapter I** section B-1). In contrast divergent channel properties, pharmacology, and regulation are mostly derived from dissimilar coding sequences for the N- and C-termini and the extracellular and intracellular segments that link transmembrane segments and channel domains.

VGSC isoforms can be classified according to their pharmacologic sensitivity to the puffer fish toxin, tetrodotoxin (TTX), as TTX-sensitive (TTX-S) or TTX-resistant (TTX-R). Channel isoforms NaV1.1, -1.2, -1.3, -1.4, -1.6, and -1.7 are classified as TTX-S, with IC_{50} values ranging from 1-25 nM. Conversely, channel isoforms NaV1.5, -1.8, and -1.9 are classified as TTX-R, with IC_{50} values ranging from 1-60 μM ¹⁶. TTX interacts directly with the outer vestibule of the channel pore to block inward sodium current³⁹. Specifically, the presence of key cysteine and serine residues in the channel pore of NaV1.5, NaV1.8, and NaV1.9 appear to underlie the reduced potency of TTX⁴⁰. Interestingly, site directed mutagenesis of channel pore phenylalanine and tyrosine residues in TTX-S isoforms to cysteine or serine can reduce the IC_{50} value by 100 to 1000 fold^{20,41}. Consequently, key substitutes of channel pore residues can make TTX-S channel isoforms resistant to TTX. Experiments in this thesis make use of this strategy

in order to pharmacologically isolate currents from transfected sodium channels in DRG neurons from native sodium currents.

VGSC isoforms are also categorized according to their tissue specific distributions. Table 1 summarizes the tissue distribution and TTX-sensitivity of mammalian VGSCs. For example, the NaV1.4 isoform is exclusively expressed in skeletal muscle^{16,42}; whereas the NaV1.5 channel isoform is highly expressed in cardiac muscle^{16,43}. Both NaV1.4 and NaV1.5 channel isoforms underlie the rapid upstroke of skeletal and cardiac muscle action potentials that ultimately results in muscle contraction. While muscle tissues predominantly express one voltage-gated sodium channel isoform, an array of VGSCs contribute to action potential generation and propagation in central and peripheral neurons. NaV1.1, NaV1.2, NaV1.3, and NaV1.6 are differentially expressed in central neurons^{16,44}. Peripheral DRG neurons express by far the greatest diversity of VGSC isoforms. DRG neurons can express NaV1.1, NaV1.3, NaV1.6, NaV1.7, NaV1.8, and NaV1.9^{36,45-47}. NaV1.3 is predominantly expressed in developing central and peripheral neurons and is not typically observed in mature neurons⁴⁸; however, NaV1.3 mRNA and protein expression appear to be upregulated with inflammation and following peripheral injury⁴⁹⁻⁵¹. Expression of NaV1.7, -1.8, and -1.9 are typically only found in small diameter DRG neurons, whereas NaV1.1 and -1.6 are found in medium and large diameter neurons⁵². NaV1.8 and NaV1.9 are interesting channels in that they have limited sequence homology to the rest of the VGSC isoforms, they are both resistant to TTX, and they underlie slowly activating/inactivating and persistent sodium currents found in small diameter DRG neurons.

Table 1:

Name	Alternative Names	Gene Name	Tissue Distribution	TTX Sensitivity (est. IC ₅₀) ^G
NaV1.1	Brain Type I	SCN1a	CNS and PNS neurons ^A	TTX-S (6 nM)
NaV1.2	Brain Type II	SCN2a	CNS neurons	TTX-S (12 nM)
NaV1.3	Brain Type III	SCN3a	CNS and PNS neurons ^B	TTX-S (4 nM)
NaV1.4	μ1 or Skm1	SCN4a	Skeletal Muscle	TTX-S (5-25 nM)
NaV1.5	h1 or Skm2	SCN5a	Cardiac Myocytes	TTX-R (16 mM)
NaV1.6	Brain Type VI	SCN8a	CNS and PNS ^C	TTX-S (1-6 nM)
NaV1.7	PN-1, hNe, or Nas	SCN9a	Sympathetic neurons and PNS neurons ^D	TTX-S (4-25 nM)
NaV1.8	PN-3 or SNS	SCN10a	PNS neurons ^E	TTX-R (60 mM)
NaV1.9	NaN, or SN-2	SCN11a	PNS neurons ^F	TTX-R (40 mM)

Table 1: Diversity of voltage-gated sodium channels (VGSCs). ^A NaV1.1 mRNA is expressed throughout the CNS and is found in large soma diameter DRG neurons⁵³. ^B NaV1.3 mRNA is expressed developmentally in CNS and PNS neurons⁴⁸. NaV1.3 expression is also upregulated following injury and inflammation^{50,51,54}. ^C NaV1.6 is found in high copy number in several populations of CNS neurons including, cerebral cortex, hippocampus, cerebellar Purkinje neurons, brainstem, spinal cord, and the nodes of Ranvier⁵⁵⁻⁵⁷. NaV1.6 mRNA expression is enriched in medium soma diameter DRG neurons⁵². ^D NaV1.7 mRNA is found in small diameter DRG neurons^{58,59}. ^E NaV1.8 mRNA is found in small and medium diameter DRG neurons⁶⁰. ^F NaV1.9 mRNA is enriched in small diameter DRG neurons⁶¹. ^G Estimated IC₅₀ values for TTX. A range of values is representative of IC₅₀ values from mouse, rat and human channel isoforms¹⁶.

4. *Altered expression and dysfunction of voltage-gated sodium channels is associated with inherited and acquired disorders of excitability.*

Voltage-gated sodium channels (VGSCs) are dynamic proteins that transition to different conformations in response to changes in the local electric field. Located in the plasma membrane, VGSCs facilitate the influx of Na⁺ ions into the cell that leads to membrane depolarization and the rapid upstroke of the action potential in nerve and muscle fibers. Consequently, VGSCs play a fundamental role in regulating excitability in cells and have important roles in a diverse array of physiological processes ranging from nerve and muscle excitation to learning and memory. The physiological importance of VGSC function is underscored by an emerging body of data that implicates dysfunction of sodium channels in many neuronal and muscle disorders of excitability. Congenital mutations in genes encoding VGSCs result in channels with abnormal properties, whose ectopic activity contributes to the altered excitability associated with epilepsy⁶², migraine⁶³, cardiac arrhythmias⁶⁴, ataxia⁶⁵, non-dystrophic myopathies⁶⁶, and extreme pain⁶⁷. Pathophysiological conditions caused by mutations in voltage-gated sodium channels are generally referred to as sodium channelopathies. Changes in expression and function of sodium channels are also believed to contribute to altered neuronal excitability associated with non-genetic, acquired disorders of excitability including multiple sclerosis⁶⁸, traumatic brain injury⁶⁹, peripheral nerve injury⁷⁰⁻⁷², and chronic and acute inflammatory pain⁷³. An in-depth discussion of the properties and phenotypes of the many muscle and neuronal sodium channelopathies and the altered function and expression of VGSCs following inflammation and peripheral injury is beyond the scope of this dissertation. Indeed whole books and over 45 published review papers are devoted to these very subjects. Instead, I briefly discuss the general characteristics of some sodium channelopathies and the evidence for altered activity and expression of VGSCs following inflammation and peripheral nerve injury.

Sodium channelopathies are rare autosomal dominant heritable disorders. To date, over 200 mutations in VGSC genes have been linked to altered excitability and human disease^{66,74}. Sodium channelopathies result from loss of function or gain of function mutations in the sodium channel genes. Loss of function mutations in VGSC genes cause truncated gene transcripts and loss of channel protein expression. Loss of VGSC protein expression is associated with depressed membrane excitability that can result in tissue specific pathologies. For example, mutations resulting in loss of NaV1.7 channel protein expression in small diameter DRG neurons, neurons responsible for transducing noxious thermal and chemical stimuli, causes congenital insensitivity to pain—a rare disorder where patients are unable to perceive any form of pain, although many other sensory modalities appear normal^{a75}. Although inherited mutations in VGSC genes can cause loss of function, many disease-causing mutations in VGSCs are gain-of function mutations, meaning the mutations manifest pathological membrane hyperexcitability through increased activity of the channel. Such mutations enhance channel activity by altering the structural integrity of channel domains important for protein-protein interactions or channel conformational change. Consequently, polymorphisms which result in gain-of-function are often localized to the channel voltage sensors, the channel inactivation gate, or sites near or within the channel pore which are hypothesized to serve as docking sites for the channel inactivation gate. Indeed biophysical characterization of many mutant channels has found that polymorphisms found within the channel inactivation gate and near or within the channel pore slow or impair channel inactivation, leading to increased persistent Na⁺ current, prolonged membrane depolarization, and membrane hyperexcitability. Mutations which slow or destabilize channel inactivation produce different disease phenotypes depending on the

^aRecent evidence suggests that some patients with congenital insensitivity to pain exhibit anosmia. Goldberg Y *et al.* 2007 *Clin Genet*, Nilsen KB *et al.* 2009 *Pain*, and Straud R. *et al.* 2011 *Eur J Pain*.

tissue-specific expression of the dysfunctional isoform. For example, mutations that impair inactivation of the skeletal muscle sodium channel NaV1.4, cause myotonia, whereas mutations that impair inactivation of the peripheral neuronal sodium channel NaV1.7, cause extreme pain. Experiments performed in this dissertation utilize channel mutations which destabilize or impair channel inactivation as a tool to explore how rate of channel inactivation affects resurgent sodium current generation.

Dysfunction of voltage-gated sodium channels is also believed to contribute to altered neuronal excitability associated with non-genetic, acquired disorders of excitability including chronic inflammatory and neuropathic pain. Following injury and inflammation axons and associated cell bodies undergo an increase in their intrinsic electrical excitability⁷¹. Accordingly, neurons in or near the site of injury can become spontaneously hyperexcitable and fire ectopic action potential bursts⁷¹. It is generally believed that altered membrane excitability is caused by changes in expression and function of receptors, enzymes, and voltage-dependent ion channels in peripheral nerves and dorsal root ganglion. More specifically, inflammation or injury induced changes in the density, distribution, and functional properties of VGSCs are hypothesized to contribute to abnormal spontaneous activity, ectopic burst firing, and membrane hyperexcitability associated with inflammation or injury⁷⁰. Indeed, prolonged exposure to prostaglandins (PGE₂), neurotrophins, and pro-inflammatory cytokines, substances found in high concentration in and near a site of injury, regulate the expression and activity of several peripheral VGSCs, including the NaV1.8 channel isoform^{72,73}. Prolonged exposure to NGF can up-regulate functional NaV1.8 expression in sensory neurons and exposure to PGE₂ shifts the voltage dependence of channel activation and increases the peak amplitude of NaV1.8 current in DRG neurons; both effects increase neuronal excitability^{76,77}. NaV1.3 which is not normally found in adult DRG neurons⁴⁹ is up-regulated by inflammation and models of peripheral nerve

injury⁷⁸⁻⁸⁰. For many injury models the exact changes in channel function or expression are highly dependent on the type of injury or insult and the time course of study. Changes in expression and function of VGSCs following inflammation and peripheral injury are summarized by two recent review articles^{70,72}. In **Chapter VI** of this dissertation I examine whether VGSC expression or function are altered in peripheral DRG neurons following contusive SCI.

C. Voltage-gated sodium channel auxiliary β -subunits structure and function

In vivo, mammalian VGSC α -subunits are associated with auxiliary β -subunits *in vivo* with a subunit stoichiometry of $1\alpha : 2\beta$ -subunits⁸¹. To date, five isoforms of auxiliary β -subunits have been identified, termed β_1 - β_4 and the β_{1A} -subunit (a splice variant of the β_1 -subunit)²². The β_1 -, β_{1a} -, and β_3 -subunits associate non-covalently with the sodium channel α -subunit whereas the β_2 - and β_4 -subunits bind covalently to the channel α -subunit through an additional cysteine residue in their extracellular loop¹⁷⁻¹⁹. It is hypothesized that VGSC α -subunits may associate with either β_1 , β_{1a} , or β_3 and β_2 or β_4 . The auxiliary β -subunits are transmembrane proteins with type I topology, i.e., they contain a long (approximately 150 amino acid residues), heavily glycosylated extracellular N-terminal domain that has an immunoglobulin-like structure with homology to cell-adhesion molecules (CAMs), a single transmembrane segment, and a short, intracellular C-terminal tail (Figure 3)⁸².

VGSC β -subunits associate with the conducting α -subunit and are implicated in modulating the biophysical properties of Na^+ channels, including channel gating, cellular localization, and pharmacology⁸³. Coexpression of auxiliary β -subunits with neuronal (Nav1.1⁸⁴, Nav1.2⁸⁵, Nav1.3⁸⁶, Nav1.6⁸⁷ and Nav1.8⁸⁸) or skeletal muscle (Nav1.4⁸⁹) sodium channel α -subunits in *Xenopus* oocytes results in enhanced current amplitudes, accelerated kinetics of current inactivation, and, in some cases shifts the steady-state

voltage-dependence of activation and inactivation⁹⁰. However, these effects appear to be critically dependent on the particular heterologous expression system as these observations are not always reproduced in primary cell cultures or mammalian cell lines^{22,91,92}. Because of conflicting observations, it remains unclear to what extent the β -subunits modify channel gating *in vivo*. VGSC β -subunits can function as CAMs in terms of their interaction with the extracellular matrix and cytoskeleton proteins and regulation of cell migration and aggregation^{22,91,93}. Evidence for the β -subunits functioning as CAMs has led to speculation that these proteins may (1) guide [traffic] sodium channel complexes to areas of high channel density such as the nodes of Ranvier^{93,94} and (2) stabilize/anchor the channel complex in the plasma membrane^{22,90}. The association of neuronal VGSC α - and β -subunits is a late event in sodium channel biogenesis; consequently it is thought that association with β -subunits could be a rate-limiting step in regulation of channel density at the cell surface and localization of sodium channels within neurons⁹⁵. The function of auxiliary β -subunits is likely necessary for normal physiology as mutations in two β -subunits, β_1 and β_4 , have been linked to generalized epilepsy with febrile seizures plus type 1 (GEFS+1)⁹⁶ and congenital long-QT syndrome⁹⁷, respectively. Finally, the presence of auxiliary β -subunits can alter the pharmacology of VGSC modulators, such as phenytoin and lidocaine, although the exact mechanisms by which they do so remain unclear⁹⁸⁻¹⁰⁰. The structure and function of VGSC auxiliary β -subunits is relevant to this dissertation, as significant evidence suggests that the VGSC auxiliary β_4 -subunit (NaV β_4) interacts with the VGSC pore to produce a novel form of channel inactivation that results in resurgent sodium current (I_{NaR}) generation¹⁰¹⁻¹⁰³.

Figure 3:

β_1 or β_3 -subunit

β_2 or β_4 -subunit

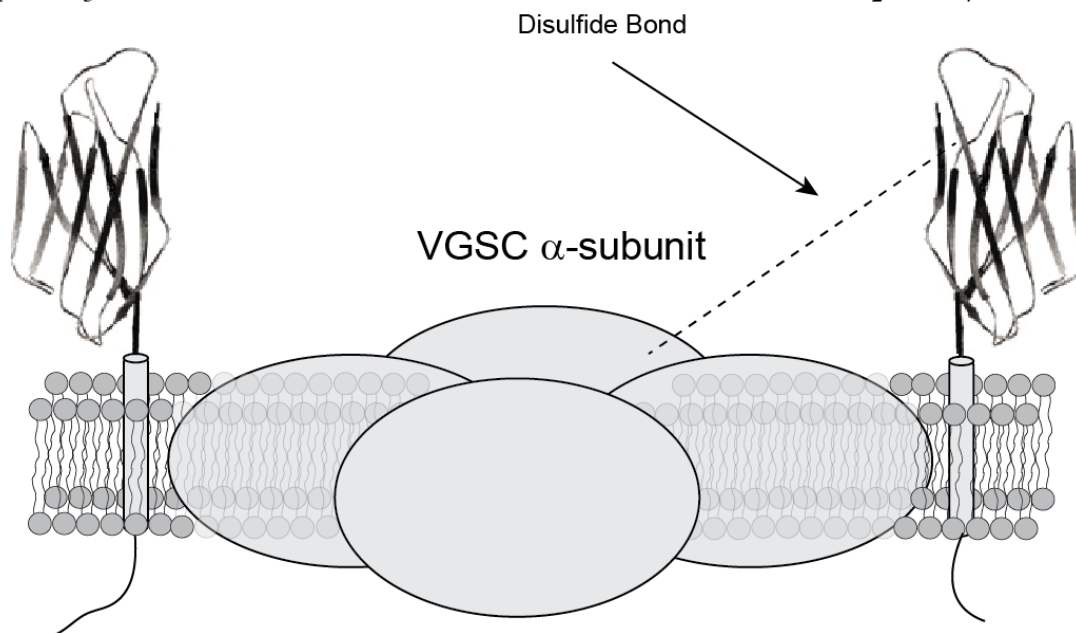


Figure 3: Structure and subunit stoichiometry of the voltage-gated sodium channel (VGSC) complex. Mammalian VGSC α -subunits are associated with auxiliary β -subunits with a subunit stoichiometry of 1 α : 2 β -subunits. Five VGSC auxiliary β -subunits have been identified β_1 - β_4 and β_{1a} . The β_1 - and β_3 -subunit are believed to associate non-covalently with the channel. The extracellular, transmembrane, and intracellular domains of the β_1 - and β_3 -subunits are all important in mediating this interaction. The β_2 - and β_4 -subunits are believed to be linked to the VGSC α -subunit by a disulfide bond (dashed line). N-terminal structure of β -subunits was adapted from Catterall *et al.* 2006¹⁰⁴.

D. *Resurgent sodium current (I_{NaR})*

VGSCs produce the large, inward sodium currents which underlie the rapid membrane depolarization phase of action potentials in nerve and muscle tissue. In addition some VGSC can also produce smaller sodium currents, which by themselves do not provide sufficient membrane depolarization to initiate an action potential, but can influence the excitable properties and signal processing functions of neurons⁷¹. One example of such a subthreshold current is the resurgent sodium current (I_{NaR}). Resurgent sodium currents are unusual sodium currents that reactivate during the falling phase of the action potential where VGSCs are normally refractory to activity.

Resurgent sodium currents were initially identified by Drs. Indira Raman and Bruce Bean, during studies where they investigated the ionic conductances that underlie the distinctive high frequency firing characteristics of cerebellar Purkinje neurons¹⁰⁵. During their characterization of transient and persistent sodium currents in cerebellar Purkinje neurons, Bean and Raman, identified a sodium current that was reactivated during membrane repolarization following a strong, brief depolarization¹⁰⁵. Raman and Bean labeled this unique current resurgent sodium current because it reactivates following a voltage-protocol that normally maximally inactivates voltage-gated sodium channels. Raman and Bean characterized the properties of resurgent current using a protocol that stepped the membrane voltage directly to +30 mV, to produce maximal inactivation of transient sodium current, and then repolarized the membrane to intermediate potentials between -10 and -80 mV. In most neuronal populations depolarization, first to +30 mV, causes sodium channels to activate and rapidly inactivate; channels remain inactivated and refractory to activity throughout membrane repolarization until the membrane has been repolarized to the resting membrane potential for several milliseconds. However, Raman and Bean found that most cerebellar Purkinje neurons expressed a slowly activating, slowly decaying inward

sodium current with kinetics that were strongly voltage dependent¹⁰⁵ during intermediate repolarization pulses. Further characterization of resurgent sodium currents in cerebellar Purkinje neurons determined that the same TTX-S VGSCs that produce I_{NaR} also produce the classic, transient Na^+ current involved in action potential generation¹⁰⁵. These observations suggested that I_{NaR} might result from an atypical form of sodium channel inactivation that allows channels to reopen during recovery from inactivation.

1. *Resurgent sodium current results from an alternative form of channel inactivation.*

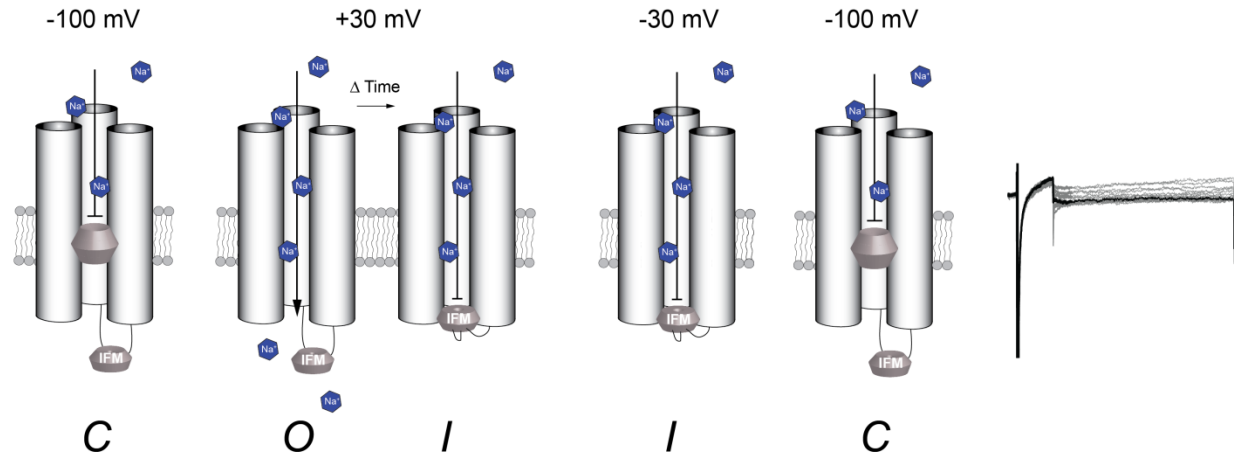
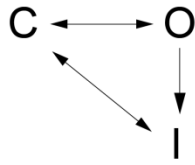
Extensive characterization of the kinetic properties of Purkinje neurons with resurgent sodium current suggested that the unique kinetics and voltage-dependence of I_{NaR} were derived from a novel recovery of the channel from an inactivated configuration that proceeds through an open state, allowing a resurgence of transient inward sodium current (as much as 10% of peak transient Na^+ current amplitude)^{105,106}. The unique recovery from channel inactivation through open states in neurons with I_{NaR} differs considerably from the process of intrinsic channel inactivation—where there is no sodium flux during recovery from channel inactivation¹⁰⁷. Normally, upon depolarization, VGSCs open and rapidly transition to a non-conducting, inactivated state. Once channels assume an inactivated conformation they are not likely to reopen and require repolarization of the membrane before they are available to open again¹⁰⁷. Also during repolarization, channels transition back [recover] to a primed closed state through non-conducting state configurations. Because inactivation of VGSCs exhibiting I_{NaR} proceeds through an open configuration, it is believed that VGSCs exhibiting I_{NaR} are inactivated by an alternative mechanism which competes with the intrinsic mechanism of channel inactivation. Accordingly, it was proposed that, in channels exhibiting I_{NaR} , inactivation is mediated by an intracellular particle that can enter into and exit from interaction with the channel only when the channel is open—yielding open channel block¹⁰⁶. Upon

depolarization, the open-channel blocker binds more rapidly than the inactivation gate, limiting the extent of fast inactivation. Upon repolarization, the blocker is expelled by inward permeating Na^+ ions¹⁰⁸, allowing I_{NaR} to flow and restoring the availability of sodium channels. In this fashion, open channel block in cells exhibiting I_{NaR} is analogous to the hooked tail currents that are seen during recovery from sodium channel block by compounds such as pancuronium and N-methylstrychnine applied to the internal recording solution^{109,110}. A schematic depicting the channel state conformations at different voltages with and without resurgent inactivation kinetics is shown in Figure 4.

Figure 4:

A

Classic State Transitions



27

B

State Transitions With I_{NaR}

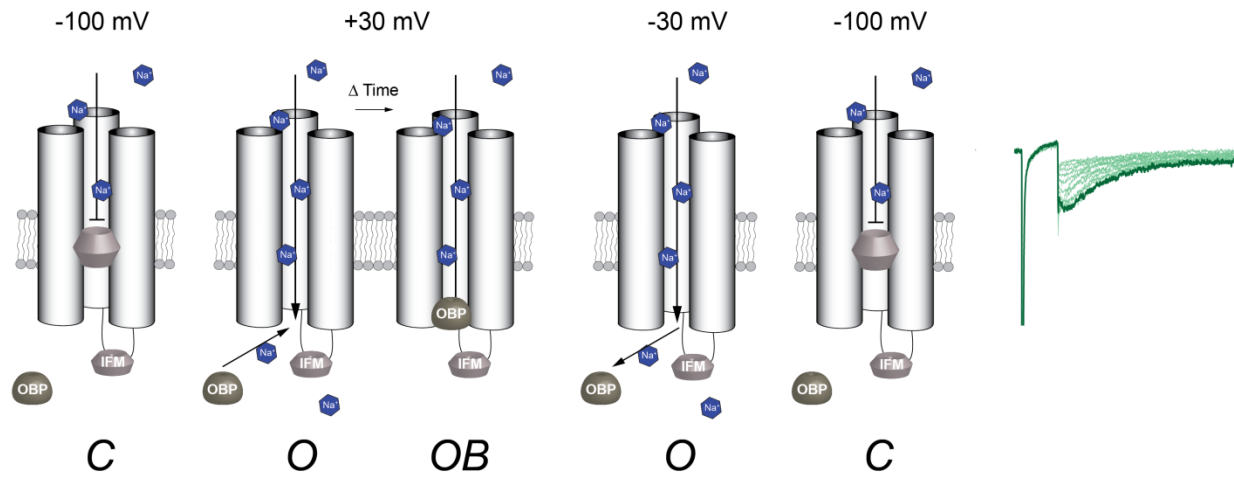
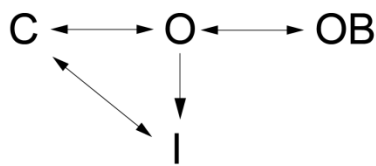


Figure 4: Model of channel state configurations with and without resurgent sodium current (I_{NaR}). The schematic of state diagrams shows the likely configuration of the sodium channel at a particular voltage (either -100 mV, +30 mV, or -30 mV) for each condition. **(A)** Shows the state conformations of the channel according to the classical understanding of sodium channel voltage-dependent state transitions. Accordingly at negative potentials the channel exists in a closed state and is ready to open. With membrane depolarization the channel undergoes complex conformational change and the channel opens allowing sodium to flow down its electrochemical gradient. Within a millisecond the sodium channel inactivates by the channel intrinsic inactivation mechanism (IFM particle). If the membrane potential is repolarized back to an intermediate potential (-30 mV) no sodium flux **(A-right)** is observed because the inactivation gate is tightly bound to the channel. Only when the membrane potential is hyperpolarized to very negative potentials is the channel reset to a closed state. The scheme **(A-left)** demonstrates that once the channel opens (O) and inactivates (I) recovery from inactivation occurs through closed (C) channel states. **(B)** Cells that exhibit resurgent sodium current can be inactivated by two competing mechanisms: the IFM particle and an open blocking particle (OBP). Channels that undergo resurgent block by OBP produce I_{NaR} . At intermediate potentials the OBP comes off the channel because the interaction is weak, allowing a resurgence of inward sodium current **(B-right)** before the channel quickly recovers to a close configuration (deactivates). Channels that undergo I_{NaR} open channel block recover faster to closed state and are ready to fire earlier than channels that undergo IFM mediated inactivation. The simplified state model for neurons exhibiting I_{NaR} **(B-left)** shows that channels that enter an open-blocked state (OB) must transition back through the channel open state (O) before they inactivate (I) or close/deactivate (C). Model for open channel block was modified from Raman and colleagues^{106,111}.

2. *Mechanism and molecular determinants of resurgent sodium current in cerebellar Purkinje neurons*

Resurgent sodium current results from a complex interaction between the VGSC α -subunit and an open channel blocker that inactivates the channel at positive potentials but is expelled from the channel during membrane repolarization, resulting in a resurgence of inward Na^+ current. The current working hypothesis is that resurgent inactivation kinetics result from open channel block by the C-terminus of the VGSC auxiliary β_4 -subunit. In addition, evidence suggests that open channel block and resurgent current are regulated by phosphorylation¹¹¹, although it remains unclear if the sodium channel α -subunit, the blocking element, or both are regulated by phosphorylation. The sections below discuss which VGSC contribute to I_{NaR} in cerebellar Purkinje neurons, the identity of the open blocking particle responsible for resurgent inactivation kinetics, and the role of phosphorylation in I_{NaR} generation.

a. *The NaV1.6 channel isoform is the major carrier of resurgent sodium current in cerebellar Purkinje neurons.*

Evidence suggests the NaV1.6 isoform underlies much of the resurgent sodium current found in cerebellar Purkinje neurons because I_{NaR} is significantly reduced in Purkinje neurons from NaV1.6 null-mice¹¹². However, the presence of residual I_{NaR} in NaV1.6 null mice suggests that in some cells, under certain conditions other isoforms can produce I_{NaR} . Indeed, in neurons of cerebellar and subthalamic nuclei significant I_{NaR} is present in the absence of NaV1.6 expression; it was suspected that NaV1.1 underlies much of the I_{NaR} present in those neurons¹¹³. Experiments by Rush and colleagues suggest that NaV1.2 is also capable of producing resurgent sodium currents¹¹⁴. Collectively, these results suggest that other channel isoforms expressed in the CNS are capable of producing I_{NaR} . As part of this dissertation I explore what channel isoforms expressed in DRG neurons are capable of producing I_{NaR} .

b. *The C-terminus of the auxiliary β_4 -subunit serves as the open channel blocker responsible for resurgent inactivation kinetics.*

Experiments by Raman and Bean demonstrated that the channel inactivation mechanism which causes resurgent sodium currents is distinct from the intrinsic inactivation mechanism of the VGSC α -subunit^{105,106,112}. Initial hypotheses for the identity of the open blocking particle included a diffusible blocking molecule such as intracellular inorganic cations or a distinct peptide or protein subunit closely associated with the channel complex¹¹¹. Application of substrate specific proteases to recordings of cerebellar Purkinje neurons made in the inside-out configuration revealed two important features of the resurgent current open channel blocker: (1) the open channel blocker was closely associated with the VGSC complex because I_{NaR} were not “washed out” after the membrane patch was excised and (2) the open channel blocker had a protein sequence with positively charged and hydrophobic/aromatic groups^{102,111}. Using the above criteria, the VGSC auxiliary β_4 subunit ($NaV\beta_4$) emerged as a candidate resurgent open channel blocker. Specifically, it is believed that the C-terminus of the β_4 subunit competes with the IFM particle to dock transiently within the channel pore¹¹⁵ before being expelled during membrane repolarization¹⁰². Several lines of experimental evidence support the claim that the C-terminus of the $NaV\beta_4$ subunit serves as the open channel blocker associated with I_{NaR} generation. First, the $NaV\beta_4$ subunit is closely associated with the VGSC α -subunit and is highly expressed in neuronal populations that exhibit I_{NaR} ¹⁹. Additionally, unlike other VGSC β -subunits, the cytoplasmic tail of the $NaV\beta_4$ -subunit contains functional groups that resemble other known VGSC blockers¹¹⁶—the cytoplasmic tail of the $NaV\beta_4$ -subunit is enriched with positively charged and hydrophobic amino acids. Bath application of a 20 amino acid peptide of the $NaV\beta_4$ -subunit C-terminus ($NaV\beta_{4,154-173}$: KKLITFILKKTREKKKECLV) restored resurgent inactivation kinetics after enzymatic degradation of the endogenous open channel

blocker^{101,102}. Finally, siRNA knockdown of NaV β_4 reduces I_{NaR} amplitude in cerebellar Purkinje neurons and bath application of the β_4 -peptide can rescue I_{NaR} amplitude and kinetics¹⁰¹. Collectively, these results suggest that the NaV β_4 -subunit likely serves as the open-channel blocker responsible for resurgent inactivation kinetics. However, this has not been established in sensory neurons.

c. Regulation of open channel block and resurgent current (I_{NaR}) generation

Although resurgent sodium currents were initially described in cerebellar Purkinje neurons, they have since been found in other CNS cell types that display fast regular spiking or burst firing^{113,117-120}. Interestingly, despite reports of resurgent inactivation kinetics in multiple CNS cell types, the majority of brain neurons do not exhibit I_{NaR} . This observation of select cell types exhibiting I_{NaR} has led many to question what mechanisms might underlie the restricted localization of resurgent sodium currents. Initially, it was hypothesized that resurgent sodium currents might only be observed in neurons expressing specific sodium channel isoforms and the open channel blocker. However, multiple reports suggest that expression of NaV1.1 or NaV1.6 (two channel isoforms suspected to contribute to I_{NaR} in CNS neurons) and NaV β_4 (the suspected resurgent current open blocking particle) are not sufficient to produce I_{NaR} because these channel subunits are expressed together in some neuronal cell types, namely hippocampal CA3 and mouse spinal neurons, that do not exhibit resurgent inactivation kinetics^{19,59,102,105,121,122}. Moreover, expression of NaV1.6 and NaV β_4 in heterologous expression systems, such as *Xenopus* oocytes⁸⁷, ND7/23 cells, (Cummins Lab unpublished observation) or hEK-293 cells^{123,124}, does not yield resurgent inactivation kinetics. Taken together these observations suggest that cell-specific regulation of channel subunits may be important in modulating open channel block and I_{NaR}

generation. Indeed, recent experimental results suggest that I_{NaR} electrogenesis may be regulated by phosphorylation¹¹¹, as well as enzymatic cleavage of the $NaV\beta_4$ -subunit.

Experiments by Raman and Grieco found that resurgent sodium currents in cerebellar Purkinje neurons were inhibited by application of broad-spectrum phosphatases¹¹¹. This observation suggests that open channel block might be regulated by phosphorylation of the channel, the blocking particle, or both. Phosphorylation of the VGCS complex has been suggested to modulate several channel electrophysiological properties including current amplitude and voltage-dependence and kinetics of channel gating¹²⁵. One intriguing possibility is that phosphorylation of the channel may modulate the kinetic rate of channel inactivation and therefore regulate the likelihood that channels might undergo open channel block rather than traditional inactivation. The rate of channel inactivation was implicated as an important factor which may affect the generation of I_{NaR} by specific channel isoforms^{113,126,127}. Specifically, slowing of channel inactivation with application of β -pompilidotoxin augments I_{NaR} amplitude in cell populations which would otherwise produce little resurgent current¹²⁷. Although phosphorylation appears to be important in the regulation of I_{NaR} electrogenesis, the specific kinases and/or phosphatases and their respective substrates are not currently known and should be examined.

In addition to being a possible substrate for regulation by kinases and phosphatases, the C-terminus of the $NaV\beta_4$ -subunit is also a target for enzymatic cleavage by β -site amyloid precursor protein (APP) cleaving enzyme 1 (BACE1). BACE1 cleavage of the $NaV\beta_4$ -subunit may regulate the affinity of the open blocking particle relative to the channel inactivation gate¹²⁸. Consequently, cell specific activity of BACE1 may regulate the generation of I_{NaR} .

3. *Resurgent sodium current contributes to burst firing of action potentials in CNS neurons.*

More recently I_{NaR} was found in other cerebellar neuron types¹¹⁷, subthalamic neurons¹¹³, mesencephalic trigeminal neurons¹²⁹, neurons of the medial nucleus of the trapezoid body¹³⁰, and large diameter DRG neurons¹³¹. The presence of I_{NaR} in multiple neuronal populations underscores the likely importance of these currents in normal physiology. Although relatively small in amplitude, I_{NaR} peaks near the threshold for action potential formation (-30 mV to -40 mV)—a range of voltages where the cell is likely to be most sensitive to small currents. Additionally, the mechanism of channel inactivation associated with I_{NaR} not only results in transient inward Na current on the downstroke of the action potential, but also permits rapid recovery and repriming of resurgent inactivated sodium channels; the presence of depolarizing current early during membrane repolarization and augmented availability of channels near threshold for action potential firing are both likely to facilitate high frequency firing of action potentials¹⁰⁵. Indeed, the presence of I_{NaR} in neuronal populations has been shown to significantly enhance neuronal excitability by facilitating high-frequency burst firing and contributing to repetitive spontaneous generation of action potentials¹³². Moreover, I_{NaR} has been found to contribute, at least in part, to the intrinsic pace making phenotype of both cerebellar Purkinje and subthalamic nucleus neurons^{132,133}. The absence of I_{NaR} in some CNS populations has been observed to compromise their excitability and reduce their capacity to function normally. Indeed cell specific knockout of $Na_v1.6$ in cerebellar Purkinje neurons results in reduced I_{NaR} , reduced rate of action potential firing, and ataxia, tremor, and impaired motor coordination¹³⁴. While the physiological role of I_{NaR} in DRG remains unclear, I hypothesize that expression of I_{NaR} may facilitate ectopic repetitive discharge of action potentials that may contribute to pain following injury.

E. Hypothesis and specific aims

Voltage-gated sodium channels (VGSCs) are complex proteins that transition to different conformations in response to changes in transmembrane voltage. Located in the plasma membrane, these dynamic proteins mediate the influx of Na⁺ ions into the cell; thus, they play a fundamental role in regulating the excitability of nerve and muscle tissue. Consequently, altered expression and/or dysfunction of voltage-gated sodium channels can contribute to altered membrane excitability associated with multiple inherited and acquired disorders of excitability.

In addition to the large inward Na⁺ currents responsible for the upstroke of the action potential, some VGSC isoforms produce smaller, subthreshold sodium currents that can influence the excitable properties and signal processing functions of neurons⁷¹. These subthreshold sodium currents can be crucial to spontaneous firing in neurons¹³³ of the central nervous system (CNS) and may contribute to the membrane potential oscillations and high frequency burst discharge of action potentials following injury in peripheral neurons. Despite the potentially crucial role of these currents in regulating excitability in nerve and muscle cells, relatively little is known about the properties of these currents or their roles in disease mechanisms. One example of a subthreshold sodium current that could contribute to altered excitability associated with disease are resurgent sodium currents (I_{NaR}).

Resurgent sodium currents are unusual currents that are active during repolarization of the membrane potential. I_{NaR} is thought to arise from a distinct inactivation mechanism that allows channels to dwell transiently in an open configuration during recovery from the inactivated state. This unique recovery is proposed to result from open-channel block by an intracellular particle that binds to the sodium channel open state preventing the channel from inactivating by its classical mechanism⁵⁶. The kinetic properties of I_{NaR} make it suitable for providing depolarizing drive early after the discharge of an AP.

Moreover, I_{NaR} may significantly enhance firing frequency during tonic firing or promote discharge of multiple APs in response to brief, supra-threshold stimuli^{2,39}. I_{NaR} was initially discovered in cerebellar Purkinje neurons⁵⁵ and was recently identified in large diameter dorsal root ganglion (DRG) neurons¹⁷. Currently, a proposed mechanism for I_{NaR} generation in cerebellar Purkinje neurons involves the requirement of phosphorylation²⁷ and the C-terminus of the auxiliary β_4 -subunit serving as the open channel blocker that allows for this unique recovery from inactivation²⁸. Evidence suggests the NaV1.6 channel isoform is capable of producing resurgent currents in cerebellar Purkinje neurons, although not all neurons expressed NaV1.6^{52,57}—suggesting other sodium channel isoforms may produce I_{NaR} under specific conditions.

While it is clear that I_{NaR} could contribute to the enhanced excitability associated with many disorders of excitability, basic knowledge of the fundamental properties of this unique current and its involvement in disease is deficient. Because the mechanisms which generate I_{NaR} are thought to be independent from the large voltage-dependent ionic conductances essential for the generation and propagation of action potentials in normal physiology¹⁰⁵, therapeutics targeted to inhibit this novel current may be efficacious in treating hyperexcitability associated with multiple diseases. Consequently, the aim of this dissertation is to understand the specific mechanisms that underlie the electrogenesis of I_{NaR} and determine if the biophysical properties of these unique currents are altered by (1) mutations that cause inherited muscle and neuronal channelopathies or (2) an experimental model of injury. Specifically, this work explores the hypothesis that I_{NaR} is increased by mutations that slow the rate of channel inactivation and contusive spinal cord injury, an experimental model of spinal cord injury known to enhance spontaneous activity in peripheral neurons.

To accomplish these goals, the following specific aims are proposed:

- 1. Characterize the properties and distribution of neurons exhibiting I_{NaR} in rat DRG neurons and determine which VGSCs expressed in DRG neurons can produce I_{NaR} .*
- 2. Determine if inherited mutations that give rise to sodium channelopathies which slow the rate of channel inactivation increase I_{NaR} amplitude.*
- 3. Explore whether temperature induced slowing of channel inactivation augments I_{NaR} amplitude in muscle and neuronal mutant channels.*
- 4. Determine if the biophysical properties of I_{NaR} are altered following contusive spinal cord injury.*

Chapter II: *Methods and materials*

This section briefly describes common methods and specific materials utilized in experimental research sections that follow.

A. *cDNA vectors*

The capacity of several VGSC isoforms to produce resurgent sodium currents was assessed by expressing recombinant channels in ND7/23 cells (mouse neuroblastoma crossed with rat neuron hybrid cell line) and dorsal root ganglion (DRG) neurons. Constructs encoding the open reading frame (ORF) for the voltage-gated sodium channel (VGSC) α -subunit isoforms rat NaV1.3 (rNaV1.3), human NaV1.4 (hNaV1.4), human NaV1.5 (hNaV1.5), mouse NaV1.6 (mNaV1.6), and human NaV1.7 (hNaV1.7), the human VGSC auxiliary β_4 -subunit, and an shRNA plasmid targeting the rat NaV1.8 (rNaV1.8) channels were used throughout the experiments in this dissertation. All constructs utilized for this thesis were previously cloned and characterized. The rat NaV1.3 subtype was previously cloned⁴¹. Briefly, the ORF of rNaV1.3 was moved from the bacterial expression pBluescript SK⁻ (pBS-SK⁻) plasmid¹³⁵ into a mammalian expression vector pcDNA3.1 (Invitrogen, San Diego, CA) that was modified to render it a low copy number plasmid¹³⁶. The human NaV1.4 subtype was previously cloned¹³⁷. The insert encoding hNaV1.4pRc/CMV¹³⁸ was sub-cloned in two steps to a RBG4 vector, yielding hNaV1.4pRBG4¹³⁹. The human NaV1.5 channel insert, originally located in a pSP64T vector¹⁴⁰, was moved into the same modified pcDNA3.1¹³⁶ expression vector as rNaV1.3 (see above) by James O. Jackson II in the laboratory of Dr. Theodore R. Cummins to enhance expression efficiency. The mouse NaV1.6 channel ORF was sub-cloned from the modified oocyte expression vector, pLCT_{1-A}⁸⁷, and inserted into the modified pcDNA3.1 vector¹³⁶ yielding the

mNav1.6pcDNA3.1 construct²⁰ used for these experiments. The human Nav1.7 channel insert was cloned into the modified pcDNA3.1 vector¹³⁶.

All experiments performed in this thesis were performed in DRG neurons—cells which express endogenous VGSCs. Specifically, DRG neurons express two populations of VGSCs—those that are sensitive to application of tetrodotoxin (TTX) [$IC_{50}=3-10nM$] collectively referred to as TTX-sensitive (TTX-S) and those that are resistant to TTX [$IC_{50}=100\mu M$]¹⁴¹. To aid in isolation and characterization of transfected sodium currents generated in DRG neurons, cDNA constructs for Nav1.3, Nav1.4, Nav1.6, and Nav1.7 were modified with a single point mutation in the VGSC ORF as previously described^{20,142} to confer high resistance to tetrodotoxin (TTX). cDNA constructs that are resistant to TTX are referred to hereinafter as Nav1.3_R, Nav1.4_R, Nav1.6_R, and Nav1.7_R, respectively (K_i, approximately 100 μM ¹⁴³). Because Nav1.5 is naturally resistant to TTX (K_i, about 2 μM), no modifications were made to the hNav1.5cDNA3.1 vector. Additional channelopathy constructs (hNav1.4_R-R1448P, hNav1.5-F1486L, mNav1.6_R-I1477T, and hNav1.7_R-I1461T) were made by inserting the respective mutation into the modified VGSC cDNA constructs using the QuikChange XL mutagenesis kit (Stratagene, La Jolla, CA, U.S.A), as described below, following the manufacturer's instructions. All mutations were confirmed by sequencing the entire VGSC ORF in each channel construct. Modification of the cDNA constructs to confer high resistance to TTX allowed for partial isolation of expressed recombinant VGSCs in DRG neurons following application of 500nM TTX.

In addition to TTX-S channels, DRG neurons also express endogenous isoforms that are TTX-R, Nav1.8 ($IC_{50}\sim 60\mu M$) and Nav1.9 ($IC_{50}\sim 40\mu M$)¹⁴³. Because application of 500 nM TTX is insufficient to pharmacologically isolate transfected currents from the endogenous Nav1.8 and -1.9 currents, genetic and pharmacological suppression of these currents was used. Nav1.9 currents are not observed under the culture and

recording conditions utilized in this dissertation (see **Chapter II-C**)^{41,144-146} and therefore were not an issue. Although NaV1.8 currents are substantially decreased with time in culture,¹⁴⁷ we used additional measures to minimize contamination of the recordings by NaV1.8 currents. Here, NaV1.8 currents were knocked down using a targeted shRNA plasmid. The NaV1.8 siRNA target sequence (GATGAGGTCGCTGCTAAGG), designed and previously characterized by Mikami and colleagues¹⁴⁸, was sub-cloned into the RNA-Ready pSIREN-DNR-DsRed Express Donor Vector (Clontech) to yield NaV1.8shpSIREN-DNR-DsRed. Cells expressing the NaV1.8 siRNA were identified based on their ability to express red fluorescent protein (DsRed). Knockdown of the NaV1.8 ionic current was verified using a specific voltage-protocol which isolates characteristic 1.8 current (NaV1.8 current has distinct channel inactivation voltage-dependence—holding the cell membrane at -60mV for 500ms inactivates almost all other wild-type VGSCs). In experiments where DRG neurons are used as an expression system for recombinant VGSC isoforms, recordings containing more than 10% NaV1.8 current (as measured as percentage of peak Na⁺ current) were excluded from analysis.

B. Mutagenesis of voltage-gated sodium channels

Site directed mutagenesis of VGSCs were performed to determine if mutations that slow the rate of channel inactivation associated with several inherited disorders of excitability increased resurgent sodium current. Site-directed mutagenesis of VGSC constructs was performed using the channel constructs listed in the previous section. Site directed mutagenesis employs the use of specifically designed mutagenic oligonucleotide primers. Primers were designed to introduce the correct base pair change and anneal to the same sequence on opposite strands of the plasmid. Additionally, primers were designed to be between 25 and 45 bases in length, with approximately 50% G-C content, a melting temperature of approximately 78°C, and 5' G-

C rich segment (G-C clamp). Mutagenic and sequencing oligonucleotide primers were designed with the aid of Vector NTI Advance 10 software (Invitrogen, Calrsbad, CA, USA) and Primer3 version 4.0 software (<http://frodo.wi.mit.edu/primer3/>). All mutagenic primers were ordered page-purified while all sequencing primers were salt-free. QuikChange II XL Site-Directed Mutagenesis Kits (Stratagene, La Jolla, CA, USA) were used according to the manufacture's protocol. Bacterial colonies were selected according to the antibiotic resistance conferred in their respective cDNA vector (Ampicillin for the VGSCs and Kanamycin for the NaV β_4 -subunit). After antibiotic-resistant colonies had grown on antibiotic/LB agar plates, individual colonies were selected using a 10 μ L pipette tip and transferred to a 14 mL round bottom Falcon tube (Becton Dickinson Labware, Franklin Lakes, NJ, USA) containing 5 mL of LB broth and the appropriate amount of antibiotic for the mini culture (25 μ L of 10 mg/mL Kanamycin for final concentration of 0.05 mg/mL per 5 mL culture; 10 μ L of 50mg/mL Ampacillin for a final concentration of 0.10 mg/mL per 5 mL culture). The mini cultures were then placed in a 37°C shaking incubator (I2400 Incubator Shaker, New Brunswick Scientific, Edison, NJ, USA) @ 300 rpm for 14 to 16 hours. For NaV1.6 and NaV1.3 30°C and 200 rpm are necessary to ensure a high fidelity yield and avoid rearrangement of the plasmid DNA product. At the end of mini culture grown up, mini culture plasmid purification was performed using the GeneJET® Plasmid Miniprep Kit (Fermentas Life Sciences Inc., Glen Burnie, MD, USA) according to the manufacturer's instruction. Once the plasmid was purified and isolated, potential mutant constructs were screened using the corresponding sequencing primers. Initial screens using restriction enzyme digests were uncommon to screen mutant constructs as they will not tell you if the sequence was altered. DNA sequencing was performed at the DNA sequencing Core Facility in the Biochemistry Biotechnology Facility of Indiana University School of Medicine (Indianapolis, IN, USA) and later through ACGT, Inc (Wheeling, IL, USA). Only after

sequence data confirmed the fidelity of the mutated cDNA constructs were maxi cultures grown in 1000 mL culture flasks with 250 mL LB broth and the appropriate amount of antibiotic (1.25 mL of 10 mg/mL Kanomycin stock for a final concentration of 50 µg/mL in 250 mL LB broth; 500 µL of the 50 mg/mL Ampacillin stock for a final concentration of 0.10 mg/mL in 250 mL LB broth). The maxi cultures were shaken at 300 rpm at 37°C for 16-18 hours before plasmid DNA was purified using the NucleoBond® Xtra Maxi Plus kit (Macherey-Nagel, Easton, PA, USA) according to the manufacturer's instructions. The Macherey-Nagel Maxi prep kit is highly recommended because, downstream applications for purified plasmid DNA, namely biolistic transfection of primary sensory DRG neurons, requires large amounts of high quality cDNA for efficient transfection. After the maxi plasmid purification was complete, concentration and purity of the cDNA constructs were checked using the Nanodrop ND-1000 Spectrophotometer (Thermo Fisher Scientific Inc., Wilmington, DE, USA) and storage and working stocks were adjusted to a concentration of 1 µg/mL with double distilled water and stored at either -20°C or 4°C, respectively.

C. *Harvest and culture of rat DRG neurons*

The primary cell expression system utilized in this dissertation is DRG neurons. Harvest and culturing of dissociated rat DRG neurons was done as previously reported^{142,149} according to guidelines provided by the Indiana University School of Medicine Laboratory Animal Resource Center. Briefly, 2-3 month old male Sprague-Dawley rats (~100-120 grams, Harlan Laboratories, Indianapolis, IN, USA) were used for DRG harvests under the guidelines set forth by the Indiana University School of Medicine Laboratory Animal Resource Center. According to said guidelines, animals were housed in the Laboratory Animal Resource Center prior to their use for the studies in a room that was artificially illuminated from 7:00 A.M. to 7:00 P.M. Care for animals was in accordance with the Guide for the Care and Use of Laboratory Animals (National Institutes of Health publication 85-23, Bethesda, MD, USA) and approved by the Institutional Animal Care and Use Committee of the Indiana University School of Medicine. Harvested rat DRG neurons were used to for gene and protein quantification and electrophysiological studies. Gene quantification was performed on excised whole DRG ganglion, while electrophysiology studies were performed on acutely cultured (2 to 5 days) DRG neurons. Although each of these downstream experimental techniques required specific processing, the sacrifice of the animal and the removal and trimming of the ganglion is done in a similar fashion.

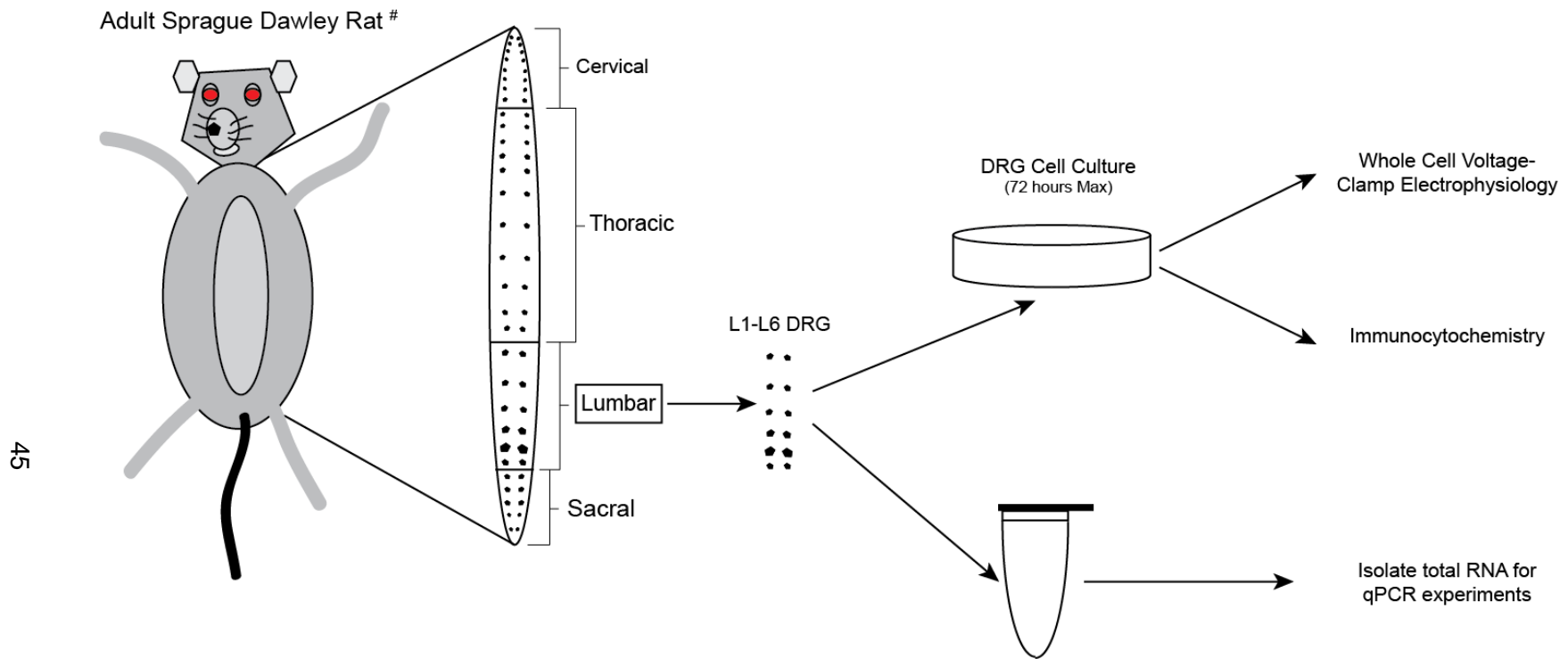
The rat DRG harvest was performed as recently described¹⁴⁴ using the lumbar L1-L6 DRG neurons. Briefly, rats were sacrificed by rendering them unconscious by exposure to CO₂ and then decapitating them. Skin and connective tissue surrounding the spinal column was cut away with sterilized tools. Once the skin is removed diamond shaped striations in the muscle surrounding the spinal column and pelvic girdle identify the location of L4-L6 DRG. The spinal column is cut away from the rat carcass by four incisions: the first made across the traverse axis 0.25 inches posterior to the end of the

diamond shaped striations, a second incision made across the traverse axis three to four inches rostral to the initial cut, and two incisions made on the dorsal axis to connect the first two incisions. After the spinal column was separated from the rat carcass the excess muscle was trimmed away before the vertebral column was cut from the rostral to the caudal axis yielding two halves of the vertebral column exposing both the spinal cord and the DRGs. The vertebral column was then placed in a 10 mL Petri dish (Corning® Inc, Corning, NY, USA) containing cold bicarbonate-free DMEM (bfDMEM). L1-L6 DRG were isolated from their pockets in the bisected vertebral column using forceps and then placed in a clean petri containing fresh cold bfDMEM. The L1-L6 DRG cell bodies were isolated from the nerve roots using forceps and a scalpel. Further processing of trimmed DRG neurons in subsequent steps depended on which experimental technique the DRG neurons were harvested for. For experiments quantifying the content of gene and protein products, trimmed, whole ganglion were further processed in lysis buffers intended to isolate either total protein or RNA according to protocols discussed later. Electrophysiology and immunohistochemistry experiments utilized dissociated and cultured DRG neurons; the following description outlines the procedure for culturing those neurons.

Once the DRG cell bodies were trimmed they were transferred using a sterile fire polished glass pipette into a 15 mL conical tube containing 600 µL of dissociation enzyme cocktail (2 mg/mL of collagenase A and D and 5 mg/mL of protease) and approximately 7 mL of bfDMEM and incubated at 37°C with moderate shaking for approximately 40 minutes. After 40 minutes, cells are spun down at 10,000 rpm for 5 minutes and liquid volume of bfDMEM and enzyme cocktail are aspirated. The DRG neurons are reconstituted in 3 mL of fresh 10% FBS DMEM complete culture medium and vigorously pipetted up and down (3 to 5 times) using a sterile glass pipette, in order to dissociate individual neurons from the clumped ganglion. Following manual

dissociation, the cells are spun down at 6,000 rpm for 5 minutes and the liquid volume of DMEM is aspirated. The DRG neurons are reconstituted in 1 mL of fresh 10% FBS DMEM complete culture medium and are vigorously dissociated by pipetting up and down (3 to 5 times) again. Following the second dissociation, cell aliquots of about 100 μ L were plated onto 12 mm glass coverslips coated with poly-D-lysine and Laminin within the wells of a 24 well plate. After 10 to 15 minutes wells were flooded with 500 μ L of complete culture media and placed in an incubator. Cultures were maintained at 37°C in a 5% CO₂ incubator and the media was changed every two days until used for either electrophysiological recordings or the coverslips were fixed on slides for immunohistochemical studies. For some experiments excised DRG neurons were processed immediately for total RNA isolation and cDNA generation for qPCR experiments (see **Chapter II-H** for details). Figure 5 illustrates the process flow chart of rat DRG neurons harvested for experiments in this thesis.

Figure 5:



45

Figure 5: Rat DRG harvest flow chart. The above flow chart illustrates that lumbar L1-L6 DRG neurons were harvested and either acutely cultured (72 hours max) for whole cell voltage-clamp electrophysiology or immunocytochemistry experiments, or processed for cell lysates immediately following harvest for qPCR experiments.[#] Adult female sprague dawley rats were used for experiments in **Chapter(s) III** and **VI** and adult male sprague dawley rats were used for experiments in **Chapter(s) IV** and **V**.

D. *Biolistic transfection of rat DRG neurons*

With the exception of a select few experiments, the majority of the work described in this dissertation was done in sensory DRG neurons. Many experiments described in the results section employed a biolistic transfection method, to transiently transfect wild-type and mutant VGSCs into DRG neurons. Biolistic transfection is a mechanical method of gene transfection that involves the high-speed propulsion of microcarriers coated with DNA that penetrate across cell membranes, delivering plasmid cDNA inside the cell. Biolistic transfections described here utilized the Helios Gene Gun System from BioRad Laboratories (Hercules, CA, USA). All recommended materials and optimized reagents, including Gold-Coat® tubing, gold, polyvinylpyrrolidone (PVP), Tubing Prep Station, Helios gene gun, gene gun barrels and cartridge holders were ordered from BioRad. Preparation of microcarrier (gold) cartridges and bombardment of cells were done using optimized protocols designed and modified based on the manufacturer's instructions. A detailed report on these transfection methods was recently published¹⁴⁴. Briefly, a 24-30 inch piece of tubing was cut to fit the saddle of the Tubing Prep Station and ultrapure grade nitrogen (Praxair Inc., Indianapolis, IN, USA) was allowed to flow at a rate of 0.3-0.4 LPM through the tubing for approximately 20 minutes to purge anything remaining in the tube and also to dry it out. While the tube is drying the microcarrier coated DNA is prepared. Approximately 15 mg of 1.0 micron gold is weighed and deposited into a tube containing 15 μ L of 0.05 M spermidine prepared from a 1:20 dilution of 1M spermidine stock in dehydrated ethanol (EtOH) [475 μ L 100% EtOH + 25 μ L 1 M spermidine stock]. It is critical that equal volumes (mg= μ L) of microcarrier and spermidine are used. The spermidine gold mixture was inverted, vortexed, and sonicated to remove clumps of gold. Next equal total volumes of cDNA were added to the spermidine gold mixture. For these experiments that commonly meant adding 7.5 μ L of rNav1.8sh-pSIREN-DNR-DsRed (at 1 μ g/mL; 7.5 μ g per

transfection) and 7.5 μL of wild-type or mutant VGSC cDNA (at 1 $\mu\text{g}/\text{mL}$; 7.5 μg per transfection) to the reaction mixture. Biolistic transfection efficiency is highly dependent on plasmid DNA attachment to gold microcarriers. The Plasmid DNA gold complex was formed next, by addition of equal volumes of 2M CaCl_2 . The addition of CaCl_2 precipitated the DNA from solution in the presence of gold microcarriers and polycation spermidine to form a stable plasma DNA-gold particle complex. The gold, spermidine, plasmid cDNA, and CaCl_2 mixture was allowed to precipitate at room temperature for 10 minutes and then the gold was pelleted, the liquid volume was removed, and the pellet was washed and reconstituted three times with fresh dehydrated EtOH (Spectrum Chemical MGF. Corp., Gardena, CA, USA). After removal of the final EtOH wash, the gold-DNA complex was then reconstituted in 1250 μL of 0.05mg/mL PVP (prepared from a 1:400 dilution of 20mg/mL PVP in EtOH storage stock; 3.125 μL 20mg/mL storage stock solution + 1246.875 μL 100% EtOH). The PVP helped the gold-DNA complex bind to the wall of the tube to form loadable cartridges that were later shot. The entire volume of PVP gold-DNA solution was transferred to a 15 mL conical tube, vortexed and mixed extensively, and then drawn into the nitrogen purged tubing using a syringe. The tubing was then carefully placed back into the Tubing Prep Station saddle. The PVP god-DNA complex sat in the tubing, undisturbed, for approximately 3-5 minutes before the liquid volume is slowly removed, leaving the gold particles attached to the tubing. Once the liquid was removed, the automatic rotation of the plastic tubing was started, and after 2 minutes time, the nitrogen was turned back on at a flow rate of 0.3-0.4 LPM for approximately 20 minutes. Cartridges were cut into 0.5 inch length cartridges using the Tubing Cutter and placed into the Helios Gene Gun Cartridge holder and the contents were shot at approximately 110 psi helium into recently dissociated DRG neurons plated onto 12 mm coverslips in 24 well plates. Unused cartridges were placed in storage tubes with a desiccator pellet and stored in a -20°C freezer. Cartridges were used for

transfection up to two weeks after their preparation. Cells shot with gold-DNA cartridges expressed DsRed protein that was visible within 16 hours of being shot. Cells were patched 24 to 72 hours post-transfection.

E. *Electrophysiology Recordings Solutions*

1. *Standard extracellular bathing (ECB) solution for electrophysiology recordings*

The standard extracellular bathing solution was used to bathe rat DRG neurons, ND7/23 cells, and hEK293 cells during all whole-cell voltage-clamp electrophysiology recordings. The composition for this solution (at ~300 mOsm) consisted of (in mM): 130 NaCl, 30 tetraethyl ammonium chloride (TEA-Cl), 1 MgCl₂, 3 KCl, 1 CaCl₂, 0.05 CdCl₂, 10 HEPES, and 10 D-Glucose. Recording solutions were adjusted using 1.0 N NaOH and D-Glucose to maintain physiological pH (pH~7.3) and osmolality values (~315 mOsm). Select experiments in transfected DRG neurons were performed in the presence and absence of 500 nM TTX [**Chapter(s) IV and V**].

2. *Standard CsF dominant electrode solution for electrophysiology recordings*

The standard CsF dominant electrode solution (at ~290 mOsm) used for all recordings in rat DRG neurons consisted of (in mM): 140 CsF, 10 NaCl, 1.1 EGTA, and 10 HEPES. Recordings solutions were adjusted using 1.0 N NaOH and D-Glucose to maintain physiological pH (pH~7.3) and osmolality values (305 mOsm).

F. *Whole-cell voltage-clamp recordings in DRG neurons*

Fire-polished electrodes were fabricated from 1.7 mm in diameter VMR Scientific (West Chester, PA, USA) capillary glass using a Sutter P-97 puller (Novato, CA, USA). For all recordings, the tip exterior contact surface of the fire polished electrodes was coated in sticky wax (KerrLab, Sybron Dental Specialties Inc., Orange, CA, USA) to minimize capacitive artifacts and allow for increased series resistance compensation. Cells on poly-D-lysine and Laminin-coated glass coverslips (12 mm) were transferred to a recording chamber containing extracellular bath solution in the presence or absence of 500 nM TTX to pharmacologically distinguish between TTX-S and TTX-R sodium currents. The majority of electrophysiology recordings were made at room temperature (22°C) in a modified 35 mm petri dish recording chamber^b. Select recordings were made in a temperature controlled recording chamber utilizing the Dagan HE-203 thermal stage regulated by a Dagan TC-10 controller (Dagan Corp., Minneapolis, MN, USA), at temperatures of 15°C, 22°C, 30°C, and 35°C ± 1°C in a 800 µL static bath with TTX present (793 µL ECB and 7 µL of 100 µM TTX).

Electrophysiology experiments make use of specialized amplifiers, microscopes, and controllers. Experimental data described here was collected from an elaborate recording setup assembled by Dr. Cummins. Recordings were made on the stage of a Nikon Eclipse TE2000-U inverted microscope (Nikon instruments Inc., Melville, NY, USA) equipped with 10X and 40X contrast objectives, dual Nikon ocular lenses, a white (Nikon TE2-PS100W) light source, and a phase contrast (Hoffman modulation contrast system) light polarizer. For select experiments, transfected cells were identified by the

^b The recording chamber was made by filling a 35 mm cell culture dish with Sylgard® (World Precision instruments Inc., Sarasota, FL, USA) by mixing equal parts of the silicone elastomer base with a curing agent. Culture dishes were cured overnight. The recording reservoir was made by removing a section of silicone in the center of the dish approximately 16 mm in diameter with a scalpel. With a 16 mm section of silicon removed the recording chamber reservoir was large enough to accommodate a 12 mm (dia) coverslip and 250 to 300 µL of ECB.

expression of green or red fluorescent protein. To identify transfected cells, the Nikon inverted microscope was outfitted with a fluorescent halogen light source and appropriate dichroic filters (DsRed dichroic filter parameters: excitation maximum=554 nm and emission maximum=591 nm; AcGFP1 dichroic filter parameters: excitation maximum=475 nm and emission maximum=505 nm). The microscope and all associated manipulators was located on an isolation, nitrogen infused, air table (50-60 psi maintained air pressure) with a 2 inch stainless steel laminate surface (62-500 Series, Technical Manufacturing Company, Peabody, MA, USA) to counter effects of transferrable vibrations. All electrophysiological experiments were performed on an air-table housed Faraday cage with multiple grounding points to minimize electrical interference. All grounding points were connected in series to a central ground that was connected to the ground input of the amplifier.

Whole-cell voltage-clamp electrophysiology recordings were conducted as previously described¹³¹. Briefly, whole-cell voltage-clamp recordings were conducted using a HEKA EPC-10 amplifier (HEKA Instruments Inc., Bellmore, NY, USA) under voltage-clamp mode. Recordings were made after obtaining a Giga-ohm seal (resistance of injected current to ground; ranging from 1-10 GΩ). Cells were selected according to their morphology, size, and for some experiments according to their expression of fluorescent protein. Fire polished recording electrodes (resistance ~1.0 to 1.60 MΩ) were back-filled with enough intracellular solution (see standard CsF dominant electrode solution) to cover the AgCl₂ coated recording filament and placed in the head stage electrode holder. For recordings made from DRG neurons transfected with recombinant channel DNA 500 nM TTX was added to the recording bath before voltage protocols were initiated to pharmacologically isolate the transfected currents from the native TTX-sensitive sodium currents. Offset potential was zeroed before patching. Capacitive artifacts were canceled using the computer-controlled circuitry of the patch

clamp amplifier. Series resistance errors were always compensated with 75-85% series resistance compensation and were typically less than 5 mV during voltage-clamp recordings. Leak currents were linearly canceled by digital P/-5 subtraction, whereby currents elicited by 5 pulses that are one-fifth of the test pulse are subtracted from the test pulse. Cells were held at a membrane potential of -100mV for recordings from transfected channels and -120 mV for recordings made from untransfected DRG neurons [see **Chapter(s) III and VI**]. For all experimental recordings membrane currents were filtered at 5 kHz, sampled at 20 kHz. Whole-cell recordings did not last for more than 45 minutes, and cells were not held in the standard bathing solution for more than 1 hour. Given the ionic solutions used for these recordings, inward sodium currents had a reversal potential of approximately +65 mV, corresponding closely to the calculated Nernst potential observed during the standard current-voltage (I-V) protocol. To encourage Gig-ohm negative pressure is applied to the cell and the cell membrane is held at -70 mV. Whole-cell recording configuration is obtained by breaking into the cell membrane once a gig-ohm seal is obtained in cell attached configuration by pulsating suction. Once whole-cell configuration is achieved the membrane RC circuit is balanced and the access resistance is compensated. Data were not recorded before 3 minutes after whole-cell configuration had been established to allow adequate time for the electrode solution to equilibrate with the intracellular contents. For recordings made from transfected DRG neurons, once the recordings began, cells underwent a series of conditioning pulses to -10 mV, to ensure rundown of any residual endogenous NaV1.9 current¹⁴³. Standard voltage-clamp protocols for recordings made from transfected DRG neurons [**Chapter(s) III, IV, and V**] were described previously¹⁵⁰. Voltage protocols for recordings made from untransfected DRG neurons [**Chapter(s) III and VI**] are described within the specific results sections. Briefly, current/voltage (I-V) relationships were determined by an incremental depolarizing step protocol, testing every +5 mV for 50 ms,

from -80 to +50 mV. To determine the fraction of channels transitioning to a fast inactivated state, a double-pulse protocol (h_{∞}/V) was used that incrementally conditioned the channels from -120 mV to -10 mV for 500 ms before testing for the fraction of channels available at -10 mV. Resurgent currents were assayed with a two-step protocol that initially depolarized the membrane to +30 mV for 20 ms before testing for inward resurgent sodium currents by hyperpolarizing the membrane potential in -5 mV increments from 0 mV to -80 mV, for 100 ms, before returning to the holding potential. Further details on the resurgent current protocol and analysis of resurgent sodium currents are provided in **Chapter II-L2**. For many experiments the rate of channel inactivation was also measured and reported. In this case the rate of channel inactivation is an “open-state” inactivation rate reported as the time constant for current decay during a +10 mV step depolarization. Current decay values were obtained from a standard Hodgkin-Huxley (m^3h) fit and reported as a τ_h value.

G. Isolation of transfected recombinant voltage-gated sodium currents in DRG neurons

For many experiments performed in this thesis DRG neurons were used as a surrogate heterologous expression system for recombinant voltage gated sodium channels. Recombinant voltage-gated sodium channels were transfected using the procedure described in **Chapter II-D** (*Biolistic transfections of rat DRG neurons*). As described previously, the recombinant channels either were already naturally resistant to TTX, as is the case with NaV1.5, or were mutated to be resistant to TTX, as with NaV1.3, NaV1.4, NaV1.6, and NaV1.7. In biolistically transfected rat DRG neurons, endogenous DRG TTX-S channels were blocked with 500 nM TTX. DRG neurons can also express endogenous NaV1.8 and NaV1.9 currents, which are resistant to TTX-R. NaV1.9 currents are rarely observed under the culture and recording conditions

used^{41,144-146}, and were therefore generally not an issue. To ensure no NaV1.9 current contamination, cells underwent a series of conditioning pulses to -10 mV once whole cell recording configuration was achieved¹⁴³. Although NaV1.8 currents were substantially decreased with time in culture¹⁵¹, I used additional measures to minimize contamination of recordings by NaV1.8 currents. Accordingly, NaV1.8 currents were knocked down using a targeted shRNA plasmid (see **Chapter II-A**) to silence native rat NaV1.8 gene expression via RNAi¹⁴⁸. Cells transfected with NaV1.8 shRNA were identified by expression of DsRed protein (NaV1.8 shRNA vector contained a DsRed sequence). Under control conditions (less than 48 hours in culture), NaV1.8 current amplitude averaged 34.9 ± 4.8 nA (n=42). To determine the efficiency of NaV1.8 shRNA knockdown, neurons were transfected with TTX-S NaV1.7 plasmid plus the NaV1.8 shRNA vector. Transfected cells (identified by red fluorescence) were recorded in the presence of 500 nM TTX (to block both endogenous and recombinant TTX-S currents in this control experiment), and the residual sodium current, which must be generated by endogenous TTX-R channels, was measured (n=17). NaV1.8 and NaV1.9 produce currents with distinctive kinetic and voltage-dependent properties that can be readily distinguished from each other and from TTX-S channels^{145,152}. In the NaV1.7 + NaV1.8 shRNA transfected cells, NaV1.9 currents were not observed, and the NaV1.8 currents were reduced by greater than 98% under our experimental conditions (Figure 6-A and -B). In addition, because NaV1.8 currents have distinctive kinetic and voltage-dependent properties¹⁵³, contamination by NaV1.8 can be determined for each individual cell expressing recombinant current. The midpoint of the voltage dependence of inactivation for NaV1.8 currents is -34.7 ± 2.0 mV, substantially more depolarized than any of the recombinant constructs investigated in this thesis (Table 5). Analysis of the voltage dependence of inactivation curve can therefore be used to determine the absolute and relative amplitude of the recombinant VGSC current and endogenous NaV1.8 current for

each individual cell (Figure 6-C). Cells that expressed NaV1.8 current with amplitudes greater than 10% of the peak recombinant current amplitude (current elicited from a 50 ms pulse to +10 mV) were excluded from the final data analysis. For the 150 cells expressing TTX-R recombinant VGSCs in **Chapter IV** the peak recombinant current amplitude averaged 36.2 ± 2.1 nA and the peak residual NaV1.8 current amplitude averaged 0.3 nA. Similar results were obtained for recordings made for **Chapter(s) III** and **V**. Taken together these data confirmed that the use of 500 nM TTX and NaV1.8 shRNA allowed effective isolation of the current produced by recombinant VGSCs in transfected DRG neurons.

Figure 6:

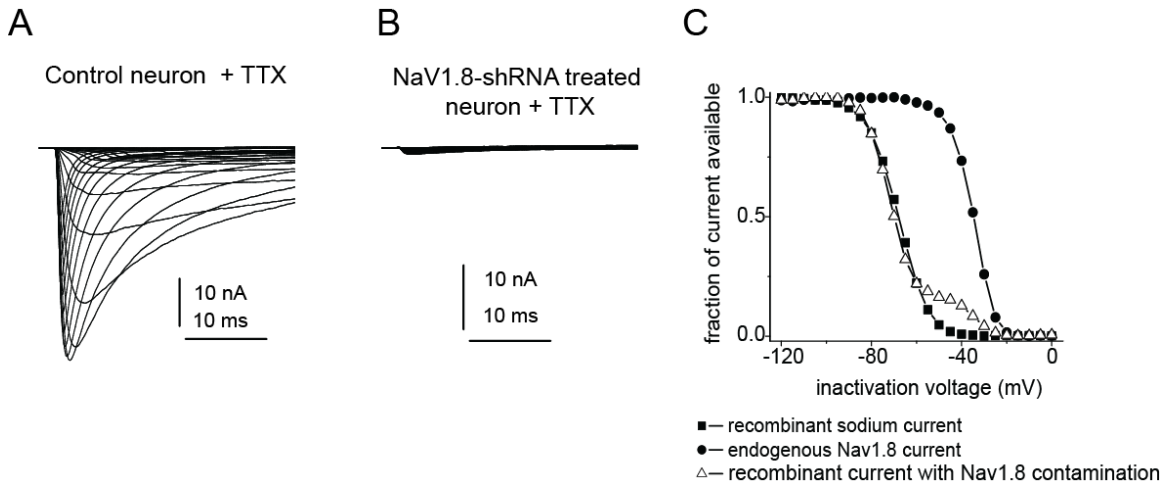


Figure 6: Reduced NaV1.8 currents following biolistic transfection of NaV1.8 shRNA. (A) Representative TTX-R currents recorded from a cultured adult rat DRG neuron in the presence of 500 nM TTX. Currents were elicited with voltage steps ranging from -80 mV to +40 mV in 10 mV increments. Current traces exhibit the slow activation and inactivation kinetics of NaV1.8 currents. (B) Representative currents recorded from a cultured adult rat DRG neuron transfected with NaV1.8-shRNA and TTX-S NaV1.7 plasmid DNA. For comparison the scale is the same as in (A). In the presence of TTX, very little sodium current is elicited. This demonstrates that the NaV1.8-shRNA transfection combined with application of 500 nM TTX effectively blocks the majority of endogenous voltage-gated sodium currents in cultured rat DRG neurons. (C) Steady-state inactivation curves for endogenous NaV1.8 currents (filled circles) recorded from the same neuron used in (A), a transfected neuron expressing recombinant NaV1.5 current without evidence of NaV1.8 contamination (closed squares), and a transfected neuron expressing recombinant NaV1.5 current with ~20% contamination by endogenous NaV1.8 currents (open triangles). NaV1.8 contamination is evidenced by the biphasic voltage-dependence of steady-state inactivation. This figure was modified from Jarecki *et al.* 2010¹⁵⁰.

H. Computational simulations of a DRG neuron and a cardiac myocyte

Computer simulations were performed to explore the impact that resurgent sodium currents generated by voltage-gated sodium channels and disease mutations might have on action potential firing. The basic approach was to use established models of DRG neuron and cardiac myocyte excitability that had been implemented into the NEURON simulation environment¹⁵⁴ and, with modifications only to the appropriate sodium channel formulation, simulate and evaluate the impact of the disease mutation and/or resurgent current blocking factor. In each model, the kinetic rate transitions of the sodium conductance were reflective of real data recorded from wild-type and mutant channels recorded from DRG neurons. Modified kinetic models used in each simulation were developed by Dr. Cummins based on data collected by myself and Dr. Brian W. Jarecki.

1. DRG neuron simulation

The DRG neuron model used for these simulations was developed previously¹⁵⁵ and included the following voltage-dependent currents: a delayed rectifier potassium current (I_{KDR}), an A-type potassium current (I_{KA}), and NaV1.8, slowly inactivating TTX-R current. The only changes made to the model were to the NaV1.7 voltage-dependent sodium current in the model. The sodium current changes were implemented in a Markov model based on the Hodgkin-Huxley formulation of NaV1.7 previously used¹⁵⁵. The diagram for the Markov model used for the simulated voltage-gated sodium conductance is shown in Figure 7. The model includes 3 closed states, a conducting open state, and 3 inactivated states. The Markov model used for the simulated voltage-gated sodium conductance with resurgent sodium current included 1 additional state, the resurgent, open blocked state (Figure 7-highlighted with the dashed box). Here the resurgent, open-blocking factor was implemented as done for a previous simulation of resurgent currents in cerebellar Purkinje neurons¹³², with slight modifications to the

transition rate expressions (Table 2). Characterization of the functional impact of the I1461T mutation in HEK293 cells¹⁵⁶ and DRG neurons [**Chapter(s) IV and V**] showed that this mutation destabilizes inactivation, shifting the voltage-dependence of inactivation in the depolarizing direction and slowing the rate of open-state inactivation. The measured values of channel availability and time constants from the recordings made in DRG neurons were used to reformulate expressions for the vertical transitions in Figure 7 (between the inactivated states and the closed and open states). The horizontal transitions were unchanged (Table 2). NEURON simulations were run with (a) 100% WT-Nav1.7, (b) 100% WT-Nav1.7 with resurgent sodium current (I_{NaR}), (c) 50% WT-Nav1.7 and 50% Nav1.7-I1461T, and (d) 50% WT-Nav1.7 and 50% WT-Nav1.7-I1461T, both with I_{NaR} . Mutant channels were simulated along with 50% wild-type channels because the PEPD mutations display autosomal dominance.

2. Cardiac myocyte simulation

The cardiac myocyte model used for these simulations was modified from previously published mathematical models of cardiac action potential firing^{157,158}, to simulate the impact of the F1486L LQT3/SIDS mutation and resurgent sodium currents. The cardiac myocyte model was based on a cardiac atrial cell model previously implemented by I. Jacobson in the neuron simulation environment¹⁵⁴. More information on the cardiac cardiac atrial cell model can be found here:

<http://senselab.med.yale.edu/ModelDB/ShowModel.asp?Model=3800>. The model includes several voltage-dependent ionic conductances: multiple delayed rectifier currents (I_{Kur} , I_{Kr} , and I_{Ks}), a time-independent inward rectifier current (I_{K1}), the fast inward sodium current (I_{Na}), the L-type calcium current ($I_{Ca,L}$) and the Na^+/Ca^{2+} exchanger current (I_{NaCa})¹⁵⁷. The only changes made to the model were to the voltage-dependent sodium current (I_{Na}). Modified I_{Na} currents were implemented using a Markov model based on the Hodgkin-Huxley formulation of Nav1.5 in the original model. The Markov formulation

was more amenable to implementation of both the F1486L effects and the resurgent open channel blocking factor. Intermediate inactivation states were not included in this formulation, as it was unclear how to model potential interactions between the resurgent current blocking factor and intermediate inactivation states. This is reasonable, as the F1486L mutation may have little or no impact on intermediate inactivation¹⁵⁹. The diagram for the Markov model used for the simulated voltage-gated sodium conductances is shown in Figure 7, and the transition rate expressions for NaV1.5 are provided in Table 3. Whole cell recordings made from DRG neurons indicate that the F1486L mutation produces moderate destabilization of inactivation, shifting the voltage dependence of inactivation by approximately 8 mV in the depolarizing direction, slowing the rate of channel inactivation, and slightly increasing persistent currents^c (Table 5). The effects of the mutation were modeled by altering the transition rates from the closed and open state into the inactivated states (Table 3). The resurgent sodium current was modeled to be similar to that of the NaV1.7, but with slight modifications to the overall expression to account for the relative resurgent sodium current amplitude observed with WT-NaV1.5 and NaV1.5-F1486L channels in our DRG recordings. NEURON simulations were run with (a) 100% WT-NaV1.5, (b) 100% WT-NaV1.5 with resurgent sodium current (I_{NaR}), (c) 50% WT-NaV1.5 and 50% NaV1.5-F1486L, and (d) 50% WT-NaV1.5 and 50% NaV1.5-F1486L, both with I_{NaR} .

^c Data not shown in **Chapter IV** Table 5. See Jarecki *et al.* 2010 in Appendix A.

Figure 7:

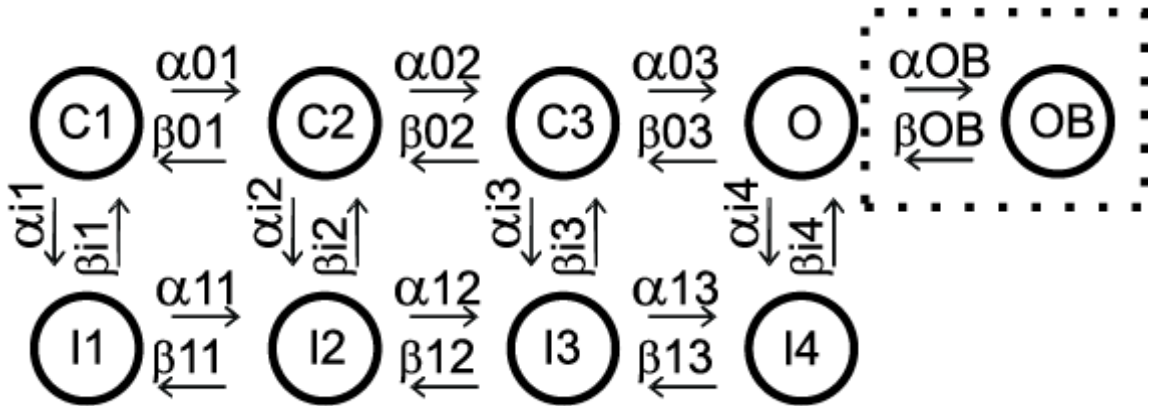


Figure 7: Diagram of the Markov models used for voltage-gated sodium channel conductances. An 8-state Markov model was used for simulation of voltage-gated sodium channel conductances without resurgent sodium currents (I_{NaR}). C1-C3, closed [non-conducting] states; O, open [conducting] state; I1-I4, inactivated [non-conducting] states. A 9-state Markov model incorporated the resurgent current, open-channel blocking factor. The OB state [within the dotted box] represents channel open channel block. For both NaV1.7 and NaV1.5 wild-type and mutant channels, the kinetic rate transitions (shown as arrows between channel states) were modified to reflect channel properties observed in recordings made from recombinant channels expressed in DRG neurons. Kinetic rate transitions between each channel state for modeled NaV1.5 and NaV1.7 channel conductances are shown in **Table 2** and **Table 3**. This figure was modified from Jarecki *et al.* 2010¹⁵⁰.

Table 2:

Transition	For Nav1.7	For Nav1.7-I1461T
α_{01}	$3 \cdot 15.5 / (1 + \exp((v-5)/(-12.08)))$	unchanged
β_{01}	$35.2 / (1 + \exp((v+72.7)/16.7))$	unchanged
α_{02}	$2 \cdot 15.5 / (1 + \exp((v-5)/(-12.08)))$	unchanged
β_{02}	$2 \cdot (35.2 / (1 + \exp((v+72.7)/16.7)))$	unchanged
α_{03}	$15.5 / (1 + \exp((v-5)/(-12.08)))$	unchanged
β_{03}	$3 \cdot (35.2 / (1 + \exp((v+72.7)/16.7)))$	unchanged
α_{11}	$3 \cdot 15.5 / (1 + \exp((v-5)/(-12.08)))$	unchanged
β_{11}	$35.2 / (1 + \exp((v+72.7)/16.7))$	unchanged
α_{12}	$2 \cdot 15.5 / (1 + \exp((v-5)/(-12.08)))$	unchanged
β_{12}	$2 \cdot (35.2 / (1 + \exp((v+72.7)/16.7)))$	unchanged
α_{13}	$15.5 / (1 + \exp((v-5)/(-12.08)))$	unchanged
β_{13}	$3 \cdot (35.2 / (1 + \exp((v+72.7)/16.7)))$	unchanged
α_{i1}	$-0.00283 + 2.003 / (1 + \exp((v+5.5266)/(-12.702)))$	unchanged
β_{i1}	$0.38685 / (1 + \exp((v+122.35)/15.29))$	$0.741 / (1 + \exp((v+135.69)/21.44))$
α_{i2}	$-0.00283 + 2.003 / (1 + \exp((v+5.5266)/(-12.702)))$	$1.669 / (1 + \exp((v+10.43)/(-9.24)))$
β_{i2}	$0.38685 / (1 + \exp((v+122.35)/15.29))$	$0.741 / (1 + \exp((v+135.69)/21.44))$
α_{i3}	$-0.00283 + 2.003 / (1 + \exp((v+5.5266)/(-12.702)))$	$1.669 / (1 + \exp((v+10.43)/(-9.24)))$
β_{i3}	$0.38685 / (1 + \exp((v+122.35)/15.29))$	$0.741 / (1 + \exp((v+135.69)/21.44))$
α_{i4}	$-0.00283 + 2.003 / (1 + \exp((v+5.5266)/(-12.702)))$	$1.05 / (1 + \exp((v+10.43)/(-9.24)))$
β_{i4}	$0.38685 / (1 + \exp((v+122.35)/15.29))$	$0.9632 / (1 + \exp((v+135.69)/21.44))$
α_{OB}	$1.1 \cdot \exp(v/1e12)$	unchanged
β_{OB}	$0.0135 \cdot \exp(v/-25)$	unchanged

Table 2: Transition rate expressions for Nav1.7 conductance simulations in a modeled DRG neuron. Transitions are as diagramed in Figure 7. Values are in ms^{-1} . Transition rate expressions were implemented into a Markov model and the modeled sodium conductances (I_{Na} +/- I_{NaR}) were integrated into a previously published DRG neuron model¹⁵⁵. This table was modified from Jarecki *et al.* 2010¹⁵⁰

Table 3:

Transition	For Nav1.5	For Nav1.5-F1486L
α_{01}	$-3 \cdot 0.32 \cdot (v+47.13) / (\exp(-0.1 \cdot (v+47.13)) - 1)$	unchanged
β_{01}	$0.08 \cdot \exp(-(v)/11)$	unchanged
α_{02}	$-2 \cdot 0.32 \cdot (v+47.13) / (\exp(-0.1 \cdot (v+47.13)) - 1)$	unchanged
β_{02}	$2 \cdot (0.08 \cdot \exp(-(v)/11))$	unchanged
α_{03}	$-0.32 \cdot (v+47.13) / (\exp(-0.1 \cdot (v+47.13)) - 1)$	unchanged
β_{03}	$3 \cdot (0.08 \cdot \exp(-(v)/11))$	unchanged
α_{11}	$-3 \cdot 0.32 \cdot (v+47.13) / (\exp(-0.1 \cdot (v+47.13)) - 1)$	unchanged
β_{11}	$0.08 \cdot \exp(-(v)/11)$	unchanged
α_{12}	$-2 \cdot 0.32 \cdot (v+47.13) / (\exp(-0.1 \cdot (v+47.13)) - 1)$	unchanged
β_{12}	$2 \cdot (0.08 \cdot \exp(-(v)/11))$	unchanged
α_{13}	$-0.32 \cdot (v+47.13) / (\exp(-0.1 \cdot (v+47.13)) - 1)$	unchanged
β_{13}	$3 \cdot (0.08 \cdot \exp(-(v)/11))$	unchanged
α_{i1}	$(1 / (0.13 \cdot (1 + (\exp(-1 \cdot (v+10.66)/11.1))))$	$1 / (0.26 \cdot (1 + (\exp(-1 \cdot (v+10.66)/11.1))))$
β_{i1}	$(0.135 \cdot \exp(-0.147 \cdot (v+80)))$	unchanged
α_{i2}	$(1 / (0.13 \cdot (1 + (\exp(-1 \cdot (v+10.66)/11.1))))$	$1 / (0.26 \cdot (1 + (\exp(-1 \cdot (v+10.66)/11.1))))$
β_{i2}	$(0.135 \cdot \exp(-0.147 \cdot (v+80)))$	unchanged
α_{i3}	$(1 / (0.13 \cdot (1 + (\exp(-1 \cdot (v+10.66)/11.1))))$	$1 / (0.26 \cdot (1 + (\exp(-1 \cdot (v+10.66)/11.1))))$
β_{i3}	$(0.135 \cdot \exp(-0.147 \cdot (v+80)))$	unchanged
α_{i4}	$(1 / (0.13 \cdot (1 + (\exp(-1 \cdot (v+10.66)/11.1))))$	$1 / (0.26 \cdot (1 + (\exp(-1 \cdot (v+10.66)/11.1))))$
β_{i4}	$(0.135 \cdot \exp(-0.147 \cdot (v+80)))$	0.001
α_{OB}	$2.5 \cdot \exp(v/1e12)$	unchanged
β_{OB}	$0.02 \cdot \exp(v/-25)$	unchanged

Table 3: Transition rate expressions for NaV1.5 conductance simulations in a modeled cardiac myocyte. Transitions are as diagrammed in Figure 7. Values are in ms^{-1} . Transition rate expressions were implemented into a Markov model and the modeled sodium conductances (I_{Na} +/- I_{NaR}) were integrated into a previously published cardiac atrial cell model¹⁵⁷. This table was modified from Jarecki *et al.* 2010¹⁵⁰.

I. *Contusive spinal cord injury model*

Studies performed in **Chapter VI** examine the potential contribution of sodium channels/currents, most notably resurgent sodium currents (I_{NaR}), following an experimental model of spinal cord injury (SCI). There are multiple models of experimental SCI including ischemic, dorsal or lateral hemisections, and contusion. Experiments in **Chapter VI** make use of the contusive SCI model because: (1) contusive SCI is the most common SCI observed in humans and (2) contusive SCI in rats has been extensively studied as a model for human SCI as it replicates the major phenotypes observed in injured patients. Contusive spinal cord injuries were carried out by Dr. Xiao-Ming Xu's laboratory personnel as described previously¹⁶⁰⁻¹⁶² using a weight-drop device developed at NYU and a protocol developed by a multicenter consortium^{163,164}. Briefly, 200-230 kg female rats were ordered and, upon arrival, allowed 5 to 7 days to acclimatize to their surroundings in the animal care facility. On the day of the surgery, rats were anesthetized with penobarbital (50mg/kg, IP), and after the animal had reached the anesthetic plain, a 1 inch skin incision was made on the dorsal midline, the musculature was retracted, the spinal column was visualized, and a stabilizer was placed between the T7 and T10 spinous processes. After the spinal process was stabilized a laminectomy was performed at T9-T10 level, exposing the dura. The surface of the spinal cord was then contused using a weight-drop impact with a 10 gram rod (2.5 mm in diameter) dropped from a height of 12.5 mm. Following the contusion the musculature was closed in 2-3 layers with sutures, and the skin was closed with wound clips. Triple antibiotic ointment was applied to the wound immediately after surgery and injured animals were placed in a temperature- and humidity-controlled chamber overnight. Manual bladder expression is carried out at least 3 times daily until reflex bladder emptying is established. For sham-operated controls, animals undergo a T9-T10 laminectomy without weight-drop contusion. All

surgical interventions and postoperative animal care were carried out in accordance with the Guide for the Care and Use of Laboratory Animals and the Guidelines of the Indiana University Institutional Animal Care and Use Committee. DRG were harvested at two weeks after contusive injury for culture or Real-time RT-PCR analysis.

J. *Conventional- and real-time- reverse transcriptase polymerase chain reaction (RT-PCR)*

Quantification of mRNA for specific targets was performed using conventional and real-time PCR techniques similar to those described previously by Wang JG *et al.* 2008¹⁶⁵ and Wu X *et al.* 2005¹⁶⁶. Briefly, fourteen days after spinal cord injury (SCI), rats were sacrificed and L1-L6 DRG neurons were harvested from both sides of the spinal column. Excised DRGs were washed twice with ice cold PBS and transferred to a fresh, RNase free microcentrifuge tube. Next, excised DRG's were processed for total RNA isolation using the RNeasy Plus Mini Kit (Qiagen Inc., Valencia, CA, USA), according to the manufacturer's instructions. If RNase isolation was performed at a later date, harvested DRG's were dissolved in RNAlater® RNA stabilization reagent (Qiagen Inc, Valencia, CA, USA), flash frozen in liquid nitrogen (~-190°C) and stored in the -80°C freezer. Harvested total RNA was reconstituted in 50 µL of nuclease free H₂O and subjected to DNase digestion using 0.5µL of TURBO DNase (Applied Biosystems, Foster City, CA, USA) enzyme and 5 µL of TURBO DNase buffer. The reaction was left in a 37°C water bath for 30 mins; at the end of 30 min 5 µL of 50 mM EGTA was added to the total RNA mixture and then placed in a thermomixer (Eppendorf AG, Hamburg Germany) at 75°C for 10 mins. Following DNase digestion, the concentration and purity of the total RNA samples was assessed by spectrophotometry (Nanodrop 1000, Thermo Fischer Scientific, Wilmington, DE, USA) and gel electrophoresis (Experion RNA StdSens Analysis Kit, BIO-RAD, Life Science Research, Hercules, CA, USA) according

to the manufacturer's instructions. Next isolated total RNA was converted to cDNA via a reverse transcriptase (RT) reaction. To increase the efficiency of reverse transcription, the iScript® cDNA Synthesis Kit (BIO-RAD), which employs random hexamer primers, was utilized. The reaction, consisting of nuclease free H₂O, RT buffer, total RNA (450-750 ng), and RT enzyme, was incubated at 25°C for 10 min, then at 42°C for 50 min, and 10 min at 70°C. Synthesized cDNA was used immediately or stored in the -80°C freezer. Important note: quantity and quality of total isolated total RNA was improved by completing DRG harvest, total RNA isolation, and cDNA conversion in a single day. Quantification of mRNA for specific targets was performed using Sybr Green real-time RT-PCR as described previously¹⁶⁷. Specific oligonucleotide primers were designed for specific targets, as well as for housekeeping (reference) genes, HPRT^d and ARBP^e, according to criteria and design software Primer Express (Applied Biosystems). In some specific cases primer sequences were taken from published sequences used by previous investigators¹⁶⁵. Each primer set was tested using isolated cDNA from brain and DRG tissue, isolated from naïve animals, to ensure primer specificity (verifying predicted amplicon size on a gel) and to optimize PCR conditions, including Mg²⁺ concentration and annealing temperature. Additional information about the primers can be found in Table 4.

Real-time PCR was performed on an ABI Prism 7500 Sequence Detector (Applied Biosystems). The PCR was performed in triplicate on each cDNA sample in a MicroAmp Optical 96-well reaction plate (Applied Biosystems). A reaction volume containing template cDNA, specific primers, SYBR Green Gene Expression Master Mix (Applied Biosystems), and uracil-N-glycosylase was loaded into each well of the reaction plate. Each plate contained a no template control (NTC) in which 4 µL of DEPC water

^d HPRT: Hypoxanthine-Guanine Phosphoribosyltransferase.

^e ARBP: Attachment Region Binding Protein

replaced cDNA. The thermal cycling program began with an initialization step: 50°C for 2 min and 95°C for 4 min for optimal uracil-N-glycosylase activity and activation of Taq DNA pol, respectively. Then 45 cycles of PCR was performed—each cycle consisted of 95°C for 15 sec for melting and 60°C for 1 min for annealing and extension.

Table 4:

Name	Rat Gene Symbol	Rat mRNA Reference	Amplicon (bp)	Primer Forward/Reverse
rNaV1.1*	SCN1a	NM_030875.1	137	ATCCGAGTCCGAAGATAGCA GTCTCGGGGAAAACAGTGAG
rNaV1.3*	SCN2a	NM_013119.1	182	AACTTGGTGCCATCAAATCC CAGATTCACACCCATGATGC
rNaV1.6*	SCN8a	NM_019266.2	274	TACAGTGGCTACAGCGGCTA TGTTTGTGACCACGCTCATT
rNaV1.7 [#]	SCN9a	NM_133289	85	GGGTTCACTATTCGTACCCCATAG TCCCGTTCACCGGTAGCA
rNaV1.8*	SCN10a	XM_001078257	151	CACGGATGACAACAGGTCAC GATCCCGTCAGGAAATGAGA
rNaV1.9 [#]	SCN11a	NM_019265	75	GGACGATGCCTCTAAAATCCA AAGAGATCCACTGGCAAGTTCTG
rNaV β_1 [#]	SCN1b	NM_017288	82	TGGTGTGCTCGTAATTATCAA CACTCTGGCGACTACGAATGTC
rNaV β_2 [#]	SCN2b	NM_012877	65	GCAATTGCTCAGAGGAGATGTT ACCGCTCCAGCTTCAGGTT
rNaV β_3 [#]	SCN3b	NM_139097	65	GGCACACAGGCCTTTTGTG TCTCCCGCCTCTTCAGTACT
rNaV β_4 [#]	SCN4b	NM_001008880	83	CAGCGAAACATCCAGGATTCTC CGGTCATCATCCTTCACTCTCA
rHPRT*	Hprt1	NM_012583.2	278	GCAGACTTTGCTTTCCTTGG TACTGGCCACATCAACAGGA
rARBP	Rplp0	NM_022402	58	CAGCCAAGGTCTGAAGCAAA CCGAATCCCATGTCCTCATC

Table 4: Primers used for qPCR experiments. qPCR primers used to quantify the gene expression of peripheral voltage-gated sodium channels (VGSCs) and their auxiliary β -subunits. The table displays the name of the target protein, the gene symbol, the rat genebank reference number, the predicted amplicon size, and the forward and reverse primers used for gene quantification. All primers are written 5' to 3'. * primers were designed and used previously by a group of scientists at the University of Cincinnati College of Medicine, Cincinnati, OH¹⁶⁵. # primers were designed to be used for both SYBR Green and Taqman PCR.

K. Immunocytochemistry: staining acutely cultured rat DRG neurons

Staining of acutely cultured rat dorsal root ganglion neurons was done with the help of Dr. Rajesh Khanna as described previously¹⁶⁸ using a modified protocol from Rick Meeker. Briefly, adult dorsal root ganglion neurons cultured on glass coverslips were washed twice with PBS (pH 7.4), and then fixed in PBS containing 4% paraformaldehyde and 4% sucrose for 5 min. The fixative was removed by washing (3x—the last time for 5 minutes) in PBS, then the cells were permeabilized with 0.25% Triton X-100 (Sigma Aldrich, St. Louis, MO, USA) for 10 minutes, followed by washing in PBS, 3 times—the last time for 5 minutes. Nonspecific antibody binding was blocked by incubating the blots overnight in PBS containing 10% bovine serum albumin (BSA, Sigma-Aldrich) diluted in 0.1 mM PBS (blocking buffer). After washing in PBS, 3 times—the last time for 5 minutes, the cells were incubated with primary antibody for 1 hour at room temperature. Primary antibodies used for these experiments were rabbit polyclonal anti-Nav β_4 antibody (Sigma Aldrich—Prestige Antibodies), diluted 1:33 in blocking, and mouse monoclonal anti β III-tubulin antibody (Abcam Inc., Cambridge, MA, USA), diluted 1:500 in 3% BSA. After incubation, the neurons were washed again with PBS, 3 times—the last time for 5 minutes, and incubated in secondary antibodies, goat anti-mouse Alexa 488 or anti-rabbit Alexa 594 (Molecular Probes, Inc., Eugene, OR), diluted at 1:1,000 in blocking solution for 45 minutes at room temperature. Coverslips were mounted in Prolong Gold Antifade (containing DAPI) mounting media (Molecular Probes, Inc.). DRG neurons were imaged on a Nikon Eclipse Ti fluorescence microscope using a 10x and 40x objective lenses and standard fluorescein isothiocyanate/Texas Red fluorescence cubes. Images were deblurred off-line by an iterative deconvolution protocol (Nikon Elements version 3.0) using a theoretical point spread function and pseudocolored for presentation.

L. Data analysis

1. Electrophysiology data analysis

Voltage-clamp data were analyzed as described by Cummins *et al.* 2005¹³¹, Jarecki *et al.* 2010¹⁵⁰, and Theile *et al.* 2010¹⁶⁹. Briefly, data was analyzed using the Pulsefit (v 8.65, HEKA Elektronik, Germany), Origin (v 7.0, OriginLab Corp., Northhampton, MA, USA), and Microsoft Excel (Microsoft Corporation, Redmond, WA, USA). Figures were made using the Adobe Photoshop CS5 and Adobe Illustrator CS5 (Adobe Systems Inc., San Jose, CA, USA). Data from individual steady-state recording conditions were fit using a standard single-phase Boltzmann distribution for activation (m^∞) and steady-state fast-inactivation (h^∞) data. Sodium current midpoint ($V_{1/2}$) and slope factors (Z) were calculated using a standard single-phase Boltzmann distribution fit according to **Eq 1**:

$$I(V) = Offset + \left(\frac{Amplitude}{1 + \exp(-(V - V_{1/2})/Z)} \right)$$

All data shown are means \pm S.E.M. Comparison of frequency [occurrence of I_{NaR}] was determined using a X^2 test. Statistical significance between current amplitudes was assessed with Microsoft Excel using single factor (one-way) ANOVA. Statistical significance of difference was accepted at P values less than 0.05.

2. Resurgent sodium current quantification and analysis

For most experiments cells were assayed for their ability to produce I_{NaR} using a step protocol that initially conditioned the cell membrane to +30 mV for 20 ms, from the holding potential (either -120 mV or -100 mV), before repolarizing the membrane potential from 0 to -80 mV (in -5 mV increments) to test for I_{NaR} . The protocol is shown below in Figure 8:

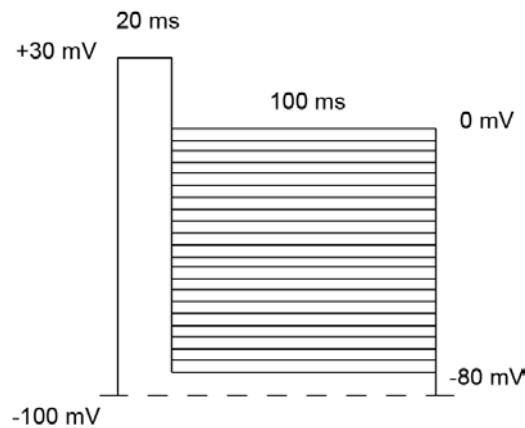


Figure 8: Standard resurgent sodium current voltage clamp protocol.

Resurgent currents display several features that were used in the identification and quantification of these currents. These properties are discussed in detail in **Chapter III (I_{NaR} in rat DRG neurons)** of this thesis. For all cells identified with I_{NaR} in this thesis, maximal peak currents during the repolarizing pulses were produced in a window of potentials from -35 to -55 mV, and were first observed around -10 mV. Resurgent currents display a distinctly non-monotonic I - V relationship between -20 to -60 mV, which was used in identifying these currents. Another property characteristic to resurgent currents is their novel gating kinetics—slow rising phase (activation) followed by a slow decaying phase. These kinetics are much slower than those of conventional sodium current evoked by depolarizing steps, which rise in less than 0.3 ms and have a dominant decay τ_h near 1 ms¹⁰⁵. Moreover, these kinetics contrasts with classic VGSC

tail currents, which are observed instantaneously following similar hyperpolarizing steps and decay within a few milliseconds.

Resurgent currents were analyzed with leak subtraction in PulseFit® (Heka) and were filtered at 1,000 Hz to reduce noise but maintain the current waveform. I_{NaR} amplitude was measured relative to the leak-subtracted baseline as shown in Figure 9. Accordingly, I_{NaR} amplitude is reported throughout the text as a relative amplitude. The relative amplitude of I_{NaR} was calculated as a percentage of the peak transient current generated during a test pulse to -10 mV from a holding potential of -100 mV, according to **Eq2**:

$$I_{NaR} \text{ amplitude}(\%) = \left(\frac{\text{Amplitude of } I_{NaR} \text{ (nA)}}{\text{Amplitude of Transient Current @ -10mV from a holding of -100mV (nA)}} \right) * 100$$

The average resurgent current amplitude for each experimental group was calculated using data from those cells in which I_{NaR} was detected. For experiments, employing transfected primary DRG neurons, data was only analyzed from those cells with minimal TTX-R contamination—cells with endogenous TTX-R currents greater than 10% of the peak current amplitude were excluded from analysis. Moreover, cells that expressed recombinant currents with peak transient sodium current amplitudes that were less than 5 nA were also excluded from the overall analysis due to concerns about measuring I_{NaR} with a low signal to noise ratio.

Figure 9:

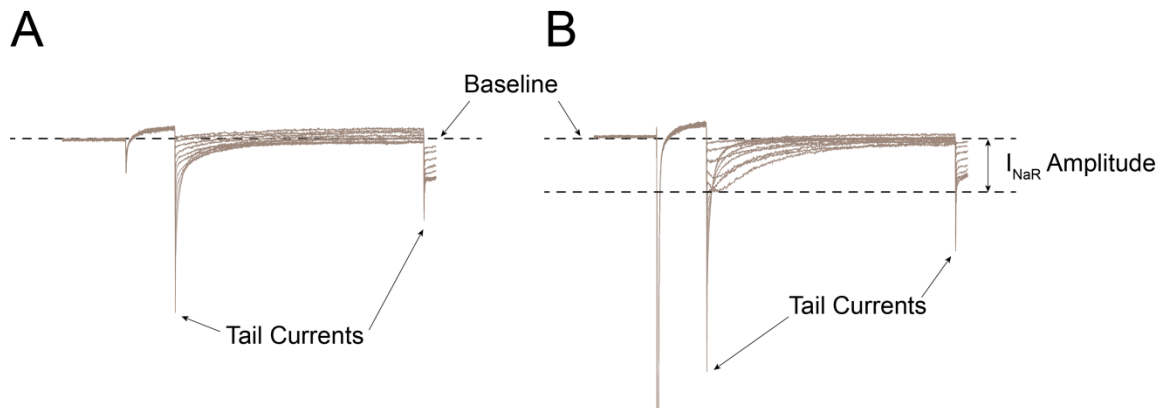


Figure 9: Quantification of resurgent sodium current amplitude. Sodium currents recorded from two different neurons. Currents were elicited with a 20 ms pulse to +30 mV followed by a 100 ms pulse to -40 mV from a holding potential of -100 mV. Tail currents can be observed in the recordings from both neurons (**A and B**). Robust resurgent current, with slower onset and decay than the tail currents (**B**), were observed in recordings from some neurons. For quantification the amplitude of I_{NaR} was measured relative to the baseline obtained at the holding potential. Relative I_{NaR} amplitude was reported as I_{NaR} amplitude (as shown above) divided by the amplitude of the transient current at -100 mV, according to **Eq 2**.

3. *qPCR data analysis*

Data from real-time RT-PCR experiments described in **Chapter(s) III and VI** were analyzed as described previously^{168,167}. Briefly, a real-time RT-PCR procedure employing SYBR Green I fluorescence dye was utilized to assess mRNA expression of sodium channel and auxiliary subunits isolated from DRG neurons (whole tissue). Quantification and comparison of gene expression data was done following a relative transformation of the raw data. Relative quantification of RT-PCR data is based on the expression of a target gene relative to a reference gene. An important consideration when using relative transformations is the identity and expression profile of the reference gene. The reference genes (internal control) should be expressed in the same cells as the target gene, the expression profile of the reference gene should be uniform under all experimental conditions, and the cycle threshold (C_t) of the reference gene should be similar to that of the target gene(s). For these experiments primers were designed for the reference genes HPRT and ARBP (see **Chapter II-H**).

The relative quantification of the target genes was determined according to the Pfaffl model¹⁷⁰. The Pfaffl model utilizes the values of two properties, C_t value (the cycle of threshold fluorescence) and primer PCR efficiency (E)—both are derived from the raw data, to estimate the relative expression ratio (R) of the target gene to the reference gene. In the Pfaffl model¹⁷⁰ the C_t value of the target is adjusted according to the E_{target} and compared to the C_t value of the reference, adjusted according to the $E_{\text{reference}}$. **Eq 3** outlines how R is derived for each target gene:

$$R = \frac{(E_{\text{target}})^{\Delta C_t \text{ target}}}{(E_{\text{reference}})^{\Delta C_t \text{ reference}}}$$

Where $\Delta C_t \text{ target}$ is the difference in C_t control and C_t treatment.

Data are displayed in figures as either % reference gene or treatment/naïve. Experimental data are based on cDNA isolated from 5-7 animals. All data shown are means \pm S.E.M. Statistical significance between current amplitudes was assessed with Microsoft Excel using a post-hoc single factor (one-way) ANOVA. Statistical significance of difference was accepted at *P* values less than 0.05.

Chapter III: *Characterization of resurgent sodium current (I_{NaR}) properties and distribution in rat dorsal root ganglion (DRG) neurons*

A. Introduction

Voltage-gated sodium channels (VGSCs) are dynamic proteins that transition to different conformations in response to changes in the transmembrane voltage. Located in the plasma membrane, these dynamic proteins mediate the influx of Na^+ into the cell; thus, they play a fundamental role in regulating the excitability of all neurons. DRG neurons express an array of voltage-gated sodium currents which regulate the firing behavior of different nerve fibers. These peripheral neurons can express two types of macroscopic sodium currents, kinetically fast tetrodotoxin-sensitive (TTX-S) currents and kinetically fast, tetrodotoxin-resistant (TTX-R) currents, which amplify generator potentials and contribute to the rapid upstroke of the action potential. Interestingly, VGSCs in DRG neurons also produce smaller, persistent and subthreshold sodium currents, which by themselves do not contribute to either the amplification of membrane depolarizations or the upstroke of the action potential, but rather can influence the action potential firing characteristics in neurons. An example of such a subthreshold current is resurgent sodium currents (I_{NaR}).

Resurgent sodium currents are unusual sodium currents that activate during the recovery phase of the action potential where VGSCs are normally refractory to activity. I_{NaR} was initially described in cerebellar Purkinje neurons⁵⁵, however, they have since been described in other cerebellar neuron types¹¹⁷, subthalamic neurons¹¹³, mesencephalic trigeminal neurons¹²⁹, and neurons of the medial nucleus of the trapezoid body¹³⁰. Although relatively small in amplitude (~3% of peak transient current), I_{NaR} exhibit slow gating kinetics and unusual voltage-dependence, with peak currents near threshold for action potential firing, which make it suitable for augmenting excitability in neurons. The mechanism for I_{NaR} electrogenesis is hypothesized to result from the C-

terminus of the NaV β_4 -subunit interacting with the pore of the VGSC α -subunit. Strong evidence suggests that the NaV1.6 channel produces the majority of I_{NaR} found in neurons as the amplitude of resurgent sodium current is significantly reduced in recordings made from cerebellar Purkinje neurons of NaV1.6 knockout mice. Curiously, small I_{NaR} has been observed in some neurons of NaV1.6 knockout animals, suggesting that other sodium channel isoforms have the capacity to produce I_{NaR} under specific conditions.

Recently, our laboratory reported the presence of I_{NaR} in large diameter mouse DRG neurons with comparable properties (i.e., voltage dependence, current amplitude, etc...) to those found in cerebellar Purkinje neurons¹³¹. In this dissertation I explore the mechanism of I_{NaR} electrogenesis in DRG neurons and determine if the biophysical properties of these unique currents are altered by mutations that cause inherited channelopathies or by a model of contusive spinal cord injury. In this section I characterize the properties and distribution of I_{NaR} found in rat DRG neurons and ask which VGSC isoforms might produce this current in DRG neurons. As much of what is known about I_{NaR} has been worked out in mice, results presented here confirm the presence of I_{NaR} in rat DRG neurons and provide foundational knowledge for experiments performed in subsequent chapters.

B. Original experimental results:

1. *Resurgent sodium currents in native rat DRG neurons*

A previous report by Dr. Cummins suggested that resurgent sodium currents (I_{NaR}) were observed in some large diameter DRG neurons from wild-type mice. To determine whether rat DRG neurons expressed I_{NaR} , I performed whole-cell voltage clamp recordings from L1-L6 DRG neurons, 3 to 24 hours after acute dissociation and plating of DRG neurons (see **Chapter II-E** for details). Briefly I_{NaR} were elicited using a strong depolarization (20 ms at +30 mV) followed by intermediate repolarization pulses to voltages ranging from +25 to -70 mV (for 100 ms)—this protocol referred to herein as the standard I_{NaR} protocol is shown in Figure 10-B. Because I_{NaR} described in cerebellar Purkinje and DRG neurons are observed at depolarized voltages and are relatively small, recordings were made with internal cesium and external TEA to block outward potassium currents which may convolute I_{NaR} measurement. I_{NaR} was recognized in recorded neurons according to the presence of several distinguishing characteristics outlined by previous investigators, including its unique voltage dependence and distinct rising and decaying kinetics. For these experiments I_{NaR} amplitude was measured as described in **Chapter II-L2** and reported as percentage of peak transient sodium current amplitude.

A previous report by Dr. Cummins suggested that I_{NaR} was not observed in small (defined as $< 35 \mu\text{m}$ in diameter or $< 35 \text{pF}$ ^f) diameter DRG neurons, but was observed in approximately 44% of large diameter DRG neurons (defined as 35-50 μm in diameter or 35-50 pF) with an average amplitude of $2.1\% \pm 0.4\%$ ¹³¹. Similar to Dr. Cummins' report, resurgent sodium currents were not observed in small (defined as soma diameter $< 35 \mu\text{m}$ or $< 35 \text{pF}$) diameter DRG neurons ($n=15$); Figure 10-A). However, robust I_{NaR}

^f Under the culture and recording conditions utilized here 1 μm is approximately 1 pF for recordings made within 24 hours.

was recorded in 14 out of 52 medium and large (defined as soma diameter $>35\ \mu\text{m}$ or $>35\ \text{pF}$) diameter cells with an average amplitude of $3.2\% \pm 0.5\%$ (Figure 10-C); although some medium and large diameter DRG neurons exhibited I_{NaR} , many produced rapidly decaying tail currents at intermediate voltages (Figure 10-D). Interestingly, of all the medium and large diameter DRG neurons recorded from, 11 of the 14 which exhibited I_{NaR} had a whole-cell capacitance ranging from 40pF to 55pF with an average of $46.9\text{pF} \pm 1.1\text{pF}$ suggesting I_{NaR} in DRG neurons exists in a very narrow subpopulation of medium diameter DRG neurons. This observation of restricted I_{NaR} exhibition is better illustrated in Figures 11-A and -B where histograms display the frequency of I_{NaR} versus the whole cell capacitance demonstrate that I_{NaR} is observed in a subpopulation of medium diameter DRG neurons.

Figure 10:

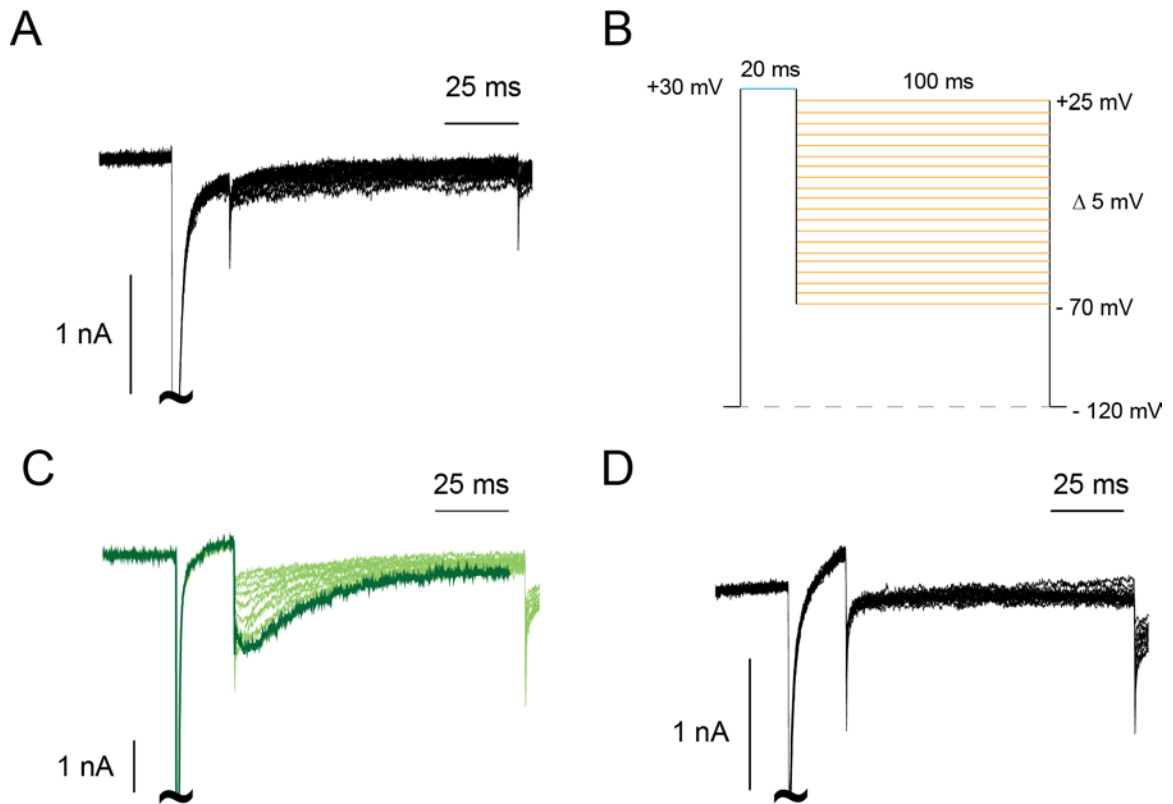


Figure 10: Resurgent sodium currents (I_{NaR}) detected in some, but not all, DRG neurons. (A) Family of sodium currents recorded from a small DRG neuron (26.49 pF). No I_{NaR} was observed in small diameter (soma diameter < 35 μ m) DRG neurons. **(B)** I_{NaR} were evoked by repolarizations to voltages ranging from +25 to -70 mV, in increments of 5 mV, after a brief depolarization to +30 mV. **(C)** Family of sodium currents recorded from a medium/large diameter, defined as (cell soma diameter > 35 μ m), DRG neuron (47.52 pF) with robust I_{NaR} . The peak I_{NaR} current trace (at -40 mV) is highlighted in **green**. **(D)** Representative sodium current trace of a medium/large diameter DRG neuron (42.13 pF) without I_{NaR} .

Figure 11:

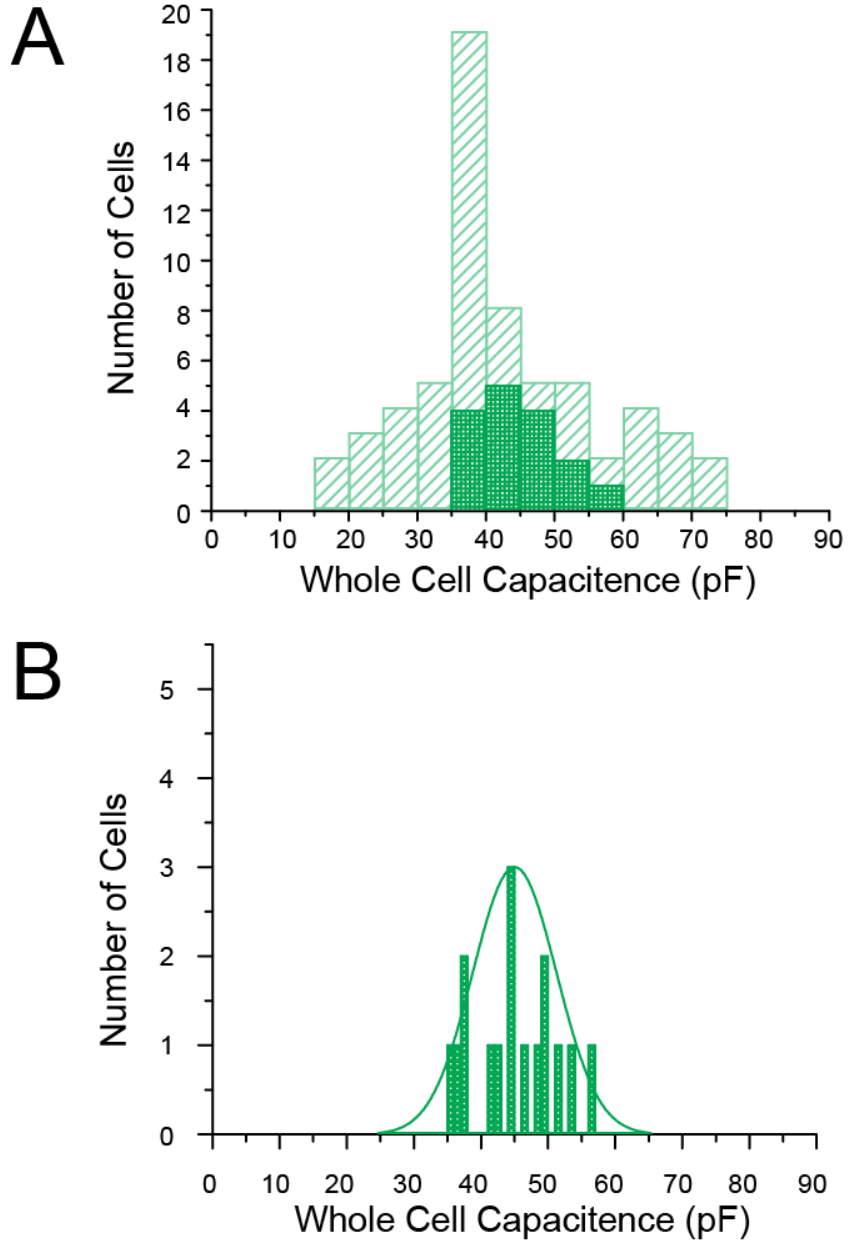


Figure 11: Distribution of native resurgent sodium currents (I_{NaR}) in rat DRG neurons. Native I_{NaR} in rat DRG neurons is observed in a narrow population of medium diameter DRG neurons (typically between 40-50pF). Frequency histograms shown in **(A)** display the number of cells expressing I_{NaR} versus the cell whole-cell capacitance (\propto to cell size). **(A)** shows the total number of cells recorded from for each cell size (bin equal to 5 pF) with hatched bars and the frequency of cells expressing I_{NaR} for each cell size with shaded bars. **(B)** shows the frequency of cells expressing I_{NaR} for each cell size (bin equal to 1pF); the data in **(B)** is fit with a normalized distribution function with the area under the curve representing the probability of a cell expressing I_{NaR} .

Next, I explored whether I_{NaR} in rat DRG neurons exhibited similar properties to those found in mouse cerebellar Purkinje and DRG neurons. Previous reports of I_{NaR} in cerebellar Purkinje and DRG neurons suggested that the current was sensitive to 500 nM TTX—suggesting I_{NaR} is produced by a TTX-S VGSC^{105,131}. To further explore the origins of these currents, three cells exhibiting I_{NaR} were exposed to 500 nM TTX and, in each case, TTX blocked the resurgent current (Figure 12-A), confirming the I_{NaR} in rat DRG neurons is produced by TTX-S VGSCs. Additionally, I_{NaR} found in rat DRG neurons exhibit voltage dependence similar to those reported in mouse cerebellar Purkinje and DRG neurons (Figure 12-B)^{105,131}. The resurgent current was first detected near -10mV, was maximal near -30mV to -40mV, and became too small and too fast to be resolved negative of -60 mV (Figure 12-C). The current also displayed kinetics characteristic of I_{NaR} with a distinct, slow rising phase followed by slow decaying phase. Near -35 mV, a potential near the peak resurgent current, the rising phase time constant, τ_m , is 2.83 ± 0.212 ms and the decay phase, τ_h , time constant is 23.3 ± 1.06 ms (Figure 12-D). These kinetics are much slower than those of conventional sodium currents evoked by depolarizing steps, which rise in < 0.3 ms and have a dominant decay τ near 1 ms⁵⁵. With repolarization to more negative potentials (-60 mV), the resurgent current is smaller, occurs with an earlier peak ($\tau_m=0.077 \pm 0.027$ ms), and decays faster ($\tau_h=12.8 \pm 15.6$ ms) (Figure 12-D). Additionally, both τ_m and τ_h are strongly voltage-dependent in the range of -60 mV to -35 mV. Collectively, these results demonstrate that I_{NaR} found in rat medium and large diameter DRG neurons exhibit similar properties to those described previously in mouse peripheral and central neurons.

Figure 12:

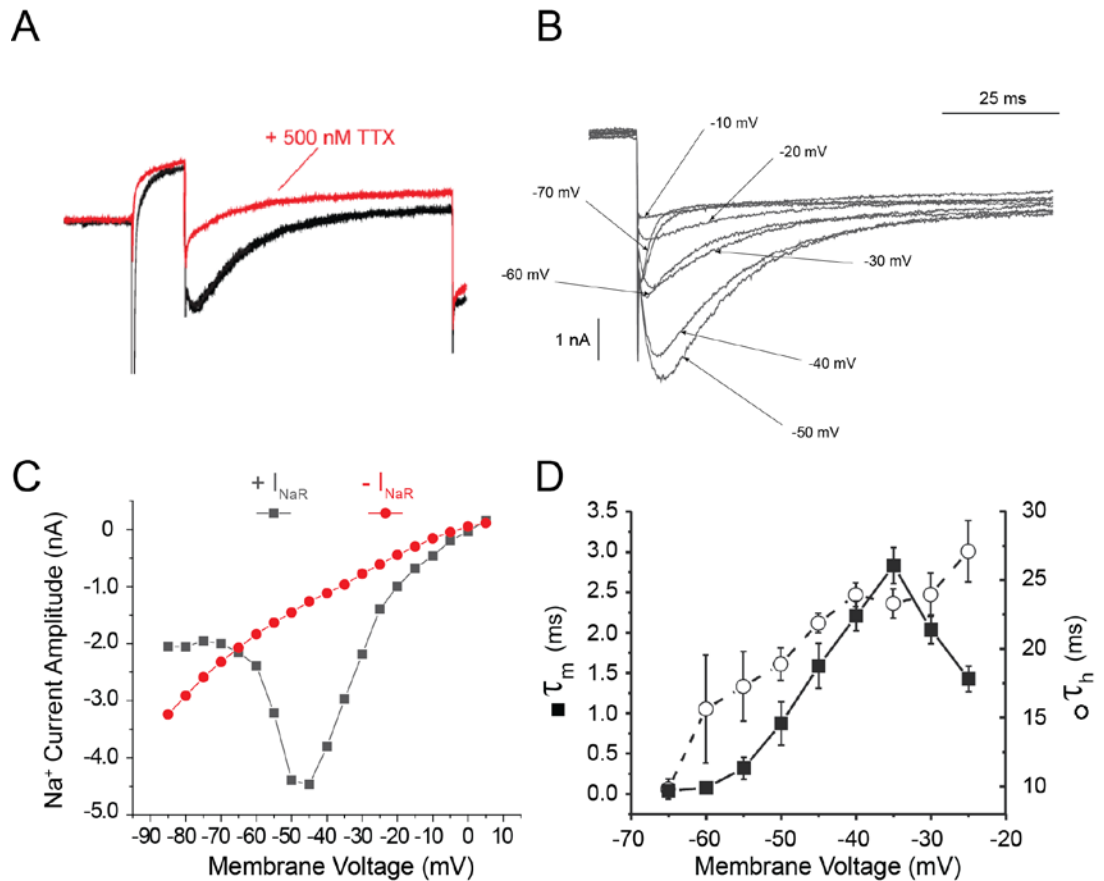


Figure 12: Properties of resurgent sodium currents (I_{NaR}) in rat DRG neurons. I_{NaR} in rat DRG neurons are produced by TTX-S VGSC. **(A)** I_{NaR} currents from a medium diameter rat DRG neuron (51 pF) before (**black trace**) and after 500 nM TTX (**red trace**). I_{NaR} in rat DRG neurons exhibit distinct voltage-dependence and kinetics similar to those observed by other investigators in mouse cerebellar Purkinje and DRG neurons. **(B)** Representative I_{NaR} current trace from medium diameter (40pF-55pF) rat DRG neurons. **(C)** The voltage dependence of I_{NaR} for the trace shown in **(B)** is shown by plotting I_{NaR} current amplitude versus the potential with which it was elicited. Cells with I_{NaR} exhibit distinct voltage-dependence between -10 mV and -80 mV (**shown in dark grey**); whereas cells with classic tail currents (no I_{NaR}) exhibit no voltage-dependence in the same voltage range (**shown in red**). **(D)** Kinetic activation (τ_m) and inactivation (τ_h) time constants plotted over a range of voltages for a cell with I_{NaR} . I_{NaR} exhibits slow activation and ultra-slow inactivation kinetics. Error bars in **(D)** are shown as \pm standard error (n=20).

2. Sodium channel auxiliary $\text{NaV}\beta_4$ subunit is expressed in rat DRG neurons.

Having established that rat DRG neurons express robust I_{NaR} , I next explored if proteins hypothesized to be important in I_{NaR} electrogenesis are present in rat DRG neurons. Previous experiments in cerebellar Purkinje neurons suggested that the $\text{NaV}\beta_4$ subunit plays an integral role in the electrogenesis of I_{NaR} ¹⁰². Specifically, experiments in cerebellar Purkinje neurons by Grieco and colleagues¹⁰² demonstrated that after enzymatic removal of I_{NaR} block, application of $\text{NaV}\beta_4$ ₁₅₄₋₁₆₇ peptide fully reconstituted open-channel block and I_{NaR} , suggesting that the cytoplasmic tail of $\text{NaV}\beta_4$ may serve as the open channel blocker that causes the alternative inactivation which causes I_{NaR} . Yu *et al.*¹⁹ demonstrated, using TaqMan quantitative RT-PCR, that expression of $\text{NaV}\beta_4$ was highest in DRG neurons⁹ compared to other tissues. Here I confirm that mRNA for the $\text{NaV}\beta_4$ -subunit is expressed in rat DRG neurons (Figure 13-A).

Because some but not all rat DRG neurons express resurgent sodium current, I have hypothesized that I_{NaR} is exhibited in neurons that have enriched expression of proteins important for I_{NaR} electrogenesis. Indeed, Yu *et al.* suggested that $\text{NaV}\beta_4$ -subunit mRNA expression was present in some small and intermediate-sized cells but was enhanced in the majority of large diameter DRG neurons¹⁹ a population of DRG neurons which express frequent resurgent sodium currents. Here I explored the cellular distribution of $\text{NaV}\beta_4$ protein expression in rat DRG neurons with the suggestion that localized or enriched expression of $\text{NaV}\beta_4$ in rat medium/large diameter DRG neurons might account for the restricted expression of I_{NaR} to a subpopulation of medium/large diameter (40 to 55 μm). To test this hypothesis acutely dissociated rat DRG neurons were stained with a polyclonal $\text{NaV}\beta_4$ antibody (see **Chapter II-K** for details). Interestingly, in rat DRG neurons, $\text{NaV}\beta_4$ is found in small, and medium/large diameter

⁹ Prepared from whole tissue.

DRG neurons (Figure 13-B). These findings suggest that restricted protein expression of NaV β_4 does not appear to account for localized expression of I_{NaR} in some medium/large diameter DRG neurons, because NaV β_4 protein is also observed in small diameter DRG neurons—cells which do not normally produce I_{NaR}.

Figure 13:

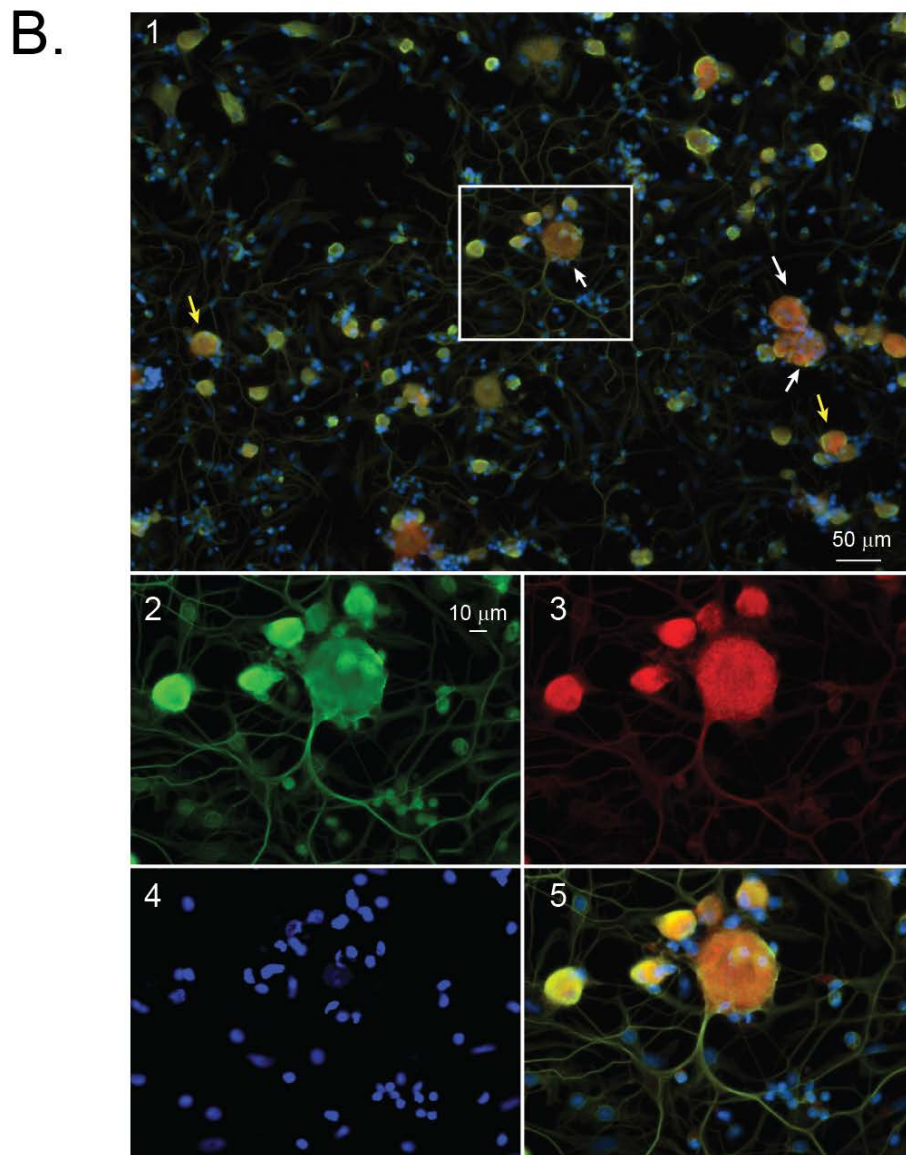
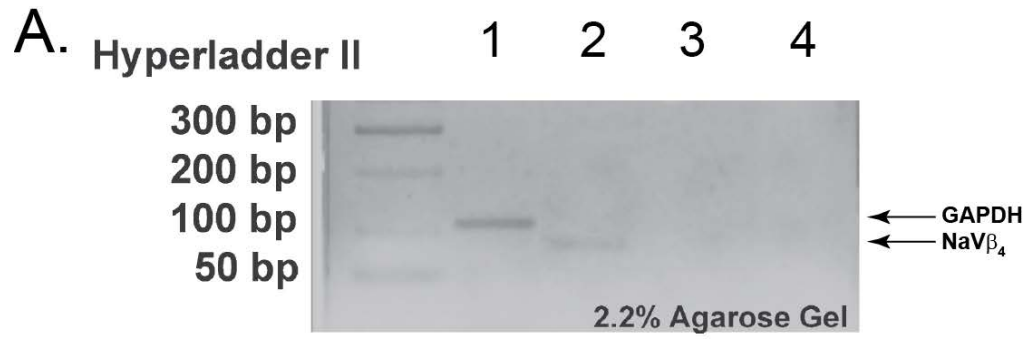


Figure 13: Suspected resurgent sodium current (I_{NaR}) open channel blocker, $NaV\beta_4$, mRNA and protein are expressed in rat DRG neurons. Previous reports by Yu *et al.* suggested $NaV\beta_4$ expression is highest in DRG neurons. Here I confirmed the presence of mRNA for $NaV\beta_4$ in rat DRG neurons. **(A)** The gel shown in Figure 3.4-A lane 2 demonstrates that mRNA for $NaV\beta_4$ is present in rat DRG neurons. Here GAPDH was used as a positive control for conventional PCR **(A-lane 1)**. $NaV\beta_4$ is detected from total RNA isolated from L1-L6 rat DRG neurons **(A-lane 2)**. No PCR product was detected when template was not included in the PCR reactions for either GAPDH or $NaV\beta_4$ **(A-lane 3 and -lane 4)**. $NaV\beta_4$ primers: forward primer—CAGCGAAACATCCAGGATTCTC; reverse primer—CGGTCATCATCCTTAC-TCTCA. **(B)** $NaV\beta_4$ protein is found in small medium and large diameter DRG neurons. Here immunostaining of rat L1-L6 DRG neurons cultured for 24 hours and stained with a polyclonal $NaV\beta_4$ antibody reveals $NaV\beta_4$ protein is found in small (white arrows) and medium/large (yellow arrows) diameter DRG neurons. **(B-1)** a 10x merged image of a culture stained with polyclonal anti- $NaV\beta_4$, monoclonal β -tubulin, and Dapi mount. **(B-2 to B-5)** are 40x images of area highlighted by the white box in **B-1**. **(B-2)** β -tubulin staining in small and medium/large diameter DRG neurons; **(B-3)** $NaV\beta_4$ staining; **(B-4)** Dapi staining; **(B-5)** merge of β -tubulin, $NaV\beta_4$, and Dapi staining. β -tubulin staining is used here as a general neuronal marker in order to demonstrate that $NaV\beta_4$ protein is present neurons. Monoclonal anti β -tubulin antibody (1:500) and polyclonal anti- $NaV\beta_4$ (1:33).

3. *Resurgent sodium currents can be produced by multiple voltage-gated sodium channels in rat DRG neurons.*

To further explore the origins of I_{NaR} found in rat DRG neurons I next explored which VGSCs, expressed in DRG neurons, can produce resurgent sodium currents. Previously, our laboratory established that I_{NaR} found in mouse¹³¹ and rat DRG neurons was sensitive to 500 nM TTX (Figure 12-A)—suggesting that I_{NaR} is produced by a TTX-S VGSC. Additionally, strong evidence from our lab and others suggests the NaV1.6 channel isoform underlies most of the I_{NaR} found in cerebellar Purkinje and DRG neurons because I_{NaR} is significantly reduced [~90%] in NaV1.6-null mice^{112,121,131}. Still, the presence of residual I_{NaR} in NaV1.6-null mice has led some to speculate that I_{NaR} may be carried by other VGSC isoforms, including NaV1.1, NaV1.2, and NaV1.5, under specific conditions^{115,127}.

I employed a strategy of expressing recombinant VGSCs in DRG neurons in order to test which VGSC isoforms can produce I_{NaR} , and therefore might contribute to native resurgent sodium current found in rat DRG neurons. Previously, Waxman and colleagues had shown that recombinant NaV1.2 and NaV1.6 channels expressed in mouse DRG neurons can generate I_{NaR} ^{114,131}—providing proof of concept that DRG neurons may be the ideal cell background for testing which VGSC isoforms can produce I_{NaR} . Here I tested whether NaV1.3, NaV1.6, and NaV1.7—three of the prominently expressed TTX-S VGSCs found in the periphery—had the capacity to generate I_{NaR} in rat DRG neurons. In these experiments modified wild-type NaV1.3, NaV1.6, and NaV1.7 channels that generate currents which can be pharmacologically isolated, were expressed in adult rat DRG neurons using a biolistic transfection technique (see **Chapter II-B and -D**). In addition to the recombinant channel of interest, neurons were also co-transfected with a second plasmid encoding for both EGFP, to help identify transfected neurons, and a specific NaV1.8 shRNA, to minimize endogenous NaV1.8

currents (see **Chapter II-A and G** for specific details). Using this expression strategy I first sought to confirm whether NaV1.6 can generate I_{NaR} when expressed in rat DRG neurons. Robust resurgent current was observed in 8 of 14 rat DRG neurons transfected with NaV1.6, with an average amplitude (expressed as a percentage of peak transient sodium current elicited with a test pulse to -10 mV) of $2.4\% \pm 0.3\%$ for those 8 neurons (Figure 14-A); these reports support previous observations by Cummins and colleagues¹³¹. Next, I tested whether NaV1.3 and NaV1.7 have the capacity to generate I_{NaR} when expressed in rat DRG neurons. Interestingly, robust I_{NaR} was observed in 5 of 21 neurons expressing NaV1.7 ($1.0\% \pm 0.5\%$) and 5 of 8 neurons expressing NaV1.3 ($3.77\% \pm 0.83\%$) (Figures 14-B and -C). Although I_{NaR} is only found in a subpopulation of untransfected medium/large diameter DRG neurons, I_{NaR} can be observed in small and large biolistically transfected neurons expressing recombinant VGSCs. Based on this observation I speculate that all DRG neurons, regardless of cell soma size, may have the capacity to produce I_{NaR} under the right experimental conditions.

Figure 14:

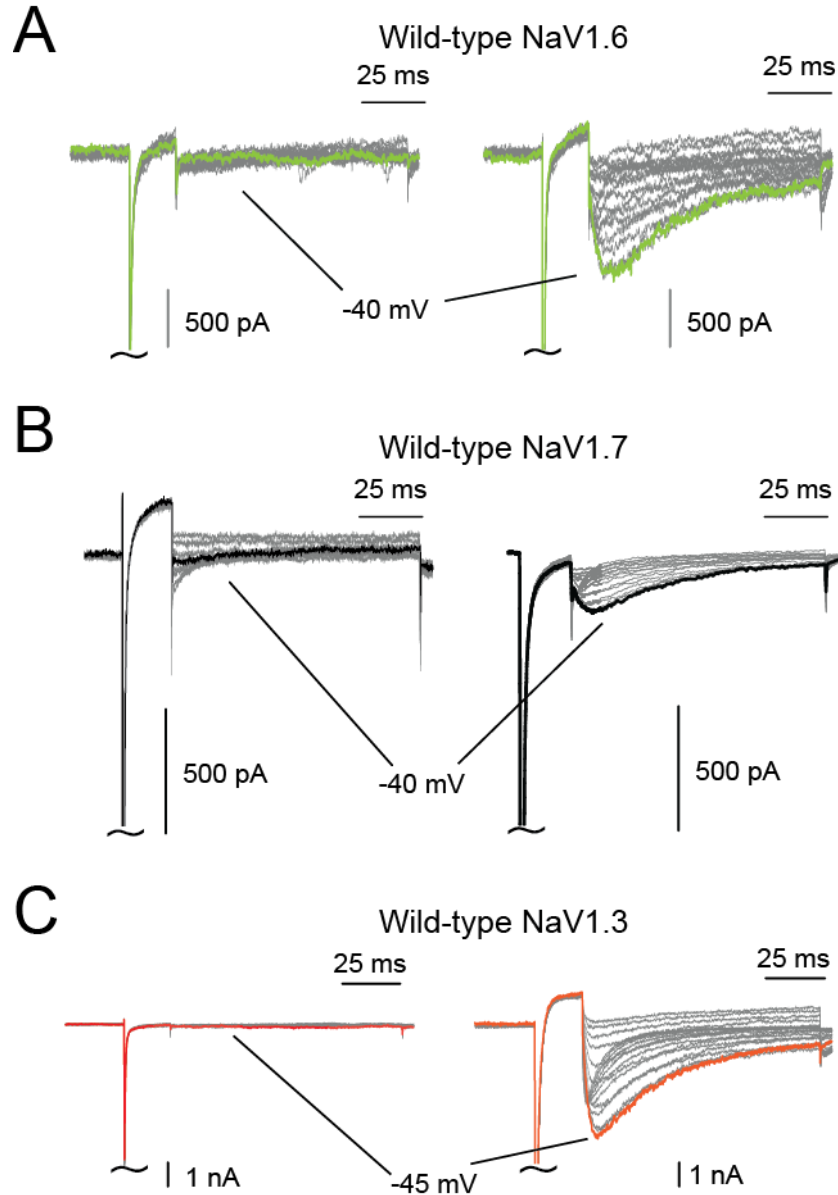


Figure 14: Resurgent sodium currents (I_{NaR}) are produced by recombinant wild-type NaV1.6, -1.7, and -1.3 channels expressed in rat DRG neurons. (A) Representative current traces recorded from rat DRG neurons expressing recombinant wild-type NaV1.6 that did not (A-left) and that did (A-right) generate I_{NaR} . (B) Representative current traces recorded from rat DRG neurons expressing recombinant wild-type NaV1.7 that did not (B-left) and that did (B-right) generate I_{NaR} . (C) Representative current traces recorded from rat DRG neurons expressing recombinant wild-type NaV1.3 that did not (C-left) and that did (C-right) generate I_{NaR} . For comparison, the peak I_{NaR} amplitude trace is highlighted in each exemplar trace with I_{NaR} and the corresponding trace is also highlighted for the exemplar trace without I_{NaR} . Currents were elicited with the standard I_{NaR} voltage protocol shown in Figure 3.1-B.

C. Discussion

In this section I explored the hypothesis that rat DRG neurons also produce resurgent sodium current and explored which VGSCs might contribute to I_{NaR} observed in rat DRG neurons. Data presented in this chapter demonstrate the following: (1) TTX-S I_{NaR} is found in a subpopulation of medium/large diameter rat DRG neurons, (2) I_{NaR} found in rat DRG neurons exhibits similar properties to those described previously in mouse central and peripheral neurons, (3) $Nav\beta_4$ subunit mRNA and protein are expressed in rat DRG neurons, and (4) Nav1.3, Nav1.6, and Nav1.7 channels have the capability of producing I_{NaR} when expressed in DRG neurons.

Native TTX-S resurgent sodium currents in peripheral DRG neurons were previously described by Cummins and colleagues. According to Cummins *et al.* 2005, I_{NaR} were not observed in small diameter mouse DRG neurons but were present in ~44% of large diameter mouse DRG neurons. In this study I confirmed the presence of TTX-S I_{NaR} in rat DRG neurons. In agreement with the previous report, I_{NaR} were not observed in small diameter rat DRG neurons but robust I_{NaR} were observed in ~27% of medium/large diameter DRG neurons. In many medium and large diameter DRG neurons peak I_{NaR} amplitude exceeded 1 nA with a relative amplitude of $3.2\% \pm 0.5\%$. These large resurgent sodium currents in rat DRG neurons exhibited similar TTX-sensitivity, voltage-dependence, and kinetic properties to those observed in mouse DRG and cerebellar Purkinje neurons. Interestingly, despite their many similarities I_{NaR} are observed slightly less frequently in rat DRG neurons compared to mouse DRG neurons (I_{NaR} present in 44% of mouse medium/large diameter DRG neurons versus 27% of rat medium/large diameter DRG neurons) and I_{NaR} amplitude is increased in rat DRG neurons compared to mouse DRG neurons (I_{NaR} amplitude in mouse: $2.1\% \pm 0.4\%$; I_{NaR} amplitude in rat: $3.2\% \pm 0.5\%$). While neither of these differences are statistically significant they highlight the fact that there may be species specific differences in I_{NaR}

localization and properties. Collectively these data demonstrate my ability to measure I_{NaR} in acutely cultured DRG neurons and show that robust I_{NaR} is present in a subpopulation of rat medium/large diameter rat DRG neurons.

Previous reports from our lab and others suggest that the Nav1.6 channel isoform is a major contributor to I_{NaR} in cerebellar Purkinje and CNS neurons. I explored which VGSC isoforms, expressed in DRG neurons, might contribute to I_{NaR} found in DRG neurons. Characterizing the individual contribution of specific channel isoforms to currents observed in primary cell cultures has been difficult due to the lack of availability of isoform selective inhibitors. Without the capability to parse out the contribution of individual isoforms to native I_{NaR} I asked a parallel question: which VGSCs expressed in DRG neurons are capable of producing I_{NaR} ? Still addressing this question comes with its own technical challenges. The mechanism of resurgent current electrogenesis is complex—resurgent inactivation kinetics are not an inherent property of the sodium channel, but rather may result from a poorly understood interaction between the Nav β_4 -subunit and the sodium channel pore. The complex nature of I_{NaR} electrogenesis has made it difficult to reconstitute the exact cellular conditions which allow for the production of I_{NaR} in heterologous expression systems. For these studies I utilized a DRG expression system previously developed by Dr. Cummins, where modified recombinant sodium channel isoforms are biolistically transfected in acutely cultured mouse DRG neurons. Using this expression system Dr. Cummins was able to show that recombinant Nav1.6 channels expressed in mouse DRG neurons can generate resurgent currents in approximately 60% of transfected neurons—indicating that cultured DRG neurons provide an opportune expression system for investigating the capability of VGSCs to generate resurgent current. I optimized the expression strategy for rat DRG neurons and demonstrated, for the first time, that the Nav1.3 and Nav1.7 channel isoforms can also produce robust I_{NaR} when expressed in DRG. Interestingly, in a previous report by

Cummins and colleagues, NaV1.4 and NaV1.7 did not produce I_{NaR} when expressed in mouse DRG neurons¹³¹. My observation of robust I_{NaR} in NaV1.7 in some rat DRG neurons, again, highlights possible species specific differences in I_{NaR} properties between rat and mouse, and underscores the importance of characterizing the properties of I_{NaR} in rat DRG neurons before exploring whether I_{NaR} is altered following injury or inflammation as most of these animal models are commonly done in rats.

Similar to Dr. Cummins' previous report, native resurgent sodium currents were found in a subpopulation of medium/large diameter rat DRG neurons and are not observed in small diameter DRG neurons. As previously discussed due to the complex nature of I_{NaR} electrogenesis, elements of the cell background, including expression of proteins involved in the generation and regulation of I_{NaR} , are likely important in determining which cells natively express I_{NaR} in DRG neurons. Moreover, the observation of I_{NaR} in a specific size class of DRG neurons suggests that there must be differential expression of some factors which allow for robust I_{NaR} in medium/large diameter DRG neurons and not in small diameter DRG neurons. Two proteins which are hypothesized to be important in I_{NaR} electrogenesis are NaV1.6, the sodium channel which underlies much of the native I_{NaR} in neurons, and NaV β_4 , the sodium channel auxiliary β -subunit which has been proposed to serve as the open-channel blocker which confers resurgent inactivation kinetics. My observation of I_{NaR} in a subpopulation of medium/large DRG neurons may be explained by enriched mRNA expression of NaV1.6⁵² and NaV β_4 ¹⁹ in that size class of DRG neurons. However, it seems unlikely that NaV1.6 and NaV β_4 expression alone is sufficient to produce I_{NaR} because (1) I_{NaR} can be produced by other VGSC isoforms including NaV1.2¹¹⁴, NaV1.3^h, and NaV1.7ⁱ and (2) I_{NaR} are not observed in neuronal populations which express both NaV1.6 and

⁹ Observation made in this report (see Figure 14-B and -C)

ⁱ Observation made in this report (see Figure 13-B)

NaV β_4 , including hippocampal CA3 neurons¹⁰⁵, spinal neurons¹²¹, or small diameter DRG^j neurons^{19,171}. This rationale is supported by experiments in hEK293 or ND7/23 cells which found that overexpression of NaV1.6 and NaV β_4 by themselves is not sufficient to generate I_{NaR} ¹²⁴. Taken together, these observations suggest that while NaV1.6 and NaV β_4 may be involved in the electrogenesis of I_{NaR} there are likely other factors which contribute to the localized genesis of I_{NaR} in a specific subpopulation of DRG neurons.

Here I speculate that candidate mechanisms which might be important for I_{NaR} generation in specific cell populations include: subcellular co-localization of NaV1.6 with the NaV β_4 subunit and post-translational regulation of subunits involved in the generation of I_{NaR} . While several reports indicate that NaV β_4 and NaV1.6 are expressed in some cells that do not produce I_{NaR} it is not clear whether both subunits are found in the same subcellular compartments. The working hypothesis of I_{NaR} electrogenesis involves close association between a VGSC capable of producing I_{NaR} and NaV β_4 . Here I speculate that NaV1.6 and NaV β_4 may not coexist in the same subcellular compartment or interact in cells which do not produce I_{NaR} but express both subunits. A report from Raman and colleagues supports such speculation, where NaV1.6 and NaV β_4 do not co-immunoprecipitate even though both subunits are expressed in hippocampal CA3 neurons and I_{NaR} is not observed¹⁰². According to this logic NaV1.6 and NaV β_4 may only associate or exist in the same subcellular compartment in a subpopulation of medium/large diameter DRG neurons resulting in localized expression of I_{NaR} . Phosphorylation has also been implicated in modulating I_{NaR} ¹¹¹. More specifically, constitutive phosphorylation appears necessary to maintain I_{NaR} amplitude in cultured cells¹¹¹. Consequently, I speculate that differential kinase or phosphatase activity in

^j Observation made in this report (see Figure 13-B)

small and medium/diameter DRG neurons might underlie the cell specific localization of I_{NaR} in peripheral DRG neurons.

The results presented in this section of my dissertation demonstrate the presence of I_{NaR} in rat DRG neurons. Specifically, I characterized the properties and distribution of this current and found that I_{NaR} exist in a subpopulation of medium/large diameter DRG neurons (40pF-55pF). Additionally, I demonstrated that NaV1.3, NaV1.6, and NaV1.7 channels have the capacity to generate I_{NaR} and therefore may contribute to resurgent currents isolated in rat DRG neurons. Although the exact role that resurgent sodium currents play in normal sensory neuronal excitability remains unclear, the observation that such a labile sodium conductance exists in a specific size class of DRG neurons, may reflect the functional modality of these sensory neurons. Having characterized the properties of I_{NaR} in rat DRG neurons, I next explore whether the properties of I_{NaR} were altered by single point mutations which slow the rate of channel inactivation or by peripheral spinal cord injury.

Chapter IV: *Mutations that slow the rate of channel inactivation and cause neuronal and muscle channelopathies increase I_{NaR} amplitude and frequency.*

I next explored whether mutations which slow the rate of channel inactivation and cause neuronal and muscle channelopathies increase I_{NaR} . This work was a collaboration between myself, Dr. Theodore Cummins, and Dr. Brian W. Jarecki, a former Department of Pharmacology and Toxicology graduate student. Although some of this work has already been published in Brian's dissertation, I briefly discuss the rationale and results of this study below because it is an important part of my graduate work. An unabridged copy of the published work is included in **Appendix A**.

A. Introduction and Hypothesis Rationale

Results from Raman and colleagues suggest that in neurons exhibiting I_{NaR} can undergo two forms of channel inactivation, which compete with each other: [classical] domain III-IV linker (IFM) mediated channel inactivation and an endogenous open-channel block^{115,127}. Evidence for two, competing forms of channel inactivation have led some to hypothesize that impairing the rate of intrinsic channel inactivation may increase the probability that the channel will undergo open-channel block, resulting in increased proclivity for an ion channel to produce I_{NaR} or increase the I_{NaR} amplitude (Figure 15). Indeed, in NaV1.6 knockout mice, I_{NaR} amplitude is decreased in cerebellar Purkinje neurons and the rate of channel inactivation is significantly faster as compared to wild-type neurons. Computer simulations modeling a cerebellar Purkinje neuron with resurgent sodium current confirmed that faster channel inactivation kinetics was likely to produce small I_{NaR} ; this observation suggested that the rate of channel inactivation is likely an important factor governing I_{NaR} electrogenesis¹³². In support of this hypothesis, artificial slowing of VGSC inactivation via β -pompilidotoxin application can increase I_{NaR} amplitude in cerebellar Purkinje neurons isolated from NaV1.6 knockout mice¹²⁷.

Collectively, these findings suggest that the rate of channel inactivation may be an important factor which determines how large I_{NaR} amplitude is and which VGSC express I_{NaR} .

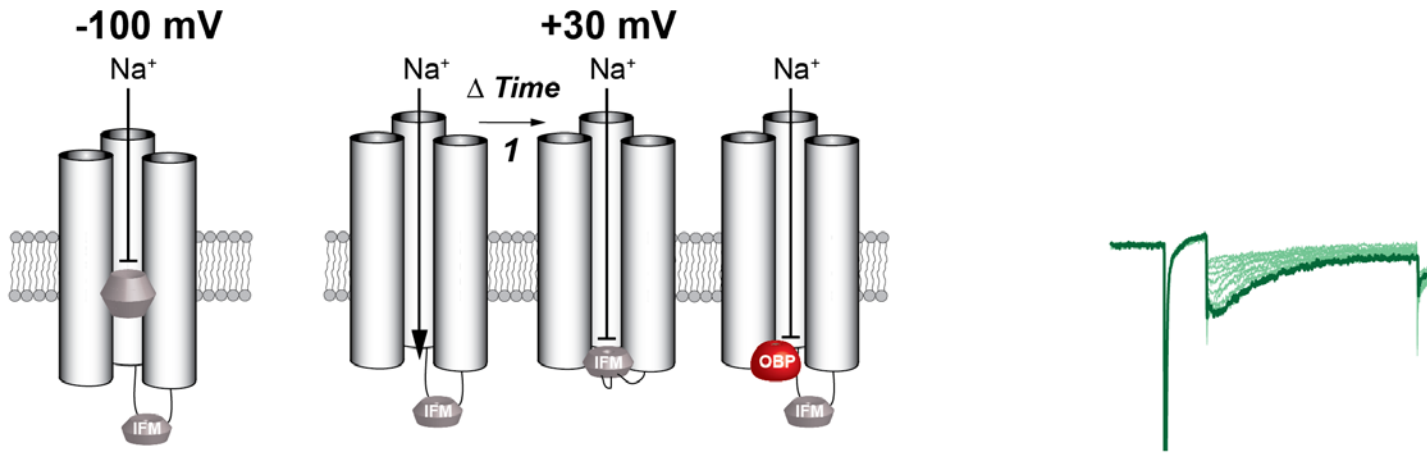
Interestingly, more than 200 different missense mutations in 7 VGSCs have been identified as causing a broad spectrum of neurological disorders, or channelopathies, in humans, including epilepsy, painful neuropathies, and non-dystrophic myopathies. In many cases these mutations either alter the stability of the dynamic channel structure, resulting in increased leak or persistent currents and/or altered voltage-dependence or kinetics of channel state conformational change. Mutant channels have been extensively studied in non-excitabile heterologous expression systems, providing substantial knowledge; however, a major concern is that the functional properties of VGSCs in muscle and neurons are not accurately reproduced in non-excitabile cells. A prime example of this phenomenon is VGSC resurgent currents. Although I_{NaR} have been recorded from neurons, it has not been possible to record resurgent currents in non-excitabile heterologous expressions systems, and it is not known whether VGSC channelopathy mutations which slow the rate of channel inactivation increase I_{NaR} .

In this study I reasoned that since application of a toxin which slows the rate of channel inactivation increases I_{NaR} then missense mutations in VGSCs that slow the rate of channel inactivation should also enhance I_{NaR} amplitude (Figure 15). Specifically, I explored the hypothesis that disease mutations which slow or destabilize sodium channel inactivation will lead to increased I_{NaR} amplitude in the mutant channels. To test my hypothesis I used the expression strategy outlined in the previous chapter. According to the expression paradigm, modified VGSCs that generate currents that can be pharmacologically isolated were expressed in adult rat DRG neurons. In addition to the recombinant channels of interest, neurons were also co-transfected with a second plasmid encoding for both EGFP (to aid in identification of transfected neurons) and a

specific shRNA, to minimize endogenous NaV1.8 currents (see **Chapter II-A** and **-G**) for further information). Using these expression strategies I found that recombinant NaV1.3, NaV1.6, and NaV1.7 channels can generate I_{NaR} when expressed in DRG neurons (see **Chapter III-Figure 14**). Moreover, my observation of I_{NaR} in approximately 45% of the all transfected neurons indicated that DRG neurons are a reasonable cell background for testing my hypothesis. Using this methodology, I demonstrated that disease mutations which slow the rate of channel inactivation in three different VGSC isoforms increased resurgent sodium current amplitude and frequency.

Figure 15:

A



B

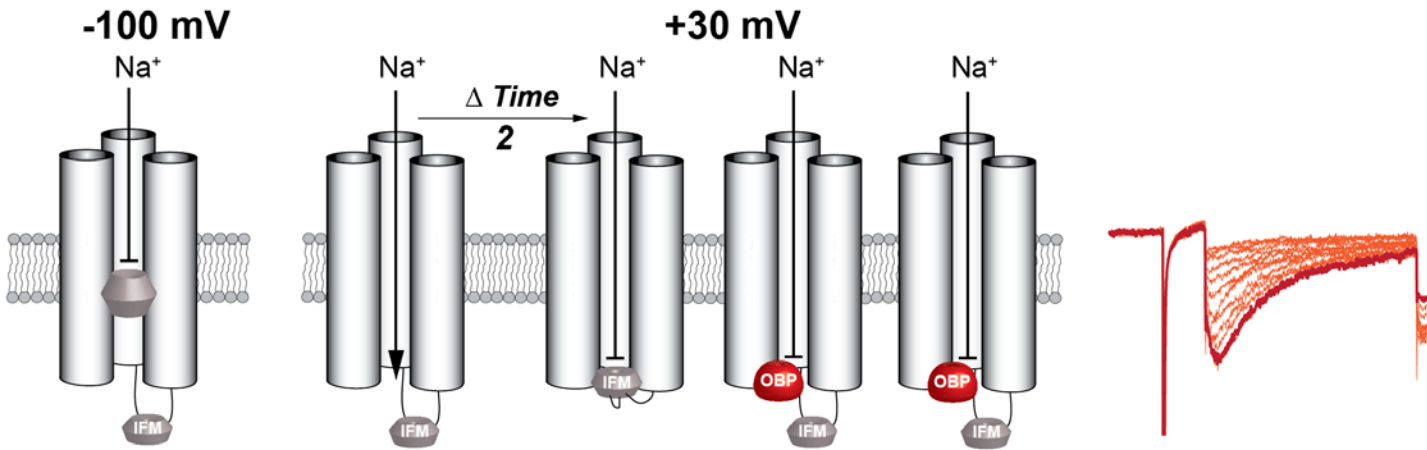


Figure 15: Rationale for increased I_{NaR} frequency and amplitude with slowed rate of channel inactivation. *IFM* represents the gate underlying normal, fast inactivation. *OBP* represents the putative blocking element that produces “open-channel block” with I_{NaR} . At very negative potentials (-100 mV) VGSCs are closed and ready to open—both IFM and OBP are unbound. Normally, with membrane depolarization VGSCs open, briefly allowing sodium to diffuse into the cell, and subsequently rapidly inactivate via the fast inactivation gate IFM. In cells with I_{NaR} channels can be inactivated by two mechanisms, either IFM or OBP, which compete with one another for the same or overlapping binding site in the channel pore. **(A)**. Under normal conditions where I_{NaR} is present, a limited number of channels are inactivated by OBP because the kinetic rate transition of the channel from open to inactivated via IFM is very fast **(A-1)**. However, when the kinetic rate transition of the channel from open to IFM inactivated is impaired by structural mutations **(B-2)** it is hypothesized that OBP is able to “out-compete” IFM for binding to the channel pore resulting in a large population of channels binding OBP and increased I_{NaR} amplitude **(B)**.

B. Original experimental results

1. *NaV1.7 PEPD mutations which slow the rate of channel inactivation increase resurgent sodium currents.*

The first mutation we examined with slowed or destabilized channel inactivation was a paroxysmal extreme pain disorder (PEPD) mutation in NaV1.7¹⁷². Highly expressed in DRG neurons, NaV1.7 channels are essential for nociception, as evidenced by single point, missense mutations causing a spectrum of pain syndromes including PEPD, and by nonsense mutations resulting in human insensitivity to pain¹⁷³. Previously, our lab has demonstrated that PEPD mutations destabilize inactivation, shifting the voltage dependence of steady-state inactivation, and impairing the rate of channel inactivation^{156,174}. Here we examined whether the PEPD mutation I1461T, located in the DIII-DIV inactivation gate, produced increased resurgent current compared to wild-type (WT) NaV1.7. When expressed in DRG neurons the NaV1.7-I1461T PEPD mutation caused a +18 mV shift in steady-state voltage dependence of inactivation and significantly impaired the rate of channel inactivation [NaV1.7-I1461T τ_h at +10 mV is 21% slower than WT NaV1.7] (Figure 16-A-D); collectively, these observations were consistent with those reported in a previous characterization of this mutant in hEK293 cells¹⁵⁶. In the previous **Chapter I** demonstrated that I_{NaR} was observed in 5 of 21 neurons transfected with WT NaV1.7 with an average of $1.0\% \pm 0.5\%$ for these five neurons. Interestingly, I_{NaR} was observed in 20 of 30 neurons expressing the NaV1.7-I1461T PEPD mutant (Figure 16-E-H). The frequency of I_{NaR} in NaV1.7-I1461T channels was significantly increased ($P < 0.05$, chi-squared test) compared to WT NaV1.7 channels (Figure 16-G). Moreover, the relative amplitude of I_{NaR} was also significantly increased ($P < 0.05$) in NaV1.7-I1461T channels ($2.0\% \pm 0.1\%$) compared to WT NaV1.7 channels (Figure 16-F and H). Because all of the currently characterized PEPD mutations significantly impaired rate of channel inactivation in NaV1.7, I hypothesized that all

PEPD mutations are likely to increase I_{NaR} generation^{156,172,174}. Indeed, in a subsequent study, led by Dr. John Theile, we demonstrated that three additional PEPD mutants, NaV1.7-M1627K, -T1464I, and V1299F, all increase I_{NaR} amplitude¹²³.

Figure 16:

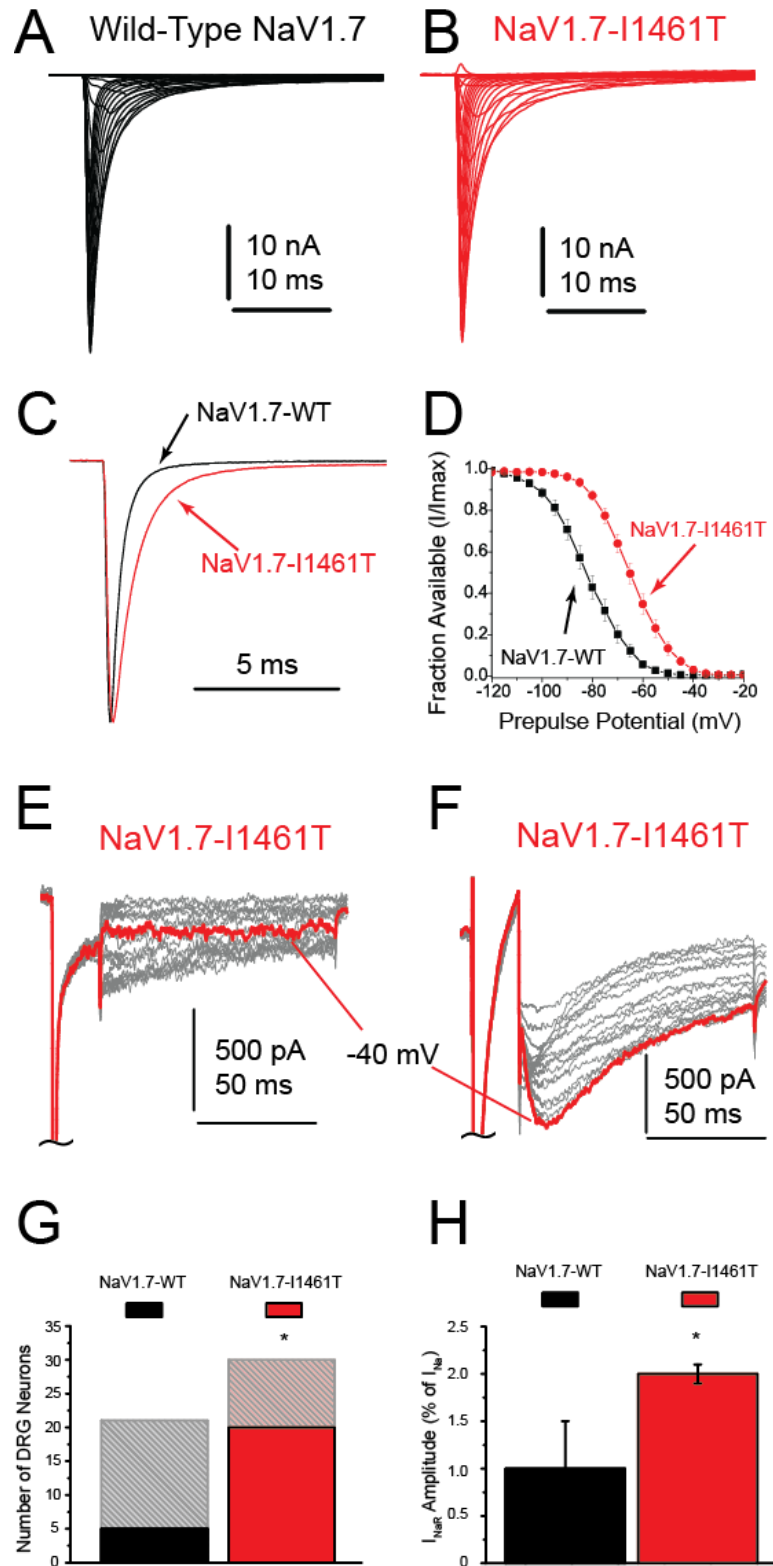


Figure 16: Resurgent current amplitude and frequency are increased in NaV1.7-I1461T PEPD mutant channels. (A) Representative NaV1.7 current traces recorded from a transfected DRG neuron. (B) Representative NaV1.7-I1461T current traces recorded from a transfected DRG neuron. Currents were elicited with step depolarizations to voltages ranging from -80 to +40 mV from a holding potential of -100 mV. (C) The painful mutation I1461T slowed the rate of inactivation of NaV1.7 (**black trace**: WT NaV1.7; **red trace**: Nav1.7-I1461T). Currents were elicited with a step depolarization to +10 mV. (D) Steady-state inactivation curves for WT NaV1.7 (**black**) and NaV1.7-I1461T (**red**) channels expressed in DRG neurons. (E and F) Representative current traces recorded from DRG neurons expressing NaV1.7-I1461T that did not (E) and that did (F) generate I_{NaR} . (G) Frequency of I_{NaR} were statistically increased (*chi-squared test*) in NaV1.7-I1461T compared to NaV1.7 WT. Solid bars represent number of cells with I_{NaR} ; hatched bars represent number total cells. (H) I_{NaR} amplitude is increased is statistically increased in NaV1.7-I1461T compared to WT NaV1.7. * Represents statistical significance ($P < 0.05$) in PEPD mutant channels from WT. Grey bars represent NaV1.7 WT and red bars represent NaV1.7-I1461T. Cultured adult DRG neurons were transfected with the recombinant VGSC construct and NaV1.8 shRNA, and recordings were done in the presence of 500 nM TTX. Resurgent sodium currents were elicited using the standard protocol described in **Chapter II-L2**. Images from panels **A-F** in **Figure 16** were modified from Jarecki *et al.* 2010¹⁵⁰.

2. *Increased resurgent sodium currents augment neuronal excitability*

Previous reports by Raman and colleagues demonstrated that resurgent current contributes to the spontaneous and high frequency firing phenotype of cerebellar Purkinje neurons^{105,132}. Based on these observations, we hypothesized that increased I_{NaR} generated by PEPD mutations might contribute to the previously observed hyperexcitability of neurons expressing PEPD mutant channels¹⁷⁴. To test this hypothesis, Dr. Cummins, Brian Jarecki and I performed computer simulations of DRG neuron excitability. Specifically, we used an established model of DRG neuron excitability¹⁵⁵ that had been implemented in the NEURON simulation environment^{154,175} and, with modifications only to the appropriate sodium channel formulation, simulated and evaluated the impact of the I1461T mutation and resurgent currents on AP firing. Mathematical models of Nav1.7 and NaV1.7-I1461 currents with and without a resurgent blocking factor were developed using a multistate Markov type model of NaV1.7 (Figure 17). For this model the resurgent blocking factor was incorporated into the Markov model using a similar strategy described by Khaliq and colleagues¹³². The rates of channel inactivation and I_{NaR} amplitude were consistent with those observed in recordings from DRG neurons expressing recombinant sodium channels. The computer simulations of action potential (AP) firing in DRG neurons indicated that destabilization and retardation of the rate of channel inactivation in NaV1.7-I1461T was sufficient to decrease the threshold for eliciting an AP. However, inclusion of the resurgent blocking factor in the Markov model led to high frequency train of APs (Figure 17-D). These results suggest that the impaired rate of channel inactivation and increased amplitude of I_{NaR} work synergistically to increase neuronal excitability. Accordingly, increased I_{NaR} and increased neuronal excitability may contribute to the extreme pain sensations associated with PEPD mutations.

Figure 17:

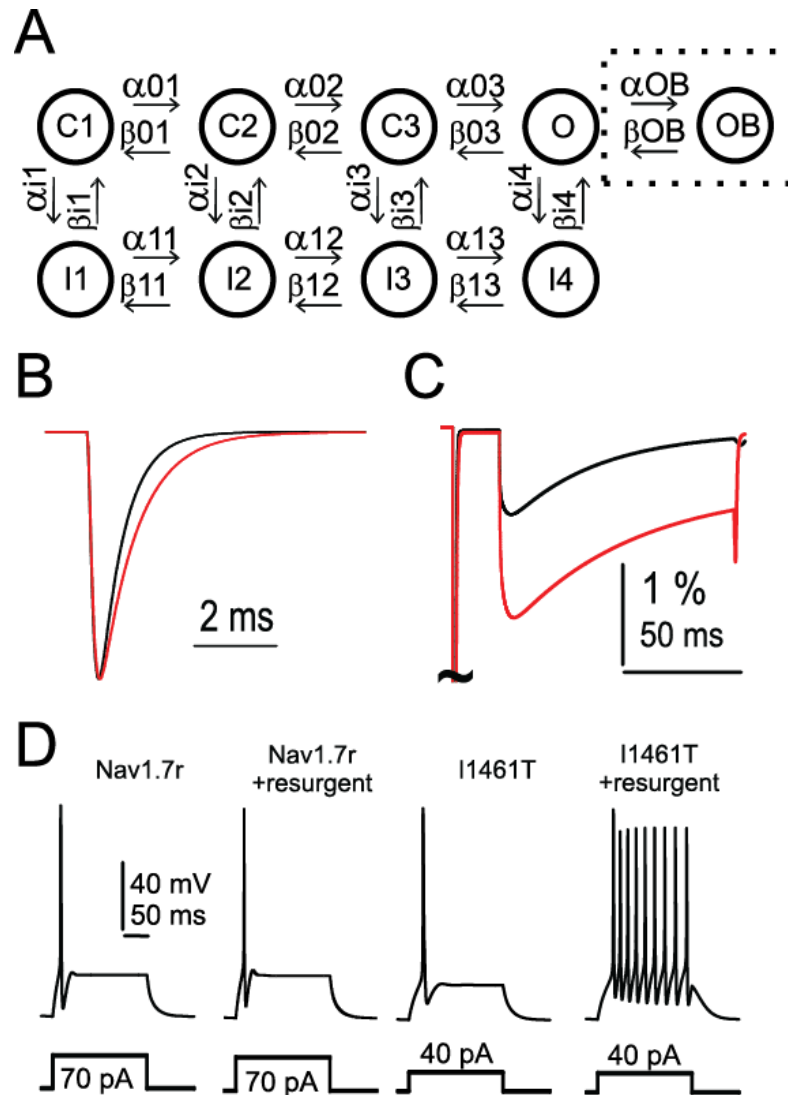


Figure 17: Computer simulation of sodium conductances and DRG neuron excitability. (A) Diagram of Markov models for VGSC conductances. An 8-state Markov model was used for simulation of VGSC conductances without I_{NaR} . C1-C3 represents closed (non-conducting) states. O represents the open (conducting) state. I1-I4 represents inactivated states, which are also non-conducting states. A nine-state Markov model incorporated the resurgent current blocking factor. The OB state (shown boxed) represents channels blocked by this factor. (B) Simulated Nav1.7 (black trace) and Nav1.7-I1461T (red trace) currents elicited by a voltage step from -100 mV to +10 mV. (C) Simulated resurgent currents generated by model Nav1.7 (black trace) and Nav1.7-I1461T (red trace) conductances. Model currents were elicited with the standard resurgent current voltage protocol described in Chapter II—L2. (D) In simulated DRG neurons with wild-type Nav1.7 channels, 70 pA of depolarizing current is required to elicit an action potential (AP) with or without resurgent current simulation. By contrast only 480 pA is need to elicit a AP in a simulated neuron with Nav1.7-I1461T channels and a train of high-frequency APs are generated when the modeled Nav1.7-I1461T channels generate resurgent currents. Figure 17 was modified from Jarecki *et al.* 2010¹⁵⁰.

3. *A NaV1.5 LQT-3/SIDS mutation which slows the rate of channel inactivation increased resurgent sodium currents and elongates the cardiac action potential Q-T interval.*

Disease mutations that impair channel inactivation are not unique to NaV1.7. Indeed, more than 50 different disease mutations that impair inactivation have been characterized in several other VGSCs, including NaV1.1 and NaV1.3 mutations associated with epilepsies, NaV1.4 associated with skeletal muscle myotonias, and NaV1.5 mutations associated with cardiac arrhythmias^{66,74}. Next we asked whether a mutation in NaV1.5, F1486L, associated with long-QT-3/sudden infant death syndrome (LQT3/SIDS), generates increased I_{NaR} . Located in the same region as the NaV1.7-I1461T PEPD mutant, the NaV1.5-F1486L mutation results in slowed rate of channel inactivation and shifts the voltage dependence of channel inactivation in the depolarizing direction¹⁵⁹. When expressed in DRG neurons, WT NaV1.5 generated I_{NaR} in 9 of 18 DRG neurons (Figure 18-A and B) with an average amplitude of 0.6 ± 0.1 % of peak sodium current. Interestingly, of 17 neurons expressing NaV1.5-F1486L channels, 8 generated I_{NaR} with significantly enhanced amplitude ($P < 0.05$) compared to WT NaV1.5 (NaV1.5-F1486L I_{NaR} amplitude: 2.0 ± 0.1 % of peak sodium current (Figure 18-C-E). As I_{NaR} are activated during repolarization, I hypothesized that increased I_{NaR} in NaV1.5 might broaden the cardiac AP, resulting in an increased QT interval and potentially lethal cardiac arrhythmias associated with LQT3/SIDS mutations. Indeed, computer simulations of I_{NaR} in a cardiac myocyte¹⁵⁷ suggest that increased I_{NaR} in the NaV1.5 LQT3/SIDS mutant channel may contribute to increased QT interval (Figure 18-F-H).

Figure 18:

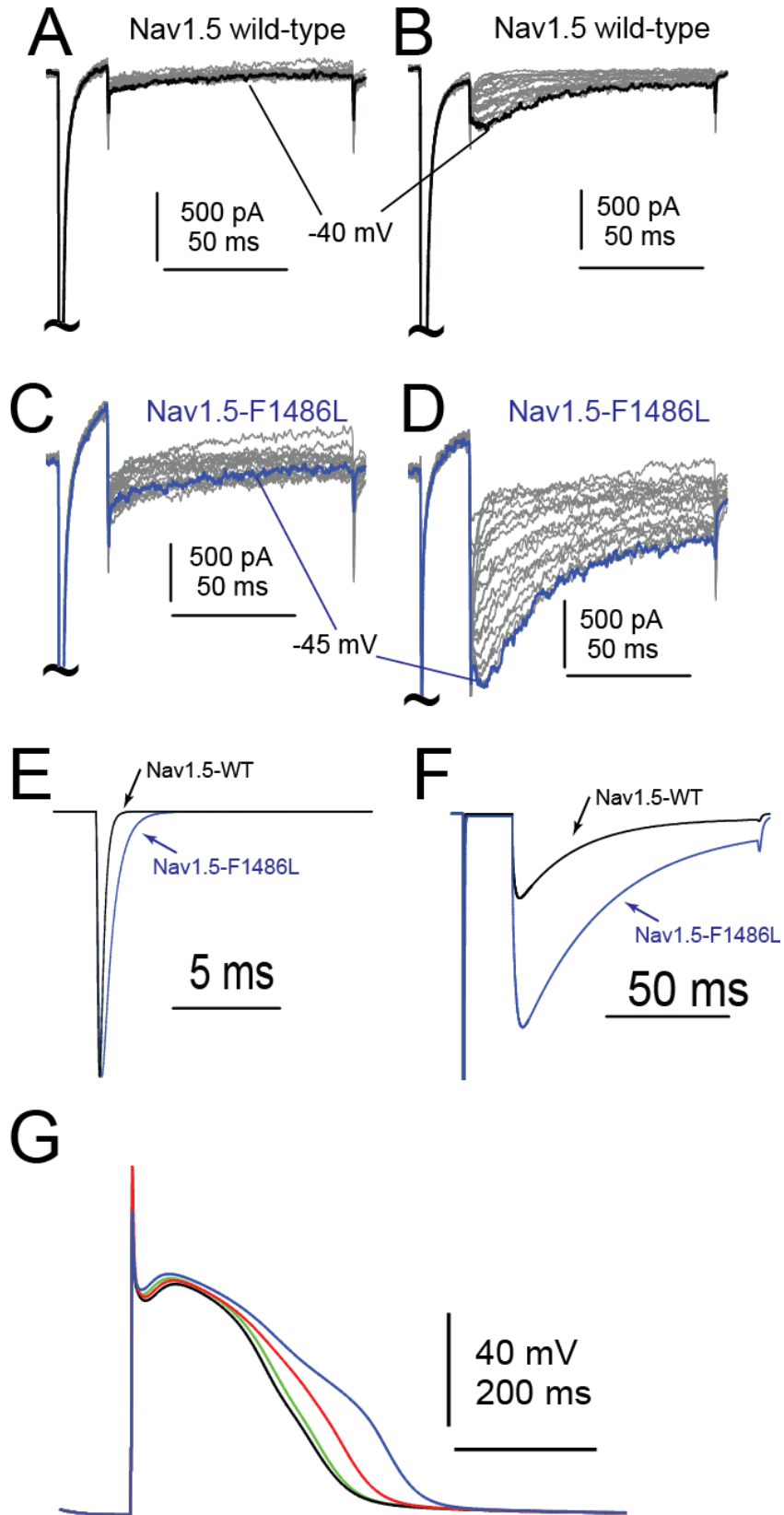


Figure 18: Increased I_{NaR} amplitude in Nav1.5-F1486L mutant channel contributes to elongated cardiac action potential. Representative current traces recorded from DRG neurons expressing wild-type Nav1.5 that did not **(A)** and that did **(B)** generate resurgent currents. Representative current traces recorded from DRG neurons expressing LQT/SIDS Nav1.5-F1486L channels that did not **(C)** and that did **(D)** generate resurgent currents. Resurgent currents were larger on average for Nav1.5-F1486L than for wild-type Nav1.5 channels. Currents were elicited with the standard resurgent current protocol described in **Chapter II-L2** and are magnified 30x relative to the peak current amplitude. **(E)** Simulated Nav1.5 (black trace) and Nav1.5-F1486L (blue trace) currents elicited by a voltage step from -100 mV to +10 mV. **(F)** Simulated resurgent currents generated by model Nav1.5 (black trace) and Nav1.5-F1486L (**blue trace**) conductances. Model currents were elicited with the standard resurgent current voltage protocol. The modeled resurgent current was 0.9% of the peak current for wild-type Nav1.5 and 1.7% of the peak current for Nav1.5-F1486L. **(G)** Simulated APs from a modeled cardiac myocyte. Little difference is seen between the APs of a model cell with wild-type Nav1.5 that did not include I_{NaR} (**black trace**) and that with wild-type Nav1.5 that did include I_{NaR} (**green trace**). Nav1.5-F1486L simulated without resurgent current generation broadened the AP (**red trace**) and this effect was exacerbated in the simulation of Nav1.5-F1486L with resurgent current generation (**blue trace**).

4. *Nav1.4 PMC mutations that slow the rate of channel inactivation increased resurgent sodium currents*

I also examined whether a mutation that slows the rate of channel inactivation in Nav1.4 and causes paramyotonia congenital (PMC) induces I_{NaR} . Specifically I asked if the Nav1.4-R1448P mutation¹⁷⁶, which alters the outermost extracellular charged residue in the DIV voltage sensor, and the Nav1.4-T1313M mutation¹⁷⁷, which alters the structure of the IFM inactivation gate, increased I_{NaR} . The R1448P mutation is of particular interest because it produces a severe slowing of channel inactivation relative to the other mutations in this study—nearly a 10-fold slowing of channel inactivation relative to WT Nav1.4 (Figure 19-A). This is likely due to the important role of translocation of the DIV voltage-sensor in coupling channel inactivation to activation. In contrast to the other mutant VGSCs examined in this report, the R1448P mutation causes a hyperpolarizing shift in the steady-state voltage dependence of inactivation. In a previous study, I_{NaR} were not detected in any of 41 mouse Nav1.8-null DRG neurons transfected with WT Nav1.4¹³¹. Consistent with those data, I did not detect I_{NaR} in any of the 11 neurons expressing Nav1.4 (Figure 19-B). Interestingly, despite the inability of WT Nav1.4 to carry I_{NaR} , Nav1.4-R1448P produced robust resurgent sodium current in 13 of 20 neurons with average relative amplitude of $4.8\% \pm 0.7\%$ of peak sodium current (Figure 19-C). The Nav1.4-T1313M also produced robust I_{NaR} in 2 of 12 neurons with amplitudes of 3.12% and 9.52% (Figure 19-D). Although Nav1.4-R1448P and Nav1.4-T1313M mutations both slow the rate of channel inactivation, albeit to varied degrees, and increase I_{NaR} amplitude, they have opposite effects on steady-state voltage-dependence of inactivation (Nav1.4-R1448P mutant causes a -14.3 mV shift whereas Nav1.4-T1313M causes a +9 mV shift). Thus, at least for Nav1.4, slowing the rate of channel inactivation seemed to be crucial to the production of I_{NaR} , and the impact of the mutation on the voltage dependence of inactivation may be less important. Resurgent

currents generated by NaV1.4 are likely to increase repetitive AP firing in skeletal muscle, which is one of the hallmarks of PMC. Indeed, mathematical modeling of I_{NaR} and computer simulations of skeletal muscle suggest that increased I_{NaR} in the NaV1.4 PMC mutants likely contributes to the myotonic burst observed in mutant channels¹⁷⁸.

Figure 19:

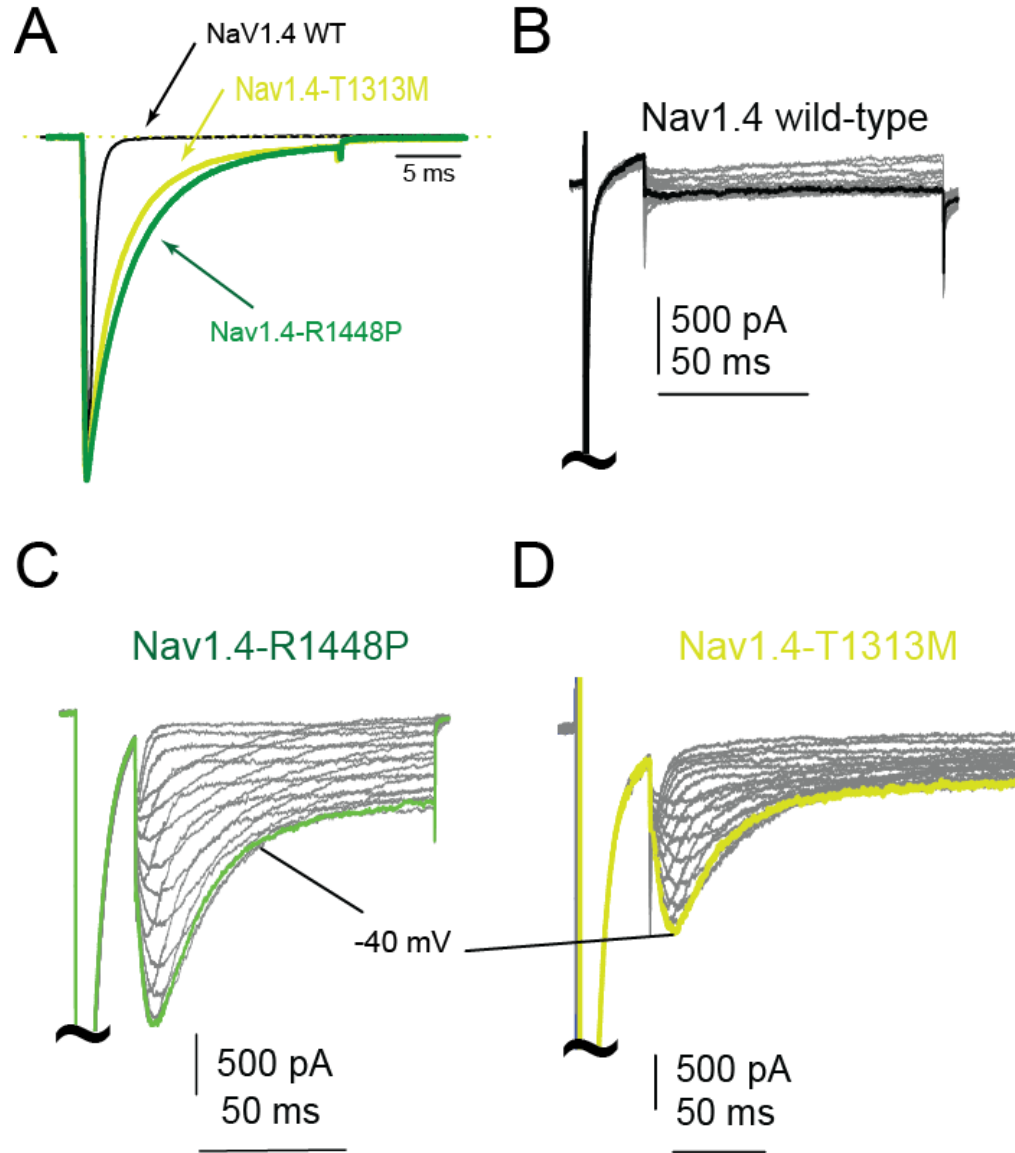


Figure 19: Paramyotonia congenita mutations induce I_{NaR} in Nav1.4 mutants that slow the rate of channel inactivation . (A) The paramyotonia R1448P and T1313M mutation cause a pronounced slowing of the rate of Nav1.4 inactivation. Currents were elicited with a step depolarization to +10 mV. Resurgent currents were not detectable in any of the neurons expressing wild-type Nav1.4 channels (B). By contrast, the majority of neurons expressing Nav1.4-R1448P channels generated robust I_{NaR} (C). I_{NaR} was also observed in 2 of 12 DRG neurons expressing Nav1.4-T1313M (D). T1313M and R1448P I_{NaR} was significantly increased ($P < 0.05$) compare to WT Nav1.4. Resurgent currents were elicited with the protocol shown in **Chapter II-2L** and are magnified 20x relative to the peak current amplitude.

Table 5:

Construct	$V_{1/2}$ Inactivation ^a (mV)	τ_h ^b (ms)	I_{NaR} Amplitude ^c (% I_{Na})
NaV1.7	-80.1 ± 1.6 ($n=25$)	0.85 ± 0.06 ($n=23$)	1.0 ± 0.5 ($n=5$ of 21)
NaV1.7-I1461T	-61.8 ± 1.3^d ($n=37$)	1.07 ± 0.07^d ($n=35$)	2.0 ± 0.1^d ($n=20$ of 30)
NaV1.5	-88.1 ± 1.7 ($n=20$)	0.9 ± 0.07 ($n=20$)	0.6 ± 0.1 ($n=9$ of 18)
NaV1.5-F1486L	-80.1 ± 1.6 ($n=18$)	1.31 ± 0.14^d ($n=15$)	2.0 ± 0.4^d ($n=8$ of 17)
NaV1.4	-77.3 ± 2.1 ($n=11$)	0.34 ± 0.03 ($n=11$)	None detected ($n=0$ of 11)
NaV1.4-R1448P	-91.1 ± 2.4^d ($n=20$)	3.92 ± 0.25^d ($n=21$)	4.2 ± 0.6^d ($n=13$ of 20)
NaV1.4-T1313M	-68.8 ± 2.0^d ($n=12$)	1.89 ± 0.35^d ($n=12$)	3.12% and 9.52% ($n=2$ of 12)
NaV1.6	-71.3 ± 1.9 ($n=17$)	1.02 ± 0.1 ($n=17$)	2.4 ± 0.3 ($n=8$ of 14)
NaV1.6-I1477T	-58.6 ± 1.2^d ($n=18$)	1.25 ± 0.09 ($n=18$)	15.3 ± 3.4^d ($n=7$ of 14)

Table 5: Biophysical properties of wild-type and mutant channels. ^a Midpoint voltage of steady-state inactivation curve, as determined with a standard Boltzmann distribution fit. ^b Time constant for current decay during +10 mV step depolarization. ^c Resurgent sodium current was measured with the protocol shown in Figure 3.1 and reported as a percentage of the peak current amplitude elicited by a step depolarization to -10 mV. The average resurgent current amplitude was only calculated from those cells in which resurgent current was detected. ^d Indicates statistical significance ($P < 0.05$) versus respective wild-type channel.

C. Discussion

Resurgent currents (I_{NaR}) are unique sodium currents, active at voltages where the channel is normally refractory to activity and have been shown to be crucial to spontaneous and high frequency firing in specific populations of central neurons^{105,112,132}. More recent data suggests I_{NaR} are also present in peripheral DRG neurons. Mechanistically, I_{NaR} is hypothesized to arise from a distinct inactivation mechanism, which competes with the intrinsic channel inactivation gate. This alternative form of channel inactivation allows channels to dwell transiently in an open configuration, producing a resurgence of inward sodium current as the channel recovers from the inactivated state to a closed configuration. Although the exact molecular determinants of I_{NaR} remain poorly understood, strong evidence suggests NaV1.6 likely carries the majority of I_{NaR} because it was greatly reduced (by ~90%) in neurons isolated from NaV1.6-null mice^{17, 52, 57}.

Because the mechanism which inactivates the channel to produce I_{NaR} is hypothesized to compete with intrinsic channel inactivation it has been hypothesized that the rate of channel inactivation may be an important factor in the electrogenesis of this current. In support of this hypothesis, artificial slowing of VGSC inactivation via β -pompilidotoxin application did, increase I_{NaR} amplitude in cerebellar Purkinje neurons isolated from NaV1.6 knockout mice¹²⁷. These data confirmed that the rate of channel inactivation is likely an important factor in I_{NaR} amplitude and also suggested that NaV1.1 or NaV1.2 may be capable of producing I_{NaR} . Subsequent reports have suggested that I_{NaR} is not a property intrinsic to NaV1.6 and may be produced by other VGSCs under specific conditions. Indeed, Rush and colleagues demonstrated that NaV1.2 is capable of producing I_{NaR} ¹¹⁴ and my data (see **Chapter III**) suggest that NaV1.3, NaV1.7 can carry I_{NaR} .

I further explored (in collaboration with Brian Jarecki) whether I_{NaR} could be produced by muscle VGSCs and asked whether single point mutations associated with multiple inherited disorders of excitability increased I_{NaR} . Our data show that NaV1.4 and NaV1.5 channels have the capability to generate resurgent currents. Additionally, we demonstrated that a mutation associated with paroxysmal extreme pain disorder (PEPD) in the human peripheral neuronal sodium channel NaV1.7, a paramyotonia congenital (PMC) mutation in the human skeletal muscle sodium channel NaV1.4, and a long-QT3/SIDS mutation in the human cardiac sodium channel NaV1.5 all substantially increased the amplitude of I_{NaR} in an optimized adult rat-derived DRG neuronal expression system. Importantly, computer simulations indicated that increased I_{NaR} associated with the NaV1.7 PEPD mutation could induce high frequency action potential (AP) firing in nociceptive neurons and that increased I_{NaR} associated with the NaV1.5 LQT3/SIDS mutation could broaden the AP in cardiac myocytes; both observations are consistent with the hypothesized pathophysiological alterations in membrane excitability associated with extreme pain or cardiac arrhythmias in PEPD and LQT3/SIDS, respectively. Collectively, these results indicate that resurgent currents are associated with multiple channelopathies and are likely to be important contributors to neuronal and muscle disorders of excitability.

Data presented here provide further evidence that the rate of channel inactivation is likely an important factor in I_{NaR} electrogenesis. Specifically, these data in conjunction with the previous study indicating that pharmacological slowing of channel inactivation via toxin application could augment I_{NaR} amplitude, suggest that slowed rate of channel inactivation is sufficient to induce or increase I_{NaR} amplitude in some VGSC isoforms. Still, close examination of the data indicate that rate of channel inactivation is likely not the sole determinant of I_{NaR} amplitude—nor is the rate of channel inactivation [relative to other VGSC isoforms] a good predictor of the proclivity of a given isoform to carry I_{NaR} .

For example, NaV1.8 channel inactivation is far slower than any of the mutant channels tested here, yet it does not appear that NaV1.8 is capable of producing classic I_{NaR} ¹⁵⁰. Moreover, the NaV1.6 channel's relatively slow rate of inactivation was speculated to be important in conferring large I_{NaR} in several peripheral and central neurons, yet several VGSC isoforms, with faster rates of channel inactivation, including WT NaV1.3, -1.5, and -1.7 appear capable of producing resurgent sodium currents with comparable amplitudes. Consequently, other factors must also contribute to the propensity of specific VGSC isoforms to generate I_{NaR} , such as association with the proposed open channel [resurgent] blocker (NaV β_4), or differential post translational regulation of I_{NaR} electrogenesis in each VGSC isoform.

Data presented here suggest that I_{NaR} are likely to play a role in the functional consequences of inherited neuronal and muscle channelopathies. In addition, these data, in conjunction with previous reports¹²⁷, suggest that any manipulation that slows or destabilizes inactivation has the potential to induce or increase I_{NaR} . Several post translational modifications, including phosphorylation¹⁷⁹, altered calcium signaling²⁰, and oxidation¹⁸⁰, have been reported to slow the rate of channel inactivation. Curiously, phosphorylation of the channel complex has previously been implicated in the mechanism of I_{NaR} electrogenesis¹¹¹. I propose that these alterations could also result in abnormal resurgent current generation. The induction of I_{NaR} likely contributes to the more extreme electrophysiological changes and disease sequelae that can be associated with both inherited and acquired disorders of neuronal and muscle excitability.

Chapter V: *Differential temperature dependence of resurgent sodium currents in muscle and neuronal channelopathies*

A. Introduction

Inherited mutations in voltage-gated sodium channels cause a diverse array of human disorders of excitability including painful neuropathies⁶⁷, cardiac arrhythmias⁶⁴, epilepsy⁶², and non-dystrophic myopathies⁶⁶. These sodium channelopathies are congenital disorders, caused by single-point mutations in channel encoding genes that produce different disease phenotypes depending on the tissue-specific expression of the dysfunctional isoform and the consequences of the mutation on channel properties. While the sodium channelopathies may appear unrelated due to their dissimilar phenotypes and diverse tissue localization, the underlying molecular dysfunctions are often strikingly similar in their biophysical mechanisms.

A fundamental feature that links these disorders is their episodic nature. Most sodium channelopathies are paroxysmal in nature, characterized by periodic or sudden onset of symptoms in patients who are often otherwise healthy¹⁸¹. Episodic attacks can be precipitated by a multitude of factors ranging from specific agents such as exercise^{182,183}, direct mechanical stress¹⁸⁴, and ingestion of potassium rich food¹⁸⁵, as well as psychological⁶⁶ and environmental^{184,186} factors. Although there is substantial information on the triggers that precipitate the symptoms for many sodium channelopathies, the underlying mechanisms are poorly understood.

We have observed that disease-associated mutations that cause *paroxysmal extreme pain disorder* (PEPD), in the peripheral neuronal sodium channel NaV1.7, and *paramyotonia congenita* (PMC), in the skeletal muscle sodium channel NaV1.4, cause an increase in the amplitude of resurgent sodium currents¹⁵⁰ (**see Chapter IV and Appendix A**). Mechanistically, increased I_{NaR} in neuronal and muscle channelopathies is thought to result, at least in part, from the slowed rate of open-state channel

inactivation induced by many disease mutations¹²³. We postulated that additional manipulations that slow or destabilize channel inactivation have the potential to induce or increase I_{NaR} . Temperature is an important environmental factor known to slow VGSC gating and is reported to precipitate symptomatic attacks in several episodic channelopathies. Specifically, in many patients with the non-dystrophic skeletal muscle channelopathy, *paramyotonia congenita*, episodic attacks of muscle stiffness are reliably precipitated by exposure to cold temperature¹⁸⁷. In addition, although the data are less compelling, some reports suggest that patients with PEPD experience episodes of pain following exposure to cold temperatures¹⁸⁴. Here, we tested the hypothesis that I_{NaR} associated with PEPD and PMC disease-causing mutations increases inversely with temperature. To test our hypothesis we investigated how temperature affected kinetics of fast inactivation and I_{NaR} generation in two disease mutants (NaV1.7 I1461T and NaV1.4 R1448P) associated with two distinct disorders (PEPD and PMC, respectively) where cold has been reported to trigger episodic attacks.

B. Original experimental results

1. Cold temperature induces slowing of NaV1.4 and NaV1.7 channel inactivation kinetics

I first examined how channel inactivation kinetics are altered in response to changes in the recording temperature for both wild-type and mutant channels. Sodium currents were recorded from dissociated DRG neurons expressing recombinant wild-type (WT) or mutant channels. As we have previously reported¹⁵⁰, this expression system allows detailed characterization of voltage-gated sodium currents, including I_{NaR} , which are difficult to study in non-excitable cell backgrounds. NaV1.7-WT, NaV1.4-WT, NaV1.7-I1461T, and NaV1.4-R1448P currents were pharmacology isolated from native TTX-S DRG currents with application of 500 nM TTX as described previously¹⁵⁰. In addition to the recombinant channel of interest, neurons were co-transfected with a second plasmid encoding DsRed, to aid in identification of transfected neurons, and a specific NaV1.8 shRNA, to minimize the endogenous TTX-resistant NaV1.8 currents. Individual recordings were made in a static bath environment at 35°, 30°, 22°, and 15°C. In DRG neurons a decrease in recording temperature produced a general slowing of gating kinetics at all voltages for all transfected recombinant channels. More specifically the rate of open-state channel inactivation was significantly ($P < 0.05$) slowed as temperature was decreased in both NaV1.7- and NaV1.4-WT and mutant channels (Figure 20-A), with minimal effects on channel activation. The Tau-h (τ_h) values over the temperature range are shown in Table 6 and are displayed in Figure 20-B as an Arrhenius plot, which plots inactivation kinetics as a function of temperature. The slopes from the fits of these data yield energies of activation for NaV1.7-WT, NaV1.4-WT, NaV1.7-I1461T, and NaV1.4 R1448P of 9.04 ± 1.33 , 9.34 ± 2.12 , 8.09 ± 1.55 , and 8.70 ± 1.20 kcal/mol, respectively. These values are proportional over this temperature range

to Q_{10}^k values of 1.74, 1.75, 1.49, and 1.65 for NaV1.7-WT, NaV1.4-WT, NaV1.7-I1461T, and NaV1.4-R1448P. Collectively, these data indicate that (1) the rate of channel inactivation is impaired by the I1461T mutation in NaV1.7 and the R1448P mutation in NaV1.4, (2) channel inactivation rate is temperature sensitive in both wild-type and mutant channels, and (3) disease causing mutations in NaV1.7 (I1461T) and NaV1.4 (R1448P) do not alter the temperature dependence of the rate of channel inactivation. Because the rate of channel inactivation does not show increased temperature dependency in either of the mutant channels compared to wild-type, cold induced slowing of channel inactivation, by itself, is unlikely to be able to trigger the episodic bouts of myotonia and pain observed in patients with PMC and PEPD, respectively.

^k The temperature coefficient, Q_{10} , is a measure of the rate of change of a biological or chemical system as a consequence of increasing the temperature by 10°C

Figure 20:

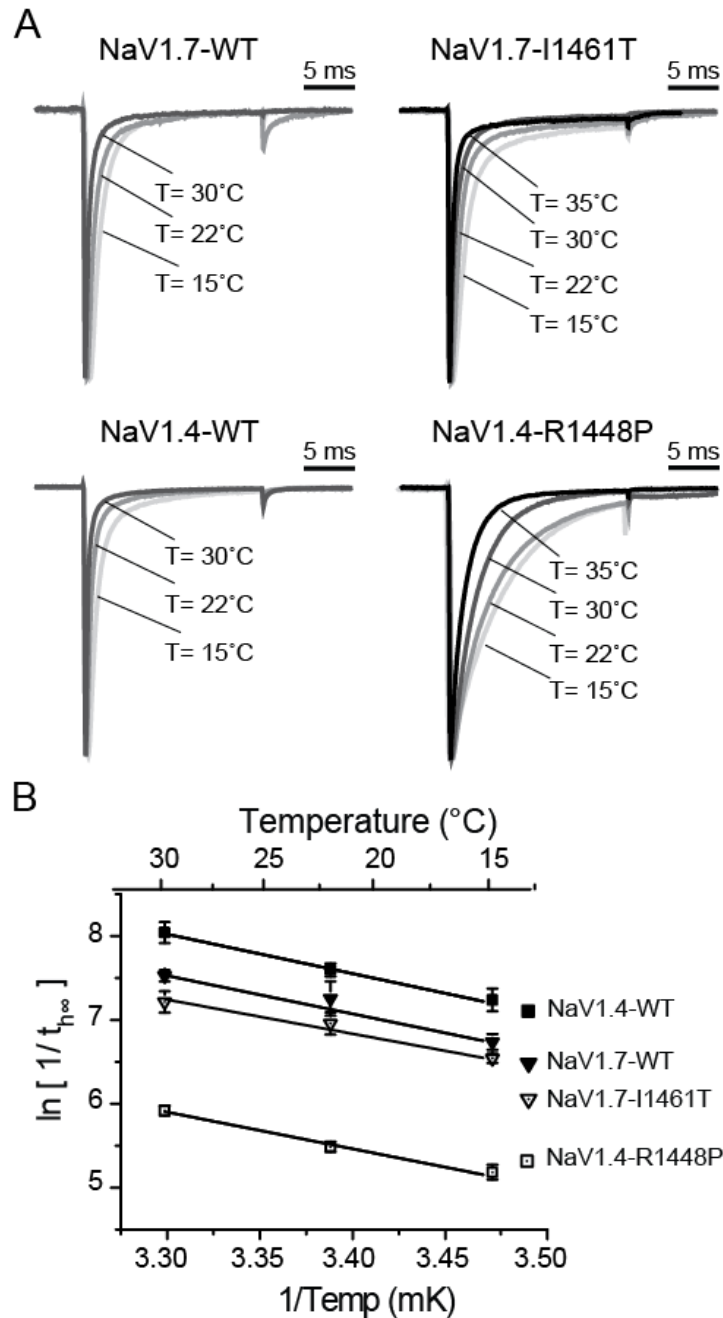


Figure 20: Temperature slows channel open-state inactivation in NaV1.7-WT, NaV1.4-WT, NaV1.7-I1461T, and NaV1.4-R1448P. Recombinant channels were transfected in DRG neurons and individual recordings were made at each temperature (15°C to 35°C) as indicated by arrow. **(A)** Representative currents elicited by a voltage step from -100mV to +10 mV. **(B)** Transformed inactivation rate time constants (τ_h) are plotted as a function of temperature (mK) in the Arrhenius plot. Data for each channel was linearly fitted with the slope of the line corresponding to the activation energy. Corresponding values for activation energy and Q_{10} are reported in the text.

2. Cold Temperature increases I_{NaR} in NaV1.4-R1448P PMC Mutant but not NaV1.7-I1461T PEPD Mutant Channels

Next I examined whether I_{NaR} amplitude was temperature sensitive in mutant and wild-type channels. In a previous study we reported that recombinant WT NaV1.7, but not WT NaV1.4, was capable of producing I_{NaR} when transfected in DRG neurons (recording temperature $T=22^{\circ}\text{C}$)¹⁵⁰; and I_{NaR} amplitude was increased in neuronal and skeletal muscle disease mutants NaV1.7-I1461T and NaV1.4-R1448P ($T=22^{\circ}\text{C}$)¹⁵⁰. Here we show that while I_{NaR} amplitude is significantly greater with NaV1.7-I1461T channels than with WT-NaV1.7 channels, NaV1.7-I1461T I_{NaR} amplitude is not sensitive to changes in temperature (Figure 21-A and -C); the relative I_{NaR} amplitude for NaV1.7-I1461T channels was not significantly different at each tested temperature ($4.5 \pm 0.8\%$ at $T=15^{\circ}\text{C}$; $4.1 \pm 0.7\%$ at $T=22^{\circ}\text{C}$; $4.6 \pm 0.6\%$ at $T=30^{\circ}\text{C}$; $4.7 \pm 0.5\%$ at $T=35^{\circ}\text{C}$). In contrast, I_{NaR} in NaV1.4-R1448P mutant channels exhibits substantial temperature sensitivity (Figure 21-B and -C). I_{NaR} amplitude in NaV1.4-R1448P is highest at the low temperatures, where the rate of channel inactivation is slowest, and decreases in amplitude as the recording temperature increased ($8.5\% \pm 1.5\%$ at 15°C ; $4.1\% \pm 0.5\%$ at 22°C ; $2.6\% \pm 0.4\%$ at 30°C ; $1.87\% \pm 0.2\%$ at 35°C). Previous reports suggested I_{NaR} amplitude is correlated to the rate of channel inactivation (τ_h)¹²³. Here I report that slowed kinetics of inactivation with decreased temperatures correlated, at least to some extent, with increased I_{NaR} in NaV1.4-R1448P (Figure 21-D bottom, $R^2=0.47$); in contrast no correlation existed between I_{NaR} amplitude and the slowed kinetics of inactivation with decreased temperature in the NaV1.7-I1461T mutant. In addition we examined if I_{NaR} amplitude was temperature sensitive in WT-NaV1.7 and WT-NaV1.4 channels. Preliminary findings suggest I_{NaR} amplitude may be temperature sensitive in WT NaV1.7, however, I was unable to record from enough cells expressing WT-NaV1.7 with I_{NaR} to make statistically based conclusions. It is important to note that I_{NaR} was not detected in

any cells expressing WT-NaV1.4 at any temperature even though the kinetics of channel inactivation were retarded at cold temperatures. These data show that although inactivation is impaired and robust I_{NaR} are generated at 22°C in both the NaV1.7-I1461T and the NaV1.4-R1448P mutants, the two mutations show very different temperature sensitivities.

Figure 21:

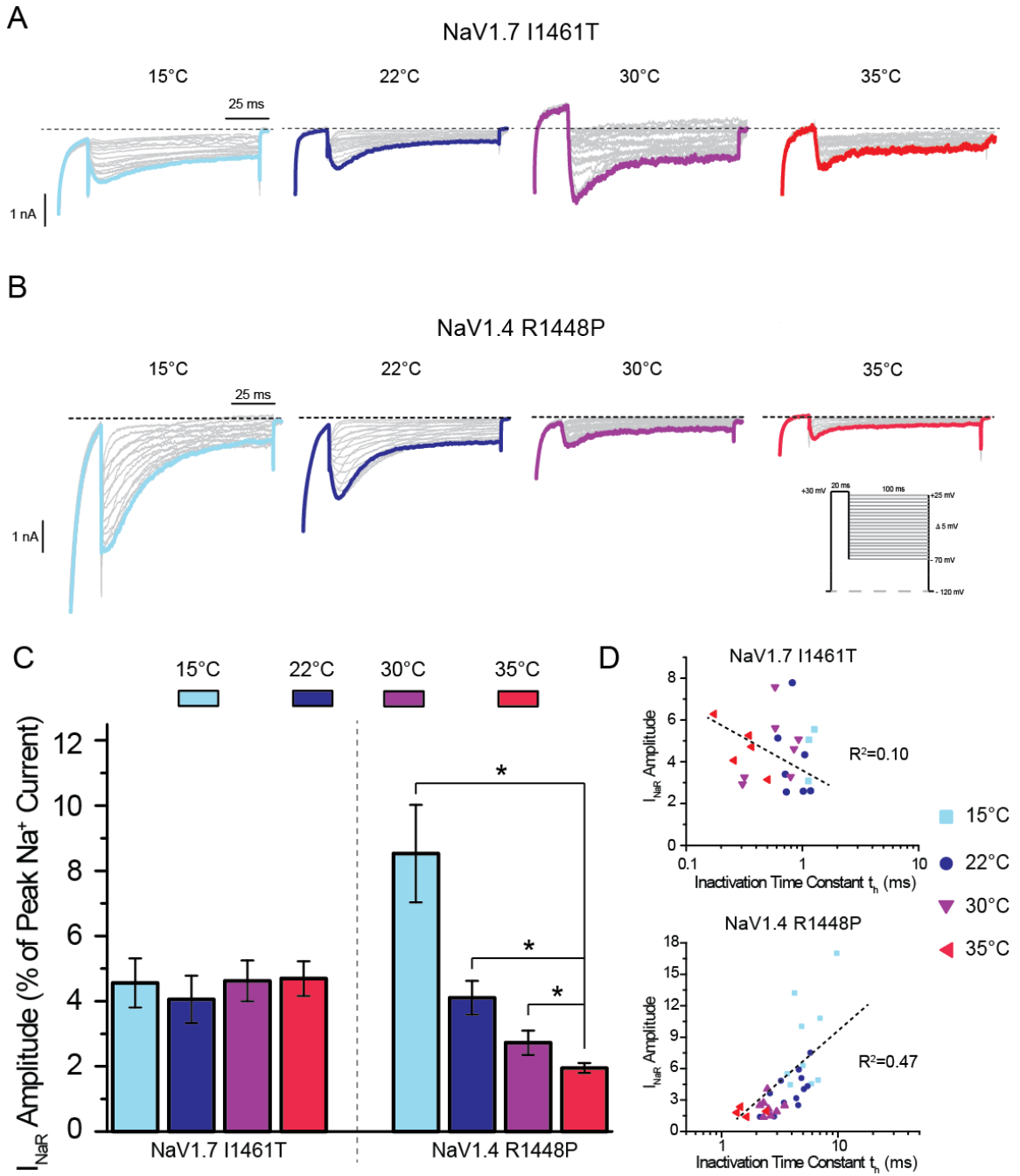


Figure 21: Temperature alters resurgent current (I_{NaR}) amplitude from the NaV1.4-R1448P (PMC) but not NaV1.7-I1461T (PEPD) mutant channels. (A) Representative I_{NaR} traces recorded from DRG neurons expressing NaV1.7-I1461T at 15°, 22°, 30°, and 35°C. (B) Representative I_{NaR} traces recorded from DRG neurons expressing NaV1.4-R1448P at 15°, 22°, 30°, and 35°C. The voltage protocol to elicit I_{NaR} is pictured in B-inset. (C) Comparison of the relative I_{NaR} amplitude, expressed as a percentage of peak transient current for wild-type and mutant VGSCs. *Indicates statistically significant differences between 35°C and other temperatures tested ($P < 0.05$) for each given isoform. (D) Relative I_{NaR} amplitude from individual cells at 15°, 22°, 30°, and 35°C plotted as a function of open-state inactivation time constant (τ_h) for NaV1.7-I1461T (*Top*) and NaV1.4-R1448P (*bottom*). In both cases the dashed line represents the linear trend line for the data.

3. *Temperature sensitivity of I_{NaR} is determined, at least in part, by the location of the mutation*

I next asked what could account for the differential temperature sensitivities of the PEPD and PMC mutant I_{NaR} . To determine whether the differences in PEPD and PMC mutant responses to temperature are related to the channel isoform tested or, alternatively, the location of the mutation, we generated a PMC mimic mutation in the voltage sensor of NaV1.7 (R1599P) and examined how the kinetics of channel gating and I_{NaR} generation are affected by changes in temperature. As with the NaV1.4-R1448P mutation, the NaV1.7-R1599P mutation had no significant effect on the kinetics or voltage-dependence of channel activation (data not shown) but significantly slowed the rate of channel inactivation and caused a slight hyperpolarizing shift in the voltage dependence of inactivation ($V_{1/2}$) when compared to WT-NaV1.7 (see Table 6). Similar to the other channel constructs tested in this report, lower temperatures caused with a general slowing in channel gating kinetics (Figure 22-A). Indeed, we observed the rate of channel open-state inactivation to be significantly slower ($P < 0.05$) at each subsequent temperature tested ($T = 30^\circ\text{C}$, 22°C , and 15°C). The τ_h values over the temperature range from 15°C to 30°C are reported in Table 6 and displayed in Figure 22-B as an Arrhenius plot compared to WT NaV1.7. The activation energy and the Q_{10} value of the temperature range were 8.57 ± 1.99 kcal/mol and 1.61, respectively. Although channel inactivation kinetics were significantly slowed with temperature, the Arrhenius plot indicates there was no change in temperature dependence over the range of temperatures tested compared to WT. As predicted, the NaV1.7-R1599P mutation significantly increases I_{NaR} compared to WT-NaV1.7 (Table 6). In addition, as seen in Figure 22-C and -D, the NaV1.7-R1599P mutant exhibited some temperature dependence in I_{NaR} amplitude, at least between 30°C and 22°C ($2.46\% \pm 0.5\%$ at $T = 30^\circ\text{C}$ and $7.7\% \pm 0.7\%$ at $T = 22^\circ\text{C}$); however, I_{NaR} amplitude appears to plateau at

lower temperatures ($7.2\% \pm 2.0\%$ at $T=15^{\circ}\text{C}$) even as the rate of channel inactivation slows. Also, as with the NaV1.4-R1448P mutant channel, the rate of channel inactivation was correlated with I_{NaR} amplitude (Figure 22-E, $R^2=0.82$). Collectively these results suggest that the location of the mutation is an important factor in conferring temperature sensitive I_{NaR} in disease associated mutations in neuronal and muscle tissue.

Figure 22:

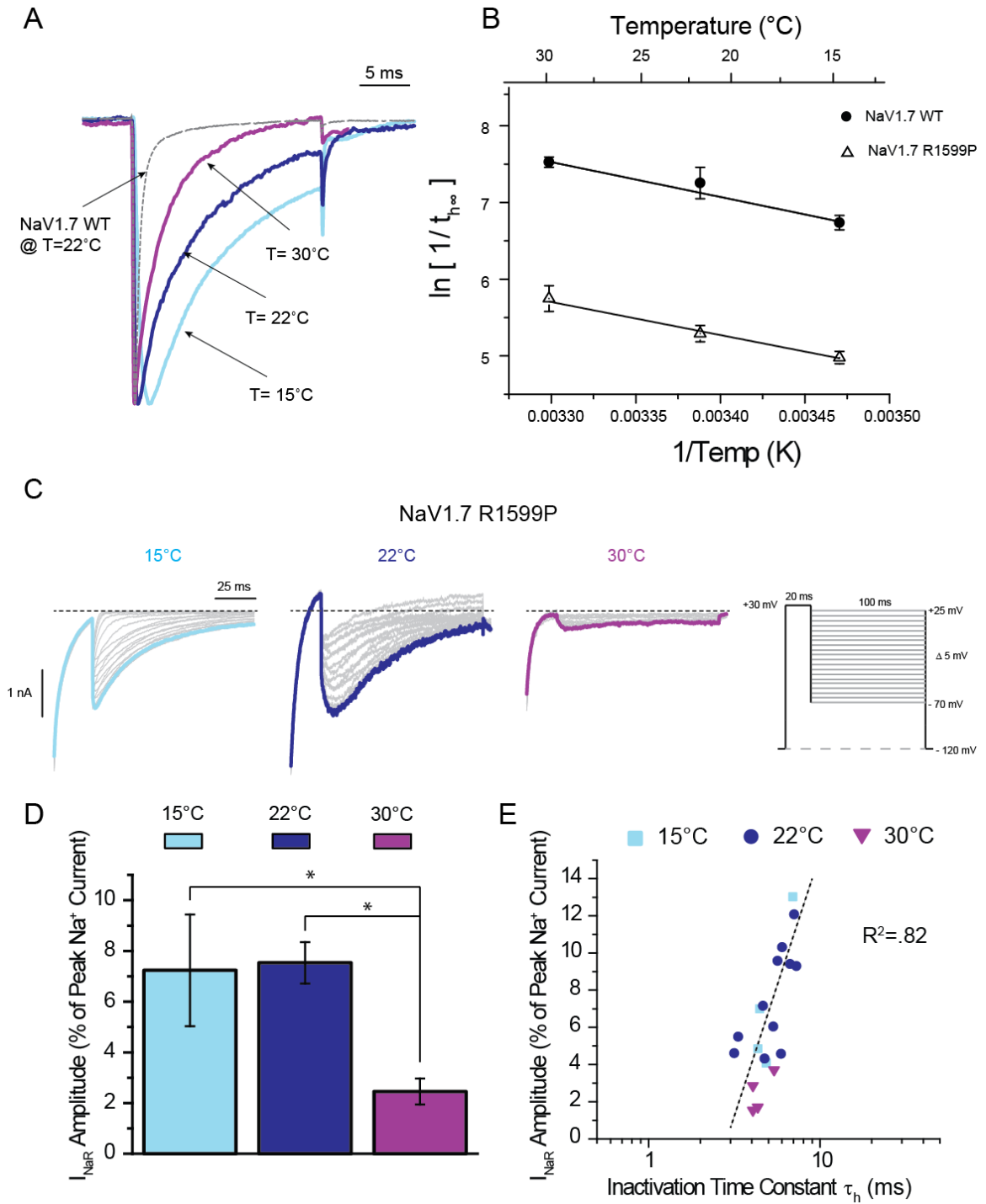


Figure 22: Temperature slows channel open-state inactivation in NaV1.7-R1599P and increases I_{NaR} amplitude. (A) Representative currents elicited by a voltage step from -100mV to +10mV. (B) Transformed open-state inactivation rate time constants are plotted as a function of temperature (K) in the Arrhenius plot. Data for NaV1.7-R1599P and WT-NaV1.7 are linearly fitted over the temperature range with the slope of the line corresponding to the activation energy. Corresponding values for activation energy and Q_{10} are reported in the text. (C) Representative I_{NaR} traces recorded from DRG neurons expressing NaV1.7-R1599P at 15°, 22°, and 30°C. (D) Comparison of the relative I_{NaR} amplitude observed over the temperature range. *Indicates statistically significant differences between 30°C and other temperatures tested ($P < 0.05$). (E) Relative I_{NaR} amplitude from individual cells at 15°, 22°, 30°C plotted as a function of open-state inactivation time constant (τ_h). Dashed line represents the linear trend line for the data—Corresponding R^2 values are found in the text.

Table 6:

Construct	Current Density (pA/pF)		$V_{1/2}$ Steady-State Inactivation (mV)		Inactivation Time Constant [τ_h] (ms) ^B		Resurgent Current Amplitude (%) ^A	
NaV1.7 Wild-Type								
15°C	-890 ± 305	n=10	-73.8 ± 2.5	n=10	1.24 ± 0.12 ‡	n=10	1.4	n=1/10
22°C	-1176 ± 335	n=8	-70.3 ± 2.5	n=6	0.73 ± 0.17 ‡	n=7	0.5 ± 0.1	n=3/7
30°C	-1122 ± 225	n=4	-67.0 ± 4.1	n=4	0.54 ± 0.04	n=4	Not detected	n=0/4
NaV1.7-I1461T								
15°C	-685 ± 122	n=16	-61.8 ± 1.5 ‡	n=16	1.48 ± 0.09 * ‡	n=16	4.6 ± 0.7	n=3/16
22°C	-1996 ± 382 *	n=9	-56.3 ± 1.9	n=9	1.03 ± 0.17 *	n=9	4.1 ± 0.7	n=7/9
30°C	-1438 ± 443	n=14	-53.8 ± 2.5	n=14	0.81 ± 0.09 *	n=14	4.6 ± 0.6	n=7/14
35°C	-902 ± 249	n=9	-54.5 ± 2.7	n=8	0.41 ± 0.05	n=9	4.7 ± 0.5	n=5/9
NaV1.7-R1599P								
15°C	-863 ± 141	n=20	-75.7 ± 2.2 ‡	n=20	7.29 ± 0.52 ‡	n=20	7.2 ± 2.0 ‡	n=4/20
22°C	-1012 ± 149	n=13	-76.2 ± 4.2 ‡	n=6	5.35 ± 0.48 ‡	n=13	7.7 ± 0.8 ‡	n=12/13
30°C	-1415 ± 359	n=13	-61.1 ± 2.3	n=13	3.58 ± 0.36	n=13	2.5 ± 0.5	n=4/13
NaV1.4 Wild-Type								
15°C	-1839 ± 468	n=8	-76.0 ± 2.1	n=8	0.77 ± 0.10 ‡	n=8	Not detected	n=0/8
22°C	-2128 ± 298	n=17	-76.5 ± 1.5	n=17	0.53 ± 0.04 ‡	n=17	Not detected	n=0/17
30°C	-1791 ± 635	n=4	-70.5 ± 4.0	n=4	0.33 ± 0.04	n=4	Not detected	n=0/4
NaV1.4-R1448P								
15°C	-1175 ± 245	n=13	-90.2 ± 4.0 *	n=13	5.88 ± 0.52 * ‡	n=13	8.5 ± 1.5 * ‡	n=9/13
22°C	-1633 ± 221	n=18	-90.8 ± 1.6 * ‡	n=35	4.29 ± 0.25 * ‡	n=18	4.1 ± 0.5 * ‡	n=11/18
30°C	-1698 ± 278	n=15	-82.3 ± 2.5 *	n=21	2.76 ± 0.18 *	n=15	2.6 ± 0.4 *	n=9/15
35°C	-1863 ± 607	n=5	-55.2 ± 4.2	n=5	1.73 ± 0.25	n=5	1.9 ± 0.2	n=4/5

Table 6: Comparison of NaV1.7 and NaV1.4 wild-type and mutant channel biophysical properties. ^AResurgent current amplitude is measured as a percentage of peak transient sodium current. ^B τ_h values are open state inactivation rate time constants for current decay during a +10 mV step depolarization. Time constants were obtained from a standard Hodgkin-Huxley (m^3h) fit. *Statistical significance from data value at 35°C (p-value < 0.05). †Statistical significance from data value at 30°C (p-value < 0.05).

C. Discussion

Changes in temperature are known to exacerbate the clinical manifestations of many channelopathies— triggering pain in some patients, and muscle cramping and myotonia in others. Although recording temperature is known to influence the gating properties of ion channels^{188,189} and, in some cases, augment impaired channel function, enhanced temperature associated slowing of mutant channel inactivation, by itself, appears insufficient to explain augmented excitability associated with many episodic channelopathies^{138,177,190,191}. Although it has been speculated that other channel processes or biochemical interactions, secondary to impaired channel inactivation, may underlie the episodic nature of these disorders¹⁸¹, identifying potential candidates has been difficult. Interestingly, channel mutations associated with PMC and PEPD, two disorders where cold temperature is reported to precipitate episodic attacks, exhibit impaired rate of channel inactivation and increased resurgent sodium currents (I_{NaR})— which together are believed to underlie the enhanced excitability associated with both disorders. In this study we asked if exposure to cold temperature augments impaired inactivation kinetics and increases I_{NaR} amplitude in PMC and PEPD disease mutants. My data confirmed previous findings that channel inactivation kinetics are temperature sensitive—channel inactivation kinetics are very fast near normal body temperature and slow as temperature is decreased for both wild-type and mutant channels. Importantly, the results presented here demonstrate that temperature associated slowing of channel inactivation kinetics results in increased I_{NaR} amplitude in the PMC mutant, NaV1.4-R1448P, but not the PEPD mutant, NaV1.7-I1461T. My results indicate the phenotypic differences in temperature sensitivity between PMC and PEPD depend on the location of the inherited mutations as well as isoform specific differences. Given our computational modeling data that suggests I_{NaR} can contribute to pathological hyperexcitability, we propose that temperature sensitive I_{NaR} in NaV1.4-R1448P may be an important factor in

triggering episodic bouts of myotonia, and may help explain how cold temperature impaired inactivation kinetics in PMC mutant channels results in a sudden and dramatic change in membrane excitability.

At the molecular level, I_{NaR} are thought to arise following relief of ultra-fast open channel block by an intracellular blocking particle that competes with the normal channel inactivation mechanism^{102,115}. Accordingly, mutations that slow channel inactivation kinetics are likely to increase the probability that channels will undergo resurgent (open-channel) block rather than inactivation, resulting in increased I_{NaR} amplitude. Our previous work demonstrated that the degree to which mutations slow the kinetics of channel inactivation is an important determinant of I_{NaR} amplitude¹²³. In the present study we hypothesized that cold temperature-induced slowing of channel inactivation would increase I_{NaR} amplitude and, because increased I_{NaR} is predicted to contribute to the etiology of the different disorders, we rationalized that temperature sensitive I_{NaR} might contribute to the unexplained cold-induced trigger associated with PMC and, to a lesser extent, PEPD. Interestingly, although channel inactivation is temperature sensitive in both disease mutants, I_{NaR} amplitude is temperature sensitive in only the PMC mutant (NaV1.4-R1448P). To help understand this, we asked whether this observation was due to differences in the location of the two mutations. The NaV1.7 PEPD I1461T mutation lies within the domain III-IV linker deemed to serve as the putative inactivation gate (the IFM particle) of the channel, whereas the NaV1.4 PMC mutant, R1448P, alters the outer most charged residue in the VGSC domain IV voltage sensor, which is involved in coupling activation to inactivation¹³⁸. Both mutations are reported to have negligible effects on channel activation and appreciably slow the rate of channel inactivation^{138,156} (albeit to different degrees), but cause opposite shifts in the voltage-dependence of steady state fast inactivation, suggesting that the two mutations perturb channel inactivation in different ways. Indeed, previous characterization of

NaV1.7-I1461T indicate that this mutation destabilizes docking of the IFM particle with its intra-pore docking sites, resulting in impaired rate of channel inactivation and increased persistent currents^{156,172}. Conversely, the NaV1.4-R1448P mutation impairs outward mobility of the domain IV voltage sensor, uncoupling channel activation from inactivation, resulting in delayed translocation of the inactivation gate and reduced accessibility of intrapore binding sites, resulting in slowed current decay^{138,183}. While previous data indicates slowing of channel inactivation is an important determinant of resurgent current amplitude, our observation of temperature insensitive I_{NaR} in NaV1.7-I1461T indicates the rate of channel inactivation is not likely the sole determinant. Moreover, our observation of temperature sensitive I_{NaR} in domain IV voltage sensor mutations but not in a mutation within the inactivation gate suggest the location of the mutation, and ultimately how inactivation is impaired is likely to be important in conferring temperature sensitive I_{NaR} .

My previous findings suggest that sequence differences among channel isoforms may also be important determinants of I_{NaR} amplitude (**see Chapter III and IV**)¹⁵⁰. Sequence differences among channel isoforms are known to be responsible for isoform specific differences in pharmacology, voltage-dependence, and kinetics of channel gating^{192,193}. Although several wild-type sodium channels have been reported to be capable of producing I_{NaR} , NaV1.6 produces I_{NaR} in the greatest frequency and amplitude and wild-type NaV1.4 did not produce detectable I_{NaR} when expressed in DRG neurons¹⁵⁰. Initially we postulated that wild-type NaV1.4 did not produce I_{NaR} because the rate of channel inactivation was significantly faster than the other wild-type channels. However, because mutations [NaV1.4-R1448P and NaV1.4-T1313M (**see Chapter IV**)], which impair the rate of channel inactivation allow NaV1.4 mutant channels to produce robust I_{NaR} , it was predicted that if inactivation kinetics were slowed with cold temperature, WT NaV1.4 would also produce I_{NaR} . Surprisingly, WT NaV1.4 did not produce I_{NaR} even at

cold temperatures where inactivation kinetics are slowed to rates where other isoforms produced robust I_{NaR} . This observation and the fact that the domain IV voltage sensor mutation in NaV1.7 (R1599P) did not completely reproduce the temperature sensitive I_{NaR} observed in NaV1.4-R1448P provide additional evidence that differences in isoform sequences are also important determinants of I_{NaR} amplitude.

Data presented in this chapter were recorded from DRG neurons expressing recombinant wild-type and mutant voltage-gated sodium channels. Previously we have shown that DRG neurons are an optimal cell background to study I_{NaR} , as they express the specific auxiliary subunits and regulatory proteins necessary for I_{NaR} generation. For our purposes DRG neurons were used because it is the natural cell background for NaV1.7 and because these neurons have proven to be an optimal surrogate expression system for studying I_{NaR} in NaV1.4. Although the $NaV\beta_4$ subunit (the I_{NaR} open-channel blocker) is expressed in skeletal muscle¹⁹, I_{NaR} have not yet been observed in myocytes. Our data suggests that WT NaV1.4 is unlikely to produce I_{NaR} in myocytes, at least under normal conditions. Although a few studies have examined sodium currents in myocytes biopsied from patients with PMC, unfortunately, I_{NaR} was not tested for in these studies. Interestingly, the increased I_{NaR} with decreased temperature correlates well with increased spontaneous activity in biopsied muscle from a PMC patient over the same temperature range¹⁹⁴. Although our data indicate that increased I_{NaR} may contribute to the previously unexplained cold induced trigger of muscle stiffness and myotonia in PMC, these observations should be confirmed using biopsied muscle tissue from PMC patients (or transfected myocytes) using appropriate protocols and conditions for eliciting I_{NaR} .

Voltage-gated sodium channels (VGSCs) are critical determinants of excitability in nerve and muscle tissue. As sodium channels are critically important for initiating and propagating action potentials, mutations which alter channel structure and activity are

believed to produce profound changes in membrane excitability resulting in ectopic signaling and pathology. Indeed, sodium channelopathies encompass a diverse array of disorders of excitability with distinct symptoms including extreme pain, seizures, myotonia, and cardiac arrhythmia. Although symptomatically unrelated, many channelopathies are episodic in nature and share similar factors that precipitate attacks. In this study we explored the mechanism by which cold temperature causes episodic myopathy in PMC and extreme pain in PEPD. Inherited mutations associated with PEPD and PMC were thought to manifest hyperexcitability by enhancing the open probability of the channel by slowing the kinetics of channel inactivation and increasing persistent sodium current. As a consequence of impairing inactivation we now know that many of these mutations increase I_{NaR} amplitude. Importantly, computer simulations of a DRG neuron¹⁵⁰ and a skeletal muscle fiber¹⁷⁸ indicate increased I_{NaR} could substantially exacerbate the effects of the disease mutation on cellular excitability and might underlie the burst discharge of action potentials common to many neurological disorders. Although, cold temperature is known to slow VGSC inactivation kinetics, the sensitivity of fast inactivation kinetics to cooling is not enhanced by mutations associated with PMC, where cold induced myopathy is a defining characteristic. This observation has led some to speculate that the cold induced trigger in PMC arises from a ‘threshold effect’¹⁹⁵. Our results indicate that the disease mutant gain of function which may be responsible for the cold induced myotonia is not enhanced temperature dependence of channel inactivation kinetics, but rather increased I_{NaR} amplitude as a consequence of further impairment of channel inactivation. Moreover, while slowed kinetics of channel inactivation and increased I_{NaR} may underlie the cold sensitive trigger in PMC it is important to consider that this mechanism may not be conserved for all episodic disorders of excitability where cold temperature is implicated—our results with the NaV1.7-I1461T PEPD mutation underscore this point. Taken together these results

suggest that increased resurgent sodium currents may be involved in the previously unexplained cold induced episodic myotonia in PMC.

Chapter VI: *Increased resurgent sodium currents in rat DRG neurons following contusive spinal cord injury (SCI)*

A. Introduction

Traumatic spinal cord injury (SCI) results not only in motor impairment below the site of injury, but also chronic pain that can persist for years and significantly impact patient quality of life¹⁹⁶. Most pain associated with SCI is neuropathic in origin and occurs at or below the level of the lesion. SCI induced pain can occur spontaneously (stimulus independent) or in response to stimuli that are either normally innocuous or noxious, resulting in either allodynia or hyperalgesia—respectively. Regardless of the level or severity of the injury, an estimated sixty to eighty percent of persons who have sustained SCI experience clinically significant pain at some time after injury¹⁹⁷⁻²⁰⁰. For some patients this pain can impact the quality of life to a greater extent than even the motor impairment^{201,202}, often negatively influencing patient rehabilitation and recovery²⁰³. Unfortunately, chronic pain associated with SCI is progressive in nature^{197,201} and available treatments are, often, either not effective or have significant side effects²⁰⁴. Although substantial progress has been made in our understanding of the etiology and origins of SCI induced pain, development of more effective therapeutics has been hindered by our incomplete understanding of the underlying molecular dysfunctions which contribute to development and progression of this painful phenotype.

Pain associated with SCI is hypothesized to result, generally, from increased neuronal excitability as a consequence of either enhanced excitatory mechanisms or a loss or reduction of inhibition^{196,205-208}. Abnormal pain sensations can originate from abnormalities in the peripheral nerve fibers (peripheral nervous system, PNS) or in the central nervous system (CNS). Because spinal cord lesions impact the CNS directly [via trauma], neuropathic pain associated with SCI is hypothesized to result from

sensitization and plastic remodeling of neurons associated with the spinothalamic pain-signaling pathway, such that, post-injury, these neurons become spontaneously hyperexcitable. Indeed, experimental and clinical studies have demonstrated that secondary neurons in the dorsal horn of the spinal cord²⁰⁹ and neurons within the ventroposterior lateral (VPL) thalamus²¹⁰ can become hyperexcitable after SCI. Mechanistically, initiation and maintenance of hyperexcitability in neurons of the dorsal horn and thalamus have been linked to microglial^l and astrocyte activation^{206,209,211} and altered expression and function of ion channels²⁰⁷.

Although hyperexcitability of peripheral, sensory neurons can contribute to pain associated with peripheral nerve injury and inflammation, altered function of peripheral neurons, caudal to the lesion site, have been largely ignored for SCI pain. Interestingly, pain fails to develop in patients with complete lesions and spinal cord deafferentation,²¹² underscoring the importance of peripheral inputs from nociceptive, sensory neurons in the development and/or maintenance of some types of SCI pain. More recent evidence suggests that, similar to central neurons of the spinothalamic tract, peripheral, sensory neurons, below the site of the lesion, are also sensitized following SCI. A study by Walters E.T. *et al.* (2010) found that 3 days following a moderate thoracic (T10) spinal cord injury, 75% of small diameter L4/L5 DRG neurons from rats exhibited elevated incidence of spontaneous activity and soma hyperexcitability when compared with untreated or sham-treated animals. Increased spontaneous activity in SCI animals was greatest below the level of the lesion and failed to decline over 8 months²¹³. Importantly, increased intrinsic spontaneous activity in small diameter DRG neurons correlated with increased mechanical and thermal hypersensitivity of sites below the injury level; these results suggest a potentially important and previously undefined contribution of below-

^l Post-SCI microglial activation results in release of several proinflammatory cytokines, prostaglandin E2, reactive oxygen species (ROS), ATP, excitatory amino acids, and nitric oxide (NO)—all of which are believed to contribute to remodeling of CNS circuitry and hyperexcitability.

level, primary nociceptors to post SCI pain²¹³. Consequently, the goal of this study was to explore the underlying mechanisms which contribute to spontaneous activity and hyperexcitability of below level DRG neurons following contusive SCI.

Expression and function of ion channels can be dynamically regulated following peripheral injury. More recent evidence suggests that altered expression and function of VGSCs may also contribute to the etiology of pain associated with SCI. Indeed, increased expression of the NaV1.3 channel isoform [4 weeks after injury] in the spinal cord and the thalamus appear to underlie hyperexcitability and pathophysiology of CNS neurons following SCI²⁰⁷. Moreover, peritoneal administration of antiepileptics and local anesthetics, compounds which target VGSCs, are moderately effective in the treatment of neuropathic pain following SCI²¹⁴. Here I explored the hypothesis that altered expression or function of VGSCs are associated with the increased spontaneous activity and hyperexcitability of below level DRG neurons previously reported to contribute to pain following contusive SCI. To test this hypothesis I used the rat T10 contusive SCI model and harvested L1-L6 DRG neurons and assessed changes in function and expression of VGSCs using whole cell voltage-clamp electrophysiology and real time RT-PCR 14 days after injury.

B. *Original experimental results*

A recent report by Walters *et al.*²¹³ indicated that following T10 contusive SCI, increased spontaneous activity and hyperexcitability of small diameter L1-L6 DRG neurons correlated to increased thermal and mechanical hyperalgesia in injured animals. Here I explored the hypothesis that, following injury, increased SA and hyperexcitability of peripheral DRG neurons results from increased expression and dysfunction of specific VGSCs. To examine the effects of injury on sodium currents we cultured L1-L6 DRG neurons from rats 14 days post contusive injury as well as those from sham surgery and

age-match naïve [control] animals. Contusive spinal cord injury and sham surgery animals were prepared as described in **Chapter II-I**. Sodium currents were recorded, in voltage-clamp configuration, as described in **Chapter II-C** and **F**. Although Walters *et al.*²¹³ focused only on the function of small diameter, nociceptive neurons following SCI, in this study I recorded from both small (~15 μm^{m} to 35 μm^{m}) and medium/large (>35 μm^{n}) cell soma diameter neurons. Recordings were made from at least 15 cells in each size class from each treatment group. Neurons were cultured in the presence of 30ng/mL NGF^o with most recordings completed within 12 hours of dissociation.

^m Typically C-type nociceptive neurons

ⁿ Typically A δ - and A β -type multimodal neurons

^o 30ng/mL NGF was added to the standard culture media to maintain the expression of NaV1.8 over the 12 hour recording period. See Dib-Hajj *et al.*, 1998, Hinson *et al.*, 1997, and Fjell *et al.*, 1999 for rationale.

1. *14 days post T10 contusive SCI, VGSC TTX-S, TTX-R, and persistent current densities are unaltered in acutely dissociated L1-L6 DRG neurons*

DRG neurons express an array of voltage-gated sodium currents which regulate the firing behavior of different nerve fibers, including persistent sodium currents. Interestingly, DRG neurons express two classes of persistent sodium currents: persistent currents associated with the rapidly inactivating TTX-S VGSCs and NaV1.8 (as seen on the top of Figure 23-C) and ultra-slow persistent currents believed to be produced by NaV1.9 (as seen on the top of Figure 23-D). The two types of persistent currents can be distinguished according to their differing voltage dependence: persistent currents observed at -10 mV are mostly produced by rapid inactivating TTX-S VGSC and NaV1.8, whereas at persistent currents observed at -60 mV is likely produced by NaV1.9¹⁴⁵. I examined the impact of contusive injury on TTX-S, TTX-R, and persistent currents in DRG neurons because increases in either macroscopic TTX-S or TTX-R current following injury has been associated with cell soma membrane hyperexcitability and increases in persistent sodium currents increase spontaneous discharge of action potentials—each of which were observed in below level DRG neurons following contusive spinal cord injury. The amount of TTX-S and TTX-R currents expressed in each cell were estimated using kinetic subtraction and a pre-pulse inactivation protocol described previously²¹⁵. Here, persistent currents were estimated two ways: (1) persistent currents were estimated using the current elicited from a 100 msec pulse to -60 mV from a holding potential of -120 mV (Figure 23-C right) and (2) persistent currents were also estimated as the current remaining at the end of a 50 msec test depolarization (average of the last 5 msec) to -10mV from a holding potential of -120 mV (Figure 23-C left).

Fourteen days post-contusive SCI minimal changes in TTX-S, TTX-R, and persistent sodium current density were observed. Current densities^p for each type of sodium current are reported for each experimental condition in Table 7, and are shown in Figure 23. These findings contrast previous results from other models of peripheral injury, namely axotomy^{215,216} and peripheral inflammation⁷⁷, which suggested that the current amplitudes of TTX-S and TTX-R currents are dynamically regulated following injury. Interestingly, in medium/large DRG neurons I observed a small but significant increase in TTX-S and TTX-R current density in sham surgery animals as compared to both naïve [control] and injured animals (Figure 23-A and -B). Collectively these results suggest that increases in TTX-S, TTX-R, or persistent sodium currents likely do not underlie the reported increase in SA or hyperexcitability of small diameter DRG neurons following contusive SCI.

^p Current Density is a measure of functional [active] channels in the membrane and is expressed as the ratio of current magnitude per surface area unit.

Figure 23:

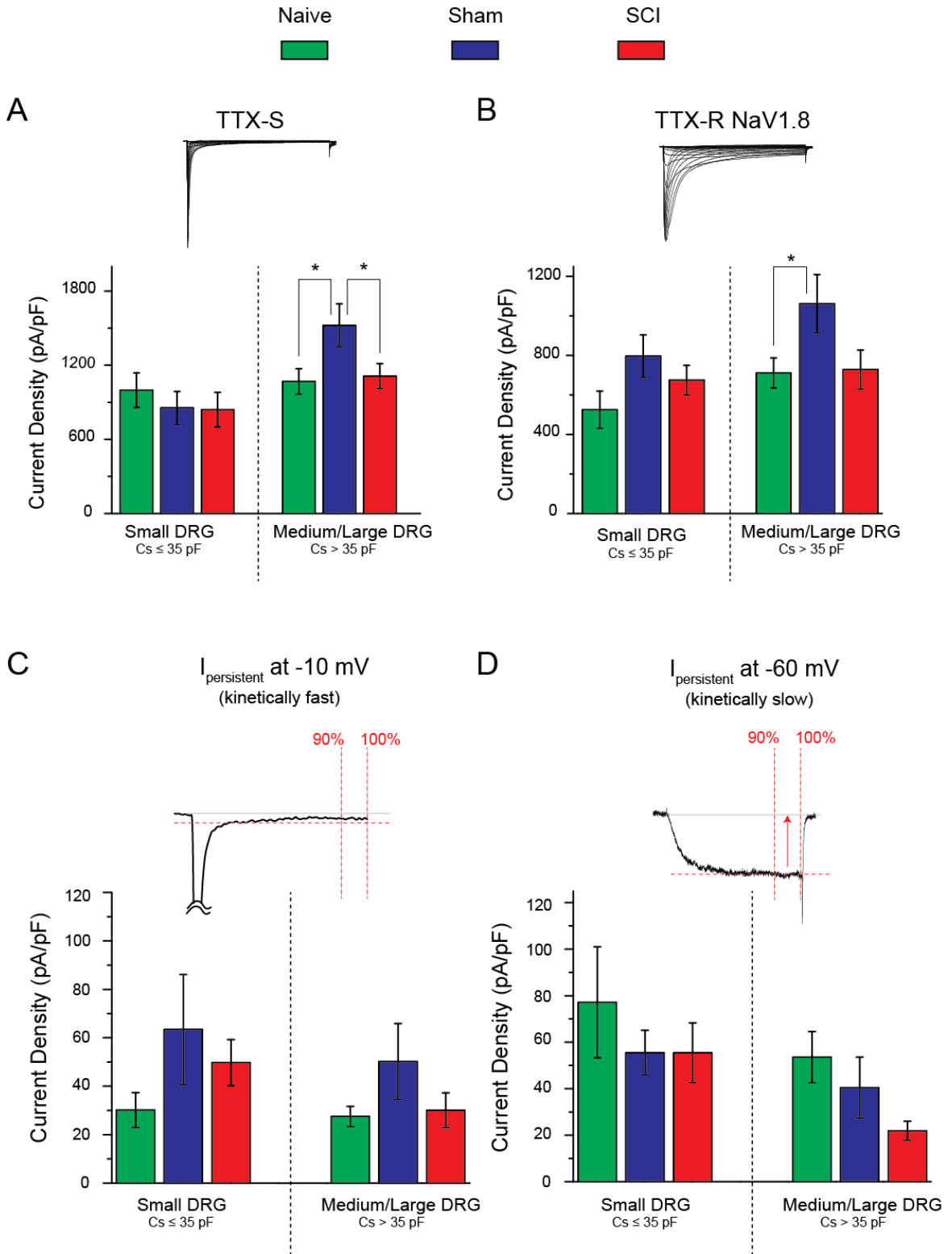


Figure 23: No change in TTX-S, TTX-R, or persistent sodium current density 14 days post contusive SCI. Current densities were calculated by dividing the estimated peak currents [for each current] by the whole-cell capacitance. TTX-S **(A)** and TTX-R **(B)** current densities were estimated in naïve, sham, and SCI neurons with the help of post hoc kinetic subtraction—see Cummins TR *et al.* 1997 for more details²¹⁵. TTX-S and TTX-R current densities were estimated using a .pre-pulse inactivation protocol (500 msec pre-pulses) with a -10 mV test pulse. TTX-R current densities were estimated through kinetic subtraction of the total current elicited at the -10 mV test pulse—with the magnitude of TTX-S current was equal to the total current less the subtracted TTX-R current. Kinetically fast $I_{\text{persistent}}$ **(C)** current density was estimated as the current remaining during the last 5 msec of a 50 msec test pulse to -10 mV from a holding potential of -120 mV. Kinetically slow $I_{\text{persistent}}$ **(D)** current density was estimated as the current remaining during the last 10 msec of a 100 msec test pulse to -60 mV from a holding potential of -120 mV. Generally, TTX-S, TTX-R, or persistent current densities were not affected by sham surgery or SCI injury when compared to control. Significant increases ($P < 0.05$) in TTX-S **(A)** and TTX-R **(B)** current densities were observed from medium/large soma diameter sham-surgery DRG neurons. Values of current density for each condition displayed in **Table 7**. Error bars indicate \pm SE.

2.. 14 days post contusive SCI resurgent sodium current (I_{NaR}) amplitude is increased

I hypothesized that increased I_{NaR} following SCI may contribute to membrane potential oscillations and high frequency burst discharge of action potentials observed in peripheral neurons following injury. To test this hypothesis, I_{NaR} were recorded from small and medium/large diameter DRG using the standard I_{NaR} protocol—described in **Chapter II-L2**. For more in depth details on I_{NaR} recording conditions or analysis please reference **Chapter II-L2**.

Here I report that contusive SCI caused a dramatic increase in I_{NaR} amplitude at the 14 day time point (see representative traces in Figure 24-A). Overall, in recordings made from DRG neurons of all sizes, I_{NaR} amplitude, measured as a percentage of peak transient current amplitude, was significantly ($P < 0.05$) increased from $3.39\% \pm 0.47\%$ in naïve animals to $6.14\% \pm 0.49\%$ in SCI animals (Figure 24-B). When the data is segregated, according to cell soma diameter, I_{NaR} is still significantly increased in medium/large neurons from injured animals (Figure 24-C). Although I_{NaR} are normally observed in medium/large diameter neurons¹³¹ (see **Chapter III**), robust I_{NaR} are now observed in some small diameter DRG neurons (Figure 24-C left) following contusive SCI. In control neurons, resurgent sodium currents are nearly abolished by 500 nM TTX, suggesting that I_{NaR} are produced by one of the TTX-S VGSC isoforms expressed in DRG neurons [either NaV1.1, -1.3, -1.6, or -1.7]; it is believed that the majority of native I_{NaR} is produced by NaV1.6. To test if I_{NaR} , found in DRG neurons from sham or SCI animals, is also sensitive to TTX, 500 nM TTX was added to the bath solution following select recordings. Indeed, I_{NaR} found in sham (data not shown) and SCI (Figure 24-D) neurons is completely abolished by 500 nM TTX.

Figure 24:

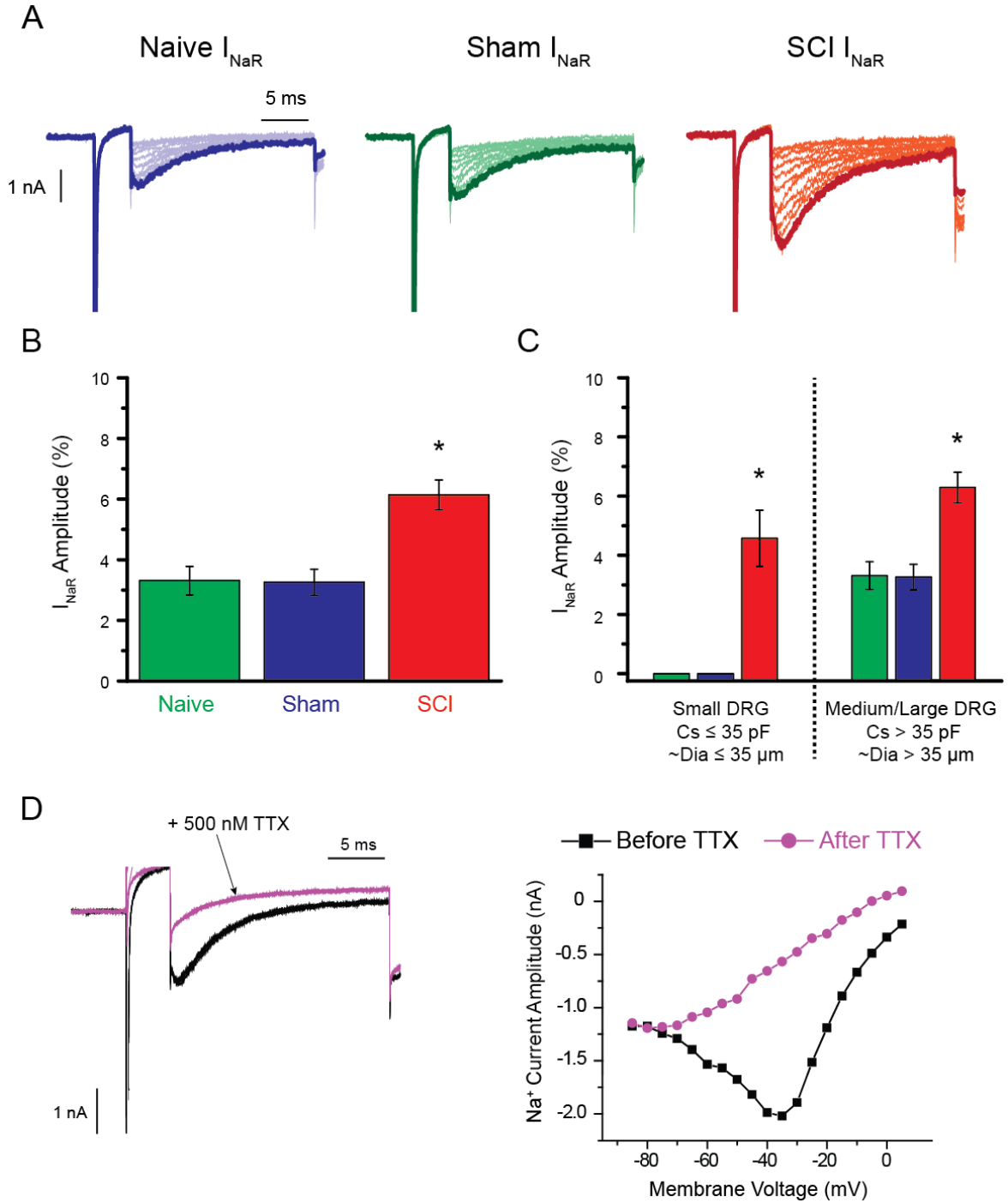


Figure 24: Increased resurgent sodium current (I_{NaR}) amplitude in small and medium/large soma diameter DRG neurons 14 days post contusive SCI. I_{NaR} are elicited according to a voltage protocol where the membrane voltage is transitioned from a holding potential of -120 mV to +30 mV for 20 msec and then repolarized to intermediate voltages of 0 mV to -80 mV in increments of 5 mV. **(A)** Representative current traces of I_{NaR} from naïve, sham, and SCI animals 14 days post spinal cord injury. **(B)** 14 days post contusive SCI I_{NaR} amplitude is significantly increased ($P < 0.05$) from ~3.3% of peak I_{Na} to ~6.3% I_{Na} . **(C)** Under control conditions I_{NaR} is never observed in small soma diameter DRG neurons and is approximately 3.3% of peak I_{NaR} following contusive SCI robust I_{NaR} is now observed in small diameter DRG neurons (~4.6%) and I_{NaR} amplitude is increased to from 3.3% of I_{Na} to ~6.3% of I_{Na} post injury. In **Figures B and C** averages are representative of only cells that exhibit I_{NaR} . 500 nM TTX was added to the bath of end of some SCI recordings. As shown in the representative current trace **(D-left)** and voltage dependence **(D-right)** 500 nM TTX abolished I_{NaR} from SCI recordings—suggesting increased I_{NaR} post injury is also produced by TTX-S VGSCs. Error bars indicate \pm SE. * Represents statistical significance ($P < 0.05$) as determined by one-way ANOVA.

Previously I have shown that I_{NaR} are only observed in a subpopulation of medium diameter DRG neurons—cells expressing I_{NaR} are typically between 35 to 60 μm cell soma diameter (see **Chapter III**). Shown in Figure 25-A is a histogram displaying the frequency of I_{NaR} versus the whole cell capacitance (bin size 5 pF) for recordings made from naïve, sham, and SCI neurons. In sham animals, I_{NaR} is also restricted to a subpopulation of medium/large soma diameter DRG neurons—between 35 and 65pF. Interestingly, not only is I_{NaR} amplitude increased in SCI neurons but I_{NaR} is now observed in smaller (as small as 28 μm) and larger (up to 138 μm) diameter DRG neurons. The observation of a broader distribution of neurons exhibiting I_{NaR} is more pronounced in the histogram shown in Figure 25-B where the frequency of I_{NaR} is shown versus the whole cell capacitance (bin size 1 pF). Here the data is fitted according to a normally distributed function and the area under the curve approximates the likelihood that a cell of a given soma diameter will express I_{NaR} . Finally, following SCI I_{NaR} amplitude increases as cell soma diameter increases; remarkably, I_{NaR} amplitude can be as much as 14% of peak current amplitude in large cells following SCI (Figure 25-C). Taken together these results demonstrate that following SCI (1) I_{NaR} amplitude is significantly increased compared to control and (2) I_{NaR} amplitude is found in a broader population of DRG neurons—including small and very large diameter.

Figure 25:

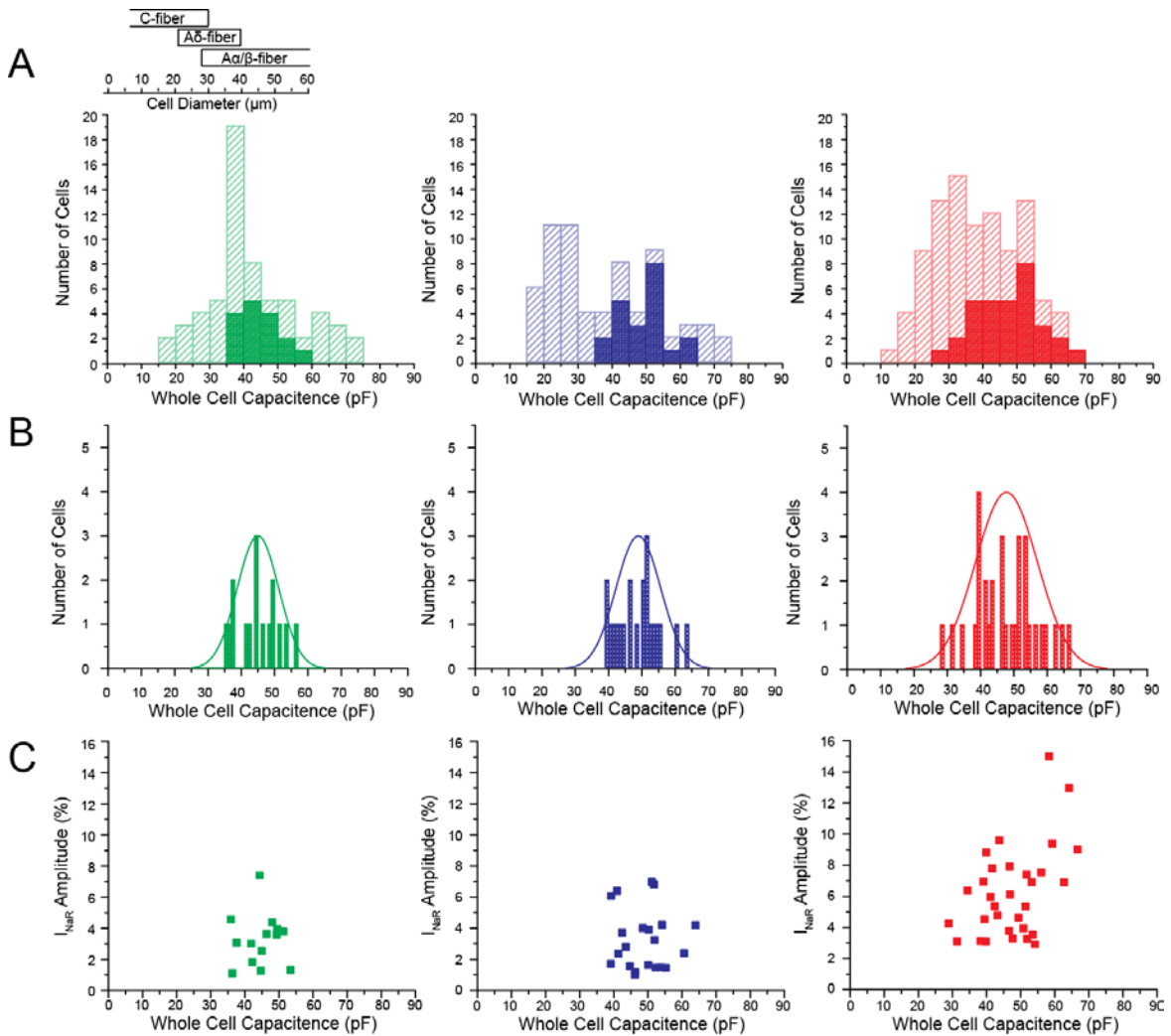


Figure 25: Following contusive SCI resurgent sodium current (I_{NaR}) is found in a broader population of DRG neurons. In naïve and sham surgery DRG neurons I_{NaR} is only observed in a narrow population of DRG neurons (typically between 40-50pF). Following contusive SCI [at 14 days] I_{NaR} can be observed in small diameter DRG and are found in greater frequency in larger soma diameter DRG neurons (50pF and larger). Frequency histograms shown in **(A and B)** display the number of cells expressing I_{NaR} versus the cell whole-cell capacitance (\propto to cell size). **(A)** shows the total number of cells recorded from for each cell size (bin equal to 5 pF) with hatched bars and the frequency of cells expressing I_{NaR} for each cell size with shaded bars. **(B)** shows the frequency of cells expressing I_{NaR} for each cell size (bin equal to 1pF); the data in **B** is fit with a normalized distribution function with the area under the curve representing the probability of a cell expressing I_{NaR} . **(C)** shows a scatter plot of I_{NaR} amplitude versus whole cell capacitance. According to **(C)**, there is a positive correlation between I_{NaR} amplitude and cell size—following SCI I_{NaR} amplitude is increased overall but I_{NaR} amplitude is greatest in larger cells. The ruler shown above **(A)** demonstrates the correlation of whole cell capacitance to cell soma diameter (1:1 for recordings made from neurons less than 24 in culture); additionally, the ruler shows the predicted modality of the neuron according to cell soma diameter (see Lawson SN et al 1985).

3. *Increased I_{NaR} in SCI neurons does not result from slowed rate of channel open-state inactivation*

Previously, I demonstrated that two factors can influence I_{NaR} amplitude: (1) the channel isoform carrying I_{NaR} and (2) the rate of channel open-state inactivation (see **Chapter IV** and **V**). In an effort to explain the origins of increased I_{NaR} in SCI neurons I examined whether a correlation existed between I_{NaR} amplitude and the rate of channel inactivation. I_{NaR} amplitude was plotted versus the kinetic time constant for open state inactivation for each recording made from naïve, sham, and SCI neurons. As seen in Figure 26, no correlation exists between I_{NaR} amplitude and rate of sodium channel inactivation. Additionally, for cells expressing I_{NaR} , little difference in the time constant for channel open state inactivation exists among naïve and sham neurons with small amplitude I_{NaR} and SCI neurons with greater I_{NaR} amplitude. In fact, with the exception of a few outliers, naïve, sham, and SCI neurons had similar τ_h values. Collectively, these results suggest that a post injury slowing in channel inactivation is not responsible for the observed increase in I_{NaR} amplitude.

Figure 26:

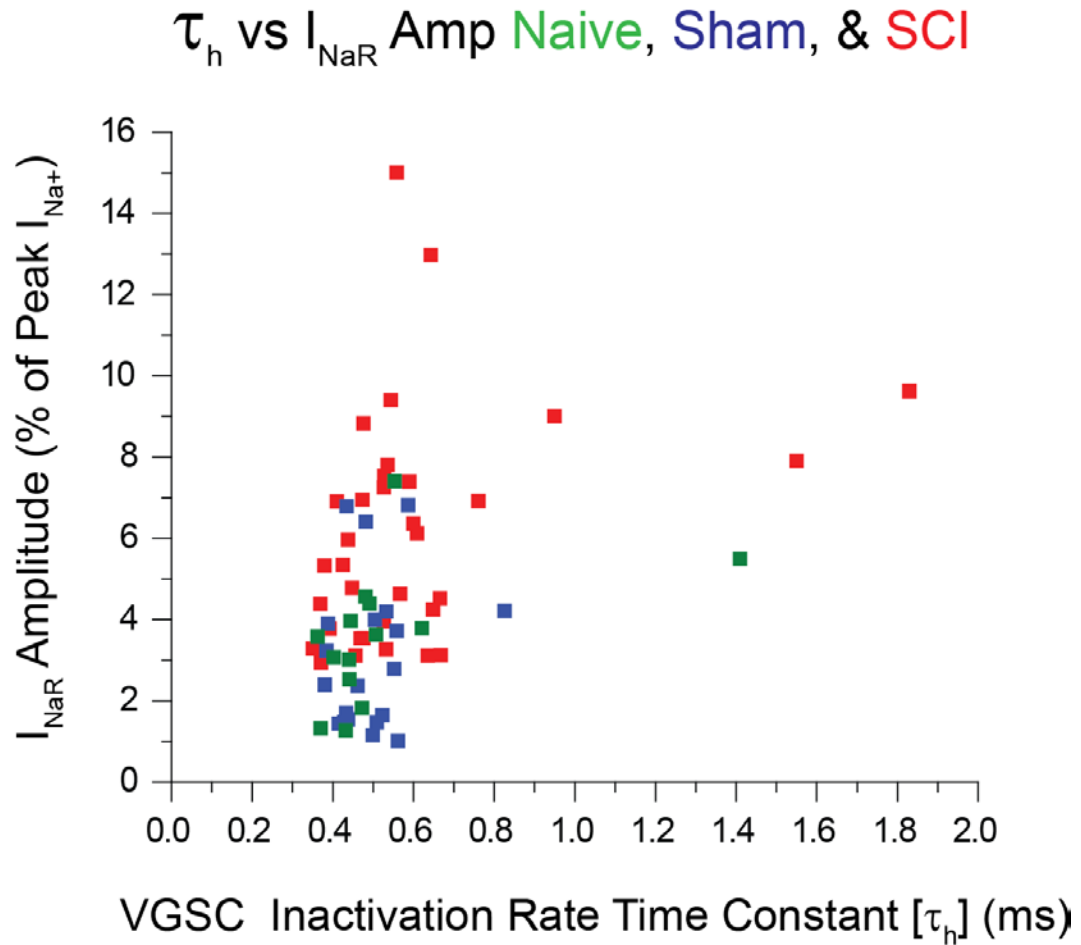


Figure 26: Increased resurgent sodium current (I_{NaR}) amplitude following contusive SCI is not explained by slowed rate of channel open-state inactivation (τ_h). Previously it was demonstrated that there is a strong correlation between rate of VGSC inactivation and I_{NaR} amplitude for some VGSC isoforms. The scatter plot above shows I_{NaR} amplitude (measured as % of peak I_{Na+}) versus the corresponding time constant for open-state inactivation for each recording. With the exception of few outliers no correlation exists for I_{NaR} amplitude in naïve, sham, or SCI neurons. Each box represents a single recording with I_{NaR} from naïve (*green*), sham (*blue*), or SCI (*red*) DRG neurons.

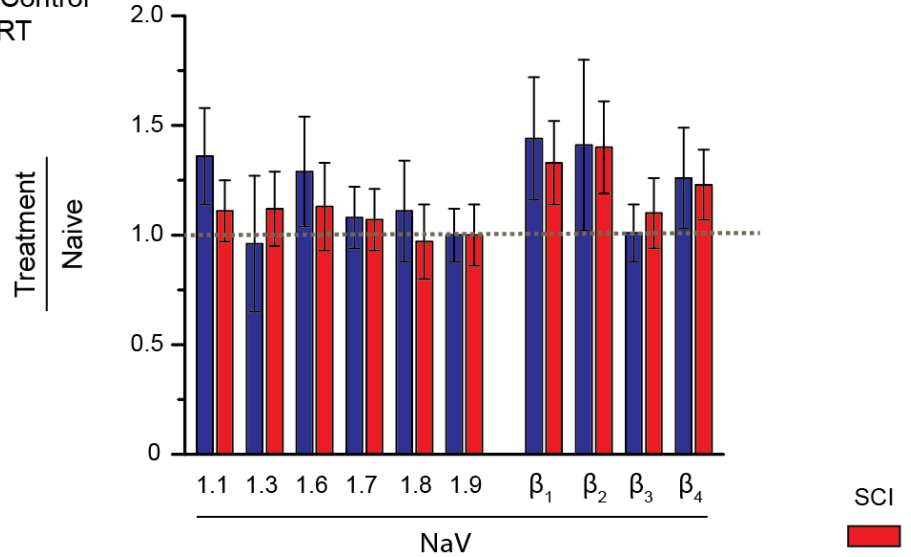
4. *Increased DRG excitability and I_{NaR} amplitude is not supported by gene expression increases in voltage-gated sodium channel isoform and associated β -subunits*

Several voltage-gated sodium channel subunits have been implicated in I_{NaR} generation. Previously, I have demonstrated that NaV1.3, -1.6, and -1.7 are capable of producing I_{NaR} . Additionally results from several studies suggest the NaV β_4 -subunit interacts with the VGSC to produce resurgent inactivation kinetics^{101,102}. Consequently, I next explored whether changes in NaV1.1, -1.6, -7 or β_4 -subunit gene expression contributes to the injury induced increase in I_{NaR} amplitude. Changes in mRNA expression for VGSCs were evaluated using techniques in real-time, SYBR Green RT-PCR and specific primers described in **Chapter II-J** (Table 4). For these experiments total RNA was isolated from excised whole ganglion (L1-L6) for each experimental condition. Raw gene expression C_t values for individual targets were normalized according to a selected internal standard (HPRT in Figure 27-A and ARBP Figure 27-B); normalized gene expression data is shown as the ratio of treatment (either sham or SCI) to naive. As shown in Figure 27, no significant changes in VGSCs or VGSC auxiliary β -subunits are observed in either sham or SCI neurons. Lack of changes in gene expression described here is supported by the minimal changes observed in TTX-S, TTX-R, and persistent current density (Figure 23). Collectively, these results suggest that ganglion wide alterations of select voltage-gated sodium channel isoforms or the NaV β_4 -subunit mRNA expression are not responsible for increased I_{NaR} amplitude following contusive SCI.

Figure 27:

A

Internal Control
HPRT



B

Internal Control
ARBP

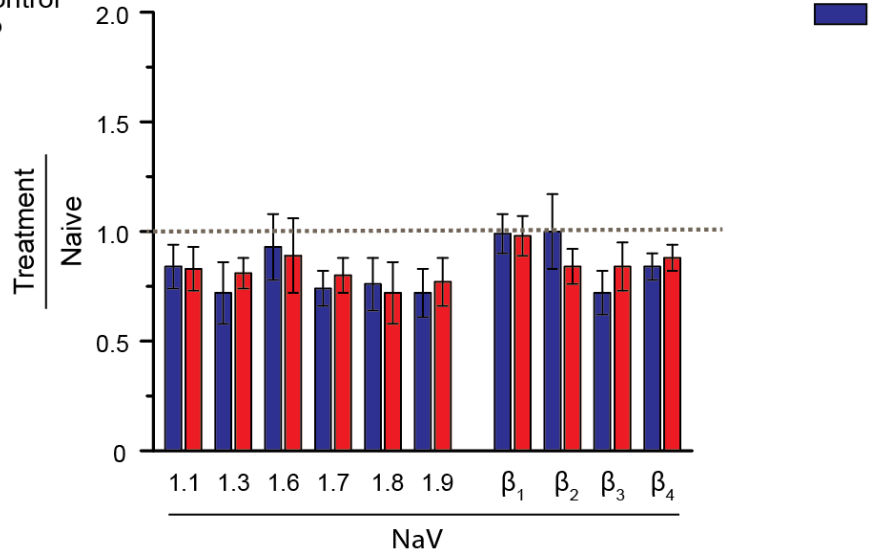


Figure 27: No change in voltage-gated sodium channel (VGSC) subunit expression following contusive SCI. mRNA expression of voltage-gated sodium channel (VGSC) isoforms and auxiliary NaV β -subunits are quantified using real-time SYBR Green RT-PCR—results are displayed in the bar graphs above. Relative quantification of mRNA expression for specific gene targets are shown relative to internal control(s) HPRT (**A**) and ARBP (**B**). Relative quantification was achieved using the Pfaffl model which makes use of target cycle threshold (C_t) values target primer efficiency, internal control C_t values, and internal control primer efficiencies. Sham and SCI gene expression data is shown normalized to naïve gene expression.

Table 7:

Small Soma Dia. DRG Neurons						
	Whole Cell Capacitance (pF) [§]	Current Density				I _{NaR} Amplitude (% peak I _{Na})
		TTX-S	TTX-R	Persistent (@ -10 mV)	Persistent (@ -60 mV)	
Naïve	25.6 ± 5.4	-997.9 ± 139.3 (n=14)	-525 ± 94.1 (n=15)	-30.2 ± 7.2 (n=15)	-77.1 ± 23.9 (n=14)	N/A (n=0/15)
Sham	24.5 ± 4.8	-854.2 ± 133.6 (n=30)	-796.2 ± 107.5 (n=31)	-63.4 ± 22.7 (n=25)	-55.4 ± 9.7 (n=31)	N/A (n=0/32)
SCI	27.4 ± 5.5	-840 ± 139 (n=38)	-674.4 ± 74.6 (n=39)	-49.7 ± 9.5 (n=31)	-55.5 ± 12.9 (n=40)	4.6 ± 1 (n=3/43)
SCI (with I_{NaR})	31.6 ± 2.8	-3268 ± 565 € (n=3)				
Medium/Large Soma Dia. DRG Neurons						
	Whole Cell Capacitance (pF) [§]	Current Density (pA/pF)				I _{NaR} Amplitude (% peak I _{Na})
		TTX-S	TTX-R	Persistent (@ -10 mV)	Persistent (@ -60 mV)	
Naïve	50.9 ± 17.1	-1069 ± 102.5 (n=43)	-710.9 ± 75.7 (n=31)	-27.5 ± 4.2 (n=34)	-53.6 ± 11 (n=34)	3.2 ± 0.5 (n=14/52)
Naïve (with I_{NaR})	45 ± 6.2	-1623.8 ± 191.1€ (n=17)				
Sham	55.1 ± 17	-1522.7 ± 174.1 (n=38)	-1061.2 ± 147.3 #* (n=17)	-50.2 ± 15.7 (n=11)	-40.4 ± 13.1 (n=17)	3.3 ± 0.4 (n=21/38)
Sham (with I_{NaR})	48.9 ± 6.7	-2144.3 ± 225.7 € (n=21)				
SCI	51.7 ± 16.1	-1112 ± 100.2 (n=57)	-727.7 ± 99.2 (n=21)	-30.1 ± 7.2 (n=23)	-21.9 ± 4.1 (n=27)	6.3 ± 0.5 * (n=31/58)
SCI (with I_{NaR})	53.5 ± 18.6	-1411 ± 138.7 € (n=31)				

Table 7: Biophysical properties of naïve, sham, and SCI L1-L6 DRG neurons 14 days post contusive SCI. The table above show the values for the data displayed in **Figures 23-25** for small and medium/large soma diameter DRG neurons. Column two in each table displays the average whole cell capacitance for each group of neurons. \$ for whole cell capacitance \pm SD. € denotes statistical significance ($P < 0.05$) of TTX-S current density for those that have I_{NaR} from those that don't have I_{NaR} with in each condition. #* denotes statistical significance of naïve TTX-R current density from naïve and SCI. * denotes statistical significance ($P < 0.05$) of SCI I_{NaR} amplitude compared to sham and naïve.

D. Discussion

Chronic pain is a prevalent consequence of spinal cord injury (SCI) that can persist for years and significantly impact patient quality of life. As a result of a traumatic, often violent, injury, the pain associated with SCI is complex and characterized as neuropathic in origin. Several potential mechanisms have been associated with SCI pain, but the exact molecular mechanisms contributing to chronic pain following SCI are incompletely understood. SCI is known to trigger changes in electrophysiological properties of several areas of the central nervous system (CNS), including dorsal horn nociceptive projecting and thalamic neurons^{197,206}. Accordingly, pain associated with SCI was thought to originate exclusively from injury induced abnormalities in the CNS according to several mechanisms including, excitation of secondary spinal cord projection neurons⁸⁰, loss of inhibitory neurons near the lesion site²¹⁷, and remodeling of ion channel expression in the spinothalamic tract leading to amplified pain signaling²¹⁰. Interestingly, a more recent report indicates that increased spontaneous activity and hyperexcitability of peripheral DRG neurons (below the level of the lesion) may contribute to the development and maintenance of some types of SCI pain²¹³. Importantly, augmented excitability of small diameter DRG neurons correlated with mechanical allodynia and thermal hyperalgesia in animals post injury²¹³. In this study I explored the hypothesis that altered expression or function of VGSCs contributes to the altered excitability of peripheral DRG neurons following contusive SCI.

Here I report no changes in sodium channel TTX-S, TTX-R, or persistent current density 14 days post contusive injury. In support of this observation I also report no change in VGSC subunit gene expression, as determined by real-time RT PCR. Interestingly, I observed increased I_{NaR} amplitude in SCI DRG neurons when compared to those observed in control (sham and naïve) cells. Additionally, in control neurons I_{NaR} is observed in only a narrow size range of medium/large soma diameter DRG neurons;

14 days post contusive SCI, I_{NaR} is observed in a broader more diverse population of DRG neurons—including small diameter and larger diameter DRG neurons. Collectively, these results suggest that increased I_{NaR} following SCI may contribute to the altered excitability in peripheral DRG neurons and pain following injury.

Because of their important role in the initiation and propagation of action potentials, the contribution of altered expression and dysfunction of VGSCs to hyperexcitability and pain associated with peripheral nerve injury has been extensively studied^{36,70}. Indeed, results from several studies indicate that sodium channel expression and function can be dynamically regulated in animal models of acute and chronic inflammation and peripheral nerve injury. Additionally, altered activity and expression of VGSCs in dorsal horn spinal cord neurons has been shown to contribute to altered excitability and pain following SCI^{197,206}. More specifically, abnormal expression of NaV1.3 in thalamic neurons^{218,219} and increased expression of NaV1.3 and increased ramp and persistent currents in dorsal horn neurons^{80,220} have been observed following SCI. In this report I explored whether altered expression or activity of VGSCs contributed to the reported increase in spontaneous activity and membrane hyperexcitability of small diameter L1-L6 DRG neurons following T10 contusive SCI.

Here we initially hypothesized that increased TTX-S, TTX-R, and resurgent sodium currents (I_{NaR}) in peripheral DRG neurons might contribute to the observed membrane hyperexcitability and increased persistent sodium currents might underlie the increased spontaneous activity of the small diameter DRG following injury. In contrast to my initial hypothesis, no changes in VGSC TTX-S, TTX-R, or persistent currents were observed in small diameter DRG neurons following contusive SCI. In support of these data, I did not observe altered gene expression of NaV1.7, NaV1.8, or NaV1.9—the three major contributors of sodium current found in small diameter DRG neurons.

Although, I_{NaR} are not normally observed in small diameter DRG neurons under control conditions, following contusive SCI I observed robust resurgent sodium currents in several small diameter DRG neurons. Although small in amplitude, I_{NaR} are known to have a profound impact on membrane excitability because of their unique voltage dependence and kinetics. Indeed, I_{NaR} are known to contribute to the high frequency burst firing phenotype of several types of CNS neurons. Accordingly, increased I_{NaR} in small diameter DRG neurons is predicted to contribute to hyperexcitability of neurons following injury. Although others have speculated that I_{NaR} may also contribute to spontaneous activity (SA) in some types of neurons, we rationalize that because I_{NaR} is stimulus dependent—that is to say resurgent kinetics require an initial depolarization before their unique qualities can impact membrane excitability—it is unlikely that I_{NaR} contributes to the initial, spontaneous action potential—even though it likely contributes to the bursting nature of the subsequent [spontaneous] action potentials. Taken together these observations suggest that (1) altered gene expression of sodium channel subunits or augmented TTX-S, TTX-R, or persistent currents do not appear to underlie any of the injury induced electrophysiological changes observed in small diameter DRG neurons and (2) increased I_{NaR} in small diameter DRG neurons may contribute to the augmented membrane excitability post injury.

Although the Walters et al²¹³ study focused solely on the excitability of small diameter DRG neurons post contusive SCI, I also explored whether the properties of medium and large soma diameter DRG neurons were altered following injury. Here I reasoned that this study should also profile the properties and expression of VGSCs in medium and large diameter neurons because augmented excitability of DRG neurons following injury correlated with increased mechanical hypersensitivity—a phenotype proposed to result from altered electrophysiological properties of medium and large DRG neurons. In contrast to small diameter neurons, I did observe some small, but

statistically significant increases in TTX-S and TTX-R sodium current densities in sham medium/large diameter neurons when compared to recordings made from naïve and SCI cells. Although results from several previous studies^{221,222} suggest that a similar increase in TTX-S or TTX-R currents (~30% increase) results in increased excitability of these neurons, it not known whether the excitability of medium/large diameter L1-L6 DRG neurons are altered following SCI. Interestingly, these data distinguish the fact that sham surgery, in this case a laminectomy without a controlled weight drop on the exposed spinal cord, may represent a mild form of injury and inflammation even though it serves as a type of control. Sham surgery is commonly used as a control in spinal cord injury animal models to assess functional motor deficits because animals that undergo sham surgery still maintain motor function below the site of the lesion. In this way sham surgery is really a control best used to assess altered motor function following injury and may not be the ideal control used for pain studies because the laminectomy associated with the sham surgery likely causes minor injury and induces inflammation in the surrounding tissue. With this perspective it is easy to understand how sham surgery might cause changes in VGSC function, as VGSC function and expression are known to be modified by mild injury and inflammation. Despite not observing any changes in TTX-S, TTX-R, or persistent current densities in medium and large diameter neurons following contusive SCI, I did observe a statistically significant increase [near doubling] in I_{NaR} amplitude when compared to control. Additionally, I_{NaR} were observed in a more diverse size population of DRG neurons post injury (from small to large cell soma diameter), whereas I_{NaR} are generally reserved to a subpopulation of medium diameter DRG neurons under control conditions. Again, although it is not clear whether medium and large diameter DRG neurons are hyperexcitable following contusive SCI, our lab's previous observations using *in silico* modeling to predict resurgent current's impact on excitability would suggest such an increase would likely contribute to membrane

hyperexcitability. Taken together these observations suggest increased I_{NaR} in medium and large diameter DRG neurons might contribute to mechanical hypersensitivity observed in SCI animals.

Traumatic injury to the spinal cord results in a myriad of electrophysiological changes that can result in intractable pain. Pain associated with SCI is complex and evidence suggests that it arises from dysfunction of neurons at the site of injury as well as remodeling of neuronal excitability above and below the lesion site. In this study I explored the hypothesis that increased expression and function of VGSCs underlie the reported increase in spontaneous activity and cell soma hyperexcitability observed in below level DRG neuron cell bodies following injury. The most significant findings of this study relate to injury induced increase in resurgent sodium current. Previously I have demonstrated that I_{NaR} is increased by inherited mutations which slow the rate of channel inactivation. Importantly, data from computer simulations suggest that increased I_{NaR} by these mutant channels is sufficient to induce membrane hyperexcitability associated with these inherited disorders, including extreme pain disorders, myopathies, and cardiac arrhythmias. Although increased I_{NaR} has been shown to be increased by mutations which cause inherited disorders of excitability, it was previously unknown whether the properties of I_{NaR} were altered by inflammation or peripheral nerve injury. In this report we have shown that following contusive SCI (1) I_{NaR} is found in both small and large diameter DRG neurons (I_{NaR} is only observed in a subpopulation of medium/large diameter DRG neurons under control conditions) and (2) I_{NaR} amplitude is significantly increased (nearly twice as large in medium and large diameter DRG neurons) when compared to sham and naïve controls. It is predicted that both of these changes may contribute to the cell soma hyperexcitability of L1-L6 DRG neurons following contusive SCI.

1. *Future Directions*

While my observation of increased I_{NaR} following contusive SCI is novel several important questions remain unanswered as I prepare this manuscript for publication. Two questions that stand out are, (1) does increased I_{NaR} correlate with increased excitability and pain following spinal cord injury and (2) what mechanisms are responsible for increased I_{NaR} in both small and medium diameter L1-L6 DRG neurons following contusive SCI? In the next sections of this discussion I elaborate on these important questions and propose a set of experiments which attempt to address them.

a. Does increased I_{NaR} in L1-L6 DRG neurons correlate with augmented excitability and pain following SCI?

The overarching goal of this study was to provide some insight into what mechanisms contribute to increased spontaneous activity and cell soma hyperexcitability in L1-L6 DRG neurons following a moderate T10 contusive SCI. Interestingly I did observe some increases in resurgent sodium current in both small and medium/large diameter DRG neurons which are predicted to contribute to some of the reported changes in excitability following SCI—particularly cell soma hyperexcitability. Although this observation is intriguing, in its present form, it falls short of the ultimate goal of the study because I have not yet demonstrated that increased I_{NaR} correlates with increased excitability and pain following spinal cord injury.

In order to address whether increased I_{NaR} in SCI neurons correlates with increased excitability following injury, future experiments should explore whether intrinsically hyperexcitable neurons following injury express robust I_{NaR} . This can be accomplished by utilizing an experimental setup with both standard electrophysiological recording hardware and instruments to measure cellular excitability with voltage-sensitive dyes. For these experiments cells would be cultured and recorded from as they were previously only now voltage sensitive dyes will be added to a standard

extracellular bath recording solution and the culture will be scanned for spontaneously hyperexcitable cells. Once a cell is identified as intrinsically excitable, that cell would be recorded from, in whole cell voltage clamp mode, to quantify I_{NaR} amplitude. Here voltage sensitive dyes should be utilized, not only because they provide a high throughput method of identifying spontaneously hyperexcitable neurons in culture, but also because the unique composition of the intracellular patch solution makes it difficult to record sodium currents in voltage-clamp mode after first examining whether the cell is hyperexcitable in current clamp configuration. If the results of these experiments reveal that intrinsically hyperexcitable cells have robust I_{NaR} it suggests that the injury induced increased in I_{NaR} amplitude is one factor which contributes to altered excitability of these neurons following SCI.

The Walters et al.²¹³ report demonstrated that increased spontaneous activity and cell soma hyperexcitability correlated with increased pain behavior (mechanical and thermal hypersensitivity) in animals following contusive SCI. In this report I have demonstrated that 14 days post contusive SCI, I_{NaR} amplitude is increased in some small and medium/large diameter L1-L6 DRG neurons and I speculate that these increases contribute to the altered pain behavior observed in animals. In order to address whether increased I_{NaR} in below level DRG neurons contributes to pain following SCI, future experiments should explore whether elimination of I_{NaR} in peripheral DRG neurons of SCI animals alters pain behavior in these animals. Here, an experiment approach employing virally packaged shRNAs, targeted to the $NaV\beta_4$ -subunit could be used to suppress I_{NaR} . Virally packaged shRNAs could be delivered by injecting herpes simplex virus (HSV) containing shRNAs for the $NaV\beta_4$ -subunit into the intrathecal space surrounding L4/L5 DRG. Here $NaV\beta_4$ is targeted because of its suspected role in I_{NaR} electrogenesis. According to several reports, resurgent inactivation kinetics are not an intrinsic property of the channel, but rather a result of the channel pore interacting with

the C-terminus of auxiliary β_4 -subunit—a closely associated member of the channel protein complex¹⁰². Because of its proposed role in the electrogenesis of I_{NaR} it has been hypothesized that either genetic knockdown of $NaV\beta_4$ or inhibition of the sodium channel interaction with $NaV\beta_4$ with a small molecule would result in reduced I_{NaR} amplitude. Indeed, a recent report by Bant and colleagues¹⁰¹ suggests that siRNA knock down of the $NaV\beta_4$ -subunit can reduce I_{NaR} amplitude in cerebellar Purkinje neurons. Here, I propose that behavioral tests (Hargreaves Test and mechanical sensitivity test using Von Frey filaments) will be performed on SCI injured animals (control) as well as SCI animals injected with either virally packaged $NaV\beta_4$ shRNA or scramble shRNA. If the injection of viral shRNA targeted to the $NaV\beta_4$ subunit yields suppression of mechanical or thermal hypersensitivity in animals following SCI, then it may be concluded that increased I_{NaR} contributes to the enhanced pain behaviors observed following contusive SCI.

b. *What mechanisms are responsible for increased I_{NaR} in L1-L6 DRG neurons following contusive SCI?*

The two most prominent observations of this study were that following contusive SCI I_{NaR} amplitude was increased and I_{NaR} were observed in a more diverse and expansive population of DRG neurons following injury^q. I have reasoned that there are numerous possible explanations for increased I_{NaR} ranging from the simplistic and straightforward, increased I_{NaR} resulting from augmented mRNA or protein expression of VGSCs ($NaV1.3$, -1.6 , or -1.7) which carry I_{NaR} or $NaV\beta_4$ (the auxiliary β -subunit responsible integral for resurgent inactivation kinetics) or increased propensity for other VGSCs in DRG neurons—other than $NaV1.6$ —to produce I_{NaR} following injury, to the abstract and poorly understood, I_{NaR} is increased as a result of altered post-translational

^q Under control conditions I_{NaR} are only observed in a subpopulation of medium diameter DRG neurons

modification of proteins involved in the electrogenesis of I_{NaR} (recall constitutive phosphorylation is apparently necessary for I_{NaR} ¹¹¹ although it remains unclear if the sodium channel, the β_4 -subunit, or both are regulated by phosphorylation). As part of this study I explored the change in gene expression hypothesis by profiling the mRNA expression of VGSCs and the VGSC β -subunits from whole DRG ganglion following injury. Results from these experiments demonstrated that following contusive SCI VGSC mRNAs are not altered, suggesting that ganglion wide changes in VGSC gene expression are not responsible for increased I_{NaR} amplitude in DRG neurons following injury. Although interesting, the results from these experiments are negative and have left me without any mechanism to explain the injury induced increase in I_{NaR} amplitude. Below I discuss preliminary data from experiments which have tested two promising alternative hypotheses: (1) increased I_{NaR} results from an increased propensity of VGSCs, other than NaV1.6, to produce I_{NaR} following injury and (2) increased I_{NaR} results from upregulated NaV β_4 gene expression in SCI neurons which express I_{NaR} .

In this study I have reported that not only is I_{NaR} amplitude increased but that this unique current is now observed in a more expansive population of DRG neurons following contusive SCI. Indeed, under control conditions I_{NaR} is observed in only a subclass of medium diameter neurons (39 to 60pF); following injury I_{NaR} can also be observed in small and large diameter DRG neurons, with whole cell capacitance ranging from 28 to 75pF. DRG neurons do not represent a uniform population of cells, but rather a diverse, heterogeneous collection of cells that, depending on their function or modality, can express different combinations ion channels or receptors. The observation that I_{NaR} is observed in a broader size range of DRG neurons following injury raises the possibility that I_{NaR} may be produced by alternative VGSC isoforms following injury. Previous data from our lab suggests that native I_{NaR} in DRG neurons is likely expressed by NaV1.6, because I_{NaR} is not observed in DRG neurons from NaV1.6 knockout animals¹³¹. The

observation that native I_{NaR} is produced by Nav1.6 is unsurprising because it is highly expressed in medium diameter DRG neurons⁵². My observation that I_{NaR} is observed across all size classes of DRG neurons following injury suggests that I_{NaR} may be produced by other sodium channels than Nav1.6. Interestingly, we now know that I_{NaR} can be produced by other VGSC isoforms under certain conditions, namely Nav1.3 and Nav1.7 (see **Chapter III**). Consequently, I have hypothesized that increased I_{NaR} amplitude in DRG neurons following contusive SCI results from increased propensity of Nav1.7 to produce I_{NaR} following injury. To test this hypothesis I suggest using the Nav1.7 selective tarantula toxin, *ProTx-II*²²³, to determine if increased I_{NaR} following contusive SCI is produced by Nav1.7. Accordingly, after naïve and SCI neurons exhibiting I_{NaR} are identified using whole-cell voltage clamp recordings, 10nM *ProTx-II* would be added directly to the bath recording solution and the I_{NaR} voltage-clamp protocol would be repeated²²³. The magnitude and kinetics of I_{NaR} following drug addition would be compared to those observed before drug addition for each experiment to determine if I_{NaR} in SCI neurons is produced by Nav1.7 (paired format experimental analysis). If addition of *ProTx-II* yields altered amplitude or kinetics of I_{NaR} in naïve and SCI neurons and if *ProTx-II* addition to SCI neurons yields more frequent suppression of I_{NaR} , when compared to naïve, then it may be concluded that increased I_{NaR} produced by Nav1.7 contributes to the injury induced increase in I_{NaR} following contusive SCI.

A second alternative hypothesis related to my results is that increased I_{NaR} amplitude following SCI is due to local upregulation of Nav β_4 in cells that express I_{NaR} . As part of this study I have shown that no changes in VGSCs or sodium channel auxiliary β -subunits gene expression were observed 14 days post contusive SCI. At first glance these results appear to suggest that altered I_{NaR} amplitude may not result from upregulation VGSC gene expression, but it is important to consider that these results were obtained from whole ganglion DRG lysates. Moreover, because I_{NaR} expressing

neurons represent a minority (estimated at 35% of all DRG neurons) of the total population of cells found in the DRG ganglion, changes in gene expression could have been missed if they did not occur uniformly across the entire population. For example, consider the possibility that following SCI VGSC subunit gene expression is unaltered ganglion wide, but altered only in cells that express I_{NaR} . Under such a scenario, changes in a small population of cells might be lost in the variability because the majority of cells have unchanged levels of expression. Accordingly, I hypothesize that increased I_{NaR} following SCI results from augmented $NaV\beta_4$ expression in neurons that express I_{NaR} . To test this hypothesis cells exhibiting I_{NaR} could be isolated following recordings and subjected to single-cell real-time RT-PCR. More specifically, $NaV\beta_4$ -subunit expression would be profiled, given its role I_{NaR} electrogenesis, in cells with and without I_{NaR} in control and injured neurons. Results from this series of experiments would determine (1) if $NaV\beta_4$ -subunit expression is enhanced in cells that express I_{NaR} and (2) if $NaV\beta_4$ expression is augmented in SCI neurons that express I_{NaR} when compared to control. Preliminary results, shown in Figure 28, indicate that (1) $NaV\beta_4$ gene expression is increased in SCI neurons with I_{NaR} compared to naïve neurons with I_{NaR} , (2) $NaV\beta_4$ expression in SCI neurons is increased in cells with greater I_{NaR} , (3) $NaV\beta_4$ expression is increased in cells that express I_{NaR} when compared to cells without I_{NaR} , and (4) $NaV\beta_4$ expression is unchanged between SCI and control neurons that do not express I_{NaR} . This last observation might explain why $NaV\beta_4$ was unchanged ganglion wide—as the majority of cells do not express I_{NaR} . Although these results demonstrate the feasibility of the experimental techniques and design, they are preliminary and I recognize that these experiments would need to be repeated before any conclusions could be finalized.

Figure 28:

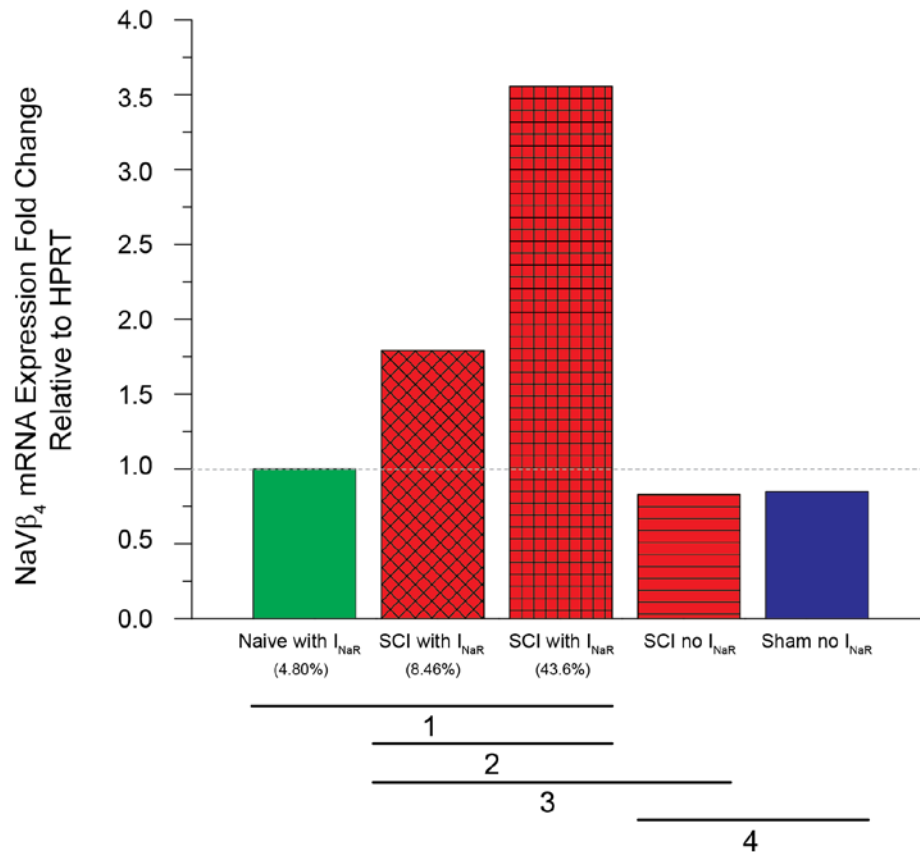


Figure 28: NaVβ₄ mRNA expression is augmented in SCI neurons with resurgent sodium current (I_{NaR}). NaVβ₄ expression from single cells was quantified using real-time Taqman RT-PCR. mRNA was isolated from single cells following whole cell voltage-clamp recordings from naïve, sham, and SCI neurons using a protocol adapted from Chi XX et al 2010²²⁴. Briefly, cells were sucked up into a nuclease free glass pipette, flash frozen in liquid nitrogen, and stored at -80°C until processed. Each isolated cell was treated with 0.25 uL of RNase inhibitor and subjected to a reverse transcriptase reaction using random hexamer primers—approximately 15uL of cDNA was generated from each cell. Because expression of target genes is extremely small in the single cell preparation, cDNA was preamplified for 14 cycles using 0.05x of each target Taqman PCR primer. Preamplification products were diluted 1:5 and 2.5 uL of diluted preamplification product was used in a 10 uL qPCR reaction containing 1x Taqman Gene Expression Master Mix, 1x GOI primers, and nuclease free water. Quantification of NaVβ₄ mRNA expression are shown relative to internal control HPRT. Relative quantification was achieved using the Pfaffl model which makes use of target cycle threshold (Ct) values target primer efficiency, internal control Ct values, and internal control primer efficiencies. Sham and SCI gene expression data is shown normalized to naïve gene expression. Each bar in the graph above is representative of data from a single cell. From these data four preliminary indications are observed: **(1)** NaVβ₄ gene expression is increased in SCI neurons with I_{NaR} compared to naïve neurons with I_{NaR}, **(2)** NaVβ₄ expression in SCI neurons is increased in cells with greater I_{NaR}, **(3)** NaVβ₄ expression is increased in cells that express I_{NaR} when compared to cells without I_{NaR}, and **(4)** NaVβ₄ expression is unchanged between SCI and control neurons that do not express I_{NaR}.

Chapter VII: *Thesis unifying discussion*

The major focuses of this dissertation were to understand the mechanism and molecular determinants of resurgent sodium currents (I_{NaR}) in dorsal root ganglion (DRG) neurons and to determine if these currents were altered by inherited mutations which impair channel inactivation or by peripheral nerve injury. Results from this dissertation characterized the presence of I_{NaR} in a subpopulation of medium/large diameter DRG neurons and determined that multiple voltage-gated sodium channel isoforms expressed in DRG neurons can produce I_{NaR} . Additionally, this dissertation found that muscle and neuronal channelopathy mutations, which slow the rate of channel inactivation, increase I_{NaR} amplitude; moreover, data from this dissertation demonstrated that temperature sensitive I_{NaR} produced by select skeletal muscle channelopathy mutations may contribute to episodic triggering of cold-induced myotonia. Finally, results from this dissertation demonstrated that I_{NaR} amplitude and distribution of cells exhibiting I_{NaR} in DRG neurons were both significantly increased two weeks following moderate contusive spinal cord injury (SCI). Based on the major findings outlined above, three overarching conclusions can be made concerning the body of work presented in this dissertation: (1) multiple VGSC isoforms can produce I_{NaR} , (2) rate of channel inactivation is an important factor which regulates I_{NaR} generation, and (3) I_{NaR} is increased in inherited and acquired disorders of excitability. Each of these overarching conclusions is discussed in the sections which follow.

A. Multiple VGSC isoforms can produce I_{NaR}

Resurgent sodium currents (I_{NaR}) were initially identified and characterized in cerebellar Purkinje neurons as a Na^+ current which flowed during the downstroke of an action potential¹⁰⁵. Resurgence of inward Na^+ current during membrane repolarization is hypothesized to contribute to the spontaneous, high frequency action potential firing phenotype of cerebellar Purkinje neurons^{132,225}. More recently, I_{NaR} has been identified in a subpopulation of medium/large diameter DRG neurons and other fast spiking brain neurons, including neurons of the subthalamic nucleus¹¹³, mesencephalic trigeminal neurons¹²⁹, and neurons of the medial nucleus of the trapezoid body¹³⁰. Interestingly, because I_{NaR} are only observed in select neuronal populations that fire at high frequency it was initially speculated that I_{NaR} may be carried by a subset of Na^+ channels. Single channel experiments determined that the same Na^+ channels which produce the transient, large inward Na^+ current which underlies the upstroke of the action potential also produce I_{NaR} ¹⁰⁵. Indeed, results from several experiments suggest that I_{NaR} results from a novel form of Na^+ channel inactivation that allows the channel to transiently reopen during recovery from inactivation. The novel form of channel inactivation associated with I_{NaR} is believed to result from open-channel block by an endogenous intracellular blocking particle, postulated to be the C-terminus of the VGSC auxiliary $NaV\beta_4$ -subunit^{101,102}, that is relieved by rapid repolarization from positive membrane potentials. With the suggestion that I_{NaR} resulted from an interaction between a Na^+ channel and an auxiliary β -subunit¹⁰¹⁻¹⁰³ one fundamental question remained unanswered: which VGSC isoforms could undergo resurgent, open channel block and produce I_{NaR} ?

Our lab and others have established that I_{NaR} is produced by a TTX-S VGSC, although the identity of the specific channel isoform remains controversial. The observation that I_{NaR} in $NaV1.6$ -null mice is reduced to 10-25% of that seen in wild-type

mice suggests that NaV1.6 underlies most of this current in cerebellar Purkinje¹¹² and DRG neurons¹³¹. Still the presence of residual I_{NaR} in NaV1.6 null-mice has led to the hypothesis that I_{NaR} may be produced by other VGSC isoforms under certain conditions. Indeed, cerebellar nuclear and subthalamic nuclear neurons exhibit significant I_{NaR} in the absence of NaV1.6 expression; it is suspected that NaV1.1 underlies much of the I_{NaR} present in those neurons because NaV1.1 is highly expressed in cerebellar nuclear and subthalamic nuclear neurons of NaV1.6 null-mice¹¹³. Isolating the contribution of specific Na^+ channel isoforms to I_{NaR} observed in primary cell cultures has been made difficult due to the lack of isoform specific pharmacological inhibitors. In the absence of such inhibitors, several studies have asked which VGSC isoforms can produce I_{NaR} using two strategies: expressing VGSC isoforms in hEK293 cells and recording with NaV β_4 -peptide in the recording pipette or expressing VGSCs in cultured primary cells known to be capable of producing I_{NaR} , such as DRG neurons. Using the strategy of incorporating the NaV β_4 -peptide in the recording pipette, NaV1.1²²⁶ and NaV1.5¹¹⁵ were found to be capable of producing “ I_{NaR} -like” currents. While pharmacological induction of I_{NaR} via application of peptide does not definitively demonstrate that either NaV1.1 or NaV1.5 produce I_{NaR} in vivo, results from these experiments suggest that NaV1.1 and NaV1.5 are capable of undergoing resurgent open-channel block with properties that resemble I_{NaR} recorded from brain and DRG neurons. Additionally, experiments by Waxman and colleagues demonstrated that NaV1.2¹¹⁴ is also capable of producing small resurgent sodium currents when expressed in DRG neurons. Collectively, these observations supported the notion that other VGSCs are likely capable of producing I_{NaR} .

As part of this dissertation I explored which VGSC isoforms were capable of producing I_{NaR} . For these experiments I employed a strategy similar to those used by Cummins et al¹³¹ and Rush et al¹¹⁴—whereby modified VGSCs, capable of being pharmacologically isolated, are expressed in DRG neurons and probed for their ability to

produce I_{NaR} using whole-cell voltage clamp electrophysiology. This expression strategy was employed because it has not been possible to observe I_{NaR} in traditional heterologous cell lines expressing VGSC subunits without application of the NaV β_4 -subunit peptide^{123,124,226}. Using this strategy I confirmed that NaV1.6 is capable of producing I_{NaR} and observed, for the first time, that NaV1.3, NaV1.5, and NaV1.7 were capable of producing I_{NaR} when expressed in DRG neurons (**Chapter III** and **IV**). Moreover, in collaboration with Brian Jarecki, I found that human channelopathy mutations which slow the rate of channel inactivation in NaV1.4, NaV1.5, and NaV1.7 produce increased I_{NaR} (**Chapter IV**). Table 8 summarizes which VGSC isoforms are believed to be capable of producing I_{NaR} . Collectively, the body of data presented in this dissertation confirms earlier speculation that I_{NaR} is not a property unique to the NaV1.6 channel isoform, as multiple VGSC isoforms are capable of producing I_{NaR} under both normal and pathological conditions.

Table 8:

VGSC Isoforms	Tissue Expression	Resurgent Sodium Current (I_{NaR})	
		NaV β_4 in Pipette	Expression in DRG neurons
NaV1.1	Brain/DRG	Aman et al 2009 ²²⁶	Unknown
NaV1.2	Brain	Unknown	Rush et al 2005 ¹¹⁴
NaV1.3	Brain/DRG	Unknown	Chapter III (wild-type)
NaV1.4	Skeletal Muscle	Cummins Lab ^A (WT and Mut NaV1.4)	Chapter IV (Mut NaV1.4 only)
NaV1.5	Cardiac Muscle	Wang et al 2006 ¹¹⁵ (WT NaV1.5)	Chapter IV (WT and Mut NaV1.5)
NaV1.6	Brain/DRG/Heart	Unknown	Cummins et al 2005 ¹³¹ (mouse) and Chapter III (rat)
NaV1.7	DRG/Sympathetic	Theile et al 2011 (WT and Mut NaV1.7)	Chapter III and IV (WT and Mut NaV1.7)
NaV1.8	DRG	Unknown	No ^B
NaV1.9	DRG	Unknown	Unknown

Table 8: Multiple VGSC isoforms can produce I_{NaR} . The table above summarizes data from several experiments which suggest that wild-type (WT) NaV1.1, NaV1.2, NaV1.3, NaV1.5, NaV1.6, and NaV1.7 can produce I_{NaR} when expressed in either (1) hEK293 cells +NaV β_4 peptide or (2) DRG neurons. Additionally, as part of this dissertation I have found that human channelopathy mutations (Mut) in NaV1.4, NaV1.5, and NaV1.7 produce increased I_{NaR} when expressed in DRG neurons. ^AUnpublished observation of the Cummins laboratory. ^BPreliminary finding.

Experiments presented in this thesis demonstrated for the first time that NaV1.5 wild-type and NaV1.4 and NaV1.5 mutant channels, which slow the rate of channel inactivation, can produce I_{NaR} when expressed in DRG neurons. Although these observations are informative it is interesting to note that adult DRG sensory neurons are not the native tissue for expression of NaV1.4 and NaV1.5, and it is not known whether either channel isoform has the capacity to produce I_{NaR} when expressed in their native cell background. Indeed, cell background has been shown to be an important factor for I_{NaR} generation as I_{NaR} cannot be observed in channels expressed in heterologous expression systems. Previous work suggests that DRG neurons and cardiac and skeletal muscle all express high levels of mRNA for the NaV β_4 -subunit—the proven open channel blocker responsible for resurgent inactivation kinetics. These observations suggest that cardiac and skeletal myocytes may have the appropriate cell environment necessary for production of I_{NaR} . Still, because NaV1.4 and NaV1.5 are not normally expressed in DRG neurons it remains unclear if either channel really has the capacity to produce I_{NaR} or the production of I_{NaR} in both channels is simply an artifact precipitated by expression in a foreign cell background. Consequently, additional experiments are needed to determine whether NaV1.4 and NaV1.5 wild-type and mutant channels can produce I_{NaR} in skeletal and cardiac myocytes.

B. *Rate of channel inactivation is an important factor which regulates I_{NaR} generation but it is not the sole determinant*

Resurgent sodium currents are an unusual type of sodium current that reactivates during mild repolarizations following a strong, brief depolarization. Normally, upon depolarization, VGSC open and rapidly transition to a non-conducting, inactivated state. Once channels assume an inactivated conformation they are not likely to reopen and require repolarization of the membrane potential before they are available to open again⁵. Also during repolarization, channels transition back (recover) to a conformation which is ready to open through non-conducting (closed) state configurations. I_{NaR} is thought to arise from a novel mechanism which allows for atypical recovery from channel inactivation. This novel recovery from inactivation in Na^+ channels is believed to result from open-channel block by an intracellular particle that binds to the sodium channel open state preventing the channel from inactivating by its classic mechanism¹⁰⁶. Consequently, neurons exhibiting I_{NaR} have two forms of channel inactivation, domain III-IV linker (IFM) mediated channel inactivation and endogenous open-channel block, which compete with each other for the same, or overlapping, binding sites within the channel pore^{102,115}. Evidence for two, competing forms of channel inactivation led some to hypothesize that the rate of intrinsic channel inactivation might be an important factor in I_{NaR} electrogenesis. Indeed, slowed rate of intrinsic channel inactivation via application of β -pompilidotoxin augmented I_{NaR} in neurons from NaV1.6 null-mice—neurons which would otherwise produce little I_{NaR} ¹²⁷. Additionally, it was initially proposed that the relatively slow rate of channel inactivation in the NaV1.6 channel isoform was a major factor which allowed this channel to produce the majority of I_{NaR} found in brain and DRG neurons. Collectively, these findings suggested that the rate of channel inactivation was likely an important factor which influences I_{NaR} generation.

As part of this dissertation, I explored how rate of channel inactivation influenced I_{NaR} amplitude. I found that human channelopathy mutations which slowed the rate of channel inactivation in NaV1.4, NaV1.5, and NaV1.7 all significantly increased I_{NaR} amplitude (**Chapter IV**). Parallel experiments done in collaboration with Dr. John Theile demonstrated that increased I_{NaR} amplitude was specific to channel mutations which slowed the rate of channel inactivation¹²³, but not mutations that selectively altered activation. Finally, I demonstrated that cold temperature induced slowing of channel inactivation augmented I_{NaR} amplitude in D-IV mutant channels which impair channel inactivation by uncoupling channel opening and formation of the inactivated pore (**Chapter V**). The relationship between rate of channel inactivation and I_{NaR} amplitude in wild-type and mutant channels is summarized in Figure 29. Here I show the rate of channel inactivation and I_{NaR} amplitude for every cell expressing pharmacologically isolated recombinant channels recorded in this thesis. Analysis of the data presented in Figure 29 indicates that a loose, positive correlation exists between rate of channel inactivation and I_{NaR} amplitude—generally, the slower the rate of channel inactivation the greater the I_{NaR} amplitude. These data in conjunction with the previous study indicating that pharmacological slowing of channel inactivation via toxin application could augment I_{NaR} amplitude, suggest that slowed rate of channel inactivation is sufficient to induce or increase I_{NaR} amplitude in some VGSC isoforms.

Figure 29:

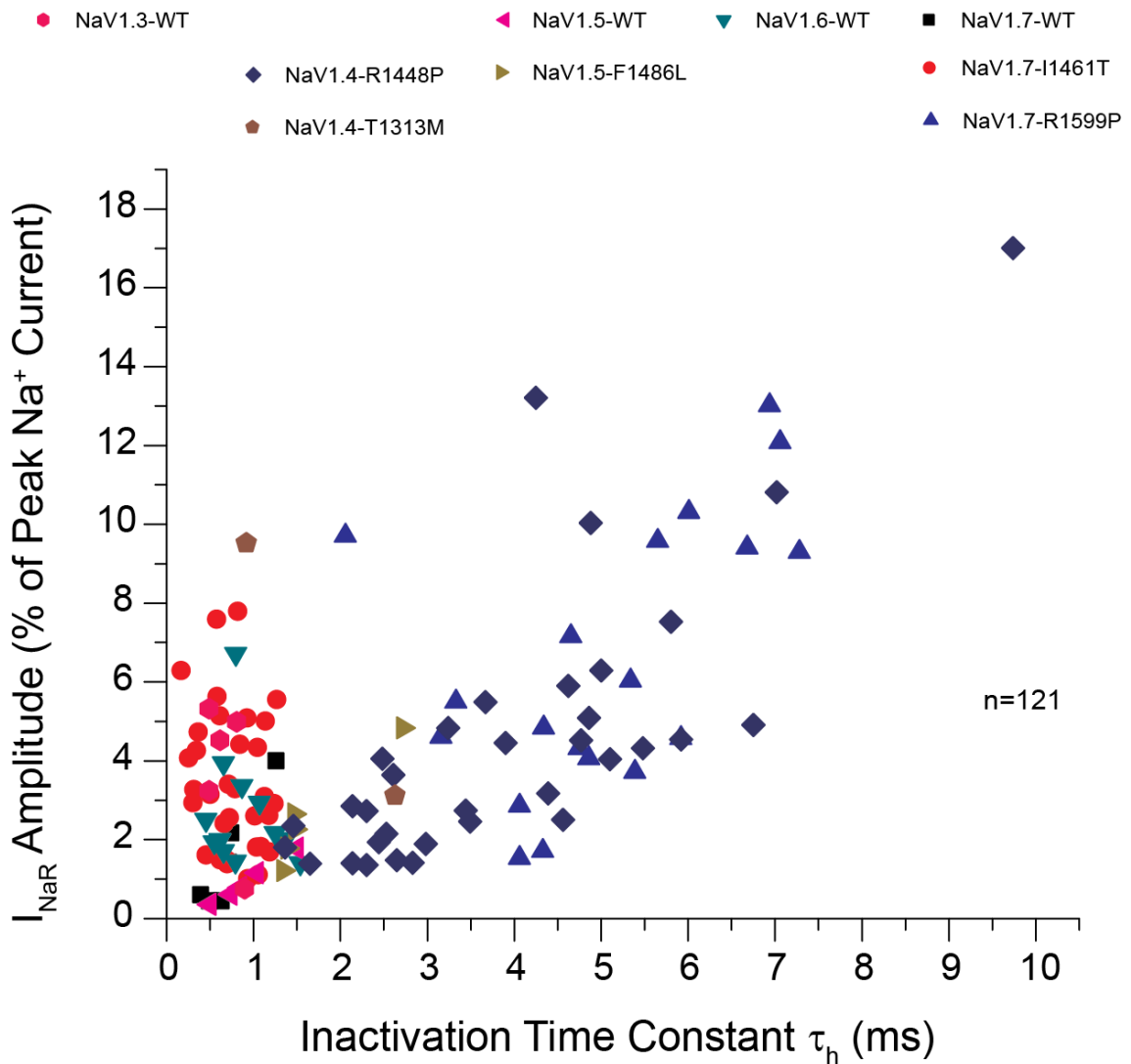


Figure 29: Rate of channel inactivation correlates to I_{NaR} amplitude for recombinant VGSCs expressed in DRG neurons. The scatter plot above shows the inactivation time constant τ_h (ms) versus I_{NaR} amplitude for the corresponding cell. Each point represents an individual recording made from biolistically transfected DRG neurons expressing wild-type (WT) or mutant recombinant VGSC isoforms including: NaV1.3-WT, NaV1.4-R1448P, NaV1.4-T1313M, NaV1.5-WT, NaV1.5-F1486L, NaV1.6-WT, NaV1.7-WT, NaV1.7-I1461T, or NaV1.7-R1599P. See the key above to reference the assigned symbol for each channel isoform. The dark grey line represents a linear line of best fit. The inactivation rate time constant was measured at +10 mV from a holding potential of -100 mV. The data presented in this figure is representative of 121 recordings from transfected neurons that exhibit I_{NaR} .

Close examination of the body of data presented in this thesis indicate that, while rate of channel inactivation is important, it is not likely the sole determinant of I_{NaR} amplitude. First, while the cumulative data shown in Figure 29 shows a correlation between slowed rate of channel inactivation and increased I_{NaR} amplitude, the correlation is weaker than would be expected if rate of channel inactivation was the sole determinant of I_{NaR} amplitude. Several additional pieces of evidence presented throughout this dissertation support the claim that the rate of channel inactivation is not the sole determinant of I_{NaR} amplitude. Two pieces of such evidence are presented in Figure 30 which summarizes the average correlation between rate of channel inactivation and I_{NaR} amplitude for NaV1.3-WT, NaV1.4-WT, NaV1.5-WT, NaV1.6-WT, NaV1.7-WT, and NaV1.8-WT. Here we see that two VGSC isoforms do not produce I_{NaR} when expressed in DRG neurons: NaV1.4 and NaV1.8. Reduced or absent I_{NaR} in NaV1.4 might be explained by the fast rate of channel inactivation; however, cold-temperature induced slowing of channel inactivation does not induce I_{NaR} in NaV1.4-WT channels (**Chapter V**) while mutations which slow the rate of channel inactivation in NaV1.4 cause an increase in I_{NaR} (**Chapter IV**). Taken together these conflicting observations suggest at a minimum that simple slowing of channel inactivation is not sufficient to induce I_{NaR} —likely other factors, such as the way that channel inactivation is slowed or isoform specific regulation of the channel complex may also be important. The claim that rate of channel inactivation is not the sole determinant of I_{NaR} is also supported by my observation that the NaV1.8 channel isoform does not produce classic I_{NaR} . As seen in Figure 30, NaV1.8 has the slowest rate of channel inactivation, yet preliminary studies indicate that NaV1.8 does not produce I_{NaR} . This observation contrasts with my initial hypothesis, which predicted that NaV1.8 would produce the greatest amplitude of I_{NaR} based on its significantly slower rate of channel inactivation relative

to the other VGSC isoforms which can exhibit I_{NaR} in DRG neurons (NaV1.3, NaV1.5, NaV1.6, and NaV1.7). The absence of I_{NaR} in NaV1.8 suggests that I_{NaR} is likely modulated by other factors than rate of channel inactivation. The final piece of evidence concerns the relationship between rate of channel inactivation and I_{NaR} amplitude among the wild-type VGSC isoforms which produce I_{NaR} when expressed in DRG neurons (Figure 30). Here we see that while NaV1.3-WT, NaV1.5-WT, NaV1.6-WT, and NaV1.7-WT all have statistically indistinguishable time constants for channel inactivation, NaV1.3-WT and NaV1.6-WT produce significantly ($P < 0.05$) greater I_{NaR} amplitude than NaV1.5-WT and NaV1.7-WT (Table 9). Again, the observation of differential I_{NaR} amplitude among channel isoforms with similar rates of channel inactivation suggest that other factors, besides rate of channel inactivation, regulate I_{NaR} generation.

Figure 30:

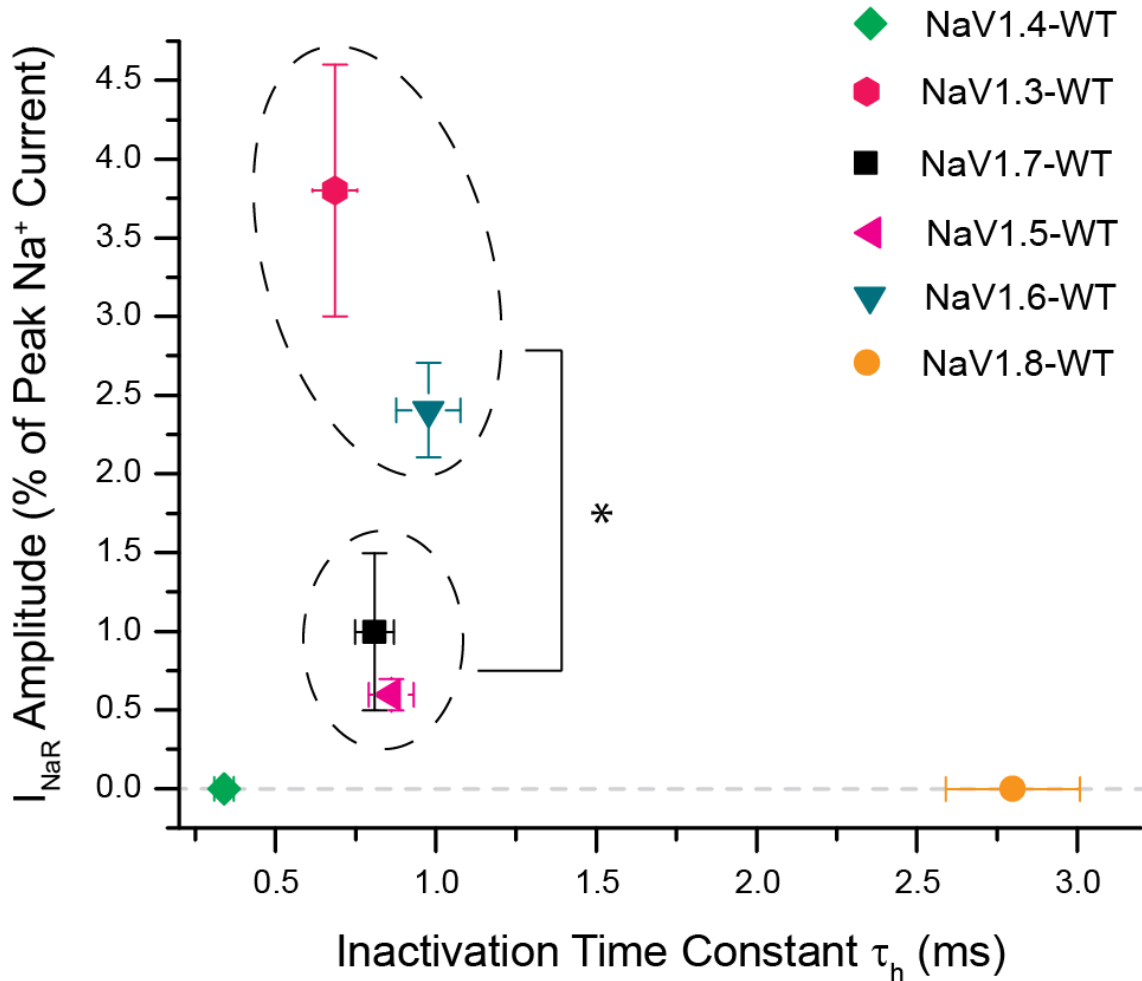


Figure 30: Summary of average correlation between rate of channel inactivation and I_{NaR} amplitude for wild-type VGSC isoforms. The scatter plot above shows the average inactivation rate time constant τ_h (ms) versus the average I_{NaR} amplitude for the corresponding wild-type (WT) voltage gated sodium channel isoform. Taken together this data would suggest that rate of channel inactivation is not the sole determinant for I_{NaR} because NaV1.3-WT, NaV1.5-WT, NaV1.6-WT, and NaV1.7-WT all have similar rates of channel inactivation yet NaV1.3-WT and NaV1.6-WT have significantly greater I_{NaR} amplitude and NaV1.8-WT, which has the slowest rate of channel inactivation, does not produce I_{NaR} . Each point shows standard error bars for both average I_{NaR} amplitude and inactivation rate time constant. Each point is representative of between 5 to 23 cells (see **Table 9** for exact numbers). The green diamond is representative of NaV1.4-WT, the red hexagon is representative of NaV1.3-WT, the black square is representative of NaV1.7-WT, the pink triangle is representative of NaV1.5-WT, the blue triangle is representative of NaV1.6-WT, and the orange circle is representative of NaV1.8-WT. For both NaV1.4-WT and NaV1.8-WT no I_{NaR} were observed. NaV1.3-WT, NaV1.5-WT, NaV1.6-WT, and NaV1.7-WT all have statistically indistinguishable time constants of channel inactivation. However, NaV1.5-WT and NaV1.7-WT have significantly ($P < 0.05$, one way anova) decreased I_{NaR} amplitude compared with NaV1.3-WT and NaV1.6-WT (denoted by *).

Table 9:

VGSC Isoform	Inactivation Rate Time Constant (τ_h)	I_{NaR} amplitude (% of peak Na^+ Current)
NaV1.3	0.73 ± 0.07 (n=8)	3.8 ± 0.8 (n=5 of 8) [#]
NaV1.5	0.90 ± 0.07 (n=20)	0.6 ± 0.1 (9 of 18)
NaV1.6	1.02 ± 0.10 (n=17)	2.4 ± 0.3 (8 of 14) [#]
NaV1.7	0.85 ± 0.06 (n=23)	1.0 ± 0.5 (n=5 of 21)
NaV1.4	0.34 ± 0.03 (n=11) [‡]	None Detected (n=0 of 11)
NaV1.8	2.84 ± 0.21 (n=10) [‡]	None Detected (n=0 of 11)

Table 9: Relationship between rate of channel inactivation and I_{NaR} amplitude in wild-type VGSCs. Table 9 displays the values shown in **Figure 30**. VGSC isoforms NaV1.3, NaV1.5, NaV1.6, and NaV1.7 have statistically indistinguishable rates of channel inactivation. [‡]NaV1.4 and NaV1.8 have statistically significant faster and slower rates of channel inactivation than the aforementioned group of VGSCs. [#] I_{NaR} amplitude produced by NaV1.3-WT and NaV1.6-WT is significantly greater than I_{NaR} amplitude produced by NaV1.5-WT and NaV1.7-WT. In each case significant is in reference to statistically significant ($P < 0.05$) according to post-hoc student t-test.

Research by Raman and colleagues has identified two additional factors which may be important likely important for I_{NaR} generation: affinity of the blocking particle (NaV β_4) for the Na⁺ channel isoform and differential regulation of the resurgent sodium channel complex. Differential affinity of the blocking particle for different VGSC isoforms was first suggested by Raman and colleagues, who found that cerebellar Purkinje and subthalamic neurons, expressing different VGSC isoforms, exhibit I_{NaR} with different kinetics of open channel block^{113,126}. With respect to data presented in this dissertation, differential affinity of the resurgent, open-blocking particle among channel isoforms is supported by the observation that VGSCs with similar rates of channel inactivation can produce disparate amplitudes of I_{NaR} . Moreover, inability for NaV1.4 and NaV1.8 to produce I_{NaR} could also be explained by differential affinity of the C-terminus of the NaV β_4 -subunit for the channel pore—decreased affinity would mean no I_{NaR} in either channel results from decreased binding of NaV β_4 within the channel pore. Conversely, increased affinity could also explain the absence of I_{NaR} in NaV1.4 and NaV1.8 as tight binding of the blocking particle within each pore might mean that the blocking particle remains bound at intermediate potentials resulting in persistent channel block that is indistinguishable from intrinsic channel inactivation. My data cannot readily distinguish between these two possibilities, especially with regard to NaV1.8. The second factor which I speculate may influence I_{NaR} is differential regulation of the resurgent sodium channel complex. According to reports by Raman and colleagues, open channel block associated with I_{NaR} is regulated by phosphorylation of the channel, the blocking particle, or both¹¹¹. Because VGSC isoforms have been shown to be differentially regulated by kinases and phosphatases^{125,227} and phosphorylation of a subunit within the resurgent sodium channel complex regulates I_{NaR} , I speculate that differential regulation of VGSC subunits may also be an important factor in I_{NaR} electrogenesis. Understanding how phosphorylation regulates I_{NaR} electrogenesis is a very important and unresolved

question that should be examined in future studies. Figure 31 summarizes my working hypothesis concerning the factors which influence I_{NaR} generation and amplitude: (1) rate of channel inactivation, (2) affinity of the resurgent, open blocking particle for individual Na^+ channel isoforms, and (3) regulation of expression or function of VGSC subunits.

Figure 31:

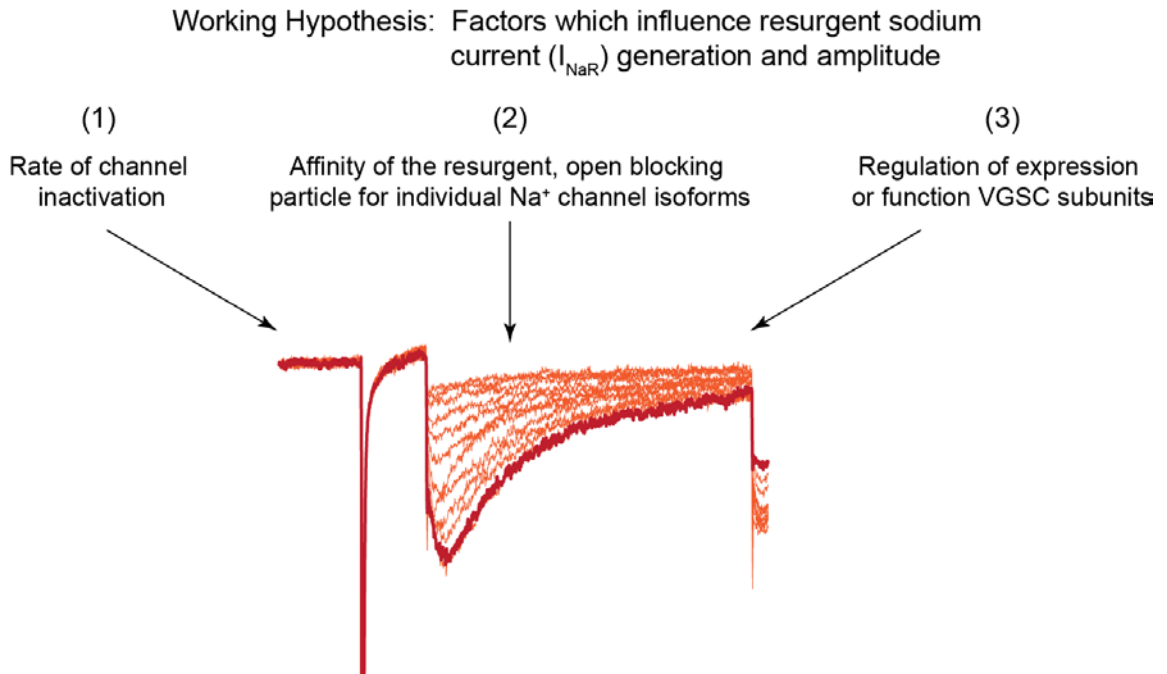


Figure 31: Working hypothesis: Factors which influence I_{NaR} generation and amplitude. The working hypothesis shown above is based on data presented in this dissertation and previous literature concerning I_{NaR} electrogenesis. **(1)** Data presented in **Chapter IV** and **-V** demonstrate that rate of channel inactivation is an important factor which regulates I_{NaR} generation. Data supporting rate of channel inactivation is summarized in **Figure 28**. **(2)** Differential affinity of the resurgent, open blocking particle for individual Na^+ channel isoforms was initially suggested by Raman and colleagues¹²⁶. Data summarized in **Figure 29** supports this claim as VGSC isoforms with similar rates of channel inactivation produce differential amplitudes of I_{NaR} . Phosphorylation of the resurgent sodium channel complex has previously been suggested to regulate I_{NaR} amplitude¹¹¹. **(3)** Here I speculate that regulation of the expression or function of VGSC subunits integral to the resurgent sodium channel complex may be another important factor which regulates I_{NaR} amplitude. Although I do not present or address (3) with an experiments presented in this dissertation, future experiments should focus on understanding the molecular regulation of I_{NaR} electrogenesis under normal and pathological conditions.

C. *Resurgent sodium current (I_{NaR}) is increased in inherited and acquired disorders of excitability*

I_{NaR} was initially described in cerebellar Purkinje neurons¹⁰⁵, however, it has been found more recently in other cerebellar neuron types¹¹⁷, subthalamic neurons¹¹³, mesencephalic trigeminal neurons¹²⁹, neurons of the medial nucleus of the trapezoid body¹³⁰, and large diameter DRG neurons¹³¹. Although relatively small in amplitude, I_{NaR} peaks near the threshold for action potential formation (-30 mV to -40 mV)—a range of voltages where the cell is likely to be most sensitive to small currents. Additionally, the mechanism of channel inactivation associated with I_{NaR} not only results in transient inward Na^+ current on the downstroke of the action potential, but also permits rapid recovery and repriming of resurgent inactivated sodium channels; the presence of depolarizing current early during membrane repolarization and augmented availability of channels near threshold for action potential firing are both likely to facilitate high frequency firing of action potentials¹⁰⁵. Indeed, the presence of I_{NaR} in neuronal populations has been shown to significantly enhance neuronal excitability by facilitating high-frequency burst firing and contributing to repetitive spontaneous generation of action potentials¹³². The presence of I_{NaR} in select CNS neuron populations that fire at high frequency is hypothesized to be necessary for fast signal processing and rapid integration of signals involved in a myriad of physiological processes including proprioception. Indeed, suppression of I_{NaR} in select CNS neurons has been shown to compromise their excitability and reduce their capacity to function normally, resulting in behavior abnormalities including ataxia, tremor, and impaired motor coordination in the whole animal¹³⁴. While I_{NaR} appears to be integral to the coordinated signal processing in some CNS neurons, the physiological role of I_{NaR} in the periphery is undefined. Knowing that I_{NaR} can have a significant impact on membrane excitability in CNS neurons, a central aim of this dissertation was to explore whether I_{NaR} were augmented

by inherited channelopathy mutations which slow the rate of channel inactivation or by peripheral nerve injury.

1. *Inherited channelopathy mutations which slow the rate of channel inactivation increase resurgent sodium currents (I_{NaR}).*

A central focus of this dissertation was to explore whether inherited channelopathy mutations which slowed the rate of channel inactivation increased I_{NaR} . The rationale for studying inherited channelopathy mutations which slow the rate of channel inactivation was derived from the observation that application of β -pompilidotoxin, which slowed the rate of channel inactivation, increased I_{NaR} ¹²⁷. Although many channelopathy mutations which slowed the rate of channel inactivation had previously been characterized, they were studied in non-excitable heterologous expression systems (ie. hEK293 cells or oocytes) under recording conditions from which it has not been possible to observe I_{NaR} ^{87,124,169}. Consequently, prior to research performed in this dissertation, it was not known whether VGSC channelopathy mutations which slow the rate of channel inactivation increase I_{NaR} . In order to determine if such channelopathy mutations increased I_{NaR} , we utilized a strategy of expressing modified recombinant VGSCs, which could be pharmacologically isolated from endogenous VGSCs, in DRG neurons using biolistic transfection methodology. This strategy allowed us to study the mutant VGSCs in a cellular background which had previously been shown to allow recombinant channels to produce I_{NaR} ^{114,131}. Using this strategy we observed, for the first time, that a paroxysmal extreme pain disorder (PEPD) mutation in the human peripheral neuronal Na^+ channel NaV1.7, a paramyotonia congenital (PMC) mutations in the human skeletal muscle Na^+ channel NaV1.4, and a long-QT type 3/ sudden infant death (SIDS) mutation in the cardiac Na^+ channel all substantially increased the amplitude of I_{NaR} (**Chapter IV**).

Because I_{NaR} contributes to enhanced intrinsic excitability of some CNS neurons, enhanced I_{NaR} produced by mutant channels was predicted to promote high-frequency repetitive firing of action potentials. Importantly, *in silico* simulations modeling excitability in nociceptive neurons and cardiac myocytes, indicated that increased I_{NaR} associated with the NaV1.7 PEPD mutation could induce high-frequency action potential firing and increased I_{NaR} associated with the NaV1.5 LQT-3/SIDS mutation could broaden the cardiac action potential (**Chapter IV**). Additionally, *in silico* modeling of a skeletal muscle fiber found that increased I_{NaR} and slowed rate of channel inactivation in NaV1.4 mutants produced a sustained burst of myotonic after-discharges, suggesting that I_{NaR} in skeletal muscle will promote myotonia—the predominant symptom of paramyotonia congenita¹⁷⁸. Close examination of the modeling data for each mutant channel indicates that slowed rate of channel inactivation and increased I_{NaR} amplitude, as a consequence of impaired inactivation, act synergistically to produce augmented action potential firing with the NaV1.7 PEPD mutant and the NaV1.4 PMC mutant, and prolonged action potential duration with the NaV1.5 LQT-3/SIDS mutant. This observation contrasts with the traditional hypothesis that impaired kinetics of inactivation and/or incomplete inactivation, alone, underlies the increased membrane excitability as a consequence of channelopathy mutations which affect channel inactivation. Consequently, data presented in this dissertation suggest, for the first time, that increased I_{NaR} could substantially exacerbate the effects of disease mutations which slow the rate of channel inactivation on cellular excitability and might underlie the burst discharge of action potentials common to many neurological disorders.

The data presented in **Chapter V** demonstrates that mutations which impair inactivation in three different VGSCs produce increased I_{NaR} when compared to wild-type channels. The observation that mutations which impair the rate of channel inactivation increase I_{NaR} in multiple channel isoforms is intriguing because a large number of

missense sodium channel mutations slow the rate of channel inactivation and, therefore, may increase I_{NaR} . Indeed, Table 10 lists 36 sodium channel mutations which slow the rate of channel inactivation and are therefore predicted to increase I_{NaR} . It is interesting to note that while this dissertation examines NaV1.7 PEPD, NaV1.4 PMC, and NaV1.5 LQT-3/SIDS mutations, Table 10 references several mutations in NaV1.1 and NaV1.3 which cause various forms of epilepsy. Future studies should examine whether NaV1.1 or NaV1.3 mutant channels produce increased I_{NaR} when expressed in DRG neurons and/or CNS neurons.

Finally, an important question that remains unresolved is whether NaV1.4 and NaV1.5 mutant channels, which produce large I_{NaR} in the adult DRG neuron expression system, are capable of producing I_{NaR} when expressed in their native environment. The data presented in this dissertation, in conjunction with the findings from previous studies^{114,131}, clearly demonstrates that DRG neurons have the appropriate cellular environment for production of I_{NaR} . Conversely, adult DRG neurons are not the native tissue for expression of NaV1.4 and NaV1.5, and it is not known whether cardiac and skeletal muscle cells have the appropriate cellular environment for the production of I_{NaR} . Previous work has demonstrated that DRG neurons, cardiac muscle, and skeletal muscle have enriched mRNA expression of the NaV β_4 -subunit, the proposed resurgent open channel blocker, suggesting that both skeletal and cardiac myocytes might express the appropriate background to allow for production of I_{NaR} . However, it is still uncertain as to whether this is true, because I_{NaR} has not yet been detected in native cardiac or skeletal muscle. Future experiments should focus on determining whether NaV1.4 and NaV1.5 mutant channels can exhibit I_{NaR} when expressed in their native cellular environment. Only after it is confirmed that I_{NaR} can be produced by NaV1.4 and NaV1.5 mutant channels found in their native environment can it be concluded that I_{NaR} is a likely disease mechanism for channel mutations expressed in muscle cells.

Table 10:

Mutation	Location	Syndrome	Δh_{inf} (mV)	Rate of inactivation	References
Nav1.1-L263V	IS5	FHM	8	slower	<u>221</u>
Nav1.1-R1648C	IV-S4	SMEI	-7	slower	<u>222</u>
Nav1.1-R1648H	IV-S4	GEFS+	-1.5	slower	<u>223</u>
Nav1.1-F1661S	IV-S5	SMEI	12	slower	<u>222</u>
Nav1.3-K354Q	I-S5-SS1 linker	epilepsy	-4	slower	<u>224</u>
Nav1.4-L266V	IS5	PMC/CAM	12	slower	<u>225</u>
Nav1.4-V445M	IS6	PAM	-3	slower	<u>226</u>
Nav1.4-S804F	IIS6	PAM	3	slower	<u>227</u>
Nav1.4-R1132Q	IIIS4-3	HypoPP	-4	slower	<u>228</u>
Nav1.4-A1152D	IIIS4S5	PMC	6	slower	<u>229</u>
Nav1.4-A1156T	IIIS4S5	PMC	5	slower	<u>173</u>
Nav1.4-G1306A	III-IV linker	PAM	5	slower	230,231
Nav1.4-G1306E	III-IV linker	PAM/PMC	12	slower	230,231
Nav1.4-T1313M	III-IV linker	PMC	+3/+17	slower	173,232
Nav1.4-T1313A	III-IV linker	PMC	11	slower	<u>233</u>
Nav1.4-L1433R	IVS3	PMC	15	slower	<u>173</u>
Nav1.4-R1448C/H/P/S	IVS4-1	PMC	-13	slower	134,172,173,234
Nav1.4-F1473S	IVS4S5	PAM	18	slower	<u>235</u>
Nav1.4-F1705I	C-term	PMC	9	slower	<u>236</u>
Nav1.5-S941N	II-III linker	LQT3	0	slower	<u>237</u>
Nav1.5-S1333Y	IIIS4-S5	SIDS/LQT3	8	slower	<u>238</u>
Nav1.5-F1486L	III-IV linker	LQT3/SIDS	14	slower	<u>155</u>
Nav1.5- Δ KPQ	III-IV linker	LQT3	-6	mixed	<u>239</u>
Nav1.5-D1595H	IVS3	DCAVA	-7	slower	<u>240</u>
Nav1.5-R1623Q	IVS4	LQT3	0	slower	<u>241</u>
Nav1.5-R1626P	IVS4	LQT3	-7	slower	<u>237</u>
Nav1.5-M1652R	IVS4-S5	LQT3	8	slower	<u>237</u>
Nav1.5-F2004L	C-term	SIDS/LQT3	5	slower	<u>155</u>
Nav1.7-V1298F	IIIS4-S5	PEPD	20	slower	<u>152</u>
Nav17-V1299F	IIIS4-S5	PEPD	21	slower	<u>152</u>
Nav1.7-I1461T	IIIS4-S5	PEPD	20	slower	152,168
Nav1.7-T1464I	III-IV linker	PEPD	19	slower	152,168
Nav1.7-M1627K	IVS4-S5	PEPD	19	slower	168,170

Table 10: VGSC channelopathy mutations that are likely to increase resurgent sodium current (I_{NaR}). The table above lists the VGSC mutations which exhibit slowed rate of channel inactivation and are predicted to cause and increase in I_{NaR} . The mutations highlighted in green are the ones that I have examined and characterized in this dissertation. According to data collected in collaboration with Dr. John Theile and not discussed in this document, three additional NaV1.7 PEPD mutations, highlighted in yellow, exhibit enhanced I_{NaR} amplitude¹⁶⁹. Finally, preliminary data, highlighted in blue and not discussed in this document, found that the NaV1.5-M1652R (LQT-3 mutation) and the NaV1.4-S804F (PAM mutation) produce augmented I_{NaR} amplitude when expressed in DRG neurons. Abbreviations: Δh_{inf} : change in voltage-dependence of steady-state inactivation. FHM: familial hemiplegic migraine; ICEGTC: intractable childhood epilepsy with generalized tonic-clonic seizures; SMEI: severe myoclonic epilepsy of infancy; GEFS+: generalized epilepsy with febrile seizures plus; HypoPP: hypokalemic periodic paralysis; PMC, paramyotonia congenital; PAM, potassium-aggravated myotonia; CAM, cold-aggravated myotonia; LQT3, long QT 3 syndrome; SIDS, sudden infant death syndrome; DCAVA, dilated cardiomyopathy with atrial and ventricular arrhythmia; PEPD paroxysmal extreme pain disorder.

2. *Resurgent sodium currents (I_{NaR}) are increased by contusive spinal cord injury (SCI)—a model of peripheral nerve injury.*

In addition to examining if I_{NaR} was affected by inherited channelopathy mutations which slow the rate of channel inactivation, I also explored whether the biophysical properties of I_{NaR} were altered following a model of peripheral nerve injury. For these experiments the model of peripheral nerve injury I utilized was a T10 contusive spinal cord injury (SCI). The T10 contusive spinal cord injury model was utilized based on recent evidence which suggested that following injury, animals exhibited increased mechanical and thermal hypersensitivity that was correlated with increased spontaneous and high frequency firing of action potentials in peripheral (L1-L6) DRG neurons. Given my previous observation that increased I_{NaR} associated with inherited channelopathies likely contributes to the high frequency burst discharge of action potentials associated with inherited disorders that cause extreme pain (**Chapter IV**), here I hypothesized that increased I_{NaR} may also contribute to the augmented membrane excitability in peripheral neurons following injury. I found that I_{NaR} amplitude was nearly doubled in SCI animals when compared with controls. Importantly, increased I_{NaR} post contusive SCI is also TTX-S and has similar kinetics and voltage dependence as those observed in naïve animals. Additionally, following SCI I_{NaR} was observed in a broader population of DRG neurons, including small diameter and large diameter DRG neurons; this finding contrasts with the observation that I_{NaR} are only observed in a subpopulation of medium/large diameter DRG neurons under control conditions. Interestingly, increased I_{NaR} in SCI neurons did not correlate with slowed rate of channel inactivation, as was observed previously with mutant channels. A number of mechanisms could underlie increased I_{NaR} two weeks post contusive SCI; here I discuss two possible explanations.

Increased I_{NaR} two weeks post contusive SCI might result from enhanced ability of multiple VGSCs to carry I_{NaR} post injury. In naïve DRG neurons, I_{NaR} is believed to be

carried by the NaV1.6 channel isoform because I_{NaR} in DRG neurons is significantly reduced in NaV1.6-null mice. However, data presented in this thesis demonstrates that NaV1.3 and NaV1.7 have the capacity to produce I_{NaR} when expressed in DRG neurons (**Chapter III**)—suggesting that under certain conditions, such as pathology, I_{NaR} may be carried by NaV1.3 and/or NaV1.7. Two pieces of experimental evidence support the hypothesis that increased I_{NaR} following SCI could result from production of I_{NaR} from multiple VGSCs. First, the observation of I_{NaR} is observed in a broader size population of DRG neurons post injury supports the claim that I_{NaR} may be produced by more than one VGSC isoform following injury. DRG neurons do not represent a uniform population of cells, but rather a diverse, heterogeneous collection of cells that, depending on their function or modality, can express different combinations of ion channels or receptors. Consequently, the presence of I_{NaR} in a broad size distribution of neurons suggests that I_{NaR} may be carried by multiple VGSCs post injury, rather than a single isoform. The second piece of evidence which suggests that increased I_{NaR} may result from the increased propensity of multiple VGSCs to carry I_{NaR} post injury can be found in **Figure 26**. Here the relationship between I_{NaR} amplitude and rate of channel inactivation is shown for naïve, sham, and SCI neurons. Although no correlation exists between I_{NaR} amplitude and rate of channel inactivation in naïve, sham, and SCI neurons, the range of correlation values for naïve and sham neurons are closely associated, whereas the correlation values for SCI neurons are more diffuse. Here, I speculate that close association of correlation values may indicate that I_{NaR} is produced by a single VGSC, whereas diffuse spread of correlation values may indicate that I_{NaR} is produced by multiple VGSCs. Future experiments utilizing bath application of the NaV1.6 selective inhibitor, 4, 9-anhydro-TTX, following each recording from control and injured neurons could help determine whether other VGSC isoforms contribute to I_{NaR} following injury.

An alternative hypothesis for why I_{NaR} is increased two weeks post contusive SCI is that gene expression for VGSCs or auxiliary β -subunits, important for I_{NaR} generation, could be upregulated following injury. Previously, I demonstrated that NaV1.3, -1.6, and -1.7 channel isoforms are capable of producing I_{NaR} in DRG neurons. Additionally, results from several studies suggest that the NaV β_4 -subunit serves as the open channel blocker which binds to the channel to produce I_{NaR} . In this report mRNA expression of VGSC isoforms and auxiliary β_4 -subunits were quantified using real-time RT-PCR from whole DRG and single cells from control and injured animals. Results from real-time RT-PCR experiments suggest increased I_{NaR} is not likely due to gross changes in expression of VGSC subunits post injury. Interestingly, preliminary data from single cell real-time RT-PCR experiments suggests that increased I_{NaR} may be due to localized upregulation of NaV β_4 -subunit in SCI neurons with I_{NaR} . Collectively, these results demonstrated that I_{NaR} amplitude and distribution of cells exhibiting I_{NaR} in DRG neurons are increased two weeks post contusive SCI. Based on previous *in silico* modeling of DRG neuron excitability, increased I_{NaR} following contusive SCI is predicted to contribute to the reported cell soma hyperexcitability of DRG neurons and increased pain behavior following injury.

D. *Final summation*

The aims of this dissertation were to understand the mechanisms which underlie the electrogenesis of I_{NaR} and determine if the biophysical properties of these unique currents are altered by either mutations that slow the rate of channel inactivation and cause inherited muscle and neuronal channelopathies, or an experimental model of peripheral nerve injury. In summary the findings of this dissertation show:

- Under normal conditions TTX-sensitive I_{NaR} is exhibited by a subpopulation of medium/large diameter DRG neurons.

- I_{NaR} can be produced by multiple VGSC isoforms when recombinant Na^+ channels are expressed in DRG neurons, including NaV1.3, NaV1.5, NaV1.6, and NaV1.7.
- I_{NaR} are increased in multiple channelopathies where channel inactivation rate is impaired. More specifically, I found that paroxysmal extreme pain disorder (PEPD) mutations in the human peripheral neuronal sodium channel NaV1.7, paramyotonia congenita (PMC) mutations in the human skeletal muscle sodium channel NaV1.4, and a long-QT-3/SIDS mutation in the human cardiac sodium channel NaV1.5 all substantially increased the amplitude of I_{NaR} .
- Increased I_{NaR} associated with the NaV1.7 PEPD mutation induced high frequency action potential firing in modeled nociceptive DRG neuron and increased I_{NaR} associated with the NaV1.5 long-QT-3/SIDS mutation broadened the action potential in a modeled cardiac myocyte; these observations suggest that increased I_{NaR} in mutant VGSCs likely play a significant role in the functional consequences of muscle and neuronal channelopathies.
- Cold temperature induced slowing of channel inactivation enhances I_{NaR} amplitude with channel mutations that impair inactivation by uncoupling channel opening and inactivation; this mechanism is likely important in triggering the cold-induced myotonia associated with paramyotonia congenita.
- I_{NaR} amplitude and distribution of cells exhibiting I_{NaR} in DRG neurons were both significantly increased two weeks following moderate contusive spinal cord injury (SCI).

Taken together, data presented in this dissertation answers questions related to the mechanism of I_{NaR} and points to a role for I_{NaR} in inherited and acquired disorders of excitability in nerve and muscle tissue. Moreover, my observation of increased I_{NaR}

following contusive SCI and increased I_{NaR} in mutant channels associated with human inherited disorders of excitability, suggests that I_{NaR} should be explored as a preclinical target for therapeutics aimed at treating inherited and acquired disorders of excitability. Because the mechanisms which contribute to I_{NaR} generation are thought to be independent of normal Na^+ channel function and because I_{NaR} appear to be selectively upregulated under pathological conditions, therapeutics targeted to inhibit I_{NaR} selectively might be efficacious at treating the ectopic high frequency firing associated with inherited and acquired disorders of excitability, while preserving the normal function of the channel.

VIII. Reference list

1. Singer, S.J. & Nicolson, G.L. The structure and chemistry of mammalian cell membranes. *Am J Pathol* **65**, 427-437 (1971).
2. Hodgkin, A.L. Evidence for electrical transmission in nerve: Part I. *J Physiol* **90**, 183-210 (1937).
3. Hodgkin, A.L. Evidence for electrical transmission in nerve: Part II. *J Physiol* **90**, 211-232 (1937).
4. Cole, K.S. & Curtis, H.J. Electric Impedance of the Squid Giant Axon during Activity. *J Gen Physiol* **22**, 649-670 (1939).
5. Curtis, H.J. & Cole, K.S. Transverse Electric Impedance of the Squid Giant Axon. *J Gen Physiol* **21**, 757-765 (1938).
6. Cole, K.S. Some physical aspects of bioelectric phenomena. *Proc Natl Acad Sci U S A* **35**, 558-566 (1949).
7. Rothenberg, M.A. Studies on permeability in relation to nerve function, ionic movements across exonal membranes. *Biochim Biophys Acta* **4**, 96-114 (1950).
8. Keynes, R.D. The ionic movements during nervous activity. *J Physiol* **114**, 119-150 (1951).
9. Hodgkin, A.L. & Katz, B. The effect of sodium ions on the electrical activity of giant axon of the squid. *J Physiol* **108**, 37-77 (1949).
10. Marmont, G. Studies on the axon membrane; a new method. *Journal of cellular physiology* **34**, 351-382 (1949).
11. Hodgkin, A.L., Huxley, A.F. & Katz, B. Measurement of current-voltage relations in the membrane of the giant axon of *Loligo*. *J Physiol* **116**, 424-448 (1952).
12. Hodgkin, A.L. & Huxley, A.F. The components of membrane conductance in the giant axon of *Loligo*. *J Physiol* **116**, 473-496 (1952).

13. Hodgkin, A.L. & Huxley, A.F. Currents carried by sodium and potassium ions through the membrane of the giant axon of *Loligo*. *J Physiol* **116**, 449-472 (1952).
14. Hodgkin, A.L. & Huxley, A.F. The dual effect of membrane potential on sodium conductance in the giant axon of *Loligo*. *J Physiol* **116**, 497-506 (1952).
15. Hodgkin, A.L. & Huxley, A.F. A quantitative description of membrane current and its application to conduction and excitation in nerve. *J Physiol* **117**, 500-544 (1952).
16. Catterall, W.A., Goldin, A.L. & Waxman, S.G. International Union of Pharmacology. XLVII. Nomenclature and structure-function relationships of voltage-gated sodium channels. *Pharmacol Rev* **57**, 397-409 (2005).
17. Messner, D.J. & Catterall, W.A. The sodium channel from rat brain. Separation and characterization of subunits. *J Biol Chem* **260**, 10597-10604 (1985).
18. Shah, B.S., *et al.* Beta3, a novel auxiliary subunit for the voltage gated sodium channel is upregulated in sensory neurones following streptozocin induced diabetic neuropathy in rat. *Neurosci Lett* **309**, 1-4 (2001).
19. Yu, F.H., *et al.* Sodium channel beta4, a new disulfide-linked auxiliary subunit with similarity to beta2. *J Neurosci* **23**, 7577-7585 (2003).
20. Herzog, R.I., Liu, C., Waxman, S.G. & Cummins, T.R. Calmodulin binds to the C terminus of sodium channels Nav1.4 and Nav1.6 and differentially modulates their functional properties. *J Neurosci* **23**, 8261-8270 (2003).
21. Okuse, K., *et al.* Annexin II light chain regulates sensory neuron-specific sodium channel expression. *Nature* **417**, 653-656 (2002).
22. Patino, G.A. & Isom, L.L. Electrophysiology and beyond: multiple roles of Na⁺ channel beta subunits in development and disease. *Neurosci Lett* **486**, 53-59 (2010).

23. Catterall, W.A. Neurotoxins that act on voltage-sensitive sodium channels in excitable membranes. *Annu Rev Pharmacol Toxicol* **20**, 15-43 (1980).
24. Catterall, W.A. Molecular properties of voltage-sensitive sodium channels. *Annu Rev Biochem* **55**, 953-985 (1986).
25. Beneski, D.A. & Catterall, W.A. Covalent labeling of protein components of the sodium channel with a photoactivable derivative of scorpion toxin. *Proc Natl Acad Sci U S A* **77**, 639-643 (1980).
26. Hartshorne, R.P. & Catterall, W.A. Purification of the saxitoxin receptor of the sodium channel from rat brain. *Proc Natl Acad Sci U S A* **78**, 4620-4624 (1981).
27. Hartshorne, R.P., Messner, D.J., Coppersmith, J.C. & Catterall, W.A. The saxitoxin receptor of the sodium channel from rat brain. Evidence for two nonidentical beta subunits. *J Biol Chem* **257**, 13888-13891 (1982).
28. Noda, M., *et al.* Primary structure of *Electrophorus electricus* sodium channel deduced from cDNA sequence. *Nature* **312**, 121-127 (1984).
29. Noda, M., *et al.* Expression of functional sodium channels from cloned cDNA. *Nature* **322**, 826-828 (1986).
30. Noda, M., *et al.* Existence of distinct sodium channel messenger RNAs in rat brain. *Nature* **320**, 188-192 (1986).
31. Stuhmer, W., *et al.* Structural parts involved in activation and inactivation of the sodium channel. *Nature* **339**, 597-603 (1989).
32. Guy, H.R. & Seetharamulu, P. Molecular model of the action potential sodium channel. *Proc Natl Acad Sci U S A* **83**, 508-512 (1986).
33. Yellen, G. The moving parts of voltage-gated ion channels. *Quarterly reviews of biophysics* **31**, 239-295 (1998).
34. Payandeh, J., Scheuer, T., Zheng, N. & Catterall, W.A. The crystal structure of a voltage-gated sodium channel. *Nature* **475**, 353-358 (2011).

35. West, J.W., *et al.* A cluster of hydrophobic amino acid residues required for fast Na(+)-channel inactivation. *Proc Natl Acad Sci U S A* **89**, 10910-10914 (1992).
36. Cummins, T.R., Sheets, P.L. & Waxman, S.G. The roles of sodium channels in nociception: Implications for mechanisms of pain. *Pain* **131**, 243-257 (2007).
37. Catterall, W.A. From ionic currents to molecular mechanisms: the structure and function of voltage-gated sodium channels. *Neuron* **26**, 13-25 (2000).
38. Tombola, F., Pathak, M.M. & Isacoff, E.Y. How does voltage open an ion channel? *Annu Rev Cell Dev Biol* **22**, 23-52 (2006).
39. Lipkind, G.M. & Fozzard, H.A. A structural model of the tetrodotoxin and saxitoxin binding site of the Na⁺ channel. *Biophys J* **66**, 1-13 (1994).
40. Kirsch, G.E., Alam, M. & Hartmann, H.A. Differential effects of sulfhydryl reagents on saxitoxin and tetrodotoxin block of voltage-dependent Na channels. *Biophys J* **67**, 2305-2315 (1994).
41. Cummins, T.R., *et al.* Nav1.3 sodium channels: rapid repriming and slow closed-state inactivation display quantitative differences after expression in a mammalian cell line and in spinal sensory neurons. *J Neurosci* **21**, 5952-5961 (2001).
42. Trimmer, J.S., *et al.* Primary structure and functional expression of a mammalian skeletal muscle sodium channel. *Neuron* **3**, 33-49 (1989).
43. Rogart, R.B., Cribbs, L.L., Muglia, L.K., Kephart, D.D. & Kaiser, M.W. Molecular cloning of a putative tetrodotoxin-resistant rat heart Na⁺ channel isoform. *Proc Natl Acad Sci U S A* **86**, 8170-8174 (1989).
44. Trimmer, J.S. & Rhodes, K.J. Localization of voltage-gated ion channels in mammalian brain. *Annu Rev Physiol* **66**, 477-519 (2004).
45. Black, J.A., *et al.* Spinal sensory neurons express multiple sodium channel alpha-subunit mRNAs. *Brain Res Mol Brain Res* **43**, 117-131 (1996).

46. Dib-Hajj, S.D., Tyrrell, L., Black, J.A. & Waxman, S.G. Na_v1, a novel voltage-gated Na channel, is expressed preferentially in peripheral sensory neurons and down-regulated after axotomy. *Proc Natl Acad Sci U S A* **95**, 8963-8968 (1998).
47. Amaya, F., *et al.* Diversity of expression of the sensory neuron-specific TTX-resistant voltage-gated sodium ion channels SNS and SNS2. *Mol Cell Neurosci* **15**, 331-342 (2000).
48. Beckh, S., Noda, M., Lubbert, H. & Numa, S. Differential regulation of three sodium channel messenger RNAs in the rat central nervous system during development. *EMBO J* **8**, 3611-3616 (1989).
49. Waxman, S.G., Kocsis, J.D. & Black, J.A. Type III sodium channel mRNA is expressed in embryonic but not adult spinal sensory neurons, and is reexpressed following axotomy. *J Neurophysiol* **72**, 466-470 (1994).
50. Kim, C.H., Oh, Y., Chung, J.M. & Chung, K. Changes in three subtypes of tetrodotoxin sensitive sodium channel expression in the axotomized dorsal root ganglion in the rat. *Neurosci Lett* **323**, 125-128 (2002).
51. Black, J.A., *et al.* Upregulation of a silent sodium channel after peripheral, but not central, nerve injury in DRG neurons. *J Neurophysiol* **82**, 2776-2785 (1999).
52. Ho, C. & O'Leary, M.E. Single-cell analysis of sodium channel expression in dorsal root ganglion neurons. *Mol Cell Neurosci* **46**, 159-166 (2011).
53. Westenbroek, R.E., Merrick, D.K. & Catterall, W.A. Differential subcellular localization of the RI and RII Na⁺ channel subtypes in central neurons. *Neuron* **3**, 695-704 (1989).
54. Waxman, S.G. The molecular pathophysiology of pain: abnormal expression of sodium channel genes and its contributions to hyperexcitability of primary sensory neurons. *Pain Suppl* **6**, S133-140 (1999).

55. Whitaker, W., *et al.* Localization of the type VI voltage-gated sodium channel protein in human CNS. *Neuroreport* **10**, 3703-3709 (1999).
56. Tzoumaka, E., *et al.* Differential distribution of the tetrodotoxin-sensitive rPN4/NaCh6/Scn8a sodium channel in the nervous system. *J Neurosci Res* **60**, 37-44 (2000).
57. Caldwell, J.H., Schaller, K.L., Lasher, R.S., Peles, E. & Levinson, S.R. Sodium channel Na(v)1.6 is localized at nodes of ranvier, dendrites, and synapses. *Proc Natl Acad Sci U S A* **97**, 5616-5620 (2000).
58. Sangameswaran, L., *et al.* A novel tetrodotoxin-sensitive, voltage-gated sodium channel expressed in rat and human dorsal root ganglia. *J Biol Chem* **272**, 14805-14809 (1997).
59. Felts, P.A., Yokoyama, S., Dib-Hajj, S., Black, J.A. & Waxman, S.G. Sodium channel alpha-subunit mRNAs I, II, III, NaG, Na6 and hNE (PN1): different expression patterns in developing rat nervous system. *Brain Res Mol Brain Res* **45**, 71-82 (1997).
60. Djouhri, L., *et al.* The TTX-resistant sodium channel Nav1.8 (SNS/PN3): expression and correlation with membrane properties in rat nociceptive primary afferent neurons. *J Physiol* **550**, 739-752 (2003).
61. Fang, X., *et al.* The presence and role of the tetrodotoxin-resistant sodium channel Na(v)1.9 (NaN) in nociceptive primary afferent neurons. *J Neurosci* **22**, 7425-7433 (2002).
62. Meisler, M.H. & Kearney, J.A. Sodium channel mutations in epilepsy and other neurological disorders. *J Clin Invest* **115**, 2010-2017 (2005).
63. Dichgans, M., *et al.* Mutation in the neuronal voltage-gated sodium channel SCN1A in familial hemiplegic migraine. *Lancet* **366**, 371-377 (2005).

64. Amin, A.S., Asghari-Roodsari, A. & Tan, H.L. Cardiac sodium channelopathies. *Pflugers Arch* **460**, 223-237 (2010).
65. Meisler, M.H., Plummer, N.W., Burgess, D.L., Buchner, D.A. & Sprunger, L.K. Allelic mutations of the sodium channel SCN8A reveal multiple cellular and physiological functions. *Genetica* **122**, 37-45 (2004).
66. Cannon, S.C. Pathomechanisms in channelopathies of skeletal muscle and brain. *Annu Rev Neurosci* **29**, 387-415 (2006).
67. Lampert, A., O'Reilly, A.O., Reeh, P. & Leffler, A. Sodium channelopathies and pain. *Pflugers Arch* **460**, 249-263 (2010).
68. Waxman, S.G. Acquired channelopathies in nerve injury and MS. *Neurology* **56**, 1621-1627 (2001).
69. Mao, Q., *et al.* The up-regulation of voltage-gated sodium channel Nav1.6 expression following fluid percussion traumatic brain injury in rats. *Neurosurgery* **66**, 1134-1139; discussion 1139 (2010).
70. Wang, W., Gu, J., Li, Y.Q. & Tao, Y.X. Are voltage-gated sodium channels on the dorsal root ganglion involved in the development of neuropathic pain? *Mol Pain* **7**, 16 (2011).
71. Devor, M. Sodium channels and mechanisms of neuropathic pain. *J Pain* **7**, S3-S12 (2006).
72. Amir, R., *et al.* The role of sodium channels in chronic inflammatory and neuropathic pain. *J Pain* **7**, S1-29 (2006).
73. Eisenhut, M. & Wallace, H. Ion channels in inflammation. *Pflugers Arch* **461**, 401-421 (2011).
74. George, A.L., Jr. Inherited disorders of voltage-gated sodium channels. *J Clin Invest* **115**, 1990-1999 (2005).

75. Cox, J.J., *et al.* An SCN9A channelopathy causes congenital inability to experience pain. *Nature* **444**, 894-898 (2006).
76. Gold, M.S. Inflammatory mediator-induced modulation of TTX-R INa: an underlying mechanism of inflammatory hyperalgesia. *Proc West Pharmacol Soc* **42**, 111-112 (1999).
77. Gold, M.S. Tetrodotoxin-resistant Na⁺ currents and inflammatory hyperalgesia. *Proc Natl Acad Sci U S A* **96**, 7645-7649 (1999).
78. Lindia, J.A., Kohler, M.G., Martin, W.J. & Abbadie, C. Relationship between sodium channel Nav1.3 expression and neuropathic pain behavior in rats. *Pain* **117**, 145-153 (2005).
79. He, X.H., *et al.* TNF-alpha contributes to up-regulation of Nav1.3 and Nav1.8 in DRG neurons following motor fiber injury. *Pain* **151**, 266-279 (2010).
80. Hains, B.C., *et al.* Upregulation of sodium channel Nav1.3 and functional involvement in neuronal hyperexcitability associated with central neuropathic pain after spinal cord injury. *J Neurosci* **23**, 8881-8892 (2003).
81. Winkelman, D.L., Beck, C.L., Ypey, D.L. & O'Leary, M.E. Inhibition of the A-type K⁺ channels of dorsal root ganglion neurons by the long-duration anesthetic butamben. *J Pharmacol Exp Ther* **314**, 1177-1186 (2005).
82. Isom, L.L., De Jongh, K.S. & Catterall, W.A. Auxiliary subunits of voltage-gated ion channels. *Neuron* **12**, 1183-1194 (1994).
83. Chahine, M., Ziane, R., Vijayaragavan, K. & Okamura, Y. Regulation of Na^v channels in sensory neurons. *Trends Pharmacol Sci* **26**, 496-502 (2005).
84. Smith, R.D. & Goldin, A.L. Functional analysis of the rat I sodium channel in xenopus oocytes. *J Neurosci* **18**, 811-820 (1998).
85. Isom, L.L., *et al.* Primary structure and functional expression of the beta 1 subunit of the rat brain sodium channel. *Science* **256**, 839-842 (1992).

86. Patton, D.E., Isom, L.L., Catterall, W.A. & Goldin, A.L. The adult rat brain beta 1 subunit modifies activation and inactivation gating of multiple sodium channel alpha subunits. *J Biol Chem* **269**, 17649-17655 (1994).
87. Smith, M.R., Smith, R.D., Plummer, N.W., Meisler, M.H. & Goldin, A.L. Functional analysis of the mouse Scn8a sodium channel. *J Neurosci* **18**, 6093-6102 (1998).
88. Vijayaragavan, K., Powell, A.J., Kinghorn, I.J. & Chahine, M. Role of auxiliary beta1-, beta2-, and beta3-subunits and their interaction with Na(v)1.8 voltage-gated sodium channel. *Biochem Biophys Res Commun* **319**, 531-540 (2004).
89. Schreibmayer, W., Wallner, M. & Lotan, I. Mechanism of modulation of single sodium channels from skeletal muscle by the beta 1-subunit from rat brain. *Pflugers Arch* **426**, 360-362 (1994).
90. Isom, L.L. I. Cellular and molecular biology of sodium channel beta-subunits: therapeutic implications for pain? I. Cellular and molecular biology of sodium channel beta-subunits: therapeutic implications for pain? *Am J Physiol Gastrointest Liver Physiol* **278**, G349-353 (2000).
91. Isom, L.L. Sodium channel beta subunits: anything but auxiliary. *Neuroscientist* **7**, 42-54 (2001).
92. Lopez-Santiago, L.F., *et al.* Sodium channel beta2 subunits regulate tetrodotoxin-sensitive sodium channels in small dorsal root ganglion neurons and modulate the response to pain. *J Neurosci* **26**, 7984-7994 (2006).
93. Isom, L.L. Beta subunits: players in neuronal hyperexcitability? *Novartis Found Symp* **241**, 124-138; discussion 138-143, 226-132 (2002).
94. Kaplan, M.R., *et al.* Differential control of clustering of the sodium channels Na(v)1.2 and Na(v)1.6 at developing CNS nodes of Ranvier. *Neuron* **30**, 105-119 (2001).

95. Schmidt, J.W. & Catterall, W.A. Biosynthesis and processing of the alpha subunit of the voltage-sensitive sodium channel in rat brain neurons. *Cell* **46**, 437-444 (1986).
96. Meadows, L.S., *et al.* Functional and biochemical analysis of a sodium channel beta1 subunit mutation responsible for generalized epilepsy with febrile seizures plus type 1. *J Neurosci* **22**, 10699-10709 (2002).
97. Medeiros-Domingo, A., *et al.* SCN4B-encoded sodium channel beta4 subunit in congenital long-QT syndrome. *Circulation* **116**, 134-142 (2007).
98. Lenkowski, P.W., Shah, B.S., Dinn, A.E., Lee, K. & Patel, M.K. Lidocaine block of neonatal Nav1.3 is differentially modulated by co-expression of beta1 and beta3 subunits. *Eur J Pharmacol* **467**, 23-30 (2003).
99. Liu, C.N., Michaelis, M., Amir, R. & Devor, M. Spinal nerve injury enhances subthreshold membrane potential oscillations in DRG neurons: relation to neuropathic pain. *J Neurophysiol* **84**, 205-215 (2000).
100. Makielski, J.C., Limberis, J.T., Chang, S.Y., Fan, Z. & Kyle, J.W. Coexpression of beta 1 with cardiac sodium channel alpha subunits in oocytes decreases lidocaine block. *Mol Pharmacol* **49**, 30-39 (1996).
101. Bant, J.S. & Raman, I.M. Control of transient, resurgent, and persistent current by open-channel block by Na channel beta4 in cultured cerebellar granule neurons. *Proc Natl Acad Sci U S A* **107**, 12357-12362 (2010).
102. Grieco, T.M., Malhotra, J.D., Chen, C., Isom, L.L. & Raman, I.M. Open-channel block by the cytoplasmic tail of sodium channel beta4 as a mechanism for resurgent sodium current. *Neuron* **45**, 233-244 (2005).
103. Lewis, A.H. & Raman, I.M. Cross-species conservation of open-channel block by Na channel beta4 peptides reveals structural features required for resurgent Na current. *J Neurosci* **31**, 11527-11536 (2011).

104. Catterall, W.A., Hulme, J.T., Jiang, X. & Few, W.P. Regulation of sodium and calcium channels by signaling complexes. *J Recept Signal Transduct Res* **26**, 577-598 (2006).
105. Raman, I.M. & Bean, B.P. Resurgent sodium current and action potential formation in dissociated cerebellar Purkinje neurons. *J Neurosci* **17**, 4517-4526 (1997).
106. Raman, I.M. & Bean, B.P. Inactivation and recovery of sodium currents in cerebellar Purkinje neurons: evidence for two mechanisms. *Biophys J* **80**, 729-737 (2001).
107. Armstrong, C.M. & Bezanilla, F. Charge movement associated with the opening and closing of the activation gates of the Na channels. *J Gen Physiol* **63**, 533-552 (1974).
108. Aman, T.K. & Raman, I.M. Inwardly permeating Na ions generate the voltage dependence of resurgent Na current in cerebellar Purkinje neurons. *J Neurosci* **30**, 5629-5634 (2010).
109. Yeh, J.Z. & Narahashi, T. Kinetic analysis of pancuronium interaction with sodium channels in squid axon membranes. *J Gen Physiol* **69**, 293-323 (1977).
110. Cahalan, M.D. & Almers, W. Block of sodium conductance and gating current in squid giant axons poisoned with quaternary strychnine. *Biophys J* **27**, 57-73 (1979).
111. Grieco, T.M., Afshari, F.S. & Raman, I.M. A role for phosphorylation in the maintenance of resurgent sodium current in cerebellar purkinje neurons. *J Neurosci* **22**, 3100-3107 (2002).
112. Raman, I.M., Sprunger, L.K., Meisler, M.H. & Bean, B.P. Altered subthreshold sodium currents and disrupted firing patterns in Purkinje neurons of Scn8a mutant mice. *Neuron* **19**, 881-891 (1997).

113. Do, M.T. & Bean, B.P. Sodium currents in subthalamic nucleus neurons from Nav1.6-null mice. *J Neurophysiol* **92**, 726-733 (2004).
114. Rush, A.M., Dib-Hajj, S.D. & Waxman, S.G. Electrophysiological properties of two axonal sodium channels, Nav1.2 and Nav1.6, expressed in mouse spinal sensory neurones. *J Physiol* **564**, 803-815 (2005).
115. Wang, G.K., Edrich, T. & Wang, S.Y. Time-dependent block and resurgent tail currents induced by mouse beta4(154-167) peptide in cardiac Na⁺ channels. *J Gen Physiol* **127**, 277-289 (2006).
116. Eaholtz, G., Scheuer, T. & Catterall, W.A. Restoration of inactivation and block of open sodium channels by an inactivation gate peptide. *Neuron* **12**, 1041-1048 (1994).
117. Afshari, F.S., *et al.* Resurgent Na currents in four classes of neurons of the cerebellum. *J Neurophysiol* **92**, 2831-2843 (2004).
118. Enomoto, A., Han, J.M., Hsiao, C.F. & Chandler, S.H. Sodium currents in mesencephalic trigeminal neurons from Nav1.6 null mice. *J Neurophysiol* **98**, 710-719 (2007).
119. Gittis, A.H., Moghadam, S.H. & du Lac, S. Mechanisms of sustained high firing rates in two classes of vestibular nucleus neurons: differential contributions of resurgent Na, Kv3, and BK currents. *J Neurophysiol* **104**, 1625-1634 (2010).
120. Gittis, A.H. & du Lac, S. Similar properties of transient, persistent, and resurgent Na currents in GABAergic and non-GABAergic vestibular nucleus neurons. *J Neurophysiol* **99**, 2060-2065 (2008).
121. Pan, F. & Beam, K.G. The absence of resurgent sodium current in mouse spinal neurons. *Brain Res* **849**, 162-168 (1999).

122. Schaller, K.L., Krzemien, D.M., Yarowsky, P.J., Krueger, B.K. & Caldwell, J.H. A novel, abundant sodium channel expressed in neurons and glia. *J Neurosci* **15**, 3231-3242 (1995).
123. Theile, J.W., Jarecki, B.W., Piekarz, A.D. & Cummins, T.R. Nav1.7 mutations associated with paroxysmal extreme pain disorder, but not erythromelalgia, enhance Navbeta4 peptide-mediated resurgent sodium currents. *J Physiol* **589**, 597-608 (2011).
124. Chen, Y., *et al.* Functional properties and differential neuromodulation of Na(v)1.6 channels. *Mol Cell Neurosci* **38**, 607-615 (2008).
125. Scheuer, T. Regulation of sodium channel activity by phosphorylation. *Seminars in cell & developmental biology* **22**, 160-165 (2011).
126. Aman, T.K. & Raman, I.M. Subunit dependence of Na channel slow inactivation and open channel block in cerebellar neurons. *Biophys J* **92**, 1938-1951 (2007).
127. Grieco, T.M. & Raman, I.M. Production of resurgent current in NaV1.6-null Purkinje neurons by slowing sodium channel inactivation with beta-pompilidotoxin. *J Neurosci* **24**, 35-42 (2004).
128. Huth, T., Rittger, A., Saftig, P. & Alzheimer, C. beta-Site APP-cleaving enzyme 1 (BACE1) cleaves cerebellar Na⁺ channel beta4-subunit and promotes Purkinje cell firing by slowing the decay of resurgent Na⁺ current. *Pflugers Arch* **461**, 355-371 (2011).
129. Enomoto, A., Han, J.M., Hsiao, C.F., Wu, N. & Chandler, S.H. Participation of sodium currents in burst generation and control of membrane excitability in mesencephalic trigeminal neurons. *J Neurosci* **26**, 3412-3422 (2006).
130. Leao, R.N., Naves, M.M., Leao, K.E. & Walmsley, B. Altered sodium currents in auditory neurons of congenitally deaf mice. *Eur J Neurosci* **24**, 1137-1146 (2006).

131. Cummins, T.R., Dib-Hajj, S.D., Herzog, R.I. & Waxman, S.G. Nav1.6 channels generate resurgent sodium currents in spinal sensory neurons. *FEBS Lett* **579**, 2166-2170 (2005).
132. Khaliq, Z.M., Gouwens, N.W. & Raman, I.M. The contribution of resurgent sodium current to high-frequency firing in Purkinje neurons: an experimental and modeling study. *J Neurosci* **23**, 4899-4912 (2003).
133. Do, M.T. & Bean, B.P. Subthreshold sodium currents and pacemaking of subthalamic neurons: modulation by slow inactivation. *Neuron* **39**, 109-120 (2003).
134. Levin, S.I., *et al.* Impaired motor function in mice with cell-specific knockout of sodium channel Scn8a (Nav1.6) in cerebellar purkinje neurons and granule cells. *J Neurophysiol* **96**, 785-793 (2006).
135. Joho, R.H., *et al.* Toxin and kinetic profile of rat brain type III sodium channels expressed in *Xenopus* oocytes. *Brain Res Mol Brain Res* **7**, 105-113 (1990).
136. Klugbauer, N., Lacinova, L., Flockerzi, V. & Hofmann, F. Structure and functional expression of a new member of the tetrodotoxin-sensitive voltage-activated sodium channel family from human neuroendocrine cells. *EMBO J* **14**, 1084-1090 (1995).
137. George, A.L., Jr., Komisarof, J., Kallen, R.G. & Barchi, R.L. Primary structure of the adult human skeletal muscle voltage-dependent sodium channel. *Ann Neurol* **31**, 131-137 (1992).
138. Chahine, M., *et al.* Sodium channel mutations in paramyotonia congenita uncouple inactivation from activation. *Neuron* **12**, 281-294 (1994).
139. Cummins, T.R., Aglieco, F. & Dib-Hajj, S.D. Critical molecular determinants of voltage-gated sodium channel sensitivity to mu-conotoxins GIIIA/B. *Mol Pharmacol* **61**, 1192-1201 (2002).

140. Gellens, M.E., *et al.* Primary structure and functional expression of the human cardiac tetrodotoxin-insensitive voltage-dependent sodium channel. *Proc Natl Acad Sci U S A* **89**, 554-558 (1992).
141. Narahashi, T. Tetrodotoxin: a brief history. *Proc Jpn Acad Ser B Phys Biol Sci* **84**, 147-154 (2008).
142. Herzog, R.I., Cummins, T.R., Ghassemi, F., Dib-Hajj, S.D. & Waxman, S.G. Distinct repriming and closed-state inactivation kinetics of Nav1.6 and Nav1.7 sodium channels in mouse spinal sensory neurons. *J Physiol* **551**, 741-750 (2003).
143. Leffler, A., Herzog, R.I., Dib-Hajj, S.D., Waxman, S.G. & Cummins, T.R. Pharmacological properties of neuronal TTX-resistant sodium channels and the role of a critical serine pore residue. *Pflugers Arch* **451**, 454-463 (2005).
144. Dib-Hajj, S.D., *et al.* Transfection of rat or mouse neurons by biolistics or electroporation. *Nat Protoc* **4**, 1118-1126 (2009).
145. Cummins, T.R., *et al.* A novel persistent tetrodotoxin-resistant sodium current in SNS-null and wild-type small primary sensory neurons. *J Neurosci* **19**, RC43 (1999).
146. Dib-Hajj, S., Black, J.A., Cummins, T.R. & Waxman, S.G. NaN/Nav1.9: a sodium channel with unique properties. *Trends Neurosci* **25**, 253-259 (2002).
147. Fjell, J., *et al.* Differential role of GDNF and NGF in the maintenance of two TTX-resistant sodium channels in adult DRG neurons. *Brain Res Mol Brain Res* **67**, 267-282 (1999).
148. Mikami, M. & Yang, J. Short hairpin RNA-mediated selective knockdown of Nav1.8 tetrodotoxin-resistant voltage-gated sodium channel in dorsal root ganglion neurons. *Anesthesiology* **103**, 828-836 (2005).

149. Caffrey, J.M., Eng, D.L., Black, J.A., Waxman, S.G. & Kocsis, J.D. Three types of sodium channels in adult rat dorsal root ganglion neurons. *Brain Res* **592**, 283-297 (1992).
150. Jarecki, B.W., Piekarz, A.D., Jackson, J.O., 2nd & Cummins, T.R. Human voltage-gated sodium channel mutations that cause inherited neuronal and muscle channelopathies increase resurgent sodium currents. *J Clin Invest* **120**, 369-378 (2010).
151. Fjell, J., *et al.* Sodium channel expression in NGF-overexpressing transgenic mice. *J Neurosci Res* **57**, 39-47 (1999).
152. Rush, A.M., Cummins, T.R. & Waxman, S.G. Multiple sodium channels and their roles in electrogenesis within dorsal root ganglion neurons. *J Physiol* **579**, 1-14 (2007).
153. Souslova, V.A., Fox, M., Wood, J.N. & Akopian, A.N. Cloning and characterization of a mouse sensory neuron tetrodotoxin-resistant voltage-gated sodium channel gene, Scn10a. *Genomics* **41**, 201-209 (1997).
154. Hines, M.L. & Carnevale, N.T. The NEURON simulation environment. *Neural Comput* **9**, 1179-1209 (1997).
155. Sheets, P.L., Jackson, J.O., 2nd, Waxman, S.G., Dib-Hajj, S.D. & Cummins, T.R. A Nav1.7 channel mutation associated with hereditary erythromelalgia contributes to neuronal hyperexcitability and displays reduced lidocaine sensitivity. *J Physiol* **581**, 1019-1031 (2007).
156. Jarecki, B.W., Sheets, P.L., Jackson, J.O., 2nd & Cummins, T.R. Paroxysmal extreme pain disorder mutations within the D3/S4-S5 linker of Nav1.7 cause moderate destabilization of fast inactivation. *J Physiol* **586**, 4137-4153 (2008).

157. Courtemanche, M., Ramirez, R.J. & Nattel, S. Ionic mechanisms underlying human atrial action potential properties: insights from a mathematical model. *Am J Physiol* **275**, H301-321 (1998).
158. Luo, C.H. & Rudy, Y. A dynamic model of the cardiac ventricular action potential. I. Simulations of ionic currents and concentration changes. *Circ Res* **74**, 1071-1096 (1994).
159. Wang, D.W., *et al.* Cardiac sodium channel dysfunction in sudden infant death syndrome. *Circulation* **115**, 368-376 (2007).
160. Liu, N., Han, S., Lu, P.H. & Xu, X.M. Upregulation of annexins I, II, and V after traumatic spinal cord injury in adult rats. *J Neurosci Res* **77**, 391-401 (2004).
161. Liu, N.K., *et al.* A novel role of phospholipase A2 in mediating spinal cord secondary injury. *Ann Neurol* **59**, 606-619 (2006).
162. Liu, N.K., *et al.* Annexin A1 reduces inflammatory reaction and tissue damage through inhibition of phospholipase A2 activation in adult rats following spinal cord injury. *J Neuropathol Exp Neurol* **66**, 932-943 (2007).
163. Gruner, J.A. & Kersun, J.M. Assessment of functional recovery after spinal cord injury in rats by reticulospinal-mediated motor evoked responses. *Electroencephalogr Clin Neurophysiol Suppl* **43**, 297-311 (1991).
164. Basso, D.M., Beattie, M.S. & Bresnahan, J.C. Graded histological and locomotor outcomes after spinal cord contusion using the NYU weight-drop device versus transection. *Exp Neurol* **139**, 244-256 (1996).
165. Wang, J.G., *et al.* The chemokine CXCL1/growth related oncogene increases sodium currents and neuronal excitability in small diameter sensory neurons. *Mol Pain* **4**, 38 (2008).

166. Wu, X., Yoo, S. & Wrathall, J.R. Real-time quantitative PCR analysis of temporal-spatial alterations in gene expression after spinal cord contusion. *J Neurochem* **93**, 943-952 (2005).
167. Fehrenbacher, J.C., Burkey, T.H., Nicol, G.D. & Vasko, M.R. Tumor necrosis factor alpha and interleukin-1beta stimulate the expression of cyclooxygenase II but do not alter prostaglandin E2 receptor mRNA levels in cultured dorsal root ganglia cells. *Pain* **113**, 113-122 (2005).
168. Brittain, J.M., *et al.* An atypical role for collapsin response mediator protein 2 (CRMP-2) in neurotransmitter release via interaction with presynaptic voltage-gated calcium channels. *J Biol Chem* **284**, 31375-31390 (2009).
169. Theile, J.W., Jarecki, B.W., Piekarz, A.D. & Cummins, T.R. Nav1.7 mutations associated with paroxysmal extreme pain disorder, but not erythromelalgia, enhance Nav β 4 peptide-mediated resurgent sodium currents. *J Physiol* (2010).
170. Pfaffl, M.W. A new mathematical model for relative quantification in real-time RT-PCR. *Nucleic Acids Res* **29**, e45 (2001).
171. Black, J.A., Renganathan, M. & Waxman, S.G. Sodium channel Na(v)1.6 is expressed along nonmyelinated axons and it contributes to conduction. *Brain Res Mol Brain Res* **105**, 19-28 (2002).
172. Fertleman, C.R., *et al.* SCN9A mutations in paroxysmal extreme pain disorder: allelic variants underlie distinct channel defects and phenotypes. *Neuron* **52**, 767-774 (2006).
173. Dib-Hajj, S.D., Cummins, T.R., Black, J.A. & Waxman, S.G. From genes to pain: Na v 1.7 and human pain disorders. *Trends Neurosci* **30**, 555-563 (2007).
174. Dib-Hajj, S.D., *et al.* Paroxysmal extreme pain disorder M1627K mutation in human Nav1.7 renders DRG neurons hyperexcitable. *Mol Pain* **4**, 37 (2008).

175. Hines, M.L. & Carnevale, N.T. NEURON: a tool for neuroscientists. *Neuroscientist* **7**, 123-135 (2001).
176. Featherstone, D.E., Fujimoto, E. & Ruben, P.C. A defect in skeletal muscle sodium channel deactivation exacerbates hyperexcitability in human paramyotonia congenita. *J Physiol* **506 (Pt 3)**, 627-638 (1998).
177. Yang, N., *et al.* Sodium channel mutations in paramyotonia congenita exhibit similar biophysical phenotypes in vitro. *Proc Natl Acad Sci U S A* **91**, 12785-12789 (1994).
178. Cannon, S.C. & Bean, B.P. Sodium channels gone wild: resurgent current from neuronal and muscle channelopathies. *J Clin Invest* **120**, 80-83 (2010).
179. Numann, R., Catterall, W.A. & Scheuer, T. Functional modulation of brain sodium channels by protein kinase C phosphorylation. *Science* **254**, 115-118 (1991).
180. Kassmann, M., *et al.* Oxidation of multiple methionine residues impairs rapid sodium channel inactivation. *Pflugers Arch* **456**, 1085-1095 (2008).
181. Ryan, D.P. & Ptacek, L.J. Episodic neurological channelopathies. *Neuron* **68**, 282-292 (2010).
182. Drenth, J.P. & Michiels, J.J. Three types of erythromelalgia. *BMJ* **301**, 985-986 (1990).
183. Lerche, H., Mitrovic, N., Dubowitz, V. & Lehmann-Horn, F. Paramyotonia congenita: the R1448P Na⁺ channel mutation in adult human skeletal muscle. *Ann Neurol* **39**, 599-608 (1996).
184. Furtleman, C.R., *et al.* Paroxysmal extreme pain disorder (previously familial rectal pain syndrome). *Neurology* **69**, 586-595 (2007).
185. Gamstorp, I. Adynamia episodica hereditaria. *Acta Paediatr Suppl* **45**, 1-126 (1956).

186. Hoffman, E.P., Lehmann-Horn, F. & Rudel, R. Overexcited or inactive: ion channels in muscle disease. *Cell* **80**, 681-686 (1995).
187. Magee, K.R. Paramyotonia congenita. Association with cutaneous cold sensitivity and description of peculiar sustained postures after muscle contraction. *Arch Neurol* **14**, 590-594 (1966).
188. Nelson, D.J. & Sachs, F. Single ionic channels observed in tissue-cultured muscle. *Nature* **282**, 861-863 (1979).
189. Beam, K.G. & Donaldson, P.L. A quantitative study of potassium channel kinetics in rat skeletal muscle from 1 to 37 degrees C. *J Gen Physiol* **81**, 485-512 (1983).
190. Hayward, L.J., Brown, R.H., Jr. & Cannon, S.C. Inactivation defects caused by myotonia-associated mutations in the sodium channel III-IV linker. *J Gen Physiol* **107**, 559-576 (1996).
191. Mitrovic, N., George, A.L., Jr., Rudel, R., Lehmann-Horn, F. & Lerche, H. Mutant channels contribute <50% to Na⁺ current in paramyotonia congenita muscle. *Brain* **122 (Pt 6)**, 1085-1092 (1999).
192. Catterall, W.A., Perez-Reyes, E., Snutch, T.P. & Striessnig, J. International Union of Pharmacology. XLVIII. Nomenclature and structure-function relationships of voltage-gated calcium channels. *Pharmacol Rev* **57**, 411-425 (2005).
193. Goldin, A.L. Diversity of mammalian voltage-gated sodium channels. *Ann N Y Acad Sci* **868**, 38-50 (1999).
194. Haass, A., *et al.* Clinical study of paramyotonia congenita with and without myotonia in a warm environment. *Muscle Nerve* **4**, 388-395 (1981).
195. Cannon, S.C. Spectrum of sodium channel disturbances in the nondystrophic myotonias and periodic paralyses. *Kidney Int* **57**, 772-779 (2000).
196. Siddall, P.J. Management of neuropathic pain following spinal cord injury: now and in the future. *Spinal Cord* **47**, 352-359 (2009).

197. Waxman, S.G. & Hains, B.C. Fire and phantoms after spinal cord injury: Na⁺ channels and central pain. *Trends Neurosci* **29**, 207-215 (2006).
198. Christensen, M.D. & Hulsebosch, C.E. Chronic central pain after spinal cord injury. *J Neurotrauma* **14**, 517-537 (1997).
199. Finnerup, N.B., Johannesen, I.L., Sindrup, S.H., Bach, F.W. & Jensen, T.S. Pain and dysesthesia in patients with spinal cord injury: A postal survey. *Spinal Cord* **39**, 256-262 (2001).
200. Siddall, P.J., McClelland, J.M., Rutkowski, S.B. & Cousins, M.J. A longitudinal study of the prevalence and characteristics of pain in the first 5 years following spinal cord injury. *Pain* **103**, 249-257 (2003).
201. Rintala, D.H., Loubser, P.G., Castro, J., Hart, K.A. & Fuhrer, M.J. Chronic pain in a community-based sample of men with spinal cord injury: prevalence, severity, and relationship with impairment, disability, handicap, and subjective well-being. *Arch Phys Med Rehabil* **79**, 604-614 (1998).
202. Anderson, C.J., Vogel, L.C., Betz, R.R. & Willis, K.M. Overview of adult outcomes in pediatric-onset spinal cord injuries: implications for transition to adulthood. *J Spinal Cord Med* **27 Suppl 1**, S98-106 (2004).
203. Nandoe Tewarie, R.D., Hurtado, A., Bartels, R.H., Grotenhuis, J.A. & Oudega, M. A clinical perspective of spinal cord injury. *NeuroRehabilitation* **27**, 129-139 (2010).
204. Namaka, M., *et al.* A treatment algorithm for neuropathic pain. *Clin Ther* **26**, 951-979 (2004).
205. Yeziarski, R.P. Pain following spinal cord injury: the clinical problem and experimental studies. *Pain* **68**, 185-194 (1996).

206. Hulsebosch, C.E., Hains, B.C., Crown, E.D. & Carlton, S.M. Mechanisms of chronic central neuropathic pain after spinal cord injury. *Brain Res Rev* **60**, 202-213 (2009).
207. Hains, B.C. & Waxman, S.G. Sodium channel expression and the molecular pathophysiology of pain after SCI. *Prog Brain Res* **161**, 195-203 (2007).
208. Eide, P.K. Pathophysiological mechanisms of central neuropathic pain after spinal cord injury. *Spinal Cord* **36**, 601-612 (1998).
209. Hains, B.C. & Waxman, S.G. Activated microglia contribute to the maintenance of chronic pain after spinal cord injury. *J Neurosci* **26**, 4308-4317 (2006).
210. Hains, B.C., Saab, C.Y. & Waxman, S.G. Changes in electrophysiological properties and sodium channel Nav1.3 expression in thalamic neurons after spinal cord injury. *Brain* **128**, 2359-2371 (2005).
211. Hansson, E. Could chronic pain and spread of pain sensation be induced and maintained by glial activation? *Acta Physiol (Oxf)* **187**, 321-327 (2006).
212. Beric, A. Post-spinal cord injury pain states. *Pain* **72**, 295-298 (1997).
213. Bedi, S.S., *et al.* Chronic spontaneous activity generated in the somata of primary nociceptors is associated with pain-related behavior after spinal cord injury. *J Neurosci* **30**, 14870-14882 (2010).
214. Teasell, R.W., *et al.* A systematic review of pharmacologic treatments of pain after spinal cord injury. *Arch Phys Med Rehabil* **91**, 816-831 (2010).
215. Cummins, T.R. & Waxman, S.G. Downregulation of tetrodotoxin-resistant sodium currents and upregulation of a rapidly repriming tetrodotoxin-sensitive sodium current in small spinal sensory neurons after nerve injury. *J Neurosci* **17**, 3503-3514 (1997).

216. Dib-Hajj, S., Black, J.A., Felts, P. & Waxman, S.G. Down-regulation of transcripts for Na channel alpha-SNS in spinal sensory neurons following axotomy. *Proc Natl Acad Sci U S A* **93**, 14950-14954 (1996).
217. Drew, G.M., Siddall, P.J. & Duggan, A.W. Mechanical allodynia following contusion injury of the rat spinal cord is associated with loss of GABAergic inhibition in the dorsal horn. *Pain* **109**, 379-388 (2004).
218. Hains, B.C., Saab, C.Y. & Waxman, S.G. Alterations in burst firing of thalamic VPL neurons and reversal by Na(v)1.3 antisense after spinal cord injury. *J Neurophysiol* **95**, 3343-3352 (2006).
219. Zhao, P., Waxman, S.G. & Hains, B.C. Sodium channel expression in the ventral posterolateral nucleus of the thalamus after peripheral nerve injury. *Mol Pain* **2**, 27 (2006).
220. Lampert, A., Hains, B.C. & Waxman, S.G. Upregulation of persistent and ramp sodium current in dorsal horn neurons after spinal cord injury. *Exp Brain Res* **174**, 660-666 (2006).
221. d'Alcantara, P., Cardenas, L.M., Swillens, S. & Scroggs, R.S. Reduced transition between open and inactivated channel states underlies 5HT increased I(Na+) in rat nociceptors. *Biophys J* **83**, 5-21 (2002).
222. Gold, M.S., Zhang, L., Wrigley, D.L. & Traub, R.J. Prostaglandin E(2) modulates TTX-R I(Na) in rat colonic sensory neurons. *J Neurophysiol* **88**, 1512-1522 (2002).
223. Schmalhofer, W.A., *et al.* ProTx-II, a selective inhibitor of NaV1.7 sodium channels, blocks action potential propagation in nociceptors. *Mol Pharmacol* **74**, 1476-1484 (2008).

224. Chi, X.X. & Nicol, G.D. The sphingosine 1-phosphate receptor, S1PR, plays a prominent but not exclusive role in enhancing the excitability of sensory neurons. *J Neurophysiol* **104**, 2741-2748 (2010).
225. Raman, I.M. & Bean, B.P. Properties of sodium currents and action potential firing in isolated cerebellar Purkinje neurons. *Ann N Y Acad Sci* **868**, 93-96 (1999).
226. Aman, T.K., *et al.* Regulation of persistent Na current by interactions between beta subunits of voltage-gated Na channels. *J Neurosci* **29**, 2027-2042 (2009).
227. Scheuer, T. & Catterall, W.A. Control of neuronal excitability by phosphorylation and dephosphorylation of sodium channels. *Biochem Soc Trans* **34**, 1299-1302 (2006).

APPENDIX A

Author permissions

Email:

To: staff@the-jci.org

From: piekarza@gmail.com

cc'd: trcummin@iupui.edu

October 28, 2011

Publishing Editor

The Journal of Clinical Investigation

Ann Arbor, Michigan 48103, USA

Dear Publisher,

I am completing my doctoral thesis at Indiana University entitled, *Increased resurgent sodium currents (I_{NaR}) in inherited and acquired disorders of excitability*. I would like permission to allow inclusion of data, modified figures, and an unabridged copy of the paper entitled, *Human voltage-gated sodium channel mutations that cause inherited neuronal and muscle channelopathies increase resurgent sodium currents*, in my thesis and permission for the Indiana University Library to make use of the thesis (i.e. reproduce, loan, distribute, or sell copies of this thesis by any means and in any form or format).

These rights will in no way restrict republication of the material in any other form by you or by others authorized by you.

The data and figures I wish to include in my thesis are reprinted from:

Jarecki, B.W.*, Piekarz, A.D.*, Jackson II, J.O., and Cummins, T.R. Human voltage-gated sodium channel mutations that cause inherited neuronal and muscle channelopathies increase resurgent sodium currents. *J Clin Invest.* **120**, 369-378 (2010).

I am aware that there is a nominal fee to be assessed to receive copyright permission and that said nominal fee applies per copy to be reprinted. How is the nominal fee assessed if an unabridged copy of this paper is present in the appendix of my thesis that is available for download through the Indiana University library website? Please let me know how I should proceed to receive your approval.

Respectfully,

Andrew D Piekarz
PhD Candidate
Department of Pharmacology and Toxicology
Indiana University School of Medicine
Indianapolis, IN 46202
Tel: (317)278-5848
Fax: (317)278-5849

Email:

To: piekarza@gmail.com and trcummin@iupui.edu

From: staff@the-jci.org

Hi Dr. Piekarz,

Thank you for your email. Since you are one of the original authors on this paper, you do not need permission to reuse data/figures. Please do cite the JCI as the source in your thesis.

The full citation, for your information:

[Human voltage-gated sodium channel mutations that cause inherited neuronal and muscle](#)

[channelopathies increase resurgent sodium currents](#)

Published in Volume 120, Issue 1 (January 4, 2010)

J Clin Invest. 2010;120(1):369–378. doi:10.1172/JCI40801.

Copyright © 2010, American Society for Clinical Investigation

If you have any other questions, please do not hesitate to contact us.

Sincerely,

Theresa Kaiser

Email:

To: Brain Jarecki bjarecki@umail.iu.edu

From: Andrew Piekarz piekarza@gmail.com

October 18, 2011

Dr. Brian W. Jarecki,

I am completing my doctoral thesis entitled, "Increased resurgent sodium currents in inherited and acquired disorders of excitability." I am writing you today because I am seeking your permission to include modified figures and data from our collaborated project entitled, "Human voltage-gated sodium channel mutations that cause inherited neuronal and muscle channelopathies increase resurgent sodium currents." I would be happy to send you an electronic copy of my thesis so that you might be able to verify that I have given you satisfactory recognition for your contribution to this work. Please email me a response indicating whether or not I have permission to include our collaborative project in my thesis.

Respectfully,

Andrew

Email (Reply):

To: Andrew Piekarz piekarza@gmail.com

From: Brain Jarecki bjarecki@umail.iu.edu

Hello Andrew:

I (Brian W. Jarecki) give you permission to use figures from our JCI paper in your thesis with the understanding that the work will be cited as a *collaborative* effort and Jarecki, Piekarz et al., 2010 will be appropriately acknowledged.

Respectfully,

Brian W. Jarecki, Ph.D

APPENDIX B

Jarecki, B.W.*, Piekarz, A.D.*, Jackson II, J.O., and Cummins, T.R. *Human voltage-gated sodium channel mutations that cause inherited neuronal and muscle channelopathies increase resurgent sodium currents. J Clin Invest.* **120**, 369-378 (2010).

* Indicates both authors contributed equally



Human voltage-gated sodium channel mutations that cause inherited neuronal and muscle channelopathies increase resurgent sodium currents

Brian W. Jarecki, Andrew D. Piekarz, James O. Jackson II, and Theodore R. Cummins

Department of Pharmacology and Toxicology, Stark Neurosciences Research Institute, Indiana University School of Medicine, Indianapolis, Indiana, USA.

Inherited mutations in voltage-gated sodium channels (VGSCs; or Nav) cause many disorders of excitability, including epilepsy, chronic pain, myotonia, and cardiac arrhythmias. Understanding the functional consequences of the disease-causing mutations is likely to provide invaluable insight into the roles that VGSCs play in normal and abnormal excitability. Here, we sought to test the hypothesis that disease-causing mutations lead to increased resurgent currents, unusual sodium currents that have not previously been implicated in disorders of excitability. We demonstrated that a paroxysmal extreme pain disorder (PEPD) mutation in the human peripheral neuronal sodium channel Nav1.7, a paramyotonia congenita (PMC) mutation in the human skeletal muscle sodium channel Nav1.4, and a long-QT3/SIDS mutation in the human cardiac sodium channel Nav1.5 all substantially increased the amplitude of resurgent sodium currents in an optimized adult rat-derived dorsal root ganglion neuronal expression system. Computer simulations indicated that resurgent currents associated with the Nav1.7 mutation could induce high-frequency action potential firing in nociceptive neurons and that resurgent currents associated with the Nav1.5 mutation could broaden the action potential in cardiac myocytes. These effects are consistent with the pathophysiology associated with the respective channelopathies. Our results indicate that resurgent currents are associated with multiple channelopathies and are likely to be important contributors to neuronal and muscle disorders of excitability.

Introduction

Voltage-gated sodium channels (VGSCs; or Nav) are crucial to the generation and propagation of the all-or-none action potentials (APs) in excitable cells, such as neurons and muscle. More than 200 different missense mutations in 7 VGSCs have been identified as causing disorders of excitability, or channelopathies, in humans (1, 2). Although these channelopathies are relatively rare, understanding the functional consequences of the disease mutations provides invaluable insight into the roles that VGSCs play in normal and abnormal excitability. Mutant channels have been extensively studied in nonexcitable heterologous expression systems, providing substantial knowledge; however, a major concern is that the functional properties of VGSCs in neurons and muscle cells are not always accurately reproduced in nonexcitable cells. A prime example of this phenomenon is VGSC resurgent currents. Although resurgent VGSC currents have been recorded from neurons, it has not been possible to record resurgent currents in nonexcitable heterologous expression systems (3–5), and it is not known whether VGSC mutations that cause channelopathies alter resurgent currents.

Resurgent sodium currents were first described in cerebellar Purkinje neurons (3) and more recently have been observed in dorsal root ganglion (DRG) neurons (4). Normally, VGSCs open, and subsequently rapidly inactivate, upon membrane depolarization. Inactivated channels cannot reopen until they have been substan-

tially hyperpolarized for many milliseconds; this is the basis for the AP refractory period (6). In contrast, resurgent currents reopen during the repolarization of the membrane potential and therefore are likely to contribute to spontaneous and high-frequency firing (7). These unusual sodium currents are proposed to result from a putative intracellular blocking factor that binds to open VGSCs and prevents classical VGSC inactivation, but unbinds during repolarization at potentials at which channels normally remain inactivated (8). In both cerebellar Purkinje and DRG neurons isolated from Nav1.6 knockout mice, resurgent currents are greatly reduced, which indicates that Nav1.6 is normally the predominant generator of resurgent currents in neurons (3, 4). However, artificial slowing of VGSC inactivation via toxin application can induce resurgent currents in Purkinje neurons isolated from Nav1.6 knockout mice, which indicates that VGSCs other than Nav1.6 may have the capacity to generate resurgent sodium currents (9). In this study, we hypothesized that disease mutations that slow or destabilize sodium channel inactivation lead to increased resurgent currents. We have previously shown that recombinant Nav1.6 channels expressed in DRG neurons can generate resurgent currents in approximately 60% of the transfected neurons (4), which indicates that DRG neurons should be an ideal cell background for testing our hypothesis. Although DRG neurons express multiple VGSCs, it is worth noting that not all isoforms are natively expressed in DRG neurons (10). Adult DRG sensory neurons can express combinations of Nav1.1, Nav1.6, Nav1.7, Nav1.8, and Nav1.9. In addition, Nav1.2, Nav1.3, and Nav1.5 are expressed, at least at low levels, in embryonic rat DRG. However, because the cellular background of DRG neurons, which may include expres-

Authorship note: Brian W. Jarecki and Andrew D. Piekarz are co-first authors and contributed equally to this work.

Conflict of interest: The authors have declared that no conflict of interest exists.

Citation for this article: *J. Clin. Invest.* 120:369–378 (2010). doi:10.1172/JCI40801.

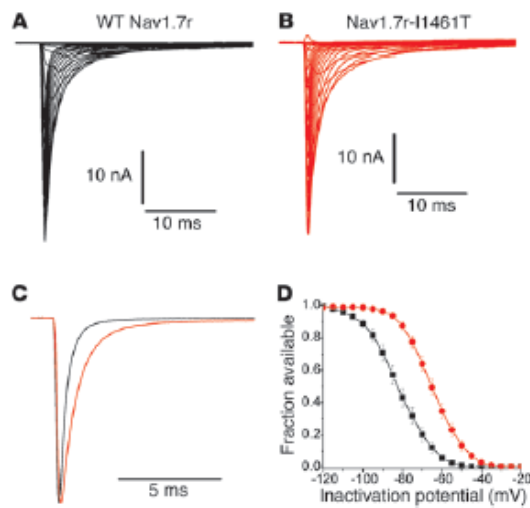


Figure 1

Currents generated by recombinant Nav1.7 channels expressed in DRG neurons. (A) Representative Nav1.7r current traces recorded from a transfected DRG neuron. (B) Representative Nav1.7r-I1461T current traces recorded from a transfected DRG neuron. Currents were elicited with step depolarizations to voltages ranging from -80 to $+40$ mV from a holding potential of -100 mV. (C) The painful mutation I1461T slowed the rate of inactivation of Nav1.7r. Black trace, Nav1.7r; red trace, Nav1.7r-I1461T. Currents were elicited with a step depolarization to $+10$ mV. (D) Steady-state inactivation curves for Nav1.7r (black) and Nav1.7r-I1461T (red) channels expressed in DRG neurons. Cultured adult rat DRG neurons were transfected with the recombinant VGSC construct and Nav1.8 shRNA, and recordings were done in the presence of 500 nM TTX.

sion of particular kinases and auxiliary subunits, is appropriate to generate resurgent sodium currents in Nav1.6, we proposed that cultured DRG neurons might provide an opportune expression system for investigating the capability of other wild-type and mutant VGSCs to generate resurgent current. Using this expression system, we showed for the first time to our knowledge that disease mutations in 3 different VGSC isoforms, associated with 3 distinct disorders of excitability, increased resurgent sodium currents. Based on our data, we propose that resurgent sodium currents play important and previously unrecognized roles in disorders of excitability.

Results

A Nav1.7 inactivation gate mutation implicated in PEPD increases resurgent sodium currents. We first asked whether a mutation in Nav1.7 that slows inactivation and causes paroxysmal extreme pain disorder (PEPD; ref. 11) generates resurgent sodium currents. Highly expressed in DRG neurons, Nav1.7 channels are essential in nociception, as evidenced by single-point missense mutations causing a spectrum of pain syndromes, including PEPD, and by nonsense

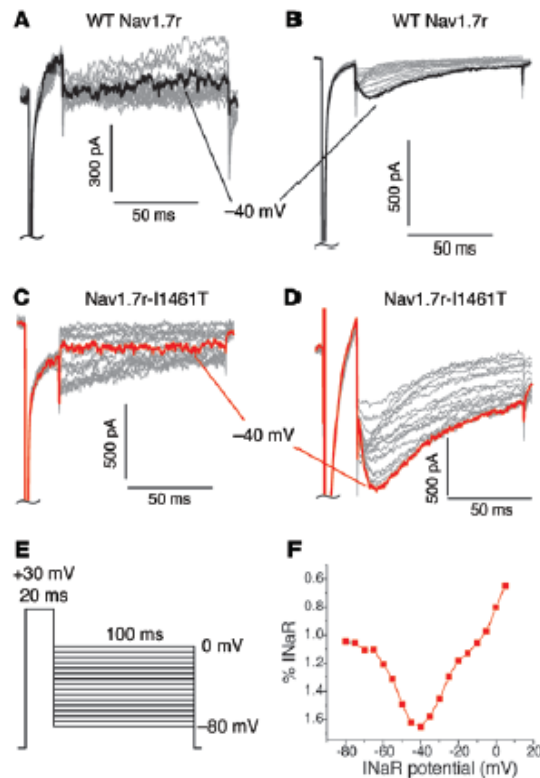
mutations resulting in human insensitivity to pain (12). Although Nav1.7 channels have not previously been shown to produce resurgent currents, PEPD mutations destabilize inactivation, shifting voltage dependence and decreasing the rate of inactivation (11, 13). Therefore, we hypothesized that PEPD mutations induce resurgent currents. We studied the Nav1.7 PEPD mutation I1461T, located within the highly conserved D3-D4 inactivation particle (IFMT) critical for VGSC inactivation (14, 15). Modified wild-type Nav1.7 and Nav1.7-I1461T (referred to herein as Nav1.7r and Nav1.7r-I1461T, respectively) channels that generate currents that can be pharmacologically isolated were expressed in adult rat DRG neurons (Figure 1, A and B). In addition to the recombinant channel of interest, neurons were also cotransfected with a second plasmid encoding for both EGFP, to help identify transfected neurons, and a specific Nav1.8 shRNA, to minimize endogenous Nav1.8 currents (see Methods for details). In DRG neurons, the I1461T PEPD mutation impaired inactivation (Figure 1, C and D, and Table 1), but did not alter activation (data not shown), of Nav1.7r channels. The persistent component, measured at the end of a 50 -ms pulse to -10 mV, was also significantly larger for Nav1.7r-I1461T chan-

Table 1

Biophysical properties of wild-type and mutant sodium channels

Construct	V _{1/2} inactivation ^A (mV)	Tau-h ^B (ms)	Persistent current ^C	Resurgent current ^D
Nav1.7r	-80.1 ± 1.6 (n = 25)	0.85 ± 0.06 (n = 23)	0.19 ± 0.16 (n = 13)	1.0 ± 0.5 (n = 5 of 21)
Nav1.7r-I1461T	-61.8 ± 1.3^E (n = 37)	1.07 ± 0.07^E (n = 35)	1.04 ± 0.25^E (n = 13)	2.0 ± 0.1^E (n = 20 of 30)
Nav1.5	-88.1 ± 1.7 (n = 20)	0.9 ± 0.07 (n = 20)	0.2 ± 0.08 (n = 15)	0.6 ± 0.1 (n = 9 of 18)
Nav1.5-F1486L	-80.1 ± 1.6 (n = 18)	1.31 ± 0.14^E (n = 15)	0.64 ± 0.15^E (n = 10)	2.0 ± 0.4^E (n = 8 of 17)
Nav1.4r	-77.3 ± 2.1 (n = 11)	0.34 ± 0.03 (n = 11)	0.17 ± 0.13 (n = 10)	None detected (n = 0 of 11)
Nav1.4r-R1448P	-91.1 ± 2.4^E (n = 20)	3.92 ± 0.25^E (n = 21)	0.95 ± 0.28^E (n = 20)	4.2 ± 0.6^E (n = 13 of 20)
Nav1.6r	-71.3 ± 1.9 (n = 17)	1.02 ± 0.1 (n = 17)	0.69 ± 0.16 (n = 11)	2.4 ± 0.3 (n = 8 of 14)
Nav1.6r-I1477T	-58.6 ± 1.2^E (n = 18)	1.25 ± 0.09 (n = 18)	7.4 ± 0.68^E (n = 14)	15.3 ± 3.4^E (n = 7 of 14)

^AMidpoint voltage of the steady-state inactivation curve, as determined with a standard Boltzmann distribution fit. ^BTime constant for current decay during $+10$ mV step depolarization. ^CPersistent current measured at 50 ms during step depolarization to $+10$ mV, reported as a percentage of peak current amplitude elicited by the step depolarization. ^DResurgent sodium current was measured with the protocol shown in Figure 2E and reported as a percentage of the peak current amplitude elicited by a step depolarization to -10 mV. The average resurgent current amplitude was only calculated from those cells in which resurgent current was detected. ^E $P < 0.05$ versus respective wild-type channel.

**Figure 2**

Resurgent currents are produced by recombinant Nav1.7 channels expressed in DRG neurons. (A and B) Representative current traces recorded from DRG neurons expressing Nav1.7r that did not (A) and that did (B) generate resurgent currents. (C and D) Representative current traces recorded from DRG neurons expressing Nav1.7r-I1461T channels that did not (C) and that did (D) generate resurgent currents. Resurgent currents were larger on average for Nav1.7r-I1461T than for Nav1.7 channels. Currents are magnified $\times 30$ relative to the peak transient current (elicited with a pulse to -10 mV) to emphasize the resurgent current components. (E) Resurgent current voltage protocol. (F) Voltage dependence of resurgent current shown in D.

with modifications only to the appropriate sodium channel formulation, simulated and evaluated the impact of the I1461T mutation and resurgent currents on AP firing. Mathematical models of Nav1.7 and Nav1.7-I1461T currents with and without a resurgent current blocking factor were developed using a multistate Markov-type model of Nav1.7 (Figure 3). The resurgent current blocking factor was implemented using the strategy developed by Khaliq et al. (18). The forward and reverse transition rate expressions for the blocking factor were adjusted (see Supplemental Table 2; supplemental material available online with this article; doi:10.1172/JCI40801DS1) in order to match the relative amplitude of the experimentally observed resurgent currents. In our model, the blocking factor-induced resurgent current was 1.0% of the peak transient current in the modeled Nav1.7 conductance and 2.0% of the peak transient current in the modeled Nav1.7-I1461T conductance (Figure 3C). The computer simulations of AP firing in DRG neurons indicated that, whereas the destabilization of inactivation caused by the I1461T mutation was sufficient to decrease the threshold for eliciting an AP, inclusion of the resurgent current blocking factor led to high-frequency trains of APs (Figure 3D). It is important to note that even when the transition rate expressions for the blocking factor were adjusted so that the wild-type resurgent current was doubled (2% of peak), a 70-pA stimulus still only elicited a single AP in the model neuron. These results indicate the resurgent current blocking factor and the I1461T mutations act synergistically to increase neuronal excitability and that resurgent currents probably contribute to the extreme pain sensations associated with PEPD mutations.

A cardiac long-QT3/sudden infant death syndrome mutation that slows inactivation increases resurgent Nav1.5 current and broadens AP waveform in a modeled myocyte. Disease mutations that impair inactivation have also been identified in several other VGSCs, including Nav1.1 and Nav1.3 mutations associated with epilepsies, Nav1.4 mutations associated with skeletal muscle myotonias, and Nav1.5 mutations associated with cardiac arrhythmias (1, 2). More than 50 different disease mutations that impair inactivation have been characterized (see Supplemental Table 1 for a partial listing). However, these mutations have all been characterized in heterologous expression systems that do not support the generation of resurgent sodium currents. Therefore, we next used the DRG expression system to determine whether the Nav1.5 mutation F1486L (19), associated with long-QT3/sudden infant death syndrome (LQT3/SIDS), generates increased resurgent currents. As was previously shown in HEK293 cells (19), the F1486L mutation, which is also located in the IFMT inactivation particle, slowed the rate of inactivation, increased the fraction of persistent currents, and shifted the voltage dependence of activation in the depolarizing direction (Table 1).

nels than for Nav1.7r channels (Nav1.7r, $0.2\% \pm 0.2\%$ of peak transient current, $n = 13$; Nav1.7r-I1461T, $1.0\% \pm 0.3\%$, $n = 22$; $P < 0.05$). These changes were identical to those observed for wild-type and I1461T Nav1.7 channels expressed in HEK293 cells (13). However, in DRG neurons, both Nav1.7r and Nav1.7r-I1461T channels also generated resurgent sodium currents. Resurgent sodium currents were observed in 5 of 21 neurons transfected with Nav1.7r (Figure 2, A and B), with an average amplitude – expressed as a percentage of the peak transient sodium current elicited with a test pulse to -10 mV – of $1.0\% \pm 0.5\%$ for these 5 neurons. Conversely, 20 of 30 neurons expressing Nav1.7r-I1461T channels produced resurgent sodium current (Figure 2, C and D). The frequency of resurgent current with Nav1.7r-I1461T channels was significantly increased ($P < 0.05$, χ^2 test) compared with Nav1.7r channels. Moreover, the relative amplitude of the resurgent current ($2.0\% \pm 0.1\%$) was also significantly greater for Nav1.7r-I1461T than for Nav1.7r channels ($P < 0.05$). Because all PEPD mutations characterized to date result in slower inactivation of Nav1.7 (11, 13), we predict that all PEPD mutations are likely to increase resurgent current generation.

A PEPD mutation that increases resurgent currents increases AP repetitive firing in simulated neurons. Based on work done in cerebellar Purkinje neurons (3), we expected increased resurgent sodium currents generated by PEPD mutations to result in spontaneous and/or repetitive APs in DRG neurons. To test this, we performed computer simulations of DRG neuron excitability. We used an established model of DRG neuron excitability (16) that had been implemented in the NEURON simulation environment (17) and,

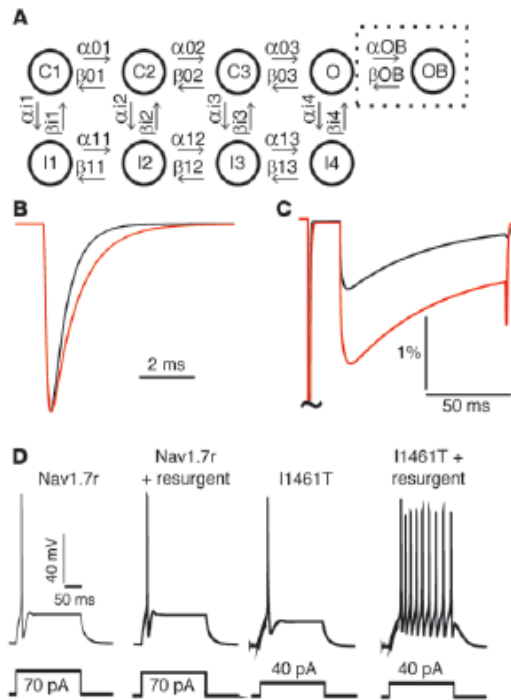


Figure 3

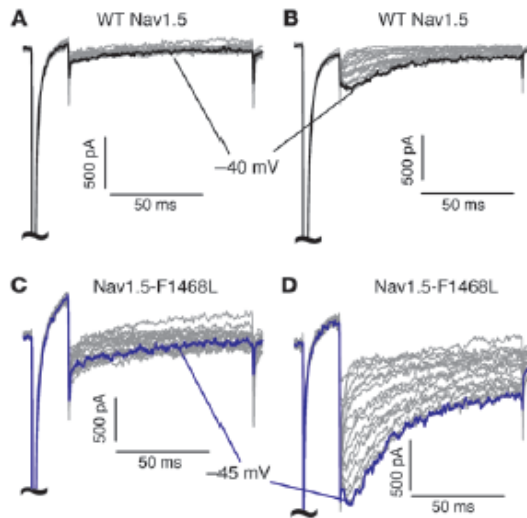
Computer simulation of sodium conductances and DRG neuron excitability. (A) Diagram of Markov models for VGSC conductances. An 8-state Markov model was used for simulation of VGSC conductances without resurgent currents. C1–C3, closed (nonconducting) states; O, open (conducting) state; I1–I4, inactivated (also nonconducting) states. A 9-state Markov model incorporated the resurgent current blocking factor. The OB state (boxed) represents channels blocked by this factor. (B) Simulated Nav1.7 (black trace) and Nav1.7-I1461T (red trace) currents elicited by a voltage step from –100 mV to +10 mV. (C) Simulated resurgent currents generated by model Nav1.7 (black trace) and Nav1.7-I1461T (red trace) conductances. Model currents were elicited with the standard resurgent current voltage protocol shown in Figure 2E. (D) In simulated DRG neurons with Nav1.7 channels, 70 pA depolarizing current is required to elicit an AP with or without resurgent current simulation. Conversely, only 40 pA is needed to elicit an AP in a simulated neuron with Nav1.7-I1461T channels, and a train of high-frequency APs is generated when the modeled Nav1.7-I1461T channels generate resurgent currents.

an average relative amplitude of $4.8\% \pm 0.7\%$ of peak. Thus, at least for Nav1.4, slowing the rate of inactivation seemed to be crucial to the production of resurgent sodium currents, and the impact of the mutation on the voltage dependence of inactivation may be less important. It should be noted that although the R1448P mutation does not alter the voltage dependence of activation, it slows deactivation (the rate at which open channels transit to the closed state; refs. 21, 23), and slower deactivation might also contribute to enhanced resurgent currents, especially in combination with slower inactivation. Resurgent currents generated by Nav1.4 are likely to increase repetitive AP firing in skeletal muscle, which is one of the hallmarks of PMC. However, it should be noted that patients with PMC can also experience episodes of muscle weakness or paralysis in addition to myotonia (24). Although resurgent currents could clearly contribute to myotonic activity associated with PMC, incomplete inactivation observed with mutant PMC channels is likely to be an important factor in muscle weakness associated with PMC (2).

A homologous inactivation gate mutation engineered into Nav1.6 channels dramatically increases resurgent currents and destabilizes transition to an inactivated state. Because Nav1.6 appears to be the predominant generator of resurgent currents in cerebellar Purkinje neurons and DRG neurons (3, 4), we next compared the amplitude of resurgent currents generated by Nav1.6 channels with those produced by the Nav1.4, Nav1.5, and Nav1.7 disease mutations. Resurgent currents were detected in 8 of 14 DRG neurons expressing wild-type Nav1.6r channels, with an average relative amplitude of $2.4\% \pm 0.3\%$ of the peak current (Figure 7A). This relative amplitude is similar to that produced by the Nav1.7r-I1461T PEPD mutant and the Nav1.5-F1486L LQT3/SIDS mutant, but slightly smaller than that produced by the Nav1.4r-R1448P PMC mutant (Figure 7C). This indicates that the resurgent currents produced by the disease mutants are indeed likely to have important impact on cellular excitability. Remarkably, gain-of-function disease mutations, to date, have not been identified in Nav1.6 channels. To determine the potential impact of mutations in Nav1.6 that impair inactivation, we next asked if a mutation in Nav1.6 (I1477T) corresponding to the I1461T mutation in Nav1.7 could increase resurgent sodium currents generated by Nav1.6. The Nav1.6r-I1477T mutation shifted the voltage dependence of inactivation in the depolarizing direction, slowed the rate of inactivation and significantly

However, 9 of 18 DRG neurons expressing wild-type Nav1.5 generated resurgent currents (Figure 4, A and B). In our expression system, the Nav1.5-F1486L LQT3/SIDS mutation significantly increased the relative amplitude of the resurgent currents (Table 1). Of 17 neurons expressing Nav1.5-F1486L channels, 8 generated resurgent currents, with an average relative amplitude of $2.0\% \pm 0.4\%$ (Figure 4, C and D). As resurgent sodium currents are activated during repolarization, we expected increased resurgent currents in Nav1.5 to broaden the AP, increase the QT interval, and thus contribute to the potentially lethal cardiac arrhythmias associated with LQT3/SIDS mutations. Mathematical modeling of resurgent sodium currents and computer simulations of a cardiac myocyte (20) indicated that this may indeed be the case (Figure 5).

A D4/S4 paramyotonia congenita mutation in Nav1.4 that replaces a charged residue and uncouples fast inactivation generates resurgent sodium currents. We next asked whether a mutation that slows inactivation of Nav1.4 and causes paramyotonia congenita (PMC) induces resurgent sodium currents. We studied the R1448P mutation (21), which alters the outermost extracellular charged residue in the sodium channel voltage sensor that couples channel activation and inactivation (22). Interestingly, although this mutation slows the inactivation of Nav1.4 currents by approximately 10-fold (Figure 6A), it causes a hyperpolarizing shift in the voltage dependence of inactivation (Table 1). In a previous study, resurgent sodium currents were not detected in any of 41 DRG neurons transfected with wild-type skeletal muscle sodium channel Nav1.4r (4). Again, we did not detect resurgent currents in any of 11 neurons expressing Nav1.4r (Figure 6B); however, 13 of 20 neurons expressing Nav1.4r-R1448P channels generated resurgent currents (Figure 6C), with

**Figure 4**

Resurgent currents are produced by Nav1.5 channels. (A and B) Representative current traces recorded from DRG neurons expressing Nav1.5 that did not (A) and that did (B) generate resurgent currents. (C and D) Representative current traces recorded from DRG neurons expressing Nav1.5-F1486L channels that did not (C) and that did (D) generate resurgent currents. Resurgent currents were larger on average for Nav1.5-F1486L than for Nav1.5 channels. Currents were elicited with the standard resurgent current protocol shown in Figure 2E and are magnified $\times 30$ relative to the peak current amplitude.

increased the persistent sodium current (Table 1). Resurgent currents were observed in 7 of 14 neurons expressing Nav1.6r-I1477T channels. Notably, these currents were approximately 8-fold larger than those produced by either Nav1.6r or Nav1.7r-I1461T channels, with an average relative amplitude of $15.3\% \pm 3.4\%$ (Figure 7C). These data suggest that mutations impairing inactivation of Nav1.6 may be lethal as a result of the proclivity of Nav1.6 to generate resurgent currents.

Discussion

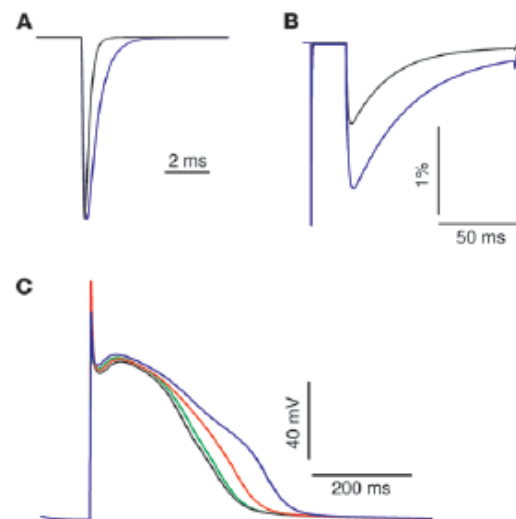
Our data show, for the first time to our knowledge, that Nav1.4, Nav1.5, and Nav1.7 channels have the capability to generate resurgent currents, and that the relative resurgent sodium current amplitudes observed with the disease mutations that impair inac-

tivation are of approximately the same magnitude as the resurgent currents generated by Nav1.6 under control conditions in cerebellar Purkinje neurons and DRG neurons (3, 4). An extensive series of studies on cerebellar Purkinje neurons indicates that resurgent currents have a major impact on excitability, contributing to spontaneous firing and accelerating the rate of repetitive firing of APs (3, 7, 8, 18, 25). As a consequence, it is predicted that the resurgent currents associated with the inherited neuronal and muscle channelopathies could markedly affect AP firing in neurons and muscle and contribute to disease pathophysiology. Indeed, our computer simulations of a DRG neuron and cardiac myocyte indicated that resurgent currents could substantially exacerbate the effects of the disease mutations on cellular excitability.

Our data provided further evidence that the sodium channel isoforms differ in their proclivity to produce resurgent sodium currents. We showed that Nav1.6 was more inclined to generate resurgent currents than Nav1.4, Nav1.5, or Nav1.7. Furthermore, the identical mutation produced a greater increase of resurgent currents in Nav1.6 than in Nav1.7 (compare Nav1.6r-I1477T data with that of Nav1.7r-I1461T; Table 1 and Figures 2 and 7). Although studies of Nav1.6 knockout mice strongly indicate that Nav1.6 is the predominant generator of resurgent currents in cerebellar Purkinje and DRG neurons (3, 4), resurgent currents have been detected in Purkinje and other central nervous system neurons from Nav1.6 knockout mice (26). Nav1.2 channels have been shown to produce resurgent currents when expressed in DRG neurons, albeit in only

Figure 5

Computer simulations of Nav1.5 currents and cardiac myocyte APs. (A) Simulated Nav1.5 (black trace) and Nav1.5-F1486L (blue trace) currents elicited by a voltage step from -100 mV to $+10$ mV. (B) Simulated resurgent currents generated by model Nav1.5 (black trace) and Nav1.5-F1486L (blue trace) conductances. Model currents were elicited with the standard resurgent current voltage protocol shown in Figure 2E. The modeled resurgent current was 0.9% of the peak current for Nav1.5 and 1.7% of the peak current for Nav1.5-F1486L. (C) Simulated APs from a modeled cardiac myocyte. There was little difference between the APs of a model cell with Nav1.5 that did not include resurgent currents (black trace) and those of a cell with Nav1.5 that did include resurgent currents (green trace). Nav1.5-F1486L simulated without resurgent current generation broadened the AP (red trace), and this effect was exacerbated in the simulation of Nav1.5-F1486L with resurgent current generation (blue trace).



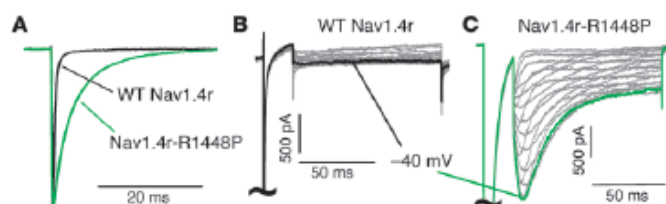


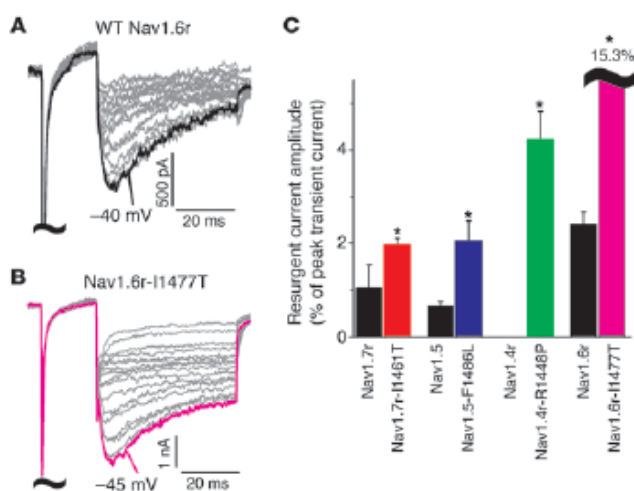
Figure 6
A PMC mutation induces resurgent currents in Nav1.4. (A) The paramyotonia R1448P mutation caused a pronounced slowing of the rate of Nav1.4r inactivation. Currents were elicited with a step depolarization to +10 mV. (B) Resurgent currents were not detectable in any of the neurons expressing Nav1.4r channels. (C) Conversely, the majority of neurons expressing Nav1.4r-R1448P channels generated robust resurgent currents. Resurgent currents were elicited with the protocol shown in Figure 2E and are magnified $\times 20$ relative to the peak current amplitude.

2 of 25 transfected cells (27). Although it is not known whether Nav1.1 and Nav1.3 channels produce resurgent currents, mutations that slow the rate of inactivation have been identified in these isoforms in patients with epilepsy (28, 29), and it is therefore conceivable that resurgent currents could contribute to the pathophysiology of some inherited epilepsies. In our study, we showed that a mutation in the voltage-sensing segment 4 of the fourth domain, as well as mutations in the IFMT inactivation particle, induced enhanced resurgent currents, which suggests that any mutation that slows the rate of open channel fast inactivation might be able to induce resurgent currents. However, it is important to note that the rate of inactivation cannot be the only determinant of resurgent current production. Nav1.8 currents are slower to inactivate than are Nav1.7r-I1461T channels. Regardless of this, cultured rat DRG neurons treated with tetrodotoxin (TTX) that produced large endogenous Nav1.8 currents, but no recombinant currents, did not produce resurgent currents ($n = 11$; see Supplemental Figure 1). Thus, other factors must also contribute to the inclination of specific VGSC isoforms to generate resurgent currents.

The data presented here, in conjunction with the findings of our previous study (4), clearly show that DRG neurons have the appropriate cellular environment for production of resurgent currents. Conversely, adult DRG sensory neurons are not the native tissue for expression of Nav1.4 and Nav1.5, and it is not known whether cardiac and skeletal muscle cells have the appropriate cellular environment for the production of resurgent currents. Data from cerebellar Purkinje neurons indicate that the auxiliary sodium channel $\beta 4$ subunit may be the putative blocking factor crucial for generation of resurgent currents with Nav1.6 channels (30). Previous work has demonstrated that DRG neurons and cardiac and skeletal muscle all express high levels of $\beta 4$ (31). However, although the $\beta 4$ subunit may be necessary, it does not appear to be sufficient. Phosphorylation of the sodium channel, the $\beta 4$ subunit, or possibly an unidentified protein also seems to be required (32), at least in cerebellar Purkinje neurons. This indicates that changes in kinase and phosphatase activity are likely to affect the generation of resurgent currents. Therefore, even if the conditions in normal cardiac and skeletal muscle are not appropriate for generation of resurgent currents, under specific, possibly pathological, conditions, these cells might express the appropriate accessory subunits and kinases. Because our optimized expression system used adult DRG neurons, in which Nav1.4 and Nav1.5 are not normally expressed, it would be of great interest to determine whether Nav1.4 and Nav1.5 wild-type and mutant channels produce resurgent sodium currents in skeletal and cardiac muscle, respectively, under either normal or pathophysiological conditions.

It is important to note that not all of the DRG neurons expressing recombinant channels capable of generating resurgent currents produced detectable resurgent currents. This further indicates that the cellular environment is a crucial determinant of resurgent current production. Regional differences in the properties of sensory afferents that affect resurgent current generation might contribute to the phenotypical association of pain with particular body

Figure 7
Nav1.6 channels generate large resurgent currents. (A and B) Representative resurgent currents recorded from a neuron expressing Nav1.6r (A) and Nav1.6r-I1477T (B) channels. Current traces are magnified $\times 20$ and $\times 5$, respectively, relative to the peak current. (C) Comparison of the relative resurgent current amplitude, expressed as a percentage of peak transient current, for wild-type and mutant VGSCs. $*P < 0.05$ versus the wild-type channel for the given isoform.





regions in PEPD. Interestingly, cells that generated detectable resurgent currents generally generated larger peak transient currents (Supplemental Table 4). Although this difference was only significant for 3 of the 7 channel constructs that generated resurgent currents, it might suggest that cellular factors underlying resurgent current generation could also affect peak current expression. However, more than 40 cells with peak transient current amplitudes greater than 20 nA were recorded that lacked detectable resurgent currents. Furthermore, the relative amplitude of resurgent currents is poorly correlated with peak transient current amplitude (Supplemental Figure 3). At this time, we do not know how DRG neurons that do and do not produce resurgent currents differ in terms of β subunit expression and/or kinase activity. Our optimized DRG expression system could be useful in identifying cellular factors that modulate resurgent currents.

Our data clearly show that resurgent sodium currents are likely to play a role in the functional consequences of inherited neuronal and muscle channelopathies. In addition, our data – in conjunction with the previous study indicating that β -pompilidotoxin can artificially induce resurgent currents in cerebellar Purkinje neurons (9) – indicate that any manipulation that slows or destabilizes inactivation has the potential to induce resurgent currents. Many posttranslational modifications have been reported to slow the rate of inactivation or increase the amplitude of persistent sodium currents, including hypoxia (33), phosphorylation (34), altered calcium signaling (35), G protein activation (36), and oxidation (37). We propose that these alterations could also result in abnormal resurgent current generation. The induction of resurgent sodium currents likely contributes to the more extreme electrophysiological changes and disease sequelae that can be associated with both inherited and acquired disorders of neuronal and muscle excitability.

Methods

Sodium channel constructs and mutagenesis

These studies used cDNA constructs encoding the human Nav1.4 open reading frame (38), the human Nav1.5 open reading frame (39), the mouse Nav1.6 open reading frame (40), and the human Nav1.7 open reading frame (41). To aid in isolation and characterization of sodium currents generated in DRG neurons by recombinant VGSCs, cDNA constructs for Nav1.4, Nav1.6, and Nav1.7 were modified with a single point mutation to confer high resistance to TTX (referred to herein as Nav1.4r, Nav1.6r, and Nav1.7r, respectively; Ki, approximately 100 μ M; ref. 42) using the QuikChange XL (Stratagene) mutagenesis kit, as previously described (35, 43). Nav1.5 channels are natively resistant to TTX (Ki, about 2 μ M); therefore, their sensitivity to TTX was not modified. Additional channelopathy constructs (Nav1.4r-R1448P, Nav1.5-F1486L, Nav1.6r-I1477T, and Nav1.7r-I1461T) were made by inserting the respective mutation into the TTX-resistant cDNA constructs using the QuikChange XL mutagenesis kit following the manufacturer's instructions (Stratagene). Mutations were confirmed by sequencing.

cDNA and cell culture and transfection

Adult rat DRG neurons were harvested and cultured as previously described (43, 44). Animal procedures were approved by the Indiana University School of Medicine Institutional Animal Care and Use Committee. Briefly, rats were rendered unconscious by exposure to CO₂ and decapitated. Cells were treated with collagenase (1 mg/ml) and papain (1 mg/ml), dissociated in DMEM supplemented with 10% fetal bovine serum, and plated on glass coverslips coated with polyornithine and laminin. Cultures were maintained at 37°C in a 5% CO₂ incubator, and media was changed

every 2 days during experimental incubation periods. The Helios Gene Gun (Bio-Rad Laboratories) was used to transiently cotransfect rat DRG neurons, as described previously (35, 43, 45, 46). Cells were cotransfected with a plasmid encoding the recombinant VGSC and an internal ribosome entry site-EGFP (IRES-EGFP) vector plasmid that also encoded a Nav1.8 shRNA (see below for details).

Electrophysiology

DRG recordings were obtained from cells 20–72 hours after transfection. Whole-cell patch-clamp recordings were conducted under voltage-clamp mode at room temperature (about 22°C) after obtaining a Giga-ohm seal (1–20 G Ω) using a HEKA EPC-10 amplifier (47). Data were acquired on a Windows-based Pentium IV computer using the Pulse program (version 8.65; HEKA Elektronik). Fire-polished electrodes (0.9–2.5 M Ω) were fabricated from 1.7-mm capillary glass using a Sutter P-97 puller (Novato), and the tips were coated with sticky wax (KerrLab) to minimize capacitive artifacts and increase series resistance compensation. The standard electrode solution consisted of 140 mM CsF, 10 mM NaCl, 1.1 mM EGTA, and 10 mM HEPES. The standard extracellular bathing solution contained 130 mM NaCl, 30 mM TEA Chloride, 1 mM MgCl₂, 3 mM KCl, 1 mM CaCl₂, 0.05 mM CdCl₂, 10 mM HEPES, and 10 mM D-glucose. Recording solutions were adjusted using D-glucose to maintain physiological pH and osmolarity values. Cells on glass coverslips were transferred to a recording chamber containing 250 μ l bathing solution. Transfected cells were selected based on their ability to express EGFP. Cells not expressing EGFP were also used for nontransfected control experiments and analysis. Voltage-clamp protocols were used to assay the biophysical properties of the recombinant sodium currents in the presence of 500 nM TTX to knock down native TTX-sensitive sodium currents. Offset potential was zeroed before patching. Capacitive artifacts were canceled using the computer-controlled circuitry of the patch clamp amplifier. Series resistance errors were always compensated with 75%–90% series resistance compensation and were typically less than 5 mV during voltage-clamp recordings. Leak currents were linearly canceled by digital P/-5 subtraction, whereby currents elicited by 5 pulses that are one-fifth of the test pulse are subtracted from the test pulse. Cells were held at a membrane potential of -100 mV. Membrane currents were filtered at 5 kHz, sampled at 20 kHz. Whole-cell patch recordings did not last more than 45 minutes, and cells were not held in the standard bathing solution for more than 1 hour. Inward sodium currents had a reversal potential of approximately +65 mV, corresponding closely to the calculated Nernst potential observed during the standard current-voltage (I/V) protocol. Data were not recorded before 3 minutes after whole-cell configuration had been established to allow adequate time for the electrode to equilibrate. Once recording started, cells underwent a series of 60 pulses of 20 ms each to -10 mV, to ensure rundown of any residual endogenous Nav1.9 current (42). I/V relationships were determined by an incremental depolarizing step protocol, testing every +5 mV for 50 ms, from -80 to +50 mV. To determine the fraction of channels transitioning to a fast-inactivated state, a double-pulse protocol (b_{∞}/V) was used that incrementally conditioned the channels from -120 to -10 mV for 500 ms before testing for the fraction of channels available at -10 mV. Resurgent currents were assayed with a 2-step protocol that initially depolarized the membrane to +30 mV for 20 ms before testing for inward resurgent sodium currents by hyperpolarizing the membrane potential in -5-mV increments from 0 mV to -80 mV, for 100 ms, before returning to the holding potential. Experimental voltage-clamp data were analyzed using Pulsefit (version 8.65; HEKA Elektronik), Origin (version 7.0; OriginLab Corp.), and Microsoft Excel software programs. Data from individual steady-state recording conditions were fit using a standard single-phase Boltzmann distribution for voltage-dependent activation (m_{∞}) and steady-state fast-inactivation



(h_{∞}) data. Midpoint ($V_{1/2}$) and slope factors (Z) were calculated using a standard single-phase Boltzmann distribution fit according to Equation 1.

Equation 1

$$I(V) = \text{Offset} + \left[\frac{\text{Amplitude}}{1 + \exp\left(\frac{V - V_{1/2}}{Z}\right)} \right]$$

Resurgent sodium current quantification and analysis

Cells were assayed for the ability to produce resurgent sodium currents using a step protocol (Figure 2E) that initially conditioned the cells to +30 mV for 20 ms, from a holding potential of -100 mV, before repolarizing the membrane potential from 0 to -80 mV (in -5-mV increments) to test for resurgent current; cells were then returned to their holding potential. Resurgent sodium currents display distinct features (25), and these were used to determine whether a cell generated resurgent currents. For example, resurgent currents display a unique voltage dependence in which the peak resurgent currents are elicited by moderately hyperpolarized potentials relative to the holding potentials during the repolarizing steps. For all cells identified with resurgent current in the current study, maximal peak currents during the repolarizing pulses were produced within a window of potentials from -35 to -50 mV (Figure 2F) and were first observed around -10 mV. Additionally, these currents displayed unique gating kinetics within the window of potentials with a noticeably slower onset and decay phase. This is in contrast with classic VGSC tail currents, which are observed instantaneously following hyperpolarizing steps and decay within a few milliseconds. In approximately 50% of the cells, resurgent currents were not detected (for example, see Figures 2, 4, and 6). Currents were analyzed with leak subtraction in PulseFit and were filtered at 1,000 Hz to reduce noise but maintain the current waveform. The resurgent current amplitude was measured relative to the leak-subtracted baseline (Supplemental Figure 2). The relative amplitude of the resurgent current was calculated as a percentage of the peak transient current by multiplying the peak resurgent current by 100 and then dividing by the peak transient current generated during a test pulse to -10 mV from a holding potential of -100 mV. The average resurgent current amplitude for each VGSC construct was only calculated using data from those cells in which resurgent current was detected. Recordings contaminated with endogenous TTX-resistant currents, determined from steady-state inactivation plots (see below), were not used for further analysis. Cells that expressed recombinant currents with peak transient sodium current amplitudes that were less than 5 nA were also excluded from the overall analysis because of uncertainties associated with measuring resurgent current amplitude in cells that had small peak current amplitudes.

Isolation of recombinant VGSC currents in DRG neurons

The goal of these experiments was to isolate and record the sodium currents generated by the recombinant VGSCs. As described above, the recombinant channels either were naturally resistant (Nav1.5), or were mutated to be resistant (Nav1.4, Nav1.6, Nav1.7), to TTX. Endogenous DRG TTX-sensitive channels were blocked with 500 nM TTX. DRG neurons can also express endogenous Nav1.8 and Nav1.9 currents, which are resistant to TTX. Nav1.9 currents are not observed under the culture and recording conditions we used (45, 46, 48, 49), and were therefore not an issue. Although Nav1.8 currents are substantially decreased with time in culture (50), we used additional measures to minimize contamination of the recordings by Nav1.8 currents. Nav1.8 currents were knocked down using a targeted shRNA plasmid (pLL3.7; targeting sequence, GATGAGGTCGCTGCTAAGG) to silence native rat Nav1.8 gene expression via RNAi (51). Additionally, the Nav1.8 shRNA was in an IRES-EGFP vector, allowing transfected

cells to be identified by their green fluorescence. The shRNA plasmid and recombinant sodium channel constructs were transfected at a ratio of 2:1. Under control conditions (less than 48 hours in culture), Nav1.8 current amplitude averaged 34.9 ± 4.8 nA ($n = 42$). To determine the efficiency of Nav1.8 shRNA knockdown, neurons were transfected with TTX-sensitive Nav1.7 plasmid plus the Nav1.8 shRNA. Cells with green fluorescence were recorded in the presence of TTX (to block both endogenous and recombinant TTX-sensitive currents in this control experiment), and the remaining TTX-resistant current, which must be generated by endogenous TTX-resistant channels, was measured ($n = 17$). Nav1.8 and Nav1.9 produce currents with distinctive kinetic and voltage-dependent properties that can be readily distinguished from each other and from TTX-sensitive currents (10, 48). In the 17 cells examined, Nav1.9 currents were not observed, and the Nav1.8 current amplitude averaged 0.5 ± 0.3 nA. Thus, endogenous Nav1.8 currents were reduced by greater than 98% under our experimental conditions (Supplemental Figure 1, A and B). In addition, because Nav1.8 currents have distinctive kinetic and voltage-dependent properties, contamination by Nav1.8 current can be determined for each individual cell expressing recombinant current. The midpoint of the voltage dependence of inactivation for Nav1.8 currents is -34.7 ± 2.0 mV, substantially more depolarized than any of the recombinant constructs investigated in the present study (see Table 1). Analysis of the voltage dependence of inactivation curve can therefore be used to determine the absolute and relative amplitude of the recombinant VGSC current and the endogenous Nav1.8 current for each individual cell (Supplemental Figure 1C). Cells that expressed Nav1.8 currents with amplitudes greater than 15% of the recombinant current amplitude were excluded from the final data analysis. In the 150 cells expressing TTX-resistant recombinant VGSCs that were used in the final analysis, the peak recombinant current amplitude averaged 36.2 ± 2.1 nA, and the peak residual Nav1.8 current amplitude averaged 0.3 nA. It is important to note that resurgent sodium currents were not observed in a control group of neurons transfected with Nav1.8 shRNA and treated with TTX that did not express recombinant TTX-resistant VGSC current ($n = 11$; Supplemental Figure 1E). Furthermore, in another control group of cultured rat DRG neurons treated with TTX that produced large endogenous Nav1.8 currents (average peak amplitude, 32 ± 8 nA; $n = 11$), resurgent currents were not observed (Supplemental Figure 1D). These data confirmed that (a) the use of TTX and the Nav1.8 shRNA allowed effective isolation of the current produced by recombinant VGSCs in transfected DRG neurons and (b) the resurgent currents recorded from DRG neurons transfected with Nav1.8 shRNA and TTX-resistant recombinant channels in the presence of 500 nM TTX were indeed generated by the recombinant channels.

Computational simulations

Simulations were performed to explore the impact that resurgent currents generated by VGSCs and disease mutants might have on AP firing. The basic approach was to use established models of DRG neuron and cardiac myocyte excitability that had been implemented in the NEURON simulation environment (17) and, with modifications only to the appropriate sodium channel formulation, simulate and evaluate the impact of the disease mutation and/or the resurgent current blocking factor.

DRG neuron simulation

The DRG neuron model used was developed previously (16) and included the following voltage-dependent currents: a delayed rectifier potassium current (I_{KDR}), an A-type potassium current (I_{KA}), and $\text{Na}_v1.8$, slowly inactivating TTX-R current. The only changes made to the model were to the Nav1.7 voltage-dependent sodium current in the model. The sodium current changes were implemented in a Markov model based on the Hodgkin-Huxley formulation of Nav1.7 previously used (16). The Markov for-



mulation is more amenable to implementation of both the I1461T effects and the resurgent blocking factor (18). Simulations were run with (a) 100% Nav1.7, (b) 100% Nav1.7 with resurgent current, (c) 50% Nav1.7 and 50% Nav1.7-I1461T, and (d) 50% Nav1.7 and 50% Nav1.7-I1461T, both with resurgent current. Mutant channels were simulated with 50% wild-type channels because the PEPD mutations displayed autosomal dominance.

Nav1.7. The diagram for the Markov model used for the simulated voltage-gated sodium conductances is shown in Figure 3A. The model includes 3 closed states, a conducting open state, and 3 inactivated states. The Markov model used for the simulated voltage-gated sodium conductance with resurgent current included 1 additional state, the open-blocked state (Figure 3A, boxed region). The resurgent current factor was implemented as done for simulation of resurgent currents in cerebellar Purkinje neurons by Khaliq et al. (18), with slight modifications to the transition rate expressions (see Supplemental Table 2).

Nav1.7-I1461T. Characterization of the functional impact of the I1461T mutation in HEK293 cells (13) and DRG neurons (present study) showed that this mutation destabilized inactivation, shifting the voltage dependence of inactivation in the depolarizing direction and slowing the rate of open-state inactivation. The measured values of channel availability and time constants of inactivation from these studies were used to reformulate expressions for the vertical transitions in Figure 3A (between the inactivated states and the closed and open states). The horizontal transitions were unchanged (Supplemental Table 2). Figure 3B compares the modeled Nav1.7 and Nav1.7-I1461T currents elicited with a step depolarization to +10 mV. The resurgent current was added to the Nav1.7-I1461T conductance model in the exact way that it was added to the wild-type Nav1.7 conductance model. Figure 3C compares the resurgent currents generated by Nav1.7 and Nav1.7-I1461T simulated conductances.

Cardiac myocyte simulation

We modified mathematical models of cardiac AP firing (20, 52) to simulate the impact of the F1486L LQT3/SIDS mutation and resurgent currents. The cardiac myocyte model (see <http://senselab.med.yale.edu/ModelDB/ShowModel.asp?model=3800>) was previously implemented by I. Jacobson in the NEURON simulation environment (17). The only changes made to the model were to the voltage-dependent sodium current (I_{Na} in the original model). Simulations were run with (a) 100% Nav1.5, (b) 100% Nav1.5 with resurgent current, (c) 50% Nav1.5 and 50% Nav1.5-F1486L, and (d) 50% Nav1.5 and 50% Nav1.5-F1486L, both with resurgent current. Mutant channels were simulated at with 50% wild-type channels because the LQT3/SIDS mutations displayed autosomal dominance.

Nav1.5. We developed a Markov model based on the Hodgkin-Huxley formulation of Nav1.5 in the original model (20, 52). The Markov formu-

lation was more amenable to implementation of both the F1486L effects and the resurgent blocking factor. Intermediate inactivation states were not included in this formulation, as it was unclear how to model potential interactions between the resurgent current blocking factor and intermediate inactivation states. This is reasonable, as the F1486L mutation may have little or no impact on intermediate inactivation (19). The diagram for the Markov model used for the simulated voltage-gated sodium conductances is shown in Figure 3A, and the transition rate expressions for Nav1.5 are provided in Supplemental Table 3.

Nav1.5 F1486L. Our data on the F1486L mutation indicate that it produces moderate destabilization of inactivation, shifting the voltage dependence of inactivation by approximately 8 mV in the depolarizing direction, slowing the rate of inactivation, and slightly increasing persistent currents. We modeled these effects by altering the transition rates from the closed and open state into the inactivated states (see Supplemental Table 3). Simulated Nav1.5 and Nav1.5-F1486L currents are shown in Figure 5A.

Nav1.5 and Nav1.5 F1486L with resurgent current. The resurgent current factor was modeled to be similar to that of Nav1.7, but with slight modifications to the overall expression to account for the relative resurgent current amplitude observed with Nav1.5 and Nav1.5-F1486L channels in our experiments (Supplemental Table 3). Simulated resurgent currents are shown in Figure 5B.

Statistics

All data are mean \pm SEM. Comparison of frequency was determined using χ^2 test. Statistical significance was assessed with Microsoft Excel using 2-tailed Student's unpaired *t* tests. Statistical significance of difference was accepted at *P* values less than 0.05.

Acknowledgments

We thank E. Thompson and M. Vasko for assistance with the Nav1.8 shRNA. B.W. Jarecki was supported by an Indiana Clinical and Translational Sciences Institute Career Development Award (PHS grant 5TL1RR025759), and A.D. Piekarsz was partially supported by NIH training fellowship NS066663. This work was supported by NIH research grant NS053422 (to T.R. Cummins).

Received for publication August 12, 2009, and accepted in revised form November 10, 2009.

Address correspondence to: Theodore R. Cummins, Indiana University School of Medicine, 950 W. Walnut St., Indianapolis, Indiana 46202, USA. Phone: (317) 278-9342; Fax: (317) 278-5849; E-mail: trcummin@iupui.edu.

- George AL Jr. Inherited disorders of voltage-gated sodium channels. *J Clin Invest*. 2005; 115(8):1990-1999.
- Cannon SC. Pathomechanisms in channelopathies of skeletal muscle and brain. *Annu Rev Neurosci*. 2006;29:387-415.
- Raman IM, Sprunger LK, Meister MH, Bean BP. Altered subthreshold sodium currents and disrupted firing patterns in Purkinje neurons of *Scn8a* mutant mice. *Neuron*. 1997;19(4):881-891.
- Cummins TR, Dib-Hajj SD, Herzog RI, Waxman SG. Nav1.6 channels generate resurgent sodium currents in spinal sensory neurons. *FEBS Lett*. 2005;579(10):2166-2170.
- Chen Y, Yu FH, Sharp EM, Beacham D, Scheuer T, Catterall WA. Functional properties and differential neuromodulation of Na(v)1.6 channels. *Mol Cell Neurosci*. 2008;38(4):607-615.
- Hodgkin AL, Huxley AF. The dual effect of membrane potential on sodium conductance in the giant axon of *Loligo*. *J Physiol*. 1952;116(4):497-506.
- Raman IM, Bean BP. Ionic currents underlying spontaneous action potentials in isolated cerebellar Purkinje neurons. *J Neurosci*. 1999;19(5):1663-1674.
- Raman IM, Bean BP. Inactivation and recovery of sodium currents in cerebellar Purkinje neurons: evidence for two mechanisms. *Biophys J*. 2001; 80(2):729-737.
- Grieco TM, Raman IM. Production of resurgent current in Nav1.6-null Purkinje neurons by slowing sodium channel inactivation with beta-pompidotaxin. *J Neurosci*. 2004;24(1):35-42.
- Rush AM, Cummins TR, Waxman SG. Multiple sodium channels and their roles in electrogenesis within dorsal root ganglion neurons. *J Physiol*. 2007;579(Pt 1):1-14.
- Fertleman CR, et al. SCN9A mutations in paroxysmal extreme pain disorder: allelic variants underlie distinct channel defects and phenotypes. *Neuron*. 2006;52(5):767-774.
- Dib-Hajj SD, Cummins TR, Black JA, Waxman SG. From genes to pain: Na v 1.7 and human pain disorders. *Trends Neurosci*. 2007;30(11):555-563.
- Jarecki BW, Sheets PL, Jackson JO II, Cummins TR. Paroxysmal extreme pain disorder mutations within the D3/S4-S5 linker of Nav1.7 cause moderate destabilization of fast inactivation. *J Physiol*. 2008;586(Pt 17):4137-4153.
- Armstrong CM, Bezanilla F, Rojas E. Destruction of sodium conductance inactivation in squid axons perfused with pronase. *J Gen Physiol*. 1973; 62(4):375-391.
- West JW, et al. A cluster of hydrophobic amino acid residues required for fast Na(+) channel inactivation. *Proc Natl Acad Sci U S A*. 1992;89(22):10910-10914.
- Sheets PL, Jackson JO II, Waxman SG, Dib-Hajj SD, Cummins TR. A Nav1.7 channel mutation associated with hereditary erythromelalgia contributes to neuronal hyperexcitability and displays reduced lidocaine sensitivity. *J Physiol*. 2007;581(Pt 3):1019-1031.



17. Hines ML, Carnevale NT. The NEURON simulation environment. *Neural Comput*. 1997;9(6):1179–1209.
18. Khaliq ZM, Gouwens NW, Raman IM. The contribution of resurgent sodium current to high-frequency firing in Purkinje neurons: an experimental and modeling study. *J Neurosci*. 2003;23(12):4899–4912.
19. Wang DW, et al. Cardiac sodium channel dysfunction in sudden infant death syndrome. *Circulation*. 2007;115(3):368–376.
20. Courtemanche M, Ramirez RJ, Nattel S. Ionic mechanisms underlying human atrial action potential properties: insights from a mathematical model. *Am J Physiol*. 1998;275(1 Pt 2):H301–H321.
21. Featherstone DE, Fujimoto E, Ruben PC. A defect in skeletal muscle sodium channel deactivation exacerbates hyperexcitability in human paramyotonia congenita. *J Physiol*. 1998;506(Pt 3):627–638.
22. Chahine M, et al. Sodium channel mutations in paramyotonia congenita uncouple inactivation from activation. *Neuron*. 1994;12(2):281–294.
23. Oxford GS. Some kinetic and steady-state properties of sodium channels after removal of inactivation. *J Gen Physiol*. 1981;77(1):1–22.
24. Heatwole CR, Moxley RT, 3rd. The nondystrophic myotonias. *Neurotherapeutics*. 2007;4(2):238–251.
25. Raman IM, Bean BP. Resurgent sodium current and action potential formation in dissociated cerebellar Purkinje neurons. *J Neurosci*. 1997;17(12):4517–4526.
26. Do MT, Bean BP. Sodium currents in subthalamic nucleus neurons from Nav1.6-null mice. *J Neurophysiol*. 2004;92(2):726–733.
27. Rush AM, Dib-Hajj SD, Waxman SG. Electrophysiological properties of two axonal sodium channels, Nav1.2 and Nav1.6, expressed in mouse spinal sensory neurons. *J Physiol*. 2005;564(Pt 3):803–815.
28. Holland KD, et al. Mutation of sodium channel SCN3A in a patient with cryptogenic pediatric partial epilepsy. *Neurosci Lett*. 2008;433(1):65–70.
29. Lossin C, Wang DW, Rhodes TH, Vanoye CG, George AL Jr. Molecular basis of an inherited epilepsy. *Neuron*. 2002;34(6):877–884.
30. Grieco TM, Malhotra JD, Chen C, Isom LL, Raman IM. Open-channel block by the cytoplasmic tail of sodium channel beta4 as a mechanism for resurgent sodium current. *Neuron*. 2005;45(2):233–244.
31. Yu FH, et al. Sodium channel beta-4, a new disulfide-linked auxiliary subunit with similarity to beta-2. *J Neurosci*. 2003;23(20):7577–7585.
32. Grieco TM, Afshari FS, Raman IM. A role for phosphorylation in the maintenance of resurgent sodium current in cerebellar Purkinje neurons. *J Neurosci*. 2002;22(8):3100–3107.
33. Hammarstrom AK, Gage PW. Hypoxia and persistent sodium current. *Eur Biophys J*. 2002;31(5):323–330.
34. Numann R, Catterall WA, Schuer T. Functional modulation of brain sodium channels by protein kinase C phosphorylation. *Science*. 1991;254(5028):115–118.
35. Herzog RI, Liu C, Waxman SG, Cummins TR. Calmodulin binds to the C terminus of sodium channels Nav1.4 and Nav1.6 and differentially modulates their functional properties. *J Neurosci*. 2003;23(23):8261–8270.
36. Ma JY, Catterall WA, Schuer T. Persistent sodium currents through brain sodium channels induced by G protein betagamma subunits. *Neuron*. 1997;19(2):443–452.
37. Kassmann M, et al. Oxidation of multiple methionine residues impairs rapid sodium channel inactivation. *Pflügers Arch*. 2008;456(6):1085–1095.
38. George AL Jr, Komisarof J, Kallen RG, Barchi RL. Primary structure of the adult human skeletal muscle voltage-dependent sodium channel. *Ann Neurol*. 1992;31(2):131–137.
39. Gellens ME, et al. Primary structure and functional expression of the human cardiac tetrodotoxin-insensitive voltage-dependent sodium channel. *Proc Natl Acad Sci U S A*. 1992;89(2):554–558.
40. Smith MR, Smith RJ, Plummer NW, Meisler MH, Goldin AL. Functional analysis of the mouse Scn8a sodium channel. *J Neurosci*. 1998;18(16):6093–6102.
41. Klagbauer N, Lacinova L, Plocker V, Hofmann F. Structure and functional expression of a new member of the tetrodotoxin-sensitive voltage-activated sodium channel family from human neuroendocrine cells. *EMBO J*. 1995;14(6):1084–1090.
42. Leffler A, Herzog RI, Dib-Hajj SD, Waxman SG, Cummins TR. Pharmacological properties of neuronal TTX-resistant sodium channels and the role of a critical serine pore residue. *Pflügers Arch*. 2005;451(3):454–463.
43. Herzog RI, Cummins TR, Ghassemi F, Dib-Hajj SD, Waxman SG. Distinct repriming and closed-state inactivation kinetics of Nav1.6 and Nav1.7 sodium channels in mouse spinal sensory neurons. *J Physiol*. 2003;551(Pt 3):741–750.
44. Caffrey JM, Eng DL, Black JA, Waxman SG, Kocsis JD. Three types of sodium channels in adult rat dorsal root ganglion neurons. *Brain Res*. 1992;592(1–2):283–297.
45. Cummins TR, et al. Nav1.3 sodium channels: rapid repriming and slow closed-state inactivation display quantitative differences after expression in a mammalian cell line and in spinal sensory neurons. *J Neurosci*. 2001;21(16):5952–5961.
46. Dib-Hajj SD, et al. Transfection of rat or mouse neurons by biolistics or electroporation. *Nat Protoc*. 2009;4(8):1118–1126.
47. Cummins TR, Rush AM, Estacion M, Dib-Hajj SD, Waxman SG. Voltage-clamp and current-clamp recordings from mammalian DRG neurons. *Nat Protoc*. 2009;4(8):1103–1112.
48. Cummins TR, Dib-Hajj SD, Black JA, Akopian AN, Wood JN, and Waxman SG. A novel persistent tetrodotoxin-resistant sodium current in SNS-null and wild-type small primary sensory neurons. *J Neurosci*. 1999;19(24):8C43.
49. Dib-Hajj S, Black JA, Cummins TR, Waxman SG. Nav/Nav1.9: a sodium channel with unique properties. *Trends Neurosci*. 2002;25(5):253–259.
50. Pjell J, Cummins TR, Dib-Hajj SD, Fried K, Black JA, Waxman SG. Differential role of GDNF and NGF in the maintenance of two TTX-resistant sodium channels in adult DRG neurons. *Brain Res Mol Brain Res*. 1999;67(2):267–282.
51. Mikami M, Yang J. Short hairpin RNA-mediated selective knockdown of Nav1.8 tetrodotoxin-resistant voltage-gated sodium channel in dorsal root ganglion neurons. *Anesthesiology*. 2005;103(4):828–836.
52. Luo CH, Rudy Y. A dynamic model of the cardiac ventricular action potential. I. Simulations of ionic currents and concentration changes. *Circ Res*. 1994;74(6):1071–1096.

CURRICULUM VITAE

Andrew D. Piekarz

EDUCATION

- August 2006-February 2012
Indiana University, Indianapolis, IN
Department of Pharmacology and Toxicology
Doctor of Philosophy (Ph.D.) in Pharmacology
Thesis: *Increased resurgent sodium currents in inherited and acquired disorders of excitability*
 - Mentor: Theodore R. Cummins, Ph.D.
- August 2002-May 2006
Saint Louis University, St. Louis, MO
Department of Biomedical Engineering, Parks College of Aviation and Engineering
Bachelor of Science (B.Sc.) in Biomedical Engineering
Thesis: *Accessible Blood Glucose Meter Docking Station*
 - Mentor: David Barnett, D.Sc.

PUBLICATIONS

- **Piekarz A.D.**, Theile J.W., Cummins T.R. Characterization of NaV1.8 resurgent sodium currents in DRG neurons. *In preparation.*
- **Piekarz A.D.**, Liu N., Hodgdon K.E., Jackson II J.O., Xu X.M., Nicol G.D., Cummins T. R. Increased resurgent sodium current following contusive spinal cord injury. *In preparation.*
- Song W., Xiao Y., Chen H., Ashpole N., **Piekarz A.D.**, Yong W., Hudmon A., Cummins T.R., Shou W. Human NaV1.5 F1486 deletion associated with long QT syndrome leads to deficiency in inactivation and reduces lidocaine sensitivity. *In review.*
- **Piekarz A.D.**, Cummins T.R. Differential temperature dependence of resurgent sodium currents in muscle and neuronal channelopathies. *In review.*
- Wilson S.M., Brittain J.M., **Piekarz A.D.**, Ballard C.J., Ripsch M.S., Cummins T.R., Hurley J.H., Khanna M., Hammes N.M., Samuels B.C., White F.A., Khanna R. Further insights into the antinociceptive potential of a peptide disrupting the N-type calcium channel-CRMP-2 signaling complex. *Channels (Austin)*. 2011 Sep 1; 5(5). *In press.*

- Theile J.W., Jarecki B.W., **Piekarz A.D.**, and Cummins T.R. NaV1.7 mutations associated with paroxysmal extreme pain disorder, but not erythromelalgia, enhance NaV and β_4 peptide-mediated resurgent sodium currents. J. Physiol. 2011 Feb; 589(Pt 3):597-608.
- Jarecki B.W.* , **Piekarz A.D.***, Jackson II J.O., Cummins T.R. Human voltage-gated sodium channel mutations that cause inherited neuronal and muscle channelopathies increase resurgent sodium currents. J. Clin. Invest., 2010 Jan; 120 (1): 369-378.
- Brittan J.M., **Piekarz, A.D.**, Wang Y, Cummins, T.R., Khanna R. An atypical role for collapsin response mediator protein 2 (CRMP-2) in neurotransmitter release via interaction with presynaptic voltage-gated calcium channels. J. Biol. Chem., 2009; 284(45):31375-90.

* denotes co-first authorship

ABSTRACTS

- Piekarz, A.D., Jackson II, J.O., Khanna R, Cummins, T.R. *Modulatory role of auxiliary β_1 - and β_2 -subunits on lidocaine's interaction with the sensory neuronal $Na_v1.7$ channel.* The National Society for Neuroscience Annual Meeting. Washington DC. Nov. 2008.
- Jarecki, B.W., Piekarz, A.D., Jackson II, J.O., Cummins T.R. *Impact of Nav1.7 – PEPD missense mutations that slow the rate of inactivation on sensory neuronal resurgent sodium currents.* Biophysical Society Annual Meeting. Boston, MA. Feb. 2009.
- Piekarz, A.D., Jackson II, J.O., Khanna R, Cummins, T.R. *Modulatory role of auxiliary β_1 - and β_2 -subunits on lidocaine's interaction with the sensory neuronal $Na_v1.7$ channel.* The Gill Symposium. Bloomington, IN. May 2009.
- Piekarz, A.D., Jarecki, B.W., Jackson II, J.O., Khanna, R., Cummins, T.R. *Missense mutations in the Nav1.4 isoform associated with paramyotonia congenital produce resurgent sodium currents.* The National Society for Neuroscience Annual Meeting. Chicago, IL. Oct. 2009.
- Jarecki, B.W., Piekarz, A.D., Jackson II, J.O., Cummins, T.R. *Resurgent sodium currents in inherited neuronal and cardiac channelopathies.* The National Society for Neuroscience Annual Meeting. Chicago, IL. Oct. 2009.
- Brittan J.M., Piekarz, A.D., Wang Y, Garcia, A.S., Cummins, T.R., Khanna R. *An atypical role for collapsin response mediator protein 2 (CRMP-2) in neurotransmitter release via interaction with presynaptic voltage-gated calcium channels.* The National Society for Neuroscience Annual Meeting. Chicago, IL. Oct. 2009.

- Piekarz, A.D., Jarecki, B.W., Jackson II, J.O., Khanna, R., Cummins, T.R. *Missense mutations in the NaV1.4 isoform associated with paramyotonia congenital produce resurgent sodium currents*. The Midwest Pain Interest Group (PIG) Meeting. Indianapolis, IN. June 2010.
- Piekarz, A.D., Jarecki, B.W., Jackson II, J.O., Khanna, R., Cummins, T.R. *Missense mutations in the NaV1.4 isoform associated with paramyotonia congenital produce resurgent sodium currents*. The Gill Symposium. Bloomington, IN. Sept. 2010.
- Piekarz, A.D., Lui N., Hodgdon, K.E., Jackson II, J.O., Nicol, G.D., Xu, X.M., and Cummins, T.R. *Altered Voltage-Gated Sodium Channel Properties Following Contusive Spinal Cord Injury (SCI)*. The National Society for Neuroscience Annual Meeting. San Diego, CA. Nov. 2010.
- Piekarz, A.D., Lui N., Hodgdon, K.E., Jackson II, J.O., Nicol, G.D., Xu, X.M., and Cummins, T.R. *Altered Voltage-Gated Sodium Channel Properties Following Contusive Spinal Cord Injury (SCI)*. The Midwest Pain Interest Group (PIG) Meeting. Chicago, IL. July 2011.
- Piekarz, A.D., Lui N., Hodgdon, K.E., Jackson II, J.O., Nicol, G.D., Xu, X.M., and Cummins, T.R. *Altered Voltage-Gated Sodium Channel Properties Following Contusive Spinal Cord Injury (SCI)*. The NIH National Graduate Student Research Conference. Bethesda, MD. Oct. 2011.
- Piekarz, A.D., Lui N., Hodgdon, K.E., Jackson II, J.O., Nicol, G.D., Xu, X.M., and Cummins, T.R. *Altered Voltage-Gated Sodium Channel Properties Following Contusive Spinal Cord Injury (SCI)*. The Gill Symposium. Bloomington, IN. Oct. 2011.
- Piekarz, A.D., Lui N., Hodgdon, K.E., Jackson II, J.O., Nicol, G.D., Xu, X.M., and Cummins, T.R. *Altered Voltage-Gated Sodium Channel Properties Following Contusive Spinal Cord Injury (SCI)*. Eli Lilly Ion Channel Mini Symposium. Indianapolis, IN. Nov. 2011.

INVITED SEMINARS

- *Increased Resurgent Sodium Current (I_{NaR}) in Inherited and Acquired Disorders of Excitability*. Neuroscience Section, National Institute of Neurological Disorders and Stroke (NINDS). National Institute of Health (NIH), Bethesda, MD. (October 2011).
- *Resurgent Sodium Current (I_{NaR}) in Inherited Disorders of Excitability*. Department of Biomedical Engineering, Parks College of Aviation and Engineering. Saint Louis University, St. Louis, MO. (October 2010).

SCHOLARSHIPS AND AWARDS

- Indiana University Department of Pharmacology and Toxicology K. K. Chen Distinguished Graduate Student Fellowship, 2010.
- Indiana Clinical and Translational Sciences Institute (CTSI) Pre-doctoral Fellowship, 2009 (declined funding).
- 1F31NS066663-01 Ruth L. Kirschstein National Research Service Award
Title: "Molecular Determinants of Resurgent Sodium Currents in Sensory Neurons."
Priority Score: 136 (2.8 percentile). July 2009-July 2011.
- GSO Education Enhancement Grant for Consumable Supplies, 2009.
- Rehabilitation Engineering Research Center on Accessible Medical Instrumentation (RERC-AMI) Design Competition Grant Recipient.
Title: *Accessible Blood Glucose Meter Docking Station*. 2006.
- Saint Louis University Jesuit Education Scholarship, 2002-2006.

RESEARCH EXPERIENCE

- **Ph.D. Graduate Student**, Indiana University School of Medicine, Indianapolis, IN (2006-2011).
Mentor: *Dr. Theodore Cummins, Ph.D.*
- Scientific Contributions:
 - Developed and optimized protocols to study the biophysical properties of voltage-gated sodium channels in transiently transfected primary sensory neurons using viral and biolistic transfection methods.
 - Used whole-cell voltage-clamp electrophysiology to characterize the biophysical and pharmacological properties of voltage-gated sodium channels from both acutely cultured neurons (cortical and DRG) and transfected mammalian heterologous cell expression systems (hEK293 and ND7/23 cells).
 - Developed a computational model to explore the impact that increased resurgent sodium currents generated by voltage-gated sodium channel disease mutants might have on action potential firing in neurons and cardiac myocytes.
 - Designed and validated siRNAs to assess functional contributions of voltage-gated sodium channels and auxiliary subunits to physiology.

- Scientific Skills:
 - Received expert training in several techniques including whole-cell voltage clamp electrophysiology, mutagenesis, cell culture, and molecular vector design and construction.
 - Cultivated collaborations with other investigators and received expert training in more advanced molecular biology and biochemistry techniques including real-time RT-PCR, siRNA design and target validation, immunocytochemistry, co-immunoprecipitation, and immunoblot.

- **Student Research Assistant**, Saint Louis University, St. Louis, MO (2005-2006).
Mentor: *Mark M. Kneuper, Ph.D.*
 - Aided in the rational design and validation of a MATLAB® program used to analyze sympathetic nerve activity from conscious animals undergoing a stress paradigm behavioral experiment.
 - Assisted graduate students and technicians troubleshoot and perform animal behavior experiments, analyze data, and perform animal surgeries.

- **Student Senior Research Project**, Saint Louis University, St. Louis, MO (2005-2006).
Advisor: *Dr. David Barnett, D.Sc.*
 - Designed a compact, user friendly accessible blood glucose monitor, designed for patients with reduced vision and dexterity.
 - Glucose meter docking station design integrated hardware capable of retrieving, storing, visually displaying, and verbalizing blood glucose readings.
 - Novel device design was capable of transmitting data wirelessly to healthcare professionals.
 - Developed software to download, catalog, and analyze transmitted data.
 - Final design recognized as innovative.

- Engineering Skills:
 - Hardware integration and knowledge of microcontroller firmware Dynamic C® and MATLAB®.
 - Knowledge of OriginLab 8® and SPSS statistical packages.

LEADERSHIP POSITIONS

- IUSM Graduate Student Organization Representative [Dept. Pharm/Tox], Indiana University School of Medicine, Indianapolis, IN (08/09-present). Supervisor: *Dr. William Sullivan Ph.D. and Dr. Lisa Kamendulis Ph.D.*
- Undergraduate Senior Project Team Leader, Saint Louis University, St. Louis, MO (2005-2006). Mentor: *David Barnett, D.Sc.*

PROFESSIONAL AFFILIATIONS

- Society for Neuroscience (SfN), student member 2007-present
- Biomedical Engineers Society (BMES), student member 2004-2006